



## UvA-DARE (Digital Academic Repository)

### Weibel-Palade body formation and release

*An odyssey through the secretory pathway*

Karampini, E.

#### Publication date

2020

#### Document Version

Final published version

#### License

Other

[Link to publication](#)

#### Citation for published version (APA):

Karampini, E. (2020). *Weibel-Palade body formation and release: An odyssey through the secretory pathway*.

#### General rights

It is not permitted to download or to forward/distribute the text or part of it without the consent of the author(s) and/or copyright holder(s), other than for strictly personal, individual use, unless the work is under an open content license (like Creative Commons).

#### Disclaimer/Complaints regulations

If you believe that digital publication of certain material infringes any of your rights or (privacy) interests, please let the Library know, stating your reasons. In case of a legitimate complaint, the Library will make the material inaccessible and/or remove it from the website. Please Ask the Library: <https://uba.uva.nl/en/contact>, or a letter to: Library of the University of Amsterdam, Secretariat, Singel 425, 1012 WP Amsterdam, The Netherlands. You will be contacted as soon as possible.

**Weibel**  
**Palade**  
**Body**  
formation  
& release

An Odyssey through  
the secretory pathway

**Ellie Karampini**

**Weibel-Palade body formation and release:  
an odyssey through the secretory pathway**

Elli Karampini

## **Colophon**

The research described in this thesis was supported by grants from the Netherlands Ministry of Health (PPOC-2015-24P) and the Landsteiner Stichting voor Bloedtransfusie Research (LSBR-1707).

Financial support for the printing of this thesis was kindly provided by Sanquin Research and the University of Amsterdam, Academisch Medisch Centrum (AMC).

ISBN: 978-94-028-2003-4

Cover and Layout: Ellie Karampini, Achilles Gerokostopoulos  
Printing: Proefschriften.nl

Copyright © 2020 Ellie Karampini

# Weibel-Palade body formation and release

## an odyssey through the secretory pathway

### **Academisch Proefschrift**

ter verkrijging van de graad van doctor  
aan de Universiteit van Amsterdam  
op gezag van de Rector Magnificus  
prof. dr. ir. K.I.J. Maex  
ten overstaan van een door het College voor Promoties ingestelde commissie,  
in het openbaar te verdedigen  
op vrijdag 24 april 2020, te 13.00 uur  
door

**Elli Karampini**

geboren te Cholargos

### **Promotiecommissie:**

Promotor: prof. dr. J.J. Voorberg, AMC-UvA

Copromotor: dr. R. Bierings, Erasmus Universiteit Rotterdam

Overige leden: prof. dr. C.J. Fijnvandraat, AMC-UvA  
prof. dr. J.D. van Buul, AMC-UvA  
dr. M.C. Wolkers, AMC-UvA  
prof. dr. F.W.G. Leebeek, Erasmus Universiteit Rotterdam  
prof. dr. K. Freson, KU Leuven  
dr. J.M.E.M. Cosemans, Universiteit Maastricht

Faculteit der Geneeskunde

## Contents

<b>Chapter 1</b>	General Introduction	<b>1</b>
<b>Chapter 2</b>	Orchestration of primary hemostasis by platelet and endothelial lysosome-related organelles	<b>9</b>
<b>Chapter 3</b>	Sec22b determines Weibel-Palade body length by controlling anterograde ER-Golgi transport	<b>23</b>
<b>Chapter 4</b>	Weibel-Palade body biogenesis is dependent on the Golgi Qa-SNARE STX5	<b>41</b>
<b>Chapter 5</b>	Exocytosis of Weibel-Palade bodies: how to unpack a vascular emergency kit	<b>57</b>
<b>Chapter 6</b>	Defective AP-3-dependent VAMP8 trafficking impairs Weibel-Palade body exocytosis in Hermansky-Pudlak Syndrome type 2 blood outgrowth endothelial cells	<b>73</b>
<b>Chapter 7</b>	Weibel-Palade body localized syntaxin-3 modulates von Willebrand factor secretion from endothelial cells	<b>93</b>
<b>Chapter 8</b>	General discussion	<b>121</b>
<b>Chapter 9</b>	Appendix	<b>133</b>
	Summary	134
	Samenvatting	136
	PhD Portfolio	138
	Publication	139
	Authors and affiliations	140
	Thank you note	142
	Curriculum vitae	143







# Chapter 1

## General Introduction

Ellie Karampini

## Introduction

Endothelial cells (ECs) form the inner lining of blood vessels, separating the blood flow from the tissue underneath, controlling the passage of molecules and the transit of white blood cells in and out of the circulation<sup>1</sup> (Figure 1A). Damaged and new vessels are repaired and generated, respectively, from pre-existing mature ECs, as they retain the capacity of cell division and migration.<sup>1</sup> In the face of vascular injury, the initial step of hemostasis includes endothelial cell activation with simultaneous sub-endothelial and basolaterally deposited collagen exposure to the blood stream.<sup>2</sup> Collagen, in conjunction with von Willebrand factor (VWF) strings that are released from activated ECs and plasma borne VWF, mediates platelet adhesion at sites of vessel wall damage. Adhesion of platelets to collagen results in platelet outside-in signaling and formation of the primary hemostatic plug, which is stabilized by cross-linking with fibrin, a product of the coagulation cascade<sup>2</sup> (Figure 1B).

## Lysosome-related organelles in primary hemostasis

ECs and platelets are the master regulators of hemostasis and they succeed in that by storing large amounts of hemostatic factors, like VWF, in specialized compartments known as lysosome-related organelles (LROs) and rapidly secrete their content upon activation. LROs that are found in ECs are the Weibel-Palade bodies (WPBs), while platelets contain two types, the  $\alpha$ - and  $\delta$ -granules.<sup>3</sup> LROs share features with the lysosomes and their formation can be separated into two steps: the initial biogenesis, either coming directly from the trans-Golgi network (TGN) or derived of multivesicular bodies (MVB), and the maturation process, where they retrieve more proteins in an AP-3 dependent manner from endosomal compartments. Platelets contain between 50 to 80  $\alpha$ -granules which appear as round or ovoid vesicles with a diameter ranging from 200-500 nm.<sup>4,5</sup> Electron tomography studies have provided evidence for morphological heterogeneity of  $\alpha$ -granules.<sup>6</sup> Tubular extensions with a size of several  $\mu$ m were found to be connected to spherical  $\alpha$ -granules. Intriguingly, tubular extensions of  $\alpha$ -granules did not contain VWF suggesting selective segregation of cargo in spherical and tubular compartments of  $\alpha$ -granules.<sup>6</sup> Proteomic studies have provided evidence for the presence of several hundreds of proteins in  $\alpha$ -granules which can be derived from both biosynthetic as well as endocytic pathways.<sup>7</sup> Platelets contain on average 3-8  $\delta$ -granules which have dimensions that are slightly smaller when compared to  $\alpha$ -granules.<sup>4</sup> In contrast to  $\alpha$ -granules,  $\delta$ -granules contain primarily small molecules like ADP/ATP and serotonin.<sup>4,8</sup> Release of ADP and serotonin from  $\delta$ -granules provides an important mechanism to further enhance autocrine and paracrine pathways of platelet activation that promote rapid formation of a platelet plug during primary hemostasis.<sup>5</sup> As outlined above, WPBs present in endothelial cells have also been classified as a highly specialized LRO, which contains cargo derived of both biosynthetic and endosomal pathways. WPBs have a distinct elongated cigar-shaped morphology and primarily store VWF in the form of condensed longitudinal tubules together with other proinflammatory and angiogenic proteins (**chapter 4**) (Figure 2). It has been established that the formation of WPBs is strictly related to VWF expression, with ectopic expression of VWF in non-endothelial cell lines leading to pseudo-WPBs.<sup>9</sup> It is now well-established that VWF is condensed into helical tubules in WPBs that rapidly “unfurl” into long VWF strings that remain anchored to the surface of endothelial cells.<sup>10-12</sup> Elegant follow-up studies by the Cutler group have convincingly shown that the dimensions of WPBs are critical for the ability of VWF to organize into long strings that are capable of efficiently capturing platelets.<sup>13</sup>

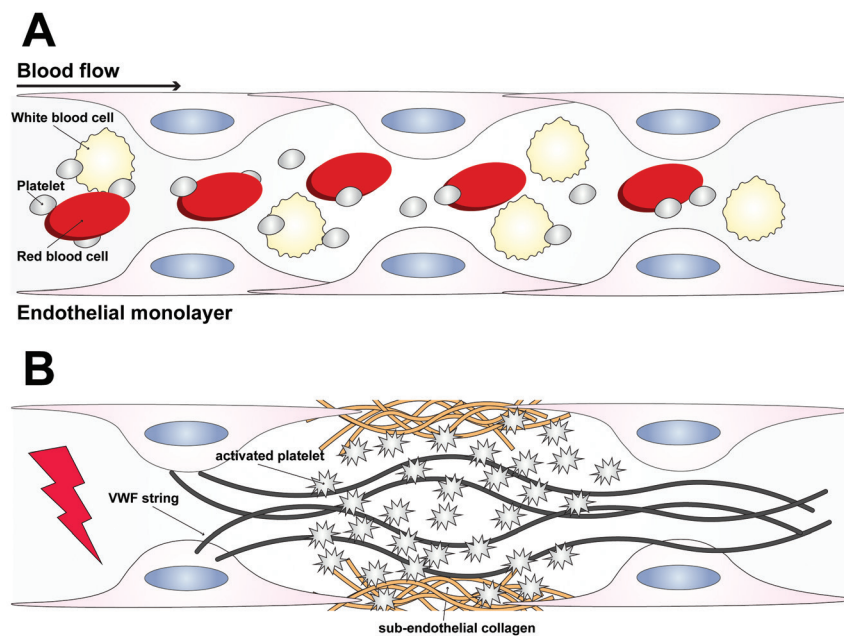


**Figure 1: Representative model of primary hemostasis.** A) Schematic representation of an endothelial cell-lined blood vessel containing blood components. B) Schematic representation of primary hemostatic plug formation at the site of vascular damage starting endothelial cell activation and collagen exposure, followed by VWF secretion and platelet activation by binding to VWF and collagen.

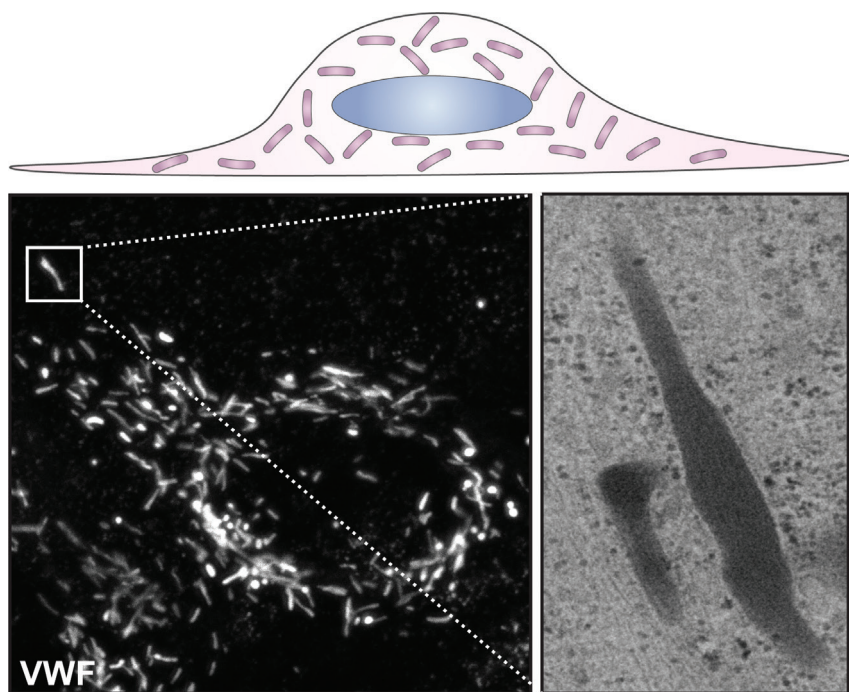


**Figure 2: Endothelial cells and Weibel-Palade bodies.** Schematic representation of an endothelial cell with cigar-shaped WPBs. Bottom left: immunofluorescent staining of VWF in ECs. Bottom right: electron microscopy image of WPBs in ECs

## Von Willebrand factor biosynthesis: the driving force WPB biogenesis

VWF is a large multimeric hemostatic protein, that is synthesized in ECs and megakaryocytes, and its monomeric structure is divided further in several domains with binding sites for factor VIII (FVIII), platelet GPIb and collagen, and with cleavage sites for furin and ADAMTS13.<sup>14</sup> In the ER, VWF monomers are converted into dimers through the formation of intermolecular disulfide bonds in the cysteine knot domain.<sup>15,16</sup> VWF dimers are subsequently transported to the Golgi, where proteolytic cleavage by furin releases the propeptide of VWF.<sup>17,18</sup> In the Golgi-apparatus, VWF dimers are converted into head-to-head linked multimers through the formation of intermolecular disulfide bonds in the D3 domain of VWF.<sup>19,20</sup> In the TGN, newly formed VWF multimers condense into helical tubules<sup>10,12,21</sup> that have been proposed to be packaged as distinct VWF quanta into newly forming WPBs.<sup>22</sup> Moreover, a recent study has provided new insights in how environmental cues can signal changes intracellularly that subsequently can alter packaging of VWF quanta in WPBs<sup>23</sup> (Figure 3).

Quantitative and qualitative defects in VWF are related to the most common bleeding disorder, Von Willebrand Disease (VWD). VWD consists of three types: VWD type 1 (VWD1) with quantitative defects in VWF plasma levels, VWD type 2 (VWD2) with qualitative defects in multimerization (2A), platelet binding (2B and 2M) and FVIII (2N) binding, and VWD type 3 (VWD3) with an almost complete lack of VWF in circulation.<sup>24–26</sup> Although most mutations that are responsible for VWD are reported to be in the VWF gene (from the promoter region to exon 52), recently studies have shown that additional genes, including ABO blood group and STXBP5, are associated with VWF plasma levels.<sup>26–28</sup> Employing patient-derived blood outgrowth endothelial cells (BOECs) it has been demonstrated that certain VWD mutations negatively affect the WPB formation or alter WPB morphology, with WPBs being absent due to VWF retention in the ER or severely deformed (shorter and rounder), respectively.<sup>25,29–31</sup>

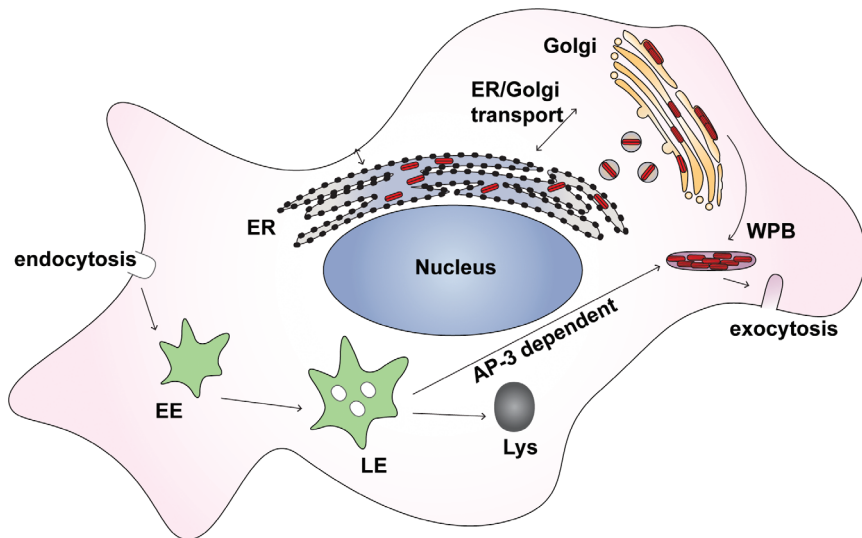


**Figure 3: Intracellular VWF trafficking and WPB formation.** VWF is dimerized at the ER and continues its maturation in the Golgi. Mature VWF condenses into tubules and stored in WPBs that emerge at the TGN. Subsequently WPBs mature in an AP-3 dependent manner and are secreted upon demand.

## WPB formation: from biogenesis to maturation

As mentioned above, the biogenesis of WPBs can be divided into two sequential steps. It has now been firmly established that condensation of VWF quanta in the TGN drives the formation of elongated WPBs.<sup>13,22</sup> Further maturation involves condensation and compaction of WPBs,<sup>21</sup> as well as recruitment of additional cargo from endosomes in an AP-3 dependent manner.<sup>32</sup> The AP-3 complex in endothelial cells has been shown to regulate an important step in WPB maturation by delivering CD63, a tetraspanin associated with CD62P in leukocyte rolling on the endothelium, to the maturing WPB<sup>32</sup> (Figure 3). Mutations in the AP3B1 gene, which results in absence of the  $\beta 1$  subunit of the AP-3 complex, occur in patients with Hermansky-Pudlak syndrome type 2 (HPS-2),<sup>33</sup> and has been shown to in vitro negatively affect the CD63 trafficking towards maturing LROs,<sup>34</sup> including WPBs (**chapter 6**). Additionally, in a recent study, it was shown that CD63 was present in intraluminal vesicles within WPBs that were released as discrete particles during WPB exocytosis.<sup>35</sup> These intriguing observations suggest that AP-3 dependent pathway promotes the incorporation of intraluminal vesicles within WPBs. In addition to the AP-3 complex additional multi-subunit complexes designated BLOC1, 2 and 3 (BLOC being the abbreviation of **biogenesis of LRO complexes**) have been implicated in the maturation of LROs in particular of pigment-containing melanosomes in melanocytes.<sup>3</sup> Two recent studies have implicated the HPS-6 subunit of the BLOC-2 complex in the biogenesis of WPBs.<sup>36,37</sup> Ma and co-workers revealed that the BLOC-2 complex plays a crucial role in tubulation and release of VWF whereas Sharda and co-workers proposed that this complex interacts with the exocyst complex which controls WPB release.<sup>36,37</sup>

## Scope of this thesis

In vesicular trafficking, organelle biogenesis and maturation, as well as organelle secretion, vesicle membranes fuse with their targets for content delivery. These fusion steps are universally governed by Soluble N-ethylmaleimide sensitive factor (NSF) attachment protein receptor (SNARE) proteins.<sup>38</sup> SNAREs are categorized into two broad classes: the v-SNAREs, where v stands for vesicle and t-SNAREs, where t stands for target. SNARE proteins interact with each other in a complex formation of a four-helix bundle, consisting of one helix from the v- and three helices from t-SNAREs (**chapter 4**). While some SNAREs have been linked to WPB exocytosis,<sup>39,40</sup> our current knowledge on which multi-protein complexes are involved in biogenesis and maturation of WPBs is not yet fully understood. The main purpose of this study is to provide insight into the regulation of biogenesis of WPBs from the trans Golgi network. In addition, we explored how additional cargo is being distributed to preformed WPBs and how these fully mature LROs subsequently deliver their hemostatic, inflammatory and angiogenic content in the vascular lumen. In **chapter 2** we provide an overview of the recent developments on the mechanisms that drive the biogenesis and maturation of LROs focusing on platelet  $\alpha$ - and  $\delta$ -granules, and endothelial cell WPBs. We continue by discussing the role of the ER-to-Golgi SNARE Sec22b in anterograde protein trafficking and WPB biogenesis (**chapter 3**). In **chapter 4**, we identify the interactome of Sec22b in ECs and evaluate the role of its binding partner STX5 in WPB formation. Next, we review recent advances in WPB exocytosis, including stimulus-dependent cascades and known exocytotic machinery (**chapter 5**). In **chapter 6** we discuss in depth the mechanisms underlying AP-3 dependent WPB maturation and how this pathway affects WPB exocytosis. In **chapter 7** we reveal the role of a newly discovered SNARE present on WPBs (STX3) in stimulus-induced WPB exocytosis. Finally, we summarize and discuss our finding in **chapter 8** and provide directions for future research.

## References

- Aird WC. Phenotypic heterogeneity of the endothelium: I. Structure, function, and mechanisms. *Circ. Res.* 2007;100(2):158–173.
- Yau JW, Teoh H, Verma S. Endothelial cell control of thrombosis. *BMC Cardiovasc. Disord.* 2015;15(1):.
- Delevoey C, Marks MS, Raposo G. Lyso-some-related organelles as functional adaptations of the endolysosomal system. *Curr. Opin. Cell Biol.* 2019;59:147–158.
- Flaumenhaft R, Sharda A. The life cycle of platelet granules. *F1000Research.* 2018;7:.
- Chen Y, Yuan Y, Li W. Sorting machineries: How platelet-dense granules differ from  $\alpha$ -granules. *Biosci. Rep.* 2018;38(5):.
- Van Nispen Tot Pannerden H, De Haas F, Geerts W, et al. The platelet interior revisited: Electron tomography reveals tubular  $\alpha$ -granule subtypes. *Blood.* 2010;116(7):1147–1156.
- Banerjee M, Whiteheart SW. How Does Protein Disulfide Isomerase Get Into a Thrombus? *Arterioscler. Thromb. Vasc. Biol.* 2016;36(6):1056–7.
- Harrison P, Martin Cramer E. Platelet  $\alpha$ -granules. *Blood Rev.* 1993;7(1):52–62.
- Voorberg J, Fontijn R, Calafat J, et al. Biogenesis of von Willebrand factor-containing organelles in heterologous transfected CV-1 cells. *EMBO J.* 1993;12(2):749–758.
- Michaux G, Abbitt KB, Collinson LM, et al. The physiological function of von Willebrand's factor depends on its tubular storage in endothelial Weibel-Palade bodies. *Dev. Cell.* 2006;10(2):223–232.
- Huang R-H, Wang Y, Roth R, et al. Assembly of Weibel-Palade body-like tubules from N-terminal domains of von Willebrand factor. *Proc. Natl. Acad. Sci. U. S. A.* 2008;105(2):482–7.
- Valentijn KM, Sadler JE, Valentijn J a, Voorberg J, Eikenboom J. Functional architecture of Weibel-Palade bodies. *Blood.* 2011;117(19):5033–43.
- Ferraro F, Mafalda Lopes da S, Grimes W, et al. Weibel-Palade body size modulates the adhesive activity of its von Willebrand Factor cargo in cultured endothelial cells. *Sci Rep.* 2016;6.
- Zhou Y-F, Eng ET, Zhu J, et al. Sequence and structure relationships within von Willebrand factor. 2012;
- Zhou YF, Eng ET, Nishida N, et al. A pH-regulated dimeric bouquet in the structure of von Willebrand factor. *EMBO J.* 2011;30(19):4098–4111.
- Springer TA. von Willebrand factor, Jedi knight of the bloodstream. *Blood.* 2014;124(9):1412–1426.
- van de Ven WJ, Voorberg J, Fontijn R, et al. Furin is a subtilisin-like proprotein processing enzyme in higher eukaryotes. *Mol. Biol. Rep.* 1990;14(4):265–75.
- Wise RJ, Barr PJ, Wong PA, et al. Expression of a human proprotein processing enzyme: Correct cleavage of the von Willebrand factor precursor at a paired basic amino acid site. *Proc. Natl. Acad. Sci. U. S. A.* 1990;87(23):9378–9382.
- Purvis AR, Gross J, Dang LT, et al. Two Cys residues essential for von Willebrand factor multimer assembly in the Golgi. *Proc. Natl. Acad. Sci. U. S. A.* 2007;104(40):15647–52.
- Dong X, Leksa NC, Chhabra ES, et al. The von Willebrand factor D'D3 assembly and structural principles for factor VIII binding and concatemer biogenesis. *Blood.* 2019;133(14):1523–1533.
- Zenner HL, Collinson LM, Michaux G, Cutler DF. High-pressure freezing provides insights into Weibel-Palade body biogenesis. *J. Cell Sci.* 2007;120(Pt 12):2117–2125.
- Ferraro F, Kriston-Vizi J, Metcalf DJ, et al. A two-tier golgi-based control of organelle size underpins the functional plasticity of endothelial cells. *Dev. Cell.* 2014;29(3):292–304.
- Lopes-da-Silva M, McCormack JJ, Burden JJ, et al. A GBF1-Dependent Mechanism for Environmentally Responsive Regulation of ER-Golgi Transport. *Dev. Cell.* 2019;1–16.
- Leebeek FWG, Eikenboom JCJ. Von Willebrand's Disease. *N. Engl. J. Med.* 2017;376(7):701–702.
- de Jong A, Eikenboom J. Von Willebrand disease mutation spectrum and associated mutation mechanisms. *Thromb. Res.* 2017;159:65–75.
- Goodeve A. Diagnosing von Willebrand disease: Genetic analysis. *Hematology.* 2016;2016(1):678–682.
- Swystun LL, Lillicrap D. Genetic regulation of plasma von Willebrand factor levels in health and disease. *J. Thromb. Haemost.* 2018;16(12):2375–2390.
- van Loon J, Dehghan A, Weihong T, et al. Genome-wide association studies identify genetic loci for low von Willebrand factor levels. *Eur. J. Hum. Genet.* 2016;24(7):1035–40.
- Wang JW, Bouwens EAM, Pintao MC, et al. Analysis of the storage and secretion of von willebrand factor in blood outgrowth endothelial cells derived from patients with von Willebrand disease. *Blood.* 2013;121(14):2762–2772.
- Valentijn KM, Eikenboom J. Weibel-Palade bodies: A window to von Willebrand disease. *J. Thromb. Haemost.* 2013;11(4):581–592.
- Starke RD, Paschalaki KE, Dyer CEF, et al. Cellular and molecular basis of von Willebrand disease: Studies on blood outgrowth endothelial cells. *Blood.* 2013;121(14):2773–2784.
- Harrison-Lavoie KJ, Michaux G, Hewlett L, et al. P-selectin and CD63 use different mechanisms for delivery to Weibel-Palade bodies. *Traffic.* 2006;7(6):647–662.

33. Wei ML. Hermansky-Pudlak syndrome: a disease of protein trafficking and organelle function. *Pigment cell Res.* 2006;19(1):19–42.
34. Dell'Angelica EC, Shotelersuk V, Aguilar RC, Gahl WA, Bonifacino JS. Altered trafficking of lysosomal proteins in Hermansky-Pudlak syndrome due to mutations in the beta3A subunit of the AP-3 adaptor. *Mol. Cell.* 1999;3(1):11–21.
35. Streetley J, Fonseca AV, Turner J, et al. Stimulated release of intraluminal vesicles from Weibel-Palade bodies. *Blood.* 2019;133(25):2707–2717.
36. Sharda A V, Harrison J, Wilkie AR, et al. VWF Exocytosis and Biogenesis of Weibel Palade Bodies in Endothelial Cells Are Differentially Controlled By Interactions between Bloc-2 and the Exocyst Complex. *Blood.* 2019;134(1):8.
37. Ma J, Zhang Z, Yang L, et al. BLOC-2 subunit HPS6 deficiency affects the tubulation and secretion of von Willebrand factor from mouse endothelial cells. *J. Genet. Genomics.* 2016;43(12):686–693.
38. Gerst JE. SNAREs and SNARE regulators in membrane fusion and exocytosis. *Cell. Mol. Life Sci.* 1999;55(5):707–734.
39. Pulido IR, Jahn R, Gerke V. VAMP3 is associated with endothelial Weibel-Palade bodies and participates in their Ca(2+)-dependent exocytosis. *Biochim. Biophys. Acta.* 2011;1813(5):1038–1044.
40. Zhu QM, Zhu Q, Yamakuchi M, Lowenstein CJ. SNAP23 Regulates Endothelial Exocytosis of von Willebrand Factor. *PLoS One.* 2015;10(8):e0118737.







## Chapter 2

# Orchestration of primary hemostasis by platelet and endothelial lysosome-related organelles

Ellie Karampini, Ruben Bierings and Jan Voorberg  
*Manuscript in preparation*

## Abstract

Megakaryocyte-derived platelets and endothelial cells store their hemostatic cargo in  $\alpha$ - and  $\delta$ -granules and Weibel-Palade bodies (WPBs), respectively. These storage granules belong to the lysosome-related organelles (LROs), a heterogeneous group of organelles that is rapidly released following agonist induced triggering of intracellular signaling pathways. Following vascular injury endothelial WPBs release their content into the vascular lumen and promote the formation of long VWF strings that form an adhesive platform for platelets. Binding to VWF strings as well as exposed subendothelial collagen activates platelets resulting in the release of  $\alpha$ - and  $\delta$ -granules which are crucial events in formation of a primary hemostatic plug. Biogenesis and secretion of LROs is pivotal for the maintenance of proper hemostasis. Several bleeding disorders have been linked to abnormal generation of LROs in megakaryocytes and endothelial cells. Recent reviews have emphasized common pathways in the biogenesis and biological properties of LROs focusing mainly on melanosomes. Despite many similarities LROs in platelet and endothelial cells clearly possess distinct properties that allow them to provide a highly coordinated and synergistic contribution to primary hemostasis by sequentially releasing hemostatic cargo. In this brief review, we discuss in depth the known regulators of  $\alpha$ - and  $\delta$ -granules in MKs/ platelets and WPBs in endothelial cells, starting from transcription factors that have been associated with granule formation to protein complexes that promote granule maturation. In addition, we provide a detailed view on the highly coordinate interplay between platelet and endothelial LROs in controlling hemostasis as well as their dysfunction in LRO related bleeding disorders.

## Introduction

Lysosome-related organelles (LROs) are specialized storage compartments that include melanosomes in skin and eye melanocytes, lytic granules of cytotoxic T cells and natural killer cells, alpha ( $\alpha$ ) and dense ( $\delta$ ) granules in platelets as well as Weibel-Palade bodies (WPB) in endothelial cells.<sup>1</sup> Originally evolving from lysosomes, they have critically adapted to a highly specialized physiological role in the storage, clustering and regulated “on demand” release of bioactive components.<sup>1</sup> In line with their evolutionary origin LROs, or as recently proposed ELROs,<sup>1</sup> share common features with endosomes.<sup>2</sup> In this review we focus on the biogenesis, morphological features and physiological role of LROs present in platelets and endothelial cells which are released in a coordinated fashion during primary hemostasis. Megakaryocytes (MKs) and platelets contain two types of LROs, the  $\alpha$ - and  $\delta$ -granules, whereas endothelial cells contain only one, the Weibel-Palade bodies (WPBs). Each type of LRO can be considered as the adaptation of the cell’s endosomes into functional secretory organelles that have evolved to specific physiological needs related to on demand cargo delivery.<sup>1</sup> Although LROs are similar enough to be placed in the same category, they differ in their stored cargoes, which is highly cell specific. In MKs,  $\alpha$ -granules contain hemostatic proteins like von Willebrand factor (VWF) and platelet factor 4 (PF4), while  $\delta$ -granules store small molecules like ATP, Ca<sup>2+</sup> and serotonin as well as the tetraspanin CD63.<sup>3</sup> Similar to  $\alpha$ -granules, WPBs primarily store VWF, along with a diverse cocktail of proinflammatory and angiogenic proteins, but also CD63.<sup>4</sup> Due to their absence or dysfunction in specific bleeding disorders, both platelet granules and WPBs have been positioned as master orchestrators of primary hemostasis.

At the site of vascular damage, endothelial cell activation drives the bulk expulsion of highly condensed VWF from WPBs and their conversion into adhesive strings, that serve as a landing platform for platelets.<sup>5</sup> Subsequently, platelet glycoprotein Ib (GPIb) and subendothelial collagen mediated interactions with VWF strings initiate an intracellular cascade of platelet activation, which leads to  $\alpha$ - and  $\delta$ -granule secretion, potentiation of platelet

aggregation, ultimately resulting in the formation of a hemostatic plug.<sup>6</sup> LRO's importance in platelet and vascular biology is highlighted by a group of heterogeneous bleeding disorders, due to defective biogenesis and maturation of LROs.

In this review, we summarize the new advances in LRO formation, highlighting the interplay and differential regulation of MK and platelet localized  $\alpha$ - and  $\delta$ -granules and endothelial cell WPBs. We discuss in depth the pathways involved in the biogenesis and maturation of the aforementioned LROs, as well as disorders that are linked to defects in these pathways.

## Biogenesis and maturation of $\alpha$ - and $\delta$ -granules in megakaryocytes and platelets

### Transcription factors in $\alpha$ - and $\delta$ -granule biogenesis

Several transcription factors including RUNX1, NF-E2, GFI1B and FLI1 have a crucial role in megakaryopoiesis and platelet formation.<sup>7,8</sup> Their importance is illustrated by defects in platelet function in patients with genetic defects in these transcription factors. *RUNX1* haplo deficiency has been linked to thrombocytopenia and both  $\alpha$ - and  $\delta$ -granule deficiencies, while *RUNX1* knock out (KO) mice lack primary hematopoiesis.<sup>9</sup> Two new studies have demonstrated that *RUNX1* haplo deficiency decreases *RAB1B* and *PLDN* expression levels which sheds light on the mechanisms for  $\alpha$ - and  $\delta$ -granule biogenesis, respectively.<sup>10,11</sup> Rab1b belongs to the small GTPase family and facilitates vesicular ER/Golgi transport, and, in the case of MKs, promotes VWF intracellular trafficking.<sup>10,12</sup> Reduced RUNX1 and Rab1b levels were proposed to lead to defective VWF maturation and decreased targeting to  $\alpha$ -granules.<sup>10</sup> RUNX1 also controls the expression of *PLDN* which encodes for pallidin or BLOC1S6, a member of the BLOC-1 complex that promotes  $\delta$ -granule formation.<sup>11,13</sup> Down-regulation of pallidin in RUNX1 haplo deficiency was suggested to underlie disrupted CD63 trafficking to  $\delta$ -granules and impaired  $\delta$ -granule biogenesis.<sup>11</sup>

NF-E2 has been described to regulate the expression of Rab27b, a small GTPase family that is strongly expressed in the MK/ platelet lineage and colocalizes with both  $\alpha$ - and  $\delta$ -granules.<sup>14</sup> *NF-E2* KO MKs lack Rab27b expression, which has been shown to regulate the number of  $\delta$ -granules per platelet.<sup>15</sup> The closely related small GTPase Rab27a deficient in ashen (*ash*) mice, a model for Griscelli Syndrome has been implicated in dense granule release (Novak et al., 2002).<sup>14-16</sup> Screening of a panel of patients with unexplained thrombocytopenia revealed defects in the gene encoding transcription factor *FLI1*.<sup>17</sup> *FLI1* is localized in the 11q24 arm on chromosome 11q. This region is deleted in patients with Jacobsen and Paris-Trousseau syndrome (collectively called 11q deletion syndromes), whose clinical symptoms include a.o. thrombocytopenia.<sup>18</sup> In accordance with its proposed role in thrombopoiesis, *Fli1*<sup>-/-</sup> mice are embryonic lethal at day 11.5 due to thrombocytopenia and abnormal vasculature development.<sup>17,18</sup> Absence of *FLI1* has previously been shown to induce macrothrombocytopenia, in addition to abnormal granule biogenesis that results in giant  $\alpha$ -granules and complete absence of  $\delta$ -granules.<sup>19</sup> Based on these findings it was suggested that FLI1 may play a role in protein packaging in  $\alpha$ -granules, while FLI1 interactions with *HPS4* and *RAB27B* may regulate  $\delta$ -granules biogenesis.<sup>7,19</sup> Dominant negative mutations in the transcription factor GFI1B have been identified in patients with Gray platelet syndrome.<sup>20,21</sup> Detailed morphological studies of patients with dominant negative GFI1B mutation revealed lack of  $\delta$ -granules as well as abnormalities in  $\alpha$ -granule contents giving rise to a "gray" appearance in blood smears in a subset of platelets.<sup>22,23</sup> The precise mechanisms underlying the observed changes in platelet LROs in patients with dominant negative GFI1B mutations remain to be identified but are most likely caused by dysregulation of developmental programs involved in thrombopoiesis and markedly reduced expression of proteins that reside in  $\alpha$ -granules.<sup>23</sup> In summary, several transcription factors have

been identified that affect the biogenesis of platelet LROs. Further elucidation of pathways controlling biogenesis of content-delivery to platelet LROs is likely to shed light on general mechanism that drive the formation of LRO compartments in other cell types including melanocytes and endothelial cells (Figure 1).

### **$\alpha$ -granule maturation: the role of VPS33B/16B complex and NBEAL2 in cargo trafficking and retention**

VPS33B is the first protein to be described as essential for  $\alpha$ -granule maturation.<sup>24,25</sup> VPS33B belongs to the family of S/M (Sec1/Munc18-like) proteins and has been proposed to promote assembly of newly forming SNARE complexes by aligning SNARE helices from target and vesicle membranes.<sup>26</sup> Mutations in *VPS33B* cause arthrogyryposis-renal dysfunction-cholestasis (ARC) syndrome, a multisystemic autosomal disorder that includes platelet deficiency.<sup>27</sup> VPS33B deficiency results in absence of  $\alpha$ -granules and reduced levels of  $\alpha$ -granule proteins like soluble cargo (fibrinogen (FGN) and VWF) and membrane proteins (CD62P) that are presumably degraded in the lysosomes.<sup>24,25</sup> Colocalization studies have shown that VPS33B is not associated with the Golgi but it is mainly found on the recycling Rab11a positive endosomes, suggesting that the VPS33B is part of the protein sorting machinery.<sup>24,25</sup> Additionally, depletion of VPS33B in MKs not only results in  $\alpha$ -granule deficiency, but also MVB maturation.<sup>28</sup> MVB have two distinct stages during maturation: type I and II and are characterized by intraluminal vesicles and electron-dense core along with intraluminal vesicles, respectively.<sup>29</sup> During MK development, MVB type I mature into type II which are the progenitors of  $\alpha$ -granules.<sup>29</sup> Downregulation of VPS33B results in nearly absence of MVB type II along with  $\alpha$ -granules, suggesting that VPS33B is primarily involved in MVB maturation and subsequent  $\alpha$ -granule formation.<sup>28</sup> VPS33B is part of the heterohexameric tethering complexes CORVET and HOPS that operate in endosome and lysosome fusion.<sup>30</sup> In addition, together with VPS16B, VPS33B forms the CHEVI-complex which is recruited in a Rab11 dependent manner to recycling endosomes.<sup>31</sup> Similar to *VPS33B*, genetic defects in the *VPS16B* encoding *VIPAS39* gene are found in patients with the ARC syndrome.<sup>32</sup> Loss of VPS16B, results in reduction of VPS33B and  $\alpha$ -granule proteins expression as well as defective  $\alpha$ -granule formation similar to *VPS33B* KO.<sup>33</sup> In a recent study, VPS33B and VSP16B are found to form a heterodimer smaller than CORVET and HOPS in MKs, which possibly does not include any other protein.<sup>24</sup> The VPS33B/16B complex localizes on recycling endosomes, which are closely related with the trans-Golgi network, and promotes protein trafficking towards MVB before finally reaching  $\alpha$ -granules.<sup>24</sup>

Another key component controlling  $\alpha$ -granule formation is NBEAL2, a protein that is mutated in the storage pool disorder gray platelet syndrome (GPS).<sup>34</sup> NBEAL2 has been described to be involved in protein sorting in MKs.<sup>35</sup> *NBEAL2* KO MKs and platelets show greatly reduced intracellular levels of  $\alpha$ -granule components such as fibrinogen (FGN) and VWF that are either sequestered by endocytosis or arrive in the  $\alpha$ -granule through biosynthetic pathways.<sup>35,36</sup> Interestingly, when compared to VPS33B/16B mutations that result in platelets which lack both soluble cargo and membrane proteins like CD62P, *NBEAL2*<sup>-/-</sup> platelets, despite missing their soluble cargo, still contain a pool of releasable CD62P.<sup>25,33,36</sup> Moreover, VPS33B and VPS16B expression is normal in *NBEAL2* KO platelets, suggesting that NBEAL2 is involved at a later stage in  $\alpha$ -granule maturation, rather than promoting the formation of  $\alpha$ -granule progenitors (MVB type II).<sup>36</sup> Recently, Kahr and co-authors suggested that NBEAL2 is required for the retention of synthesized and endocytosed cargo through interaction with CD62P, potentially as a part of a multimolecular complex, in order to allow for packaging of cargo into maturing  $\alpha$ -granules.<sup>37</sup> In the absence of NBEAL2,  $\alpha$ -granule cargo such as PF4, VWF and Fbg are not sufficiently retained allowing for their transport to Rab11 positive recycling endosomes which are subsequently exocytosed.<sup>37</sup>

Therefore, the current view on  $\alpha$ -granule maturation includes the heterodimeric CHEVI complex, composed of VPS33B and VSP16B, that promotes conversion of endosomes into

$\alpha$ -granule progenitors, the MVB type II, and  $\alpha$ -granules. After the  $\alpha$ -granule cargo has arrived at its destination, NBEAL2 retains it intralumenally thereby ensuring packaging of cargo into nascent and maturing  $\alpha$ -granules (Figure 1).

### **$\delta$ -granule maturation: proteins and complexes involved in a “kiss-and-run” maturation**

$\delta$ -granules, similarly to  $\alpha$ -granules, go through a complex maturation process that involves the delivery of specialized cargo catalyzed by several proteins and protein complexes. VPS33A has been identified as a crucial component of multisubunit tethering complexes that control  $\delta$ -granule formation.<sup>38</sup> *Vps33a*<sup>-/-</sup> mice display a prolonged bleeding time, which is attributed to decreased  $\delta$ -granule ATP and serotonin secretion, due to their reduced number.<sup>38</sup> Although this suggests that the VPS33 isoforms A and B may differentially traffic cargo towards  $\delta$ - and  $\alpha$ -granules respectively, mutations in *VPS33A* have not yet been reported.<sup>28,38</sup>

Intracellular vesicular trafficking is governed by Rab GTPases, which control specificity and directionality of the vesicles ensuring correct protein delivery to the final destination.<sup>39</sup> In the case of  $\delta$ -granule maturation, Rab32 and Rab38 play an important role by defining the delivery pathway from the endosomal compartment to the maturing  $\delta$ -granule.<sup>40</sup> Both Rabs localize on Rab7a positive MVBs, closely related to immature  $\delta$ -granule, and are required for tethering and/or fusion of cargo-containing vesicles with the maturing  $\delta$ -granule.<sup>40</sup> Double KO of *Rab32* and *Rab38*, but not the single KO, results in morphological defects and decreased presence of  $\delta$ -granules in mouse platelets, proving that they are both required for the biogenesis of  $\delta$ -granules from the MVB compartment.<sup>41</sup> Rab GTPases are considered to act as molecular switches, as they are found in an “on” GTP-bound and “off” GDP-bound state, each controlled by guanine-nucleotide-exchange factors (GEFs) and GTPase-activating proteins (GAPs), respectively.<sup>39</sup> Rab32 and Rab38 are activated by BLOC-3, a multisubunit protein complex that promotes the correct localization of Rab32/38 on its target membranes, which is an essential step in the formation and maturation of melanosomes.<sup>42</sup> Mutations in BLOC-3 subunits also lead to subtypes of the  $\delta$ -storage pool disorder Hermansky-Pudlak syndrome (HPS-1 and HPS-4),<sup>40,43,44</sup> however so far very little is known on how the BLOC-3 complex regulates formation and maturation of  $\delta$ -granules.

Similar to BLOC-3, AP-3 is another heteromeric protein trafficking complex, which promotes  $\delta$ -granule formation by delivering proteins, like LAMP2, the serotonin transporter VMAT2 and most recently SLC353D, to the forming granule.<sup>40,45</sup> Mutations in AP-3 subunits are associated with subtype HPS-2 (defect in *AP3B1*) and HPS10 (defect in *AP3D1*)  $\delta$ -storage pool disorders, which lead to complete absence or significantly lower numbers of  $\delta$ -granules along with mislocalization or decreased expression of  $\delta$ -granule cargo.<sup>45</sup>

Contrary to  $\alpha$ -granule formation,  $\delta$ -granules may follow a “kiss-and-run” maturation step, where luminal content in addition to membrane bound proteins are exchanged between two maturing granules.<sup>46</sup> TPC2 is a calcium release channel, which operates as a dual sensor for luminal pH and calcium.<sup>47</sup> In MKs, TPC2 is part of the  $\delta$ -granule limiting membrane and regulates the granule pH and calcium release, while it orchestrates the “kiss-and-run” events, through which  $\delta$ -granules can achieve homogenization and adjustment of their volume.<sup>46</sup> Thus, TPC2 is a key regulator of a novel layer in  $\delta$ -granule maturation.

Taken together, recent studies have shown that  $\delta$ -granule maturation is strongly tied to cargo delivery, regulated by Rab32 and Rab38 GTPases. BLOC-3 is a known GEF for both Rabs and mutations in BLOC-3 complex members result in HPS, therefore, by extension, it may regulate  $\delta$ -granule. Similarly, VPS33A is shown to regulate  $\delta$ -granule formation in mice, however, no current studies have been performed in MKs from humans nor mutations have been described to have pathophysiological significance yet. Finally,  $\delta$ -granules have an additional layer of a “kiss-and-run” mechanism that normalizes their content and promotes their maturation (Figure 1).

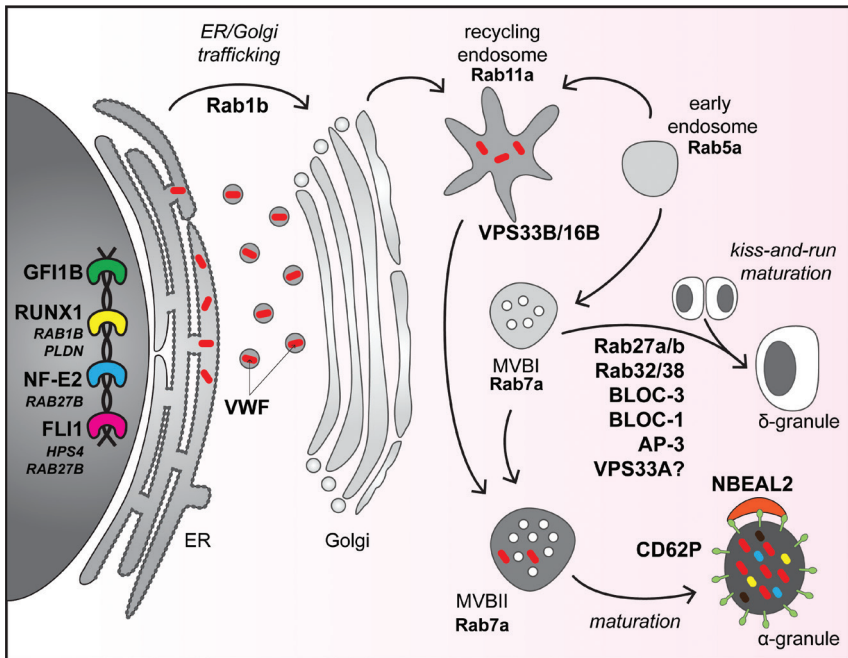


**Figure 1: Model for LRO formation in MKs/ platelets:  $\alpha$ - and  $\delta$ -granule.** In MKs, transcription factors regulate the expression of several genes that encode proteins, which are involved in the biogenesis of LROs. In the case of  $\alpha$ -granules, the first identified step of their biogenesis is the Rab1b-dependent ER-to-Golgi protein trafficking. After the newly synthesized proteins has been fully processing in the Golgi, they are found in Rab11a recycling endosomes, which serve as distribution center for new and recycled proteins. VPS33B/ 16B complex at this stage facilitate the transport of proteins to Rab7a positive MVBII, the progenitors of  $\alpha$ -granules. Protein retention in the maturing  $\alpha$ -granule and prevention of a premature release if achieved through an interaction between NBEAL2 and CD62P, that acts like a shield. On the other hand,  $\delta$ -granule progenitors are Rab7a MVBII, that supply the maturing granule with appropriate cargo. Several proteins and protein complexes have been suggested to promote  $\delta$ -granule maturation, including the well-characterized AP-3 complex, BLOC-1 and -3 and the small GTPases Rab27a/ b and Rab32/38, while VPS33A has only been described in mice. Additionally,  $\delta$ -granules have an extra step during maturation, known as “kiss-and-run”, though which they can exchange content and achieve homogenization while adjusting their volume.

## Biogenesis and maturation of Weibel-Palade bodies in endothelial cells

### VWF maturation and ER-to-Golgi protein trafficking in the biogenesis of WPBs

VWF, the main cargo of WPBs, undergoes an extensive and complex maturation process before finally being stored. VWF enters the early secretory pathway, as a single pre-pro-poly-peptide chain and, after the removal of the signal peptide, it is dimerized in the endoplasmic reticulum (ER) by the formation of disulfide bonds between the C-terminal cysteine knot (CK) domains of two proVWF monomers.<sup>48,49</sup> At this stage, the ER acts as the quality control check point that allows only VWF dimers to proceed to exit and subsequent transport to the Golgi apparatus.<sup>50,51</sup> At the Golgi, VWF dimers are further processed: the propeptide is proteolytically cleaved and VWF dimers are organized into “head-to-head” multimers, before condensing into tubules and being packaged in trans-Golgi network (TGN)-associated WPBs.<sup>5,48</sup> Blockage of any step during VWF maturation may lead to abnormal formation of WPBs, like in the case of von Willebrand disease where mutations in the *VWF* gene affect the WPB formation.<sup>52</sup> Interestingly, mutations have been reported in the D3 and C2 domains of VWF (p.Cys1130Phe and p.Cys2671Tyr, respectively) that affect ER exit

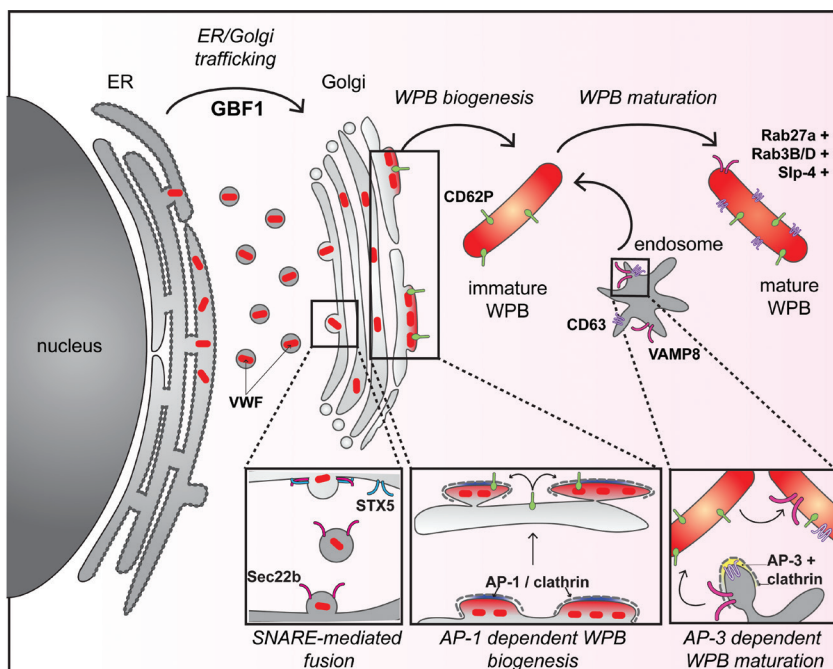


**Figure 2: Model for WPB formation in endothelial cells.** Several transcription factors have been found to positively regulate VWF expression, the driving force of WPB biogenesis. VWF exits ER in order to arrive to the Golgi in a GBF1-dependent manner. The fusion of ER-exiting vesicle is dependent of the interaction of Sec22b with the cognate SNARE on the Golgi, STX5. After VWF is fully processed and multimerized, it condenses in tubules and package in VWF quanta in the emerging granule. At this stage AP-1 localizes the TGN, by means of PI4P-rich rich domains, and acts as a corset for forming WPBs, preventing it from premature budding off. The newly synthesized WPB maintains several connections to the TGN, for the further transfer of proteins potentially like CD62P. The immature WPB undergoes a maturation process, where it acquires more proteins from the endosomal compartment in an AP-3 dependent manner. Mature WPBs are positive for the small GTPases, RAB27A, 3B and 3D as well as Slp-4 and migrate towards the periphery of the cell, ready to be secreted upon demand.

of VWF dimers and lead to VWF retention in the ER as well as the rarer occurrence of WPBs.<sup>51</sup> Similar results with ER retention of VWF and formation of abnormal WPBs have been recently shown in Sec22b KD endothelial cells.<sup>53</sup> Sec22b is a SNARE protein that regulates the fusion of COPII coated ER-exiting vesicles.<sup>54</sup> Downregulation of Sec22b affects the rate of ER-to-Golgi transport of VWF and other proteins, which consequently affects the Golgi morphology and results in the formation of short and “stubby” WPBs, probably due to Golgi fragmentation.<sup>53,55</sup> Additionally, we and others have shown that Sec22b is paired with STX5 as part of the ER-Golgi SNARE machinery, and depletion of STX5 in endothelial cells strongly affects WPB formation.<sup>56,57</sup> Depletion of STX5 in endothelial cells leads to decreased intracellular VWF storage levels and extensive Golgi dispersal, which results in the formation of shorter and rounder WPBs.<sup>56</sup> It has previously been shown that AP1/clathrin coats control WPB biogenesis at the level of the TGN.<sup>58</sup> The small GTPase Arf1 is crucial for targeting the AP-1 complex to the TGN and recently GBF1 a guanine exchange factor for members of the Arf family has been implicated in WPB biogenesis.<sup>59</sup> Intriguingly, depletion of GBF-1 resulted in accumulation of unprocessed VWF in the ER whereas very long, often bended WPBs were observed in close proximity to the TGN. The metabolic regulator 5' AMP activated kinase (AMPK) has been shown to modulate the activity of GBF-1

suggesting that environmental cues can regulate number and WPB size through their effect on ER-to-Golgi.<sup>59</sup> Taken together, these exciting findings indicate that modulation of ER-to-Golgi trafficking of VWF, can significantly alter the WPB formation by retaining VWF in the ER and thus decrease the amount of mature VWF that can be stored in WPBs, while governing morphology of WPB emerging from the TGN (Figure 2).

### **Trans-Golgi network emerging WPBs: monitoring the morphology of immature WPBs**

WPBs biogenesis is taking place at the trans-Golgi network (TGN), where VWF units, known as VWF quanta, are tightly co-packaged in the form of tubular segments in newly-synthesized WPB.<sup>55</sup> The first factor that regulates WPBs at the TGN site, is the actual morphology of the Golgi. Dispersed Golgi and TGN morphology can negatively affect the ability of endothelial cells to incorporate sufficient amount of VWF quanta in the newly-synthesized WPBs, limiting their length and affecting their string formation on the endothelial apical side.<sup>53,55,56,60</sup> The second factor that promotes WPB biogenesis is the VWF tubulation state. Endothelial cells that lack HPS6, a subunit of BLOC-2 complex associated with HPS type 6, have abnormal VWF tubulation and misshaped WPBs, potentially due to failed recruitment of proteins involved in acidification of WPB milieu.<sup>61</sup> Although the Golgi/TGN morphology sets the bar for WPB size and VWF tubulation affects the formation itself, more proteins at the site regulate WPB biogenesis like the adaptor protein 1 (AP-1) complex.<sup>58</sup> AP-1/clathrin is speculated to act as a “corset”, stabilizing the forming WPB during VWF-tubule assembly and preventing premature budding.<sup>58</sup> In parallel, discs large 1 (Dlg1) protein, associates with both mature VWF and AP-1 complex on the TGN, suggesting that Dlg1 may link VWF with a yet-unidentified transmembrane partner to the AP-1 complex.<sup>62</sup> Both AP-1 and Dlg1 knockdowns result in ablation of elongated WPBs and restrictive localization of VWF to perinuclear puncta.<sup>58,62</sup> AP-1 complex targeting and docking on the TGN is dependent on phosphatidylinositol 4 phosphate [PI(4)P]-rich domains, whose levels are determined by Golgi resident phosphatidylinositol 4 kinases (PI4Ks).<sup>63</sup> In endothelial cells, PI4KII-depletion disturbs the WPB intra-organellar environment due to abnormal VWF folding.<sup>64</sup> The resulting WPBs are shorter, suggesting a critical role for PI4KIIs in WPB biogenesis, as it could recruit AP-1 at the TGN.<sup>64</sup> At early stages of WPB biogenesis, WPBs do not leave the Golgi apparatus fast, but rather maintain multiple connections with it, for cargo delivery.<sup>65</sup> More nontubulated VWF is added to the newly formed WPB together with other proteins, until the formation is completed and the clathrin coat is removed.<sup>65</sup> In summary, WPB are formed at the TGN, which regulates their size. Their biogenesis is dependent on the recruitment of AP-1 complex at the PI4P-riched TGN domains, where, in conjunction with Dlg1 and clathrin, they create a girdle around the forming WPB. The WPB remains attached to the Golgi apparatus for the further delivery of protein cargo (Figure 2).

### **Weibel-Palade maturation: acquisition of more protein cargo**

Similar to  $\alpha$ - and  $\delta$ -granules, WPBs mature through the receipt of transmembrane cargo. WPBs, apart from soluble cargo like VWF, also contain proteins like CD62P and CD63, that follow different pathways arriving to the mature WPB. It has been shown that CD62P is accumulated to the budding WPB at the TGN through its cytoplasmic tail motif, probably while the forming WPB maintains multiple connections with the TGN as described above.<sup>65,66</sup> In contrast, CD63 is trafficked to the WPB at a later stage during maturation, following an AP-3 dependent route.<sup>66</sup> Mutations that affect the AP-3 complex formation lead to abnormal WPB maturation, with CD63 as well as SNARE proteins like VAMP8 wrongly trafficked to other cellular compartments.<sup>66,67</sup> Improper WPB formation results in reduced hormone-evoked VWF secretion, indicating that WPB maturation is a key step for fully-functional organelles.<sup>67</sup> Comparable with platelet LROs, WPBs acquire Rab proteins during the maturation process, like Rab3B and 3D and Rab27a that have been shown



LRO	Disorder	Abbreviation	Subtype	Mutated gene
<b>α-granule</b>	Gray platelet syndrome	GPS	-	<i>NBEAL2</i>
				<i>GFI1B</i>
	Quebec platelet syndrome	QPS	-	<i>PLAU</i>
	Arthrogryposis, renal dysfunction, and cholestasis syndrome	ARCS	ARCS1	<i>VPS33B</i>
ARCS2			<i>VPS16B</i>	
<b>δ-granule</b>	Hermansky-Pudlak syndrome	HPS	HPS1	<i>HPS1</i>
			HPS2	<i>AP3B1</i>
			HPS3	<i>HPS3</i>
			HPS4	<i>HPS4</i>
			HPS5	<i>HPS5</i>
			HPS6	<i>HPS6</i>
			HPS7	<i>DTNBP1</i>
			HPS8	<i>BLOC1S3</i>
			HPS9	<i>PLDN</i>
			HPS10	<i>AP3D1</i>
	Chediak-Higashi syndrome	CHS	-	<i>LYST</i>
	Griscelli syndrome	GS	GS1	<i>MYO5A</i>
			GS2	<i>RAB27A</i>
GS3			<i>MLPH</i>	
<b>Weibel-Palade body</b>	Von Willebrand disease	VWD	VWD1	<i>VWF</i>
				more genes
			VWD2	<i>VWF</i>
			VWD3	<i>VWF</i>

**Table 1:** Table of genetic disorders affecting hemostatic LRO formation.

to regulate their exocytotic behavior.<sup>68</sup> It has been suggested that Rab27a is maturation marker that arrives to the WPB at later stage, separating the WPBs into two populations: the immature Rab27a negative and the mature Rab27a positive<sup>69</sup> (Figure 2). The recruitment of Rab27a on the WPB membrane is potentially controlled by changes on the lipid/protein local environment driven by VWF.<sup>69</sup> Interestingly, although a new study sheds light on the interacting partners of mature WPB Rabs (Rab3b, Rab3d and Rab27a), it also identifies proteins that are involved in WPB biogenesis and VWF ER-to-Golgi trafficking, like the aforementioned Sec22b, STX5 and GBF1, suggesting that our knowledge on WPB formation is still incomplete.<sup>70</sup>

### Disorders associated with abnormal α-, δ-granule and WPB formation

Several disorders have been described to negatively affect the biogenesis of MK/ platelet granules and endothelial cell WPBs (Table 1). Gray platelet syndrome (GPS) is a disease that affects the α-granule formation, due to mutations in the *NBEAL2* gene, and clinically is characterized by macrothrombocytopenia and decreased platelet activity.<sup>71</sup> Similar to GPS, Quebec platelet syndrome (QPS) is an α-storage pool disorder, that is caused by mutation in *PLAU*, resulting in proteolysis of α-granule proteins, reducing their expression.<sup>72</sup> Another disorder that is presented with bleeding tendency, in addition to liver, skin and central ner-

vous system complications, is arthrogyposis, renal dysfunction, and cholestasis syndrome (ARCS). ARCS consists of two types that influence the expression of VPS33B and VPS16B, the subunits of CHEVI complex, which is responsible for  $\alpha$ -granule maturation.<sup>73</sup> Likewise, Hermansky-Pudlak syndrome (HPS) is a multisystemic disorder with ten identified genetic types, that affect skin pigmentation, hemostasis and lung tissue consistency.<sup>74</sup> The mutated genes that cause HPS primarily facilitate  $\delta$ -granule biogenesis and maturation, thus, in most cases  $\delta$ -granules are absent from the circulating platelets. Diseases that are characterized by  $\delta$ -storage pool deficiency, along with hypopigmentation, are Chediak-Higashi (CHS) and Griscelli syndrome (GS type 2). CHS is caused by mutations in the *LYST* gene, which results in decreased  $\delta$ -granule components and dysfunctional platelets, while GS2 is caused by mutations in *RAB27A*, which supports the retention of  $\delta$ -granule cargo, but the effects are dependent on the genetic background.<sup>16,75</sup> Finally, WPB biogenesis and maturation is affected in the most common bleeding disorder, known as von Willebrand disease (VWD). VWD is characterized by quantitative or qualitative defects in von Willebrand factor, the main cargo of WPBs. VWD is subcategorized into 3 types, depending on the mutations and how they alter VWF synthesis and maturation, which, in turn, can influence the biogenesis and the morphology of WPBs.<sup>52</sup>

Either derived from multivesicular bodies (MVBs) or directly formed at the TGN, LRO biogenesis and maturation is governed by universal pathways.<sup>76</sup> Hence, there are multi-systemic disorders that can alter the biogenesis of more than one LRO. Such a case is HPS, that, apart from defective  $\delta$ -granule formation, has been shown to alter  $\alpha$ -granule protein release (HPS-2, -4 and -9), whereas, it has also been described to influence WPB morphology and maturation (HPS-2 and -6).<sup>61,67,77,78</sup> Additionally, VWD, mainly VWD2 and VWD3, has been associated with impaired megakaryopoiesis and platelet dysfunction, implicating VWF-GP1b interactions in a novel role during platelet production.<sup>79-81</sup>

Taken together, LRO disorders comprise a heterogeneous group that have a multisystemic phenotype. In most cases, the bleeding tendency caused by these disorders has been attributed to a particular LRO, however, as we understand that cellular mechanisms are shared between cell types it becomes clearer that more than one LRO can be affected.

## Perspective

Although we have a better grasp on some aspects, we still need to cover a lot of ground to fathom out the tightly regulated cellular mechanisms involved in the hemostatic LRO formation. What is seemingly the most important factor in LRO biogenesis and maturation is the correct delivery of specialized cargo. It has recently been appreciated that ER-to-Golgi protein influx is the first regulatory step in LRO formation, through which the cell can control the protein supply to progenitor compartments, in response to environmental cues like glucose levels. However, the exact molecular mechanisms and protein complexes are poorly defined. Additionally, it has been described that the same type of granules can contain different packaged proteins, giving rise to subpopulations that influence modes of exocytosis.<sup>82</sup> How is cargo distributed differently? Are the same proteins monitoring different components' trafficking, and if so, what are the molecular cues for differential composition? These are questions that we cannot yet answer, which points out the need for further examination. As far the LRO cargo is concerned, recently, it has been shown that LROs contain also CD63 positive intraluminal vesicles (ILVs), that contribute to intercellular communication and modulate the targeted cells through acute secretion upon stimulation.<sup>83,84</sup> However, whether the process of ILV accumulation in LROs is intentional or unintentional, and how the cell may control this transfer are still unknown.

It is now understood that, despite the differences between LROs types, several pathways can have a universal impact in the formation of more than one granule type. Therefore, dis-

ease models, that are traditionally connected with one particular LRO, can be used to study the formation of another LRO in a different cell type. In such cases, the recent developments in induced pluripotent stem cells (iPSCs) can be utilized in LRO biology. Starting from fibroblasts, CD34 positive progenitor cells and blood outgrowth endothelial cells (BOECs), cells from various disease models can easily be reprogrammed in a pluripotent state and differentiate into different cell types, containing different LROs. In this way, the parallel monitoring of the mechanisms involved in granule formation can highlight the similarities or point out the differences.

MK/ platelet and endothelial LROs are the major players in primary hemostasis, regulating cell-cell communication and secreting bulk amounts of hemostatic proteins. Mutation in genes that govern their formation result in abnormal morphology, secretion and finally in bleeding disorders. Therefore, improved comprehension of their biogenesis and cargo retention can lead to better and more personalized treatments improving the life quality of patients.

### **Disclosure of Conflicts of Interest**

The authors state that they have no conflict of interest.

### **Acknowledgements**

We apologize to all authors whose work has been omitted owing to space restrictions, and for not always citing primary literature. Work in our lab is supported by grants from the Landsteiner Stichting voor Bloedtransfusie Research (LSBR-1244 and LSBR-1707), the Netherlands Ministry of Health (PPOC-2015-24P and PPOC-2018-21), the Dutch Thrombosis Foundation (TSN-56-2015 and TSN-2017-01) and a Research Fellowship from the European Hematology Association (EHA).

## References

- Delevoeye C, Marks MS, Raposo G. Lyso-some-related organelles as functional adaptations of the endolysosomal system. *Curr. Opin. Cell Biol.* 2019;59:147–158.
- DellAngelica EC, Mullins C, Caplan S, Bonifacino JS. Lysosome-related organelles. *FASEB J.* 2000;14(10):1265–1278.
- Whiteheart SW. Platelet granules: Surprise packages. *Blood.* 2011;118(5):1190–1191.
- Schillemans M, Karampini E, Kat M, Bierings R. Exocytosis of Weibel–Palade bodies: how to unpack a vascular emergency kit. *J. Thromb. Haemost.* 2019;17(1):6–18.
- Sadler JE. von Willebrand factor assembly and secretion. *J. Thromb. Haemost.* 2009;7(SUPPL. 1):24–27.
- Kroll MH, Harris TS, Moake JL, Handin RI, Schafer AI. Von Willebrand factor binding to platelet GpIb initiates signals for platelet activation. *J. Clin. Invest.* 1991;88(5):1568–1573.
- Zang C, Luyten A, Chen J, Liu XS, Shivasani RA. NF-E2, FLI1 and RUNX1 collaborate at areas of dynamic chromatin to activate transcription in mature mouse megakaryocytes. *Sci. Rep.* 2016;6.
- Tijssen MR, Cvejic A, Joshi A, et al. Genome-wide analysis of simultaneous GATA1/2, RUNX1, FLI1, and SCL binding in megakaryocytes identifies hematopoietic regulators. *Dev. Cell.* 2011;20(5):597–609.
- Songdej N, Rao AK. Hematopoietic transcription factor mutations: important players in inherited platelet defects. *Blood.* 2017;129(21):2873–2881.
- Jalagadugula G, Goldfinger LE, Mao G, Lambert MP, Rao AK. Defective RAB1B-related megakaryocytic ER-to-Golgi transport in RUNX1 haplo deficiency: impact on von Willebrand factor. *Blood Adv.* 2018;2(7):.
- Mao GF, Goldfinger LE, Fan DC, et al. Dysregulation of PLDN (pallidin) is a mechanism for platelet dense granule deficiency in RUNX1 haplo deficiency. *J. Thromb. Haemost.* 2017;15(4):792–801.
- Plutner H, Cox AD, Pind S, et al. Rab1b regulates vesicular transport between the endoplasmic reticulum and successive Golgi compartments. *J. Cell Biol.* 1991;115(1):31–43.
- Falcón-Pérez JM, Starcevic M, Gautam R, Dell'Angelica EC. BLOC-1, a novel complex containing the pallidin and muted proteins involved in the biogenesis of melanosomes and platelet-dense granules. *J. Biol. Chem.* 2002;277(31):28191–28199.
- Tiwari S, Italiano JE, Barral DC, et al. A role for Rab27b in NF-E2-dependent pathways of platelet formation. *Blood.* 2003;102(12):3970–3979.
- Tolmachova T, Abrink M, Futter CE, Authi KS, Seabra MC. Rab27b regulates number and secretion of platelet dense granules. *Proc. Natl. Acad. Sci. U. S. A.* 2007;104(14):5872–5877.
- Novak EK, Gautam R, Reddington M, et al. The regulation of platelet-dense granules by Rab27a in the ashken mouse, a model of Hermansky-Pudlak and Griscelli syndromes, is granule-specific and dependent on genetic background. *Blood.* 2002;100(1):128–135.
- Hart A, Melet F, Grossfeld P, et al. Fli-1 is required for murine vascular and megakaryocytic development and is hemizygously deleted in patients with thrombocytopenia. *Immunity.* 2000;13(2):167–177.
- Vo KK, Jarocha DJ, Lyde RB, et al. FLI1 level during megakaryopoiesis affects thrombopoiesis and platelet biology. *Blood.* 2017;129(26):3486–3494.
- Saultier P, Vidal L, Canault M, et al. Macrothrombocytopenia and dense granule deficiency associated with FLI1 variants: Ultrastructural and pathogenic features. *Haematologica.* 2017;102(6):1006–1016.
- Stevenson WS, Morel-Kopp MC, Chen Q, et al. GF11B mutation causes a bleeding disorder with abnormal platelet function. *J. Thromb. Haemost.* 2013;11(11):2039–2047.
- Monteferrario D, Bolar NA, Marneth AE, et al. A dominant-negative GF11B mutation in the gray platelet syndrome. *N. Engl. J. Med.* 2014;370(3):245–53.
- Marneth AE, Van Heerde WL, Hebeda KM, et al. Platelet CD34 expression and a/d-granule abnormalities in GF11B- and RUNX1-related familial bleeding disorders. *Blood.* 2017;129(12):1733–1736.
- Van Oorschot R, Hansen M, Koornneef JM, et al. Molecular mechanisms of bleeding disorder associated GF11BQ287\* mutation and its affected pathways in megakaryocytes and platelets. *Haematologica.* 2019;104(7):1460–1472.
- Ambrosio AL, Di Pietro SM. Mechanism of platelet  $\alpha$ -granule biogenesis: study of cargo transport and the VPS33B-VPS16B complex in a model system. *Blood Adv.* 2019;3(17):2617–2626.
- Lo B, Li L, Gissen P, et al. Requirement of VPS33B, a member of the Sec1/Munc18 protein family, in megakaryocyte and platelet  $\alpha$ -granule biogenesis. *Blood.* 2005;106(13):4159–4166.
- Baker RW, Jeffrey PD, Zick M, et al. A direct role for the Sec1/Munc18-family protein Vps33 as a template for SNARE assembly. *Science (80- ).* 2015;349(6252):1111–1114.
- Gissen P, Johnson CA, Morgan N V, et al. Mutations in VPS33B, encoding a regulator of SNARE-dependent membrane fusion, cause arthrogryposis-renal dysfunction-cholestasis (ARC) syndrome. *Nat. Genet.* 2004;36(4):400–404.
- Bem D, Smith H, Banushi B, et al. VPS33B regulates protein sorting into and maturation of  $\alpha$ -granule progenitor organelles in mouse megakaryocytes. *Blood.*

- 2015;126(2):133–143.
29. Heijnen HFG, Debili N, Vainchencker W, et al. Multivesicular bodies are an intermediate stage in the formation of platelet  $\alpha$ -granules. *Blood*. 1998;91(7):2313–2325.
  30. Balderhaar HJ klein., Ungermann C. CORVET and HOPS tethering complexes - coordinators of endosome and lysosome fusion. *J. Cell Sci*. 2013;126(6):1307–1316.
  31. van der Beek J, Jonker C, van der Welle R, Liv N, Klumperman J. CORVET, CHEVI and HOPS – Multisubunit tethers of the endo-lysosomal system in health and disease. *J. Cell Sci*. 2019;132(10):.
  32. Cullinane AR, Straatman-Iwanowska A, Zaucker A, et al. Mutations in VIPAR cause an arthrogryposis, renal dysfunction and cholestasis syndrome phenotype with defects in epithelial polarization. *Nat. Genet*. 2010;42(4):303–312.
  33. Urban D, Li L, Christensen H, et al. The VPS33B-binding protein VPS16B is required in megakaryocyte and platelet-granule biogenesis. *Blood*. 2012;120(25):5032–5040.
  34. Gunay-Aygun M, Falik-Zaccai TC, Vilboux T, et al. NBEAL2 is mutated in gray platelet syndrome and is required for biogenesis of platelet  $\alpha$ -granules. *Nat. Genet*. 2011;43(8):732–734.
  35. Deppermann C, Cherpokova D, Nurden P, et al. Gray platelet syndrome and defective thrombo-inflammation in Nbeal2-deficient mice. *J. Clin. Invest*. 2013;123(8):3331–3342.
  36. Kahr WHA, Lo RW, Li L, et al. Abnormal megakaryocyte development and platelet function in Nbeal2<sup>-/-</sup> mice. *Blood*. 2013;122(19):3349–3358.
  37. Lo RW, Li L, Leung R, Pluthero FG, Kahr WHA. NBEAL2 (neurobeachin-like 2) is required for retention of cargo proteins by  $\alpha$ -granules during their production by megakaryocytes. *Arterioscler. Thromb. Vasc. Biol*. 2018;38(10):2435–2447.
  38. Suzuki T, Oiso N, Gautam R, et al. The mouse organellar biogenesis mutant buff results from a mutation in Vps33a, a homologue of yeast vps33 and Drosophila carnation. *Proc. Natl. Acad. Sci. U. S. A*. 2003;100(3):1146–1150.
  39. Zhen Y, Stenmark H. Cellular functions of Rab GTPases at a glance. *J. Cell Sci*. 2015;128(17):3171–3176.
  40. Ambrosio AL, Boyle J a., Di Pietro SM. Mechanism of platelet dense granule biogenesis: Study of cargo transport and function of Rab32 and Rab38 in a model system. *Blood*. 2012;120(19):4072–4081.
  41. Aguilar A, Weber J, Boscher J, et al. Combined deficiency of RAB32 and RAB38 in the mouse mimics Hermansky-Pudlak syndrome and critically impairs thrombosis. *Blood Adv*. 2019;3(15):2368–2380.
  42. Gerondopoulos A, Langemeyer L, Liang JR, Linford A, Barr F a. BLOC-3 mutated in Hermansky-Pudlak syndrome is a Rab32/38 guanine nucleotide exchange factor. *Curr. Biol*. 2012;22(22):2135–2139.
  43. Nazarian R, Falcón-Pérez JM, Dell'Angelica EC. Biogenesis of lysosome-related organelles complex 3 (BLOC-3): A complex containing the Hermansky-Pudlak syndrome (HPS) proteins HPS1 and HPS4. *Proc. Natl. Acad. Sci. U. S. A*. 2003;100(15):8770–8775.
  44. Dell'Angelica EC. The building BLOC(k)s of lysosomes and related organelles. *Curr. Opin. Cell Biol*. 2004;16(4):458–464.
  45. Meng R, Wang Y, Yao Y, et al. SLC35D3 delivery from megakaryocyte early endosomes is required for platelet dense granule biogenesis and is differentially defective in Hermansky-Pudlak syndrome models. *Blood*. 2012;120(2):404–414.
  46. Ambrosio AL, Boyle JA, Di Pietro SM. TPC2 mediates new mechanisms of platelet dense granule membrane dynamics through regulation of Ca<sup>2+</sup> release. *Mol. Biol. Cell*. 2015;26(18):3263–3274.
  47. Pitt SJ, Funnell TM, Sitsapesan M, et al. TPC2 is a novel NAADP-sensitive Ca<sup>2+</sup> release channel, operating as a dual sensor of luminal pH and Ca<sup>2+</sup>. *J. Biol. Chem*. 2010;285(45):35039–35046.
  48. Zhou YF, Eng ET, Nishida N, et al. A pH-regulated dimeric bouquet in the structure of von Willebrand factor. *EMBO J*. 2011;30(19):4098–4111.
  49. Lippok S, Kolšek K, Löf A, et al. von Willebrand factor is dimerized by protein disulfide isomerase. *Blood*. 2016;127(9):1183–1191.
  50. Purvis AR, Gross J, Dang LT, et al. Two Cys residues essential for von Willebrand factor multimer assembly in the Golgi. *Proc. Natl. Acad. Sci. U. S. A*. 2007;104(40):15647–52.
  51. Wang JW, Groeneveld DJ, Cosemans G, et al. Biogenesis of Weibel-Palade bodies in von Willebrand's disease variants with impaired von Willebrand factor intrachain or interchain disulfide bond formation. *Haematologica*. 2012;97(6):859–866.
  52. Valentijn KM, Eikenboom J. Weibel-Palade bodies: A window to von Willebrand disease. *J. Thromb. Haemost*. 2013;11(4):581–592.
  53. Karampini E, Olins J, Mulder A, et al. Sec22b determines Weibel-Palade body length by controlling anterograde ER-Golgi transport. 2020;
  54. Mancias JD, Goldberg J. The Transport Signal on Sec22 for Packaging into COPII-Coated Vesicles Is a Conformational Epitope. 2007;403–414.
  55. Ferraro F, Kriston-Vizi J, Metcalf DJ, et al. A two-tier golgi-based control of organelle size underpins the functional plasticity of endothelial cells. *Dev. Cell*. 2014;29(3):292–304.
  56. Karampini E, Mulder A, Alphen F van, et al. STX5 regulates VWF storage and secretion in endothelial cells.
  57. Adolf F, Rhiel M, Hessling B, et al. Proteomic Profiling of Mammalian COPII and COPI Vesicles. *Cell Rep*. 2019;26(1):250-265.e5.

58. Lui-Roberts WWY, Collinson LM, Hewlett LJ, Michaux G, Cutler DF. An AP-1/clathrin coat plays a novel and essential role in forming the Weibel-Palade bodies of endothelial cells. *J. Cell Biol.* 2005;170(4):627–636.
59. Lopes-da-Silva M, McCormack JJ, Burden JJ, et al. A GBF1-Dependent Mechanism for Environmentally Responsive Regulation of ER-Golgi Transport. *Dev. Cell.* 2019;1–16.
60. Ferraro F, Mafalda Lopes da S, Grimes W, et al. Weibel-Palade body size modulates the adhesive activity of its von Willebrand Factor cargo in cultured endothelial cells. Nature Publishing Group; 2016.
61. Ma J, Zhang Z, Yang L, et al. BLOC-2 subunit HPS6 deficiency affects the tubulation and secretion of von Willebrand factor from mouse endothelial cells. *J. Genet. Genomics.* 2016;43(12):686–693.
62. Philippe M, Léger T, Desvaux R, Walch L. Discs large 1 (Dlg1) scaffolding protein participates with clathrin and adaptor protein complex 1 (AP-1) in forming weibel-palade bodies of endothelial cells. *J. Biol. Chem.* 2013;288(18):13046–13056.
63. Wang YJ, Wang J, Sun HQ, et al. Phosphatidylinositol 4 phosphate regulates targeting of clathrin adaptor AP-1 complexes to the Golgi. *Cell.* 2003;114(3):299–310.
64. da Silva ML, O'Connor MN, Kriston-Vizi J, et al. Type II PI4-kinases control Weibel-Palade body biogenesis and von Willebrand factor structure in human endothelial cells. *J. Cell Sci.* 2016;129(10):2096–2105.
65. Mourik MJ, Faas FGA, Zimmermann H, et al. Content delivery to newly forming Weibel-Palade bodies is facilitated by multiple. *Blood.* 2015;125(22):3509–3516.
66. Harrison-Lavoie KJ, Michaux G, Hewlett L, et al. P-selectin and CD63 use different mechanisms for delivery to Weibel-Palade bodies. *Traffic.* 2006;7(6):647–662.
67. Karampini E, Schillemans M, Hofman M, et al. Defective AP-3-dependent VAMP8 trafficking impairs Weibel-Palade body exocytosis in Hermansky-Pudlak Syndrome type 2 blood outgrowth endothelial cells. *Haematologica.* 2019;104(10):2091–2099.
68. Bierings R, Hellen N, Kiskin N, et al. The interplay between the Rab27A effectors Slp4-a and MyRIP controls hormone-evoked Weibel-Palade body exocytosis. *Blood.* 2012;120(13):2757–2768.
69. Hannah MJ, Hume AN, Arribas M, et al. Weibel-Palade bodies recruit Rab27 by a content-driven, maturation-dependent mechanism that is independent of cell type. *J. Cell Sci.* 2003;116(19):3939–3948.
70. Holthenrich A, Drexler HCA, Chehab T, Naß J, Gerke V. Proximity proteomics of endothelial Weibel-Palade bodies identifies novel regulator of von Willebrand factor secretion. *Blood.* 2019;134(12):979–982.
71. Albers CA, Cvejic A, Favier R, et al. Exome sequencing identifies NBEAL2 as the causative gene for gray platelet syndrome. *Nat. Genet.* 2011;43(8):735–737.
72. Hayward CP, Cramer EM, Kane WH, et al. Studies of a second family with the Quebec platelet disorder: evidence that the degradation of the alpha-granule membrane and its soluble contents are not secondary to a defect in targeting proteins to alpha-granules. *Blood.* 1997;89(4):1243–53.
73. Zhou Y, Zhang J. Arthrogryposis-renal dysfunction-cholestasis (ARC) syndrome: From molecular genetics to clinical features. *Ital. J. Pediatr.* 2014;40(1).
74. Wei A-H, Li W. Hermansky-Pudlak syndrome: pigmentary and non-pigmentary defects and their pathogenesis. *Pigment Cell Melanoma Res.* 2013;26(2):176–192.
75. Shiraiishi M, Ogawa H, Ikeda M, Kawashima S, Ito K. Platelet dysfunction in Chediak-Higashi syndrome-affected cattle. *J. Vet. Med. Sci.* 2002;64(9):751–760.
76. Marks, M. S., Heijnen, H. F.G., Raposo G. Lysosome-related organelles: Unusual compartments become mainstream. *Curr Opin Cell Biol.* 2014;25(4):495–505.
77. Meng R, Wu J, Harper DC, et al. Defective release of a granule and lysosome contents from platelets in mouse Hermansky-Pudlak syndrome models. *Blood.* 2015;125(10):1623–1632.
78. Sharda A, Kim SH, Jasuja R, et al. Defective PDI release from platelets and endothelial cells impairs thrombus formation in Hermansky-Pudlak syndrome. *Blood.* 2015;125(10):1633–1642.
79. Nurden P, Gobbi G, Nurden A, et al. Abnormal VWF modifies megakaryocytopoiesis: Studies of platelets and megakaryocyte cultures from patients with von Willebrand disease type 2B. *Blood.* 2010;115(13):2649–2656.
80. Nurden P, Debili N, Vainchenker W, et al. Impaired megakaryocytopoiesis in type 2B von Willebrand disease with severe thrombocytopenia. *Blood.* 2006;108(8):2587–2595.
81. Nurden P, Nurden AT, La Marca S, et al. Platelet morphological changes in 2 patients with von Willebrand disease type 3 caused by large homozygous deletions of the von Willebrand factor gene. *Haematologica.* 2009;94(11):1627–1629.
82. Battinelli EM, Thon JN, Okazaki R, et al. Megakaryocytes package contents into separate  $\alpha$ -granules that are differentially distributed in platelets. *Blood Adv.* 2019;3(20):3092–3098.
83. Streetley J, Fonseca A-V, Turner J, et al. Stimulated release of intraluminal vesicles from Weibel-Palade bodies. *Blood.* 2019;133(25):2707–2717.
84. Heijnen HFG, Schiel AE, Fijnheer R, Geuze HJ, Sixma JJ. Activated platelets release two types of membrane vesicles: Microvesicles by surface shedding and exosomes derived from exocytosis of multivesicular bodies and  $\alpha$ -granules. *Blood.* 1999;94(11):3791–3799.



## Chapter 3

# Sec22b determines Weibel-Palade body length by controlling anterograde ER-Golgi transport

Ellie Karampini, Jenny Olins, Aat Mulder, Carolina Jost, Dirk Geerts,  
Jan Voorberg and Ruben Bierings  
*Haematologica* 2020; in press

## Abstract

Von Willebrand factor (VWF) is a multimeric hemostatic protein that is synthesized in endothelial cells, where it is stored for secretion in elongated secretory organelles, so-called Weibel-Palade bodies (WPBs). Hemostatic activity of VWF is strongly tied to WPB length, but how endothelial cells control the dimensions of their WPBs is unclear. In this study we used a targeted shRNA screen to identify the longin-SNARE Sec22b as a novel determinant of WPB size and VWF trafficking. We found that Sec22b depletion resulted in loss of the typically elongated WPB morphology along with disintegration of the Golgi and dilation of rough ER (rER) cisternae. This was accompanied by reduced proteolytic processing of VWF, accumulation of VWF in the dilated rER and reduced basal and stimulated VWF secretion. Our data demonstrate that the elongation of WPBs, and thus adhesive activity of its cargo VWF, is determined by the rate of anterograde transport between ER and Golgi, which depends on Sec22b-containing SNARE complexes.

## Introduction

ER-to-Golgi transport is the first step in the secretory pathway.<sup>1</sup> As eukaryotic cells are vastly compartmentalized, ER is the first stop in protein production as well as the initially quality check point whether proteins are correctly folded.<sup>2</sup> Correctly folded proteins are then trafficked to the Golgi where they are additionally modified before being directed to their appropriate destination: endo/lysosome, plasma membrane or secretion.<sup>3</sup> At the *trans*-Golgi network (TGN), proteins will either enter the “constant” constitutive pathway for unimpeded release, or they are temporarily stored in secretory vesicles, often of the lysosome-related organelle (LRO) family, for regulated secretion. Storage and regulated secretion allows the immediate discharge of larger protein quantities in a correct physiological setting.<sup>4</sup>

Biogenesis of LROs is crucial for the proper function of a wide variety of cells, their importance being well-highlighted by the fact that defective LRO formation results in a vast manifestation of clinical abnormalities that include bleeding, immunodeficiency, hypopigmentation and neurological defects.<sup>5</sup> Within the LRO family, Weibel-Palade bodies (WPBs) are the storage organelles of endothelial cells (ECs).<sup>6,7</sup> WPBs primarily contain von Willebrand factor (VWF), a large multimeric hemostatic protein that serves a critical role in platelet adhesion and as chaperone for coagulation factor VIII.<sup>8</sup> WPB biogenesis is directly dependent on synthesis and correct post-translational processing of VWF.<sup>9-12</sup> WPBs have a distinct, elongated morphology that is intrinsically linked to the inherent ability of VWF multimers to self-organize in tubules when exposed to the internal milieu of the TGN.<sup>13-15</sup> Quantitative or qualitative defects in VWF, for instance due to mutations in VWF, cause von Willebrand disease (VWD), the most common inherited bleeding disorder (Leebeek and Eikenboom 2016). *VWF* mutations that affect its synthesis or processing often result in altered WPB morphology, with WPBs being either round or short.<sup>16</sup> Upon regulated release from WPBs, VWF unfurls into strings of up to 1 mm long that are anchored on the apical side of the endothelium.<sup>17,18</sup> VWF strings create an adhesive platform for platelets to initiate the formation of the initial platelet plug at site of vascular damage.<sup>19,20</sup> The adhesive capacity of VWF towards platelets and self-associating plasma VWF is proportional to WPB size.<sup>21</sup> In turn, WPB size is determined before budding from the TGN by incorporation of so-called “VWF quanta” and it was previously shown that reduced VWF synthesis or unlinking of Golgi-stacks affects WPB length.<sup>22</sup> However, how ECs control WPB size and thus hemostatic activity of VWF is largely unknown.

Due to the distinctive shape of their WPBs, ECs are an excellent model system for elucidating how cells manage formation and morphology of LROs. As WPB formation is VWF driven, monitoring intracellular VWF trafficking can be used as a tool to study the complex



mechanisms involved. VWF undergoes extensive post-translational modification during its path through the endothelial secretory pathway.<sup>23</sup> VWF enters the endoplasmic reticulum (ER) as a single pre-pro-polypeptide chain which forms tail-to-tail dimers by formation of disulfide bonds between the C-terminal cysteine knot (CTCK) domains of two proVWF monomers.<sup>24</sup> After dimerization-dependent ER exit, proVWF dimers are transported to the Golgi, where VWF propeptide is cleaved from the proVWF chain. Inter-dimer disulfide bonds between cysteines in the D3 domains lead to formation of head-to-head VWF multimers.<sup>25</sup> VWF multimers are then condensed into tubules that are packaged into newly forming WPBs that emerge from the TGN.<sup>26,27</sup>

Trafficking of proteins during formation and maturation of subcellular organelles such as WPBs is dependent on membrane fusion, which is universally controlled by SNARE proteins.<sup>28</sup> The SNARE complex consists of a v-SNARE on the vesicle membrane and t-SNAREs on the acceptor membrane which together form a four-helix bundle that allows the membranes to fuse. Although several SNAREs have been associated with WPB exocytosis,<sup>7</sup> the SNAREs taking part in WPB and LRO biogenesis are not known. The subfamily of longin-SNAREs (VAMP7, Ykt6 and Sec22b), which derives its name from an N-terminal self-inhibitory longin-domain that can fold back on the SNARE domain, controls membrane fusion events that traffic proteins to and from the Golgi.<sup>29</sup>

In this study we addressed the role of longin-SNAREs in the formation of WPBs. Using a targeted shRNA screen of longin-SNAREs in primary ECs we identify Sec22b as a novel determinant of WPB morphology. Sec22b silencing results in short WPBs, disintegration of the Golgi complex, reduced proVWF processing and retention of proVWF in a dilated ER. Our data suggest that the distinctive morphology of WPBs and thus the adhesive activity of its main cargo VWF is determined by the rate of membrane fusion between ER and Golgi, which is dependent on Sec22b-containing SNARE complexes.

## Methods

### Antibodies

Antibodies used in this study are listed in Supplemental Table I.

### Cell culture, lentiviral transfection and transduction

Pooled, cryo-preserved primary human umbilical vein endothelial cells (HUVECs) were obtained from Promocell (Heidelberg, Germany). HUVECs were cultured in EGM-18 medium; EGM-2 medium (Lonza, Basel, Switzerland, CC-3162) supplemented with 18% FCS (Bodinco, Alkmaar, Netherlands). Human embryonic kidney 293T (HEK293T) cells were obtained from ATCC (Wessel, Germany) and were grown in Dulbecco's modified Eagle medium containing D-glucose and L-glutamine (Lonza, Basel, Switzerland) supplemented with 10% FCS, 100 U/ml penicillin and 100 µg/ml streptomycin. HEK293Ts were seeded on collagen coated plates or flasks and were transfected with 3rd generation lentiviral packaging plasmids pMD2.G, pRSV-REV and pMDLg/pRRE (Addgene, Cambridge, USA) using transit-LT1 (Mirus Bio LLC, Madison, WI, USA) following the supplier's protocol. After 6-8h incubation, the medium was exchanged for EGM-18. Virus particles were collected 24 and 48 hours following transfection and were filtered through 0.45 µm pore filters in EGM-18. Two batches of virus were used to transduce HUVECs or cord blood BOECs (cbBOECs) for the period of 48 hours. Transduced ECs were selected by puromycin (0.5 µg/ml) that was added to the medium for 72 hours after the second virus installment.

### DNA constructs for shRNA silencing of longin-SNAREs, CRISPR editing and mEGFP-Sec22b-ΔSNARE

The LKO.1-puro-CMV-mEGFP-U6-shC002 vector, which simultaneously expresses mEGFP

and a non-targeting control shRNA from the CMV and U6 promoter respectively, was described previously.<sup>30</sup> shRNAs targeting Sec22b, VAMP7 and Ykt6 were obtained from the MISSION® shRNA library developed by TRC at the Broad Institute of MIT and Harvard and distributed by Sigma-Aldrich (Supplemental Table II). Fragments containing the shRNA expression cassette from the shRNA library were transferred to the LKO.1-puro-CMV-mEGFP-U6 vector by *SphI-EcoRI* subcloning. CRISPR mediated depletion of Sec22b in HUVEC was performed essentially as described previously.<sup>31</sup> LentiCRISPR\_v2 (a gift from Dr. Feng Zhang; Addgene #52961), a lentiviral vector which simultaneously expresses Cas9 endonuclease and guide RNAs (gRNAs) has been described previously.<sup>32</sup> gRNAs were designed to target exon 1 of the *SEC22B* gene using the CRISPOR Design tool (<http://crispor.tefor.net/>)<sup>3</sup> by submitting the DNA sequence of SEC22B exon 1 flanked by 100 bp up- and downstream (chromosome 1: 120,1501898-120,176,515 reverse strand; Supplemental Figure IIA). gRNA sequences were selected that have a high predicted efficiency with limited off-target effects. gRNAs used in this study are shown in Supplemental Table III and were cloned as hybridized complementary oligos (with *BsmBI* restriction site compatible overhangs on either side) into *BsmBI*-digested LentiCRISPR\_v2 plasmid. LVX-mEGFP-LIC has been described previously.<sup>33</sup> To construct a human Sec22b variant that lacks its SNARE domain (Gly135-Lys174), a synthetic Sec22b fragment was generated by gene synthesis in which codons 135-174 were removed from the 214 codon Sec22b coding sequence and which was flanked by *BsrGI* and *NotI* sites, respectively. The resulting Sec22b- $\Delta$ SNARE fragment was cloned in frame behind mEGFP in LVX-mEGFP-LIC by subcloning between *BsrGI* and *NotI* sites. All constructs were sequence verified. Lentiviral plasmids were produced in *Stbl3* bacteria.

Further details on materials and methods are found in the *Supplemental Materials and Methods*.

## Results

### Weibel-Palade body length is significantly reduced upon Sec22b silencing

To determine the role of longin-SNAREs in WPB biogenesis we performed a targeted shRNA screen against VAMP7, Ykt6 and Sec22b in human umbilical vein endothelial cells (HUVECs) and evaluated WPB morphology by VWF immunostaining. As shown in Figure 1Ai, in shCTRL, shVAMP7 and shYkt6 transduced cells, VWF was primarily stored in typical cigar-shaped WPBs. However, upon Sec22b silencing (shSec22b) (Supplemental Figure I), WPBs had lost their characteristic elongated morphology and appeared short and “stubby”. Quantification of WPB length in control and knockdown (KD) cells showed a significant reduction in WPB length after Sec22b KD, whereas no difference was found in the absence of VAMP7 or Ykt6 (Figure 1Aii). To further substantiate Sec22b’s role in WPB formation we used CRISPR-mediated *SEC22B*-editing of HUVECs (Supplemental Figure |IA, Bi, Bii). Cells depleted of Sec22b were identified by Sec22b staining (Supplemental Figure |IC). A similar reduction of WPB length was observed in ECs targeted with 3 separate gRNAs directed to exon 1 of Sec22b (Figure. 1B, Supplemental Figure IID). As a third, independent strategy we also determined WPB morphology after expression of an mEGFP-tagged non-fusogenic Sec22b variant (mEGFP-Sec22b- $\Delta$ SNARE), which lacks the SNARE domain responsible for fusion and compared these with mEGFP expressing cells (Figure 1Ci). We found that the  $\Delta$ SNARE construct had a dominant negative effect on WPB size, with WPBs significantly shorter compared to mEGFP control (Figure 1Cii). Together these results identify Sec22b as a determinant of secretory organelle size in ECs.

### Sec22b silencing results in unlinked Golgi ribbon

Since the size of nascent WPBs is regulated by incorporation of multiple so-called VWF quanta from the TGN,<sup>22</sup> we investigated TGN morphology in Sec22b-depleted cells. TGN46

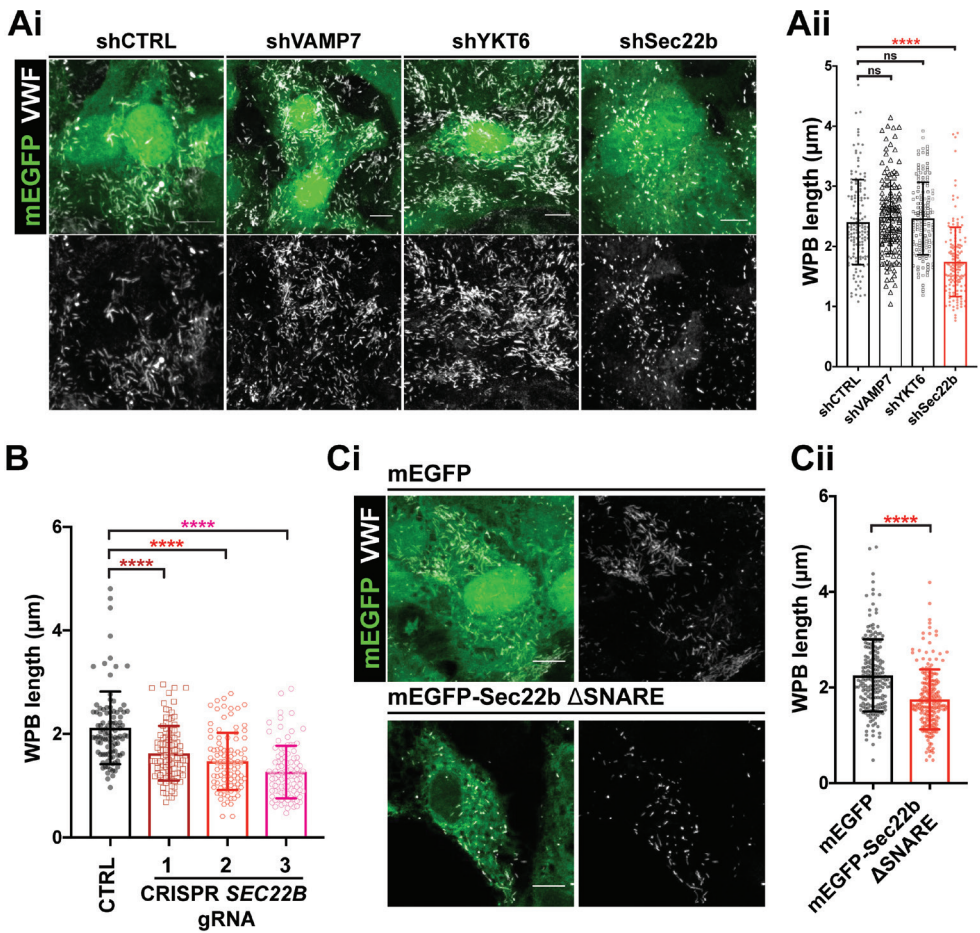


**Figure 1: Sec22b depletion and fusogenic function affects WPB elongation.** Ai) VWF immunostaining in ECs transfected with shCTRL, shVAMP7, shYKT6 or shSec22b (green channel: mEGFP expressing ECs). Aii) Quantification of WPB length in shCTRL, shVAMP7, shYKT6 and shSec22b ECs (n=3, t-test with Welch's correction, \*\*\*\* P<0.0001). B) WPB length in control and CRISPR SEC22B knockout ECs (n=3, t-test with Welch's correction, \*\*\*\* P<0.0001). Ci) VWF immunostaining in mEGFP and mEGFP-Sec22b-ΔSNARE expressing ECs (both in green). Cii) WPB length in mEGFP and mEGFP-Sec22b-ΔSNARE expressing ECs (n=3, t-test with Welch's correction, \*\*\*\* P<0.0001).

immunostaining showed that while in control cells the TGN had a compact morphology, shSec22b-treated cells exhibited a dispersed TGN morphology, consistent with an unlinked Golgi ribbon (Figure 2A-B). Quantification of the area that encompasses the entire TGN46 immunoreactivity in shSec22b and shCTRL cells revealed that, due to their fragmentation, TGNs in Sec22b depleted cells extended to a significantly larger intracellular area than the compact TGNs in control cells (Figure 2C). It has previously been described that unlinking Golgi stacks using depletion of Golgi matrix proteins or nocodazole gives rise to shorter WPBs.<sup>22</sup> When evaluating WPB length in shSec22b cells with compact vs. dispersed TGN we also observed a strong correlation between TGN dispersal and shorter WPBs (Figure 2D), which suggests that the reduction in WPB length after Sec22b depletion is (at least partly) a consequence of Golgi disintegration.

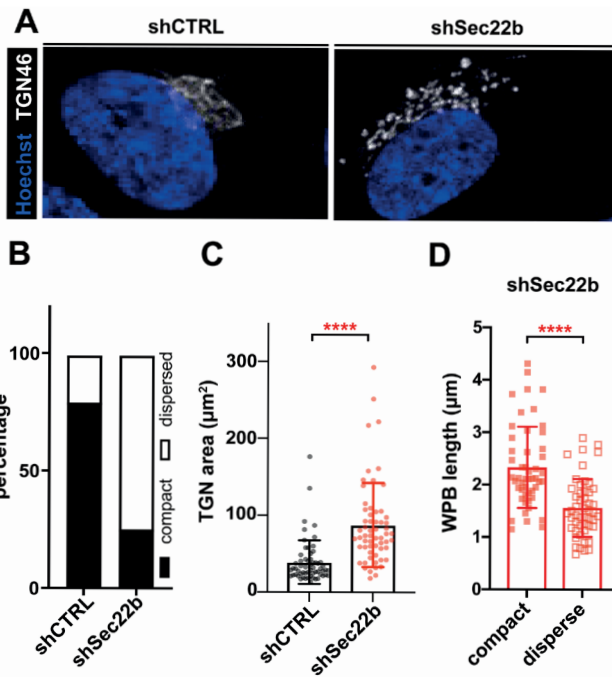


**Figure 2: Sec22b depletion results in TGN fragmentation.** A) Immunofluorescent staining of TGN (TGN46) in control and Sec22b-depleted cells (blue channel: Hoechst nuclear staining). B) Quantification of TGN dispersal in control and Sec22b KD ECs. C) Quantification of TGN area coverage in shCTRL and shSec22b ECs (n=5, t-test with Welch's correction, \*\*\*\* P<0.001). D) WPB length in Sec22b KD ECs with compact versus dispersed TGN (n=3, t-test with Welch's correction, \*\*\*\* P<0.0001, \*\*\*\* P<0.0001). Ci) VWF immunostaining in mEGFP and mEGFP-Sec22b-ΔSNARE expressing ECs (both in green). Cii) WPB length in mEGFP and mEGFP-Sec22b-ΔSNARE expressing ECs (n=3, t-test with Welch's correction, \*\*\*\* P<0.0001).

### Sec22b silencing results in decreased VWF trafficking to the Golgi and VWF retention in the ER

As Sec22b has been associated with membrane fusion events during anterograde and retrograde trafficking between ER and Golgi,<sup>29</sup> we evaluated VWF trafficking in the endothelial early secretory pathway. A key step during VWF biosynthesis is the proteolytic cleavage of proVWF into VWF propeptide and mature VWF, which takes place upon its arrival in the Golgi.<sup>34</sup> We used the intracellular ratio between the two distinct forms of VWF, proVWF (ER) and mature VWF (Golgi & post-Golgi), as a measure for ER and Golgi transport by estimating the amount of proVWF and VWF in shCTRL and shSec22b ECs (Figure 3Ai). While the total amount of mature VWF was markedly reduced in shSec22b cells, the proportion of VWF in the unprocessed proVWF form was increased. Therefore, the proVWF:VWF ratio was significantly increased in the Sec22b KD ECs (Figure 3Aii). This suggests that proteolytic processing of proVWF is reduced in the absence of Sec22b, possibly due to a reduced flux of VWF from the ER. Consistent with this we observed increased VWF immunoreactivity in reticular perinuclear structures resembling the ER after Sec22b silencing (Figure 3C). Simultaneous with - but independent of - proteolytic processing, VWF dimers oligomerize into long VWF multimers in the Golgi.<sup>10,34</sup> VWF multimer analysis using SDS-agarose gel electrophoresis showed that Sec22b silencing did not affect multimerization per se, as evidenced by high molecular weight VWF multimers in lysates of shCTRL and shSec22b ECs. However, the increased proportion of VWF dimers in the Sec22b KD cells indicates that VWF is retained at the ER (Figure 3Bi, Bii). Together this points to a reduction of anterograde ER-Golgi trafficking of VWF in the absence of Sec22b.

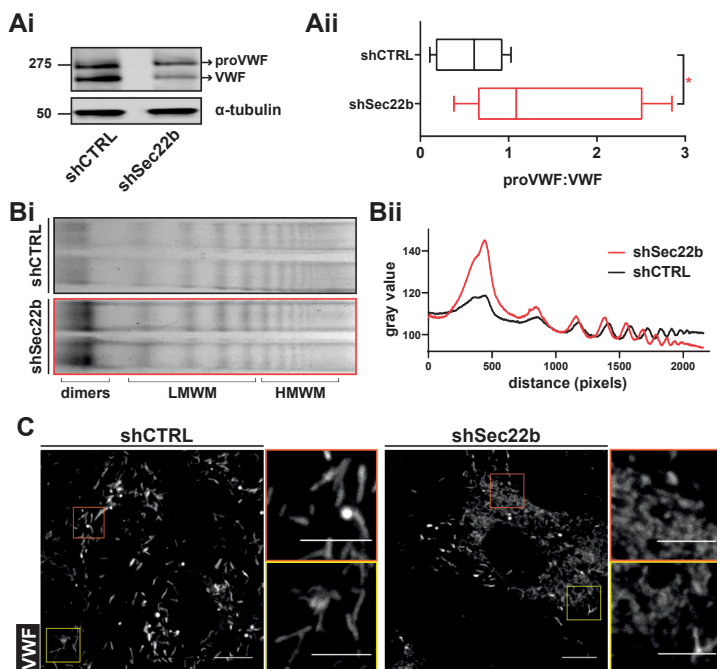


**Figure 3: Sec22b depletion results in VWF ER retention** Ai) Western blot analysis of monomeric VWF under reducing conditions in control and Sec22b KD ECs. Uncleaved (proVWF) and cleaved (VWF) forms are indicated by arrows.  $\alpha$ -tubulin is used as a loading control. Molecular weight standards are indicated on the left (kDa). Aii) ProVWF:VWF ratio in control and shSec22b ECs (n=8, paired t-test, \* P<0.05). Bi) VWF multimer blot (4 samples from 2 independent experiments) in control and Sec22b KD ECs. Bii) Line graph of the densitometry of VWF multimer bands. C) Immunofluorescent staining of VWF in shCTRL and shSec22b HUVECs (boxed areas are shown magnified on the right, size bar corresponds to 10  $\mu$ m for images or 5  $\mu$ m for boxed areas).

### Sec22b silencing results in accumulation of VWF in dilated rough ER.

Since VWF was retained in the ER, potentially along with other proteins, we used electron microscopy (EM) to examine the impact of reduced anterograde trafficking on the ER (Figure 4A). When Sec22b was silenced the rough ER (rER) appeared enlarged and ribosome-studded membrane-limited rounded structures developed with electron dense content. These rER structures represent severely dilated ER cisternae as they often retained a membranous connection to the rER. The dilated rER phenotype was observed in the majority of Sec22b depleted cells (72.9 %) (Figure 4B). Closer examination of the rER morphology revealed that apart from the round rER structures (asterisks), the luminal width of ER sheets (arrowheads) was significantly increased in Sec22b KD cells (0.29  $\mu$ m  $\pm$  0.18  $\mu$ m) when compared to control cells (0.10  $\mu$ m  $\pm$  0.01  $\mu$ m) (Figure 4C). This suggests that upon removal of Sec22b the rER expands its size dramatically, possibly to facilitate the accumulation of secretory proteins like VWF. Indeed, immunogold staining for VWF in Sec22b KD ECs localized within dilated rER and was prominently found in the round dense rER structures (Figure 4D). Taken together this shows that VWF exits the ER in a Sec22b dependent manner and upon Sec22b silencing it is retained in rER derived structures.

### ER VWF retention results in reduced VWF secretion in Sec22b depleted cells

The lack of mature VWF, as well as the shorter WPB size, prompted us to investigate how much VWF is stored and secreted in absence of Sec22b. We observed that in the Sec22b-depleted cells, intracellular VWF levels were slightly increased when compared to control cells (Figure 5A), potentially due to VWF entrapment in the ER. On the other hand, basal

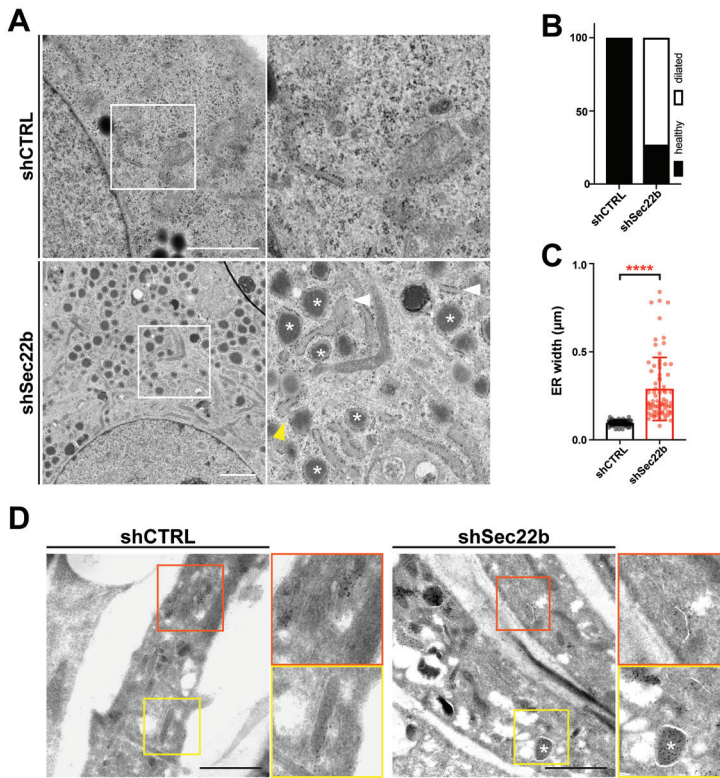


**Figure 4: VWF accumulation in dilated rough ER in Sec22b depleted ECs.** A) EM of control and Sec22b KD ECs (dilated rough ER shown by white arrowheads, ribosome-studded dilated ER by white asterisks, connection of ER structures to rER sheets in yellow arrowhead, scale bar set at 2  $\mu$ m). B) Quantification of healthy versus dilated ER in control and Sec22b KD cells. C) Quantification of ER width in control and Sec22b KD cells (t-test with Welch correction, \*\*\*\*  $P < 0.0001$ ). D) VWF immunogold staining (10 nm gold particles) in control and Sec22b KD ECs (boxed regions are magnified on the right side with the corresponding color, scale bar set at 1  $\mu$ m).

secretion was significantly decreased in Sec22b silenced cells (Figure 5Bi). Basal secretion primarily originates from unstimulated WPB release,<sup>35,36</sup> suggesting this compartment is smaller upon Sec22b depletion. In line with this, VWF release through histamine-induced WPB exocytosis was also significantly reduced (Figure 5Bii). WPBs acquire secretion competence during maturation by recruiting Rab GTPases and Rab-effectors,<sup>7</sup> so potentially this decrease could be attributed to defects in WPB maturation in Sec22b-depleted cells. We assessed whether two maturation-dependent components of the exocytotic machinery, Rab27A and Slp4-a,<sup>37,38</sup> were recruited to WPBs but found no difference between shSec22b and shCTRL cells (Supplemental Figure III). Thus, the simplest explanation for reduction in (stimulated) VWF secretion is failure of sufficient VWF to progress to a stimulus-sensitive compartment, i.e. the WPBs, because it is retained in the ER.

## Discussion

SNARE proteins are key drivers of membrane fusion that initiate and regulate specificity of membrane docking and bilayer mixing.<sup>28</sup> There is a subcategory of SNAREs, known as longin-SNAREs (Ykt6, VAMP7 and Sec22b), that generally participate in fusion events during biogenesis, maturation and exocytosis of secretory organelles in eukaryotic cells.<sup>39-43</sup> In this

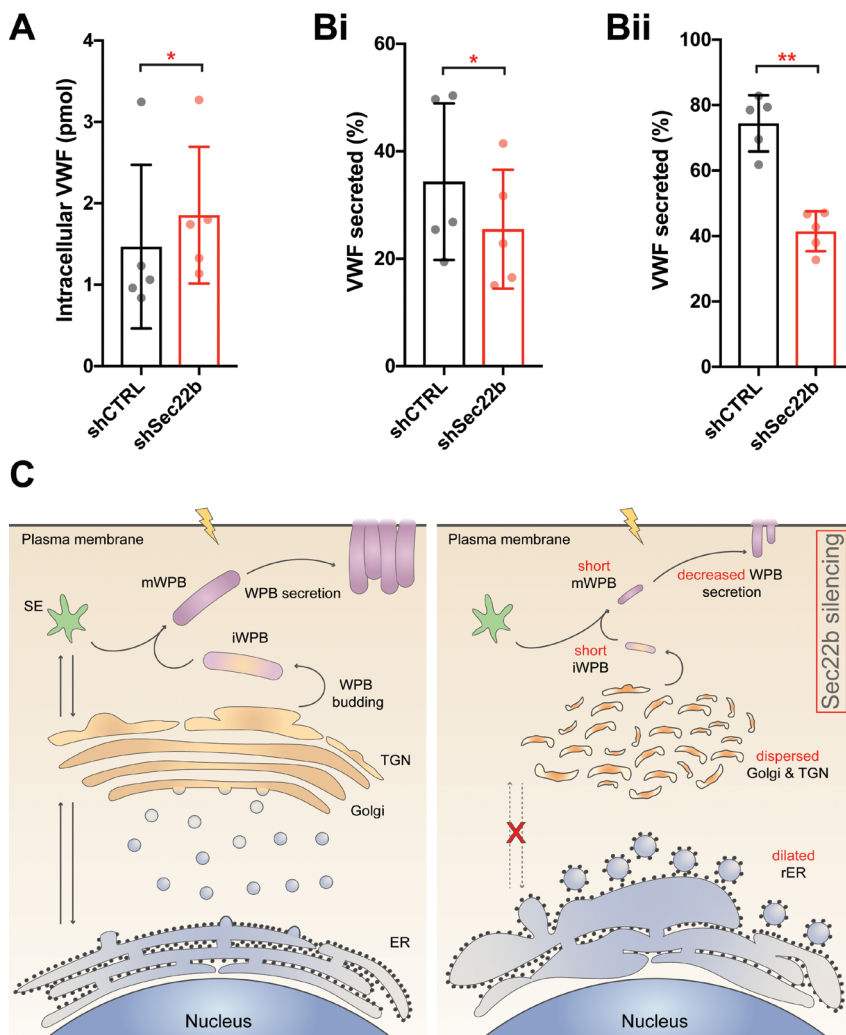


**Figure 5: Sec22b silencing results in reduced basal and stimulated secretion.** A) Intracellular VWF content in control and Sec22b-silenced ECs measured by ELISA (n=5, paired t-test, \*  $P < 0.05$ ). B) Basal VWF release presented as percentage of intracellular VWF content (n=5, paired t-test, \*  $P < 0.05$ ). Bii) Histamine-stimulated VWF release presented as percentage of intracellular VWF content (n=3 independent experiments, paired t-test, \*\*  $P < 0.01$ ). C) Proposed model of Sec22b-dependent VWF trafficking and WPB size control.

study, we used a short hairpin RNA screen targeting longin-SNAREs to identify Sec22b as a novel regulator of WPB formation and VWF trafficking, its depletion leading to short and “stubby” WPBs that were accompanied with Golgi disintegration and retention of VWF in the endoplasmic reticulum.

Sec22b is a known participant in anterograde transport of cargo in the early secretory pathway.<sup>44,45</sup> Overexpression of the Sec22b- $\Delta$ SNARE variant led to a dominant negative effect resulting in smaller WPBs, corroborating experiments that used RNAi and CRISPR strategies to deplete Sec22b expression. This is most probably a consequence of Sec22b- $\Delta$ SNARE outcompeting endogenous Sec22b while failing to properly bind with its cognate SNAREs due to the lack of the SNARE helix,<sup>46</sup> which precludes formation of a complete *trans*-SNARE complex and subsequent membrane fusion. The importance of a functional, fusion competent Sec22b has also been highlighted by mutations in the SNARE domain of

the *Drosophila* homologue of Sec22b, which caused disruption of ER-Golgi transport and resulted in cargo retention in the ER and abnormal ER morphology;<sup>47</sup> similar ER cargo retention is likely at play in Sec22b-depleted ECs in our study (Figure 3&4). Congestion of anterograde flux from the ER limits the supply of VWF to the Golgi and as WPB formation is driven by condensation of multimeric VWF in the TGN, we assume this reduction is (at least partly) responsible for the smaller size of WPBs.

The smaller WPB phenotype is likely further exacerbated by the fragmentation of the TGN (Figure 2), which was previously proposed to limit the possibility of adjacent VWF quanta copackaging into a single, extended WPB.<sup>22</sup> Interestingly, that study also demonstrated that experimental reduction of VWF trafficking by siRNA silencing of VWF synthesis led to reduction of WPB length without affecting overall Golgi morphology. The data we present here suggest that a Sec22b-dependent trafficking pathway is used both by VWF and by components that establish or maintain Golgi ribbon integrity. This is in line with previous studies of Sec22b in other models, such as an *Arabidopsis* mutant deficient for the Sec22b homolog, which displayed comparable TGN disruption.<sup>48</sup> The observed phenotype may be a consequence of defective trafficking of direct regulators of Golgi morphology, such as Golgi reassembly stacking proteins (GRASPs)<sup>49</sup> or Golgins.<sup>50</sup> Indeed, Golgi fragmentation and the concomitant length reduction of WPBs has also been observed after depletion of Golgi tethering proteins (GM130, GRASP55 and Giantin).<sup>22</sup> TGN fragmentation may also merely result from the induced imbalance in trafficking, as the phenotype was also reported after disruption of retrograde trafficking from early endosomes or within the Golgi.<sup>51,52</sup> While further investigation is required to decipher the precise role of Sec22b in the maintenance of TGN morphology, the resulting consequences highlight its indispensable function in ensuring adequate trafficking of VWF and WPB biogenesis.

Upon Sec22b silencing, dilated ER cisternae were observed accompanied by electron dense ribosome-studded rER structures that contain VWF aggregates. There is a striking resemblance with the dilated ER morphology that is observed in response to VWD causing mutations in VWF that affect its ability to dimerize and leave the ER.<sup>53,54</sup> Sec22b is recruited onto ER-derived COPII vesicles that transfer proteins from the ER to the Golgi, through interactions of its longin domain with Sec23/Sec24 of the COPII coating complex.<sup>55,56</sup> Similar dilated ER phenotypes and ER retention of secretory proteins have been previously described in chondrocytes from *sec24d* deficient zebrafish<sup>57</sup> and in pancreatic acinar cells from Sec23b<sup>sl/gt</sup> mice that additionally display lack of zymogen granules.<sup>58</sup> This suggests that the rate of COPII-mediated anterograde ER-Golgi traffic underpins the ability of ECs to shape WPBs to their typical elongated morphology.

A recent study has identified GBF1 as a dynamic regulator of anterograde VWF trafficking and WPB morphology that, dependent on external/environmental cues, controls the flux of proteins (including VWF) from ER to Golgi.<sup>59</sup> Similar to what we observed after Sec22b silencing, depletion of GBF1 led to accumulation of VWF in the ER and a reduction in the overall state of VWF proteolytic processing. However, a number of important phenotypic differences suggest that GBF1 and Sec22b operate through different mechanisms. Unlike Sec22b, GBF1 depletion did not affect Golgi morphology and, unexpectedly, resulted in unusually large WPBs that remain associated with or in close vicinity of the Golgi. Despite their length reduction, WPBs in Sec22b depleted cells normally recruited exocytotic components such as Rab27A and Slp4-a (Supplemental Figure III), contrary to the enlarged WPBs in GBF1 ablated cells which failed to acquire post-Golgi cargo and Rab27A and which were secretion incompetent.<sup>59</sup> Although their short WPBs were still agonist responsive, Sec22b-depleted ECs secreted reduced levels of VWF through the regulated and basal secretory pathway (Figure 4B), which we presume is due to a reduction in WPB pool size. These discrepancies emphasize that future studies are needed to clarify how such opposing effects on WPB formation and secretion can arise from defects in anterograde ER- Golgi transport.

In sum, our study has identified Sec22b as a new regulatory component of the endo-



thelial secretory pathway that controls VWF trafficking and the morphology of its carrier organelle the WPB. We propose a model (Figure 5C) in which secretory proteins such as VWF and components that control Golgi morphology utilize a Sec22b-dependent pathway to arrive at the Golgi, where VWF is packaged in elongated WPBs with dimensions that are proportional to the size of the Golgi. The reduction in WPB length in the absence of Sec22b is explained by a combination of retention of VWF in the ER and disintegration of the Golgi. Reduced flux of VWF through the secretory pathway ultimately decreases the amount of VWF that can be secreted by ECs that lack Sec22b function. This highlights the importance of efficient transport of VWF through the secretory pathway prior to its packaging in WPBs and identifies Sec22b as a potential determinant of plasma VWF levels. Future studies should address the impact of components of this protein complex on VWF plasma levels in patients with bleeding and thrombotic disorders.

### **Authorship**

EK, JO, and AM performed research and analyzed data; DG and CJ contributed vital reagents and expertise; EK, JV and RB designed the research; EK, JV and RB wrote the paper.

### **Acknowledgements**

This study was supported by grants from the Landsteiner Stichting voor Bloedtransfusie Research (LSBR-1707), the Netherlands Ministry of Health (PPOC-2015-24P) and the Dutch Thrombosis Foundation (TSN 2017-01).

## References

1. Gomez-Navarro, N. & Miller, E. Protein sorting at the ER-Golgi interface. *J. Cell Biol.* (2016). doi:10.1083/jcb.201610031
2. Araki, K. & Nagata, K. Protein folding and quality control in the ER. *Cold Spring Harb. Perspect. Biol.* 3, (2011).
3. Cooper, G. M. & Hausman, R. E. *The Cell: A Molecular Approach*. (Sinauer Associates Inc., U.S., 2019).
4. Halban, P. A. & Irminger, J. C. Sorting and processing of secretory proteins. *Biochemical Journal* 299, 1–18 (1994).
5. Huizing, M., Helip-Wooley, A., Westbroek, W., Gunay-Aygun, M. & Gahl, W. A. Disorders of Lysosome-Related Organelle Biogenesis: Clinical and Molecular Genetics. *Annu. Rev. Genomics Hum. Genet.* 9, 359–386 (2008).
6. Weibel, E. R. & Palade, G. E. New cytoplasmic components in arterial endothelia. *J. Cell Biol.* 23, 101–112 (1964).
7. Schillemans, M., Karampini, E., Kat, M. & Bierings, R. Exocytosis of Weibel-Palade bodies: how to unpack a vascular emergency kit. *Journal of Thrombosis and Haemostasis* 17, 6–18 (2019).
8. Sadler, J. E. Biochemistry and genetics of von Willebrand factor. *Annu. Rev. Biochem.* 67, 395–424 (1998).
9. Wagner, D. D. et al. Induction of specific storage organelles by von Willebrand factor propeptide. *Cell* 64, 403–13 (1991).
10. Voorberg, J. et al. Biogenesis of von Willebrand factor-containing organelles in heterologous transfected CV-1 cells. *EMBO J.* 12, 749–758 (1993).
11. Groeneveld, D. J. et al. Angiogenic characteristics of blood outgrowth endothelial cells from patients with von Willebrand disease. *J. Thromb. Haemost.* 13, 1854–66 (2015).
12. Schillemans, M. et al. Alternative trafficking of Weibel-Palade body proteins in CRISPR/Cas9-engineered von Willebrand factor-deficient blood outgrowth endothelial cells. *Res. Pract. Thromb. Haemost.* 3, 718–732 (2019).
13. Michaux, G. et al. The physiological function of von Willebrand's factor depends on its tubular storage in endothelial Weibel-Palade bodies. *Dev. Cell* 10, 223–232 (2006).
14. Huang, R.-H. et al. Assembly of Weibel-Palade body-like tubules from N-terminal domains of von Willebrand factor. *Proc. Natl. Acad. Sci. U. S. A.* 105, 482–7 (2008).
15. Berriman, J. A. et al. Structural organization of Weibel-Palade bodies revealed by cryo-EM of vitrified endothelial cells. *Proc. Natl. Acad. Sci. U. S. A.* 106, 17407–17412 (2009).
16. Valentijn, K. M. & Eikenboom, J. Weibel-Palade bodies: A window to von Willebrand disease. *Journal of Thrombosis and Haemostasis* 11, 581–592 (2013).
17. Dong, J. F. et al. ADAMTS-13 rapidly cleaves newly secreted ultralarge von Willebrand factor multimers on the endothelial surface under flowing conditions. *Blood* 100, 4033–4039 (2002).
18. Zheng, Y., Chen, J. & López, J. A. Flow-driven assembly of VWF fibres and webs in vitro microvessels. *Nat. Commun.* 6, 7858 (2015).
19. De Ceunynck, K., De Meyer, S. F. & Vanhoo-relbeke, K. Unwinding the von Willebrand factor strings puzzle. *Blood* 121, 270–277 (2013).
20. Sadler, J. E. von Willebrand factor assembly and secretion. *J. Thromb. Haemost.* 7, 24–27 (2009).
21. Ferraro, F. et al. Weibel-Palade body size modulates the adhesive activity of its von Willebrand Factor cargo in cultured endothelial cells. *Sci. Rep.* 6, 32473 (2016).
22. Ferraro, F. et al. A two-tier golgi-based control of organelle size underpins the functional plasticity of endothelial cells. *Dev. Cell* 29, 292–304 (2014).
23. Springer, T. A. von Willebrand factor, Jedi knight of the bloodstream. *Blood* 124, 1412–1426 (2014).
24. Zhou, Y.-F. et al. A pH-regulated dimeric bouquet in the structure of von Willebrand factor. *The EMBO Journal* 30, 4098–4111 (2011).
25. Purvis, A. R. et al. Two Cys residues essential for von Willebrand factor multimer assembly in the Golgi. *Proc. Natl. Acad. Sci. U. S. A.* 104, 15647–52 (2007).
26. Zenner, H. L., Collinson, L. M., Michaux, G. & Cutler, D. F. High-pressure freezing provides insights into Weibel-Palade body biogenesis. *J. Cell Sci.* 120, 2117–2125 (2007).
27. Mourik, M. J. et al. Content delivery to newly forming Weibel-Palade bodies is facilitated by multiple connections with the Golgi apparatus. *Blood* 125, 3509–16 (2015).
28. Jahn, R. & Scheller, R. H. SNAREs—engines for membrane fusion. *Nat. Rev. Mol. Cell Biol.* 7, 631–43 (2006).
29. Daste, F., Galli, T. & Taresté, D. Structure and function of longin SNAREs. *J. Cell Sci.* 128, 4263–4272 (2015).
30. Lenzi, C. et al. Synaptotagmin 5 regulates Ca<sup>2+</sup>-dependent Weibel-Palade body exocytosis in human endothelial cells. *J. Cell Sci.* 132, (2019).
31. Karampini, E. et al. Defective AP-3-dependent VAMP8 trafficking impairs Weibel-Palade body exocytosis in Hermansky-Pudlak Syndrome type 2 blood outgrowth endothelial cells. *Haematologica haematol.2018.207787* (2019). doi:10.3324/haematol.2018.207787
32. Sanjana, N. E., Shalem, O. & Zhang, F. Improved vectors and genome-wide libraries for CRISPR screening. *Nat. Methods* 11, 783–784 (2014).

33. van Breevoort, D. et al. STXB1 promotes Weibel-Palade body exocytosis through its interaction with the Rab27A effector Slp4-a. *Blood* 123, 3185–94 (2014).
34. Vischer, U. M. & Wagner, D. D. von Willebrand factor proteolytic processing and multimerization precede the formation of Weibel-Palade bodies. *Blood* 83, 3536–44 (1994).
35. Giblin, J. P., Hewlett, L. J. & Hannah, M. J. Basal secretion of von Willebrand factor from human endothelial cells. *Blood* 112, 957–64 (2008).
36. Lopes da Silva, M. & Cutler, D. F. von Willebrand factor multimerization and the polarity of secretory pathways in endothelial cells. *Blood* 128, 277–85 (2016).
37. Hannah, M. J. et al. Weibel-Palade bodies recruit Rab27 by a content-driven, maturation-dependent mechanism that is independent of cell type. *J. Cell Sci.* 116, 3939–3948 (2003).
38. Bierings, R. et al. The interplay between the Rab27A effectors Slp4-a and MyRIP controls hormone-evoked Weibel-Palade body exocytosis. *Blood* 120, 2757–2768 (2012).
39. Jani, R. A., Purushothaman, L. K., Rani, S., Bergam, P. & Setty, S. R. G. STX13 regulates cargo delivery from recycling endosomes during melanosome biogenesis. *J. Cell Sci.* 128, 3263–3276 (2015).
40. Koseoglu, S. et al. VAMP-7 links granule exocytosis to actin reorganization during platelet activation. *Blood* 126, 651–661 (2015).
41. Kweon, Y., Rothe, A., Conibear, E. & Stevens, T. H. Ykt6p is a multifunctional yeast R-SNARE that is required for multiple membrane transport pathways to the vacuole. *Mol. Biol. Cell* 14, 1868–81 (2003).
42. Matsui, T. et al. Autophagosomal YKT6 is required for fusion with lysosomes independently of syntaxin 17. *J. Cell Biol.* 217, 2633–2645 (2018).
43. Dai, J. et al. Vps33b regulates Vwf-positive vesicular trafficking in megakaryocytes. *J. Pathol.* 240, 108–119 (2016).
44. Zhang, T., Wong, S. H., Tang, B. L., Xu, Y. & Hong, W. Morphological and functional association of Sec22b/ERS-24 with the pre-Golgi intermediate compartment. *Mol. Biol. Cell* 10, 435–53 (1999).
45. Liu, Y. & Barlowe, C. Analysis of Sec22p in endoplasmic reticulum/Golgi transport reveals cellular redundancy in SNARE protein function. *Mol. Biol. Cell* 13, 3314–24 (2002).
46. Liu, Y., Flanagan, J. J. & Barlowe, C. Sec22p export from the endoplasmic reticulum is independent of SNARE pairing. *J. Biol. Chem.* 279, 27225–32 (2004).
47. Zhao, X. et al. Sec22 Regulates Endoplasmic Reticulum Morphology but Not Autophagy and Is Required for Eye Development in *Drosophila*. *J. Biol. Chem.* 290, 7943–7951 (2015).
48. El-Kasbi, F. et al. Arabidopsis SNARE protein SEC22 is essential for gametophyte development and maintenance of Golgi-stack integrity. *Plant J.* 66, 268–79 (2011).
49. Xiang, Y. & Wang, Y. GRASP55 and GRASP65 play complementary and essential roles in Golgi cisternal stacking. *J. Cell Biol.* 188, 237–51 (2010).
50. Wang, T., Grabski, R., Sztul, E. & Hay, J. C. p115-SNARE interactions: a dynamic cycle of p115 binding monomeric SNARE motifs and releasing assembled bundles. *Traffic* 16, 148–71 (2015).
51. Shitara, A. et al. VAMP4 is required to maintain the ribbon structure of the Golgi apparatus. *Mol. Cell. Biochem.* 380, 11–21 (2013).
52. Zolov, S. N. & Lupashin, V. V. Cog3p depletion blocks vesicle-mediated Golgi retrograde trafficking in HeLa cells. *J. Cell Biol.* 168, 747–59 (2005).
53. Wang, J. W. et al. Intracellular storage and regulated secretion of Von Willebrand factor in quantitative Von Willebrand disease. *J. Biol. Chem.* 286, 24180–24188 (2011).
54. Wang, J. W. et al. Biogenesis of Weibel-Palade bodies in von Willebrand's disease variants with impaired von Willebrand factor intrachain or interchain disulfide bond formation. *Haematologica* 97, 859–866 (2012).
55. Mancias, J. D. & Goldberg, J. The Transport Signal on Sec22 for Packaging into COPII-Coated Vesicles Is a Conformational Epitope. 403–414 (2007). doi:10.1016/j.molcel.2007.03.017
56. Adolf, F. et al. Proteomic Profiling of Mammalian COPII and COPI Vesicles. *Cell Rep.* 26, 250–265.e5 (2019).
57. Ohisa, S., Inohaya, K., Takano, Y. & Kudo, A. Sec24d encoding a component of COPII is essential for vertebra formation, revealed by the analysis of the medaka mutant, vbi. *Dev. Biol.* 342, 85–95 (2010).
58. Tao, J. et al. SEC23B is required for the maintenance of murine professional secretory tissues. *Proc. Natl. Acad. Sci. U. S. A.* 109, (2012).
59. Lopes-da-Silva, M. et al. A GBF1-Dependent Mechanism for Environmentally Responsive Regulation of ER-Golgi Transport. *Dev. Cell* 1–16 (2019). doi:10.1016/j.devcel.2019.04.006

## Supplemental Materials and Methods

### Immunoblotting

Endothelial cells were grown to confluency and lysed in NP-40 based lysis buffer (0.5% NP-40, 0.5 mM EDTA, 10 mM Tris HCl pH 7.4, 150 mM NaCl), supplemented with Complete protease inhibitor cocktail (Roche, 05056489001). Proteins were separated on a Novex® NuPAGE® 4-12% Bis-Tris gel (ThermoFisher, NP0321/NP0323) and transferred onto a nitrocellulose membrane (iBlot Transfer Stack, ThermoFisher, IB3010). Membranes were blocked with Odyssey blocking buffer (LI-COR Biosciences, Lincoln, USA, LI 927) and probed with primary antibodies and subsequently with IRDye conjugated secondary antibodies (see Supplementary Table I). Visualization of IRDye conjugated antibodies was performed by means of LI-COR Odyssey Infrared Imaging System (LI-COR Biosciences). Blot analysis for band intensities was done in Image Studio Lite (V4.0, LI-COR Biosciences) and when needed intensities were normalized to the intensity of  $\alpha$ -tubulin, which was used as a loading control.

### Fluorescence microscopy

Immunostaining and fluorescence imaging of fixed cells was performed as previously described.<sup>5</sup> Immunostained cells were mounted in MOWIOL mounting medium and images were acquired using a Leica SP8 confocal microscope (Leica, Wetzlar, Germany). Images were processed and analyzed using ImageJ (<https://imagej.nih.gov/ij/>). WPB length (major axis of cigar-shaped VWF positive structures) and TGN area (periphery of TGN46 staining) were measured as pixels and automatically converted in  $\mu\text{m}$  scale in ImageJ; box graphs were plotted in GraphPad Prism 8.

### Secretion assay

Endothelial cells were grown in 6-well plates and cultured for 7 days prior to the experiment with regular medium replacement. Basal VWF release was determined as unstimulated secretion over 24 hours in EGM-18 medium. For histamine-induced secretion cells were pre-incubated in release medium [RM: serum-free M199 (ThermoFisher, 22340) supplemented with 0.2% (w/v) bovine serum albumin (BSA) (Merck, 112018)] for 15-30 minutes prior to stimulation. Cells were stimulated in RM medium supplemented with 100  $\mu\text{M}$  histamine (Sigma-Aldrich, H7125). Lysates were obtained in NP-40 based lysis buffer supplemented with Complete protease inhibitor cocktail. VWF levels were determined by ELISA as described previously.<sup>1</sup> Secretion is expressed as relative proportion of intracellular VWF in lysates of unstimulated cells.

### VWF multimer analysis

Endothelial cell lysates, produced as described in Immunoblotting, were appropriately diluted to a final concentration of 1 nM. Samples were loaded onto freshly prepared (10 $\times$ 10 cm, 1.5 mm) agarose gels (SeaKem® HGT(P) Agarose, Lonza, 50050) (stacking gel: 0.75% Agarose, running gel: 1.8% Agarose) and separated for approximately 3 hours at 100V and 35 mA. VWF multimers were transferred to a PVDF membrane (BIO-RAD, 162-0177) overnight. Membranes were stained with an anti-VWF-HRP antibody (see Supplementary Table I). Chromogenic visualization of HRP was achieved with DAB peroxidase substrate kit (Vector Laboratories, SK-4100). Images were analyzed using ImageJ (<https://imagej.nih.gov/ij/>) and densitometry profiles were plotted in GraphPad Prism 8.

### Electron microscopy

Cells were fixed by adding double concentrated fixative to the culture dish (end concentration of fixative: 1,5% glutaraldehyde (GA) with 0.1M cacodylate buffer) and incubating for 2 hours at room temperature. After rinsing the cells 3 time with 0,1M cacodylate buffer, the cells were postfixed with 1% OsO<sub>4</sub>/0.1M cacodylatebuffer on ice for 1 hour. Dehydration followed with a

series of ethanol solutions and after that mixtures with EPON (LX112, Leadd) and ethanol 100%, and finally pure EPON. Beem capsules filled with EPON were placed on the dishes with the open face down. After EPON polymerization at 40° at the first night, followed by a day at 70°C, the beem capsules could be snapped off. 80 µm sections parallel to the surface of the Beem capsules containing the cultured cells were contrasted with uranylacetate and leadcitrate. Examination of the sections was done on a Fei Tecnai Twin transmission electron microscope (FEI, Eindhoven, Netherlands). Overlapping images were collected and stitched together into separate images, as previously described.<sup>2</sup>

### Immunoelectron microscopy

Cells were fixed in 2% PFA/0,2%GA/0,1M PHEM buffer at room temperature for 2 hours. Cells were scraped using a single use plastic scraper and collected in a pellet in 12% gelatin. Pellets were cut into smaller pieces of ~1 mm<sup>3</sup> and were impregnated with 2.3M sucrose in PBS (60 min), mounted on a stub and snap frozen in liquid nitrogen. 90 µm sections were made with a Leica EM ultracytome and were collected on grids. Grids were labeled with rabbit anti-VWF (1:1000) (see Supplemental Table I) and stained with 10 nm PAAu gold in 1%BSA/PBS following a protocol described previously.<sup>3</sup> After rinsing the sections, the grids were mounted in 0,3% uranylacetate / 2% methylcellulose solution and were examined as described above.

### Data and statistical analysis

Statistical analysis was by student's t-test and using GraphPad Prism 8 (Graphpad, La Jolla, CA, USA). Significance values are shown in the Figures and in Figure legends. Data are shown as box graphs (min. to max.), as mean ± SEM or as contingency stacked bar graphs.

## Supplemental Figures and Tables

**Supplemental Table I: Antibody reagents**

target	Species (isotype)	Label	Supplier	Cat.nr /clone	Application [concentration/dilution]
VWF	mouse (IgG <sub>2b</sub> )	-	described in <sup>4</sup>	CLB-RAG20	IF [1:1000]
α-tubulin	mouse (IgG <sub>1</sub> )	-	Sigma-Aldrich	T9026	WB [1:1000]
VWF	rabbit	-	DAKO	A0082	ELISA [6 µg/ml]
VWF	rabbit	HRP	DAKO	A0082	WB [3µg/ml], ELISA [2 µg/ml]
Sec22b	rabbit	-	Synaptic Systems	186 003	IF [2 µg/ml], WB [1 µg/ml]
TGN46	sheep	-	Bio-Rad	AHP500GT	IF [1:1000]
Rab27A	rabbit	-	described in <sup>5</sup>	B2423	IF [1:100]
Slp4-a	rabbit	-	Atlas Antibodies	HPA001475	IF [1:500]
Hoechst	-	-	Life Technologies	H-1399	IF [1:50]
rabbit IgG	donkey	680LT	Li-Cor	925-68023	WB [0.1 µg/ml]
mouse IgG	donkey	800CW	Li-Cor	925-32212	WB [0.1 µg/ml]
rabbit IgG	goat	AF633	ThermoFisher	A11011	IF [2 µg/ml]
mouse IgG	goat	AF568	ThermoFisher	A11004	IF [2 µg/ml]
mouse IgG	goat	AF488	ThermoFisher	A11004	IF [2 µg/ml]
rabbit IgG	chicken	AF647	ThermoFisher	A21443	IF [2 µg/ml]

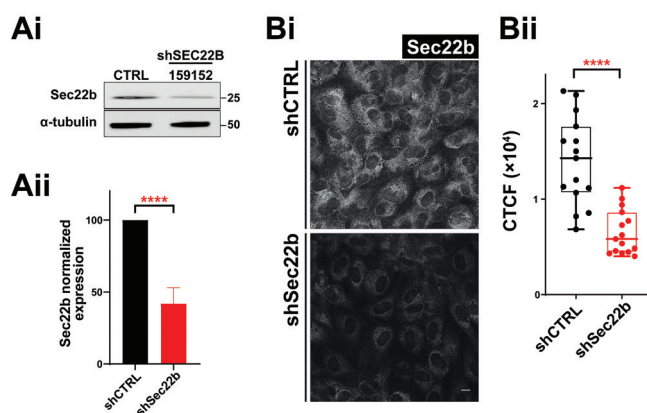
Supplemental Table II: MISSION® Library shRNAs used in this study

target	shRNA clone MISSION® library	shRNA target sequence
Sec22b	TRCN0000159152	GCCATCAATGAGATTTAACTT
	TRCN0000159288	GCCACAATTTGCTAACATTTA
VAMP7	TRCN0000059888	GCGAGGAGAAGATTGGAATT
	TRCN0000059889	GCTCACTATTATCATCATCAT
	TRCN0000059890	GAGCAGATTCTGGCTAAGATA
	TRCN0000059891	GCACTTCCATATGCCATGAAT
	TRCN0000059892	CGTACTCACATGGCAATTATT
Ykt6	TRCN0000059763	GCCGAAGTATGAGACCAAA
	TRCN0000059764	CGCATACGATGTGTCTTCCTT
	TRCN0000059765	GAGAAGCTGATCCCATGACTA
	TRCN0000059766	CGGAATGATAGTCTTGCAGGT
	TRCN0000059767	ACAGTCTAAAGCCTTCTATAA
non-targeting control (shCTRL)	-	CAACAAGATGAAGACCAAA

Supplemental Table III: SEC22B gRNAs used in this study

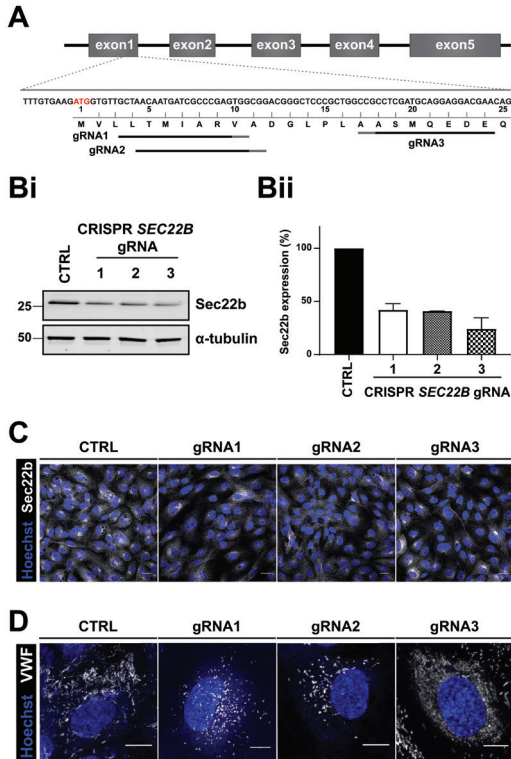
gRNA	target sequence (+PAM)	oligo	oligo sequence
gRNA1	GCTAACAATGATCGCCCGAGTGG	RBNL411	5'-caccgGCTAACAATGATCGCCCGAG-3'
		RBNL412	5'-aacCTCGGGCGATCATTGTTAGC-3'
gRNA2	AACAAATGATCGCCCGAGTGGCGG	RBNL413	5'-caccgAACAAATGATCGCCCGAGTGG-3'
		RBNL414	5'-aacCCACTCGGGCGATCATTGTTc-3'
gRNA3	TTCGTCTCTCTGCATCGAGGCGG	RBNL415	5'-caccgTTCGTCTCTCTGCATCGAGG-3'
		RBNL416	5'-aacCCTCGATGCAGGAGGACGAac-3'

Supplemental Figure I



**Supplemental Figure I: shRNA silencing of Sec22b in endothelial cells.** A) Sec22b expression in HUVEC lysates after Sec22b silencing determined using immunoblotting (Ai). α-tubulin was used as a loading control. Molecular weight indicators are shown on the right in kDa. (Aii) Quantification of Sec22b expression in Sec22b silenced endothelial cells normalized to shCTRL treated cells. Bi) Immunostaining of Sec22b in shCTRL- and shSec22b-treated HUVECs. Bii) Quantification of Sec22b immunoreactivity (corrected total cell fluorescence, CTCF) in shCTRL- and shSec22b-treated cells.

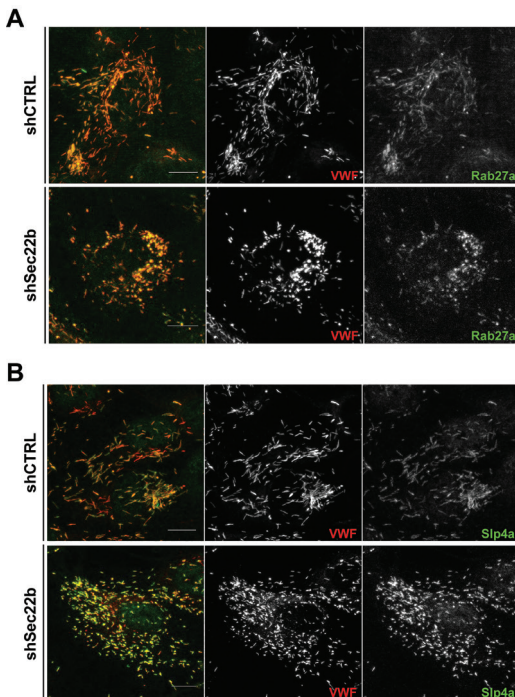
## Supplemental Figure II



## Supplemental Figure II: Analysis of bulk populations of Sec22b CRISPR-engineered HUVECs

A) Graphic representation of gRNA design at the exon 1 of *SEC22B* for CRISPR/Cas9 knock out generation. gRNAs and PAMs are indicated underneath the sequence and translated region. Bi) WB analysis of Sec22b expression in control and gRNA1, 2 and 3 samples ( $\alpha$ -tubulin as loading control). Bii) Bar graph of Sec22b normalized expression in control and CRISPR knock out cells. C) Immunofluorescent staining of Sec22b in CTRL, gRNA1, gRNA2 and gRNA3 HUVECs (blue channel: nucleus staining). D) Immunofluorescent staining of VWF in CTRL, gRNA1, gRNA2 and gRNA3 HUVECs (blue channel: nucleus staining). shSec22b-treated HUVECs. Bii) Quantification of Sec22b immunoreactivity (corrected total cell fluorescence, CTCF) in shCTRL- and shSec22b-treated cells.

## Supplemental Figure III



## Supplemental Figure III: Maturation of WPBs is not affected shSec22b-silenced endothelial cells.

A) Immunofluorescent staining of VWF (red) and Rab27A (green) in shCTRL and shSec22b HUVECs (scale bar set at 10  $\mu$ m, merge of channels on the left). B) Immunofluorescent staining of VWF (red) and Slp4a (green) in shCTRL and shSec22b HUVECs (scale bar set at 10  $\mu$ m, merge of channels on the left).

## Supplemental References

1. Schillemans M, Karampini E, van den Eshof B, et al. The Weibel-Palade body localized SNARE syntaxin-3 modulates Von Willebrand factor secretion from endothelial cells. *Arterioscler. Thromb. Vasc. Biol.* 2018;in press:1–31.
2. Faas FGA, Avramut MC, van den Berg BM, et al. Virtual nanoscopy: generation of ultra-large high resolution electron microscopy maps. *J. Cell Biol.* 2012;198(3):457–69.
3. Peters PJ, Bos E, Griekspoor A. Cryo-immunogold electron microscopy. *Curr. Protoc. cell Biol.* 2006;Chapter 4:Unit 4.7.
4. Stel H V, Sakariassen KS, Scholte BJ, et al. Characterization of 25 monoclonal antibodies to factor VIII-von Willebrand factor: relationship between ristocetin-induced platelet aggregation and platelet adherence to subendothelium. *Blood.* 1984;63(6):1408–1415.
5. Bierings R, Hellen N, Kiskin N, et al. The interplay between the Rab27A effectors Slp4-a and MyRIP controls hormone-evoked Weibel-Palade body exocytosis. *Blood.* 2012;120(13):2757–2768.





# Chapter 4

## Weibel-Palade body biogenesis is dependent on the Golgi Qa-SNARE STX5

Ellie Karampini, Jenny Olins, Aat Mulder, Floris van Alphen,  
Dirk Geerts, Carolina Jost, Maartje van den Biggelaar, Jan Voorberg  
and Ruben Bierings

*Manuscript in preparation*

## Abstract

Von Willebrand factor (VWF), a multimeric hemostatic protein primarily synthesized in endothelial cells (ECs), facilitates the arrest of platelets from the circulation at the site of vascular damage and initiates the primary hemostatic plug. VWF is temporarily stored in endothelial storage organelles, the Weibel-Palade bodies (WPBs), whose biogenesis and morphology are strongly related to VWF anterograde trafficking and Golgi morphology. We have previously identified Sec22b, an ER-to-Golgi SNARE, as a novel regulator of WPB elongation through its involvement in Golgi integrity and VWF anterograde transport. In this study we aimed to further elucidate the molecular determinants of WPB morphology by looking into the role of endothelial Sec22b interaction partners. Using a mass spectrometry-based approach we identified a vast array of proteins within the Sec22b interactome that potentially regulate WPB biogenesis and morphology, including the Golgi Qa-SNARE STX5. To investigate the role of STX5 in WPB biogenesis we depleted STX5 in endothelial cells using shRNA silencing and followed WPB biogenesis and ER and Golgi morphology using confocal and electron microscopy. STX5 depleted ECs exhibited decreased WPB length, ER dilation and extensive Golgi fragmentation. This subsequently led to reduced intracellular VWF levels and reduced stimulus-induced VWF secretion. Finally, we examined the whole proteome changes in shSTX5 and shSec22b KD ECs and found that STX5 downregulation resulted in a drastic alteration of the proteome, that negatively affected several intracellular compartments. Taken together our study has identified STX5 as a novel SNARE protein that plays a major role in WPB formation and VWF release.

## Introduction

Von Willebrand factor (VWF) is a large multimeric hemostatic protein that is primarily synthesized in endothelial cells and that acts as a chaperone of factor VIII as well as an adhesive grid for initiation of a platelet plug.<sup>1</sup> VWF follows a complex maturation process that includes dimerization and multimerization in the ER and the Golgi respectively, and proteolytic cleavage of the propeptide from the mature protein chain.<sup>2-4</sup> Subsequently, mature VWF multimers are condensed into tubules that are tightly packaged into newly forming storage organelles that emerge from the *trans*-Golgi network (TGN), the Weibel-Palade bodies (WPBs).<sup>5,6</sup> Biogenesis of WPBs is closely linked to VWF synthesis, which is highlighted by the absence of WPBs in VWF knockout endothelial cells and their reconstitution in non-endothelial cells by ectopic expression of VWF.<sup>7-9</sup> WPBs play an important role during primary hemostasis as they ensure the immediate delivery of sufficiently large amounts of VWF to the vessel lumen in response to vascular injury, whereupon VWF tubules unfurl into long platelet-decorated VWF strings on the apical side of the endothelium.<sup>1,10-13</sup>

WPBs have a very distinct, elongated morphology: their cigar-shaped structure consists of densely packed helical tubules of VWF multimers running along the length of the organelle enwrapped by a tightly fitted endomembrane.<sup>14-16</sup> VWF strings' length and adhesive properties have been correlated with WPB morphology and more specifically WPB length; shorter WPBs generate shorter VWF strings with lower adhesive capacity for platelets and plasma VWF.<sup>17</sup> Although WPB length is known to be determined by the morphology of the Golgi as well as by levels of VWF synthesis,<sup>17,18</sup> only recently has control of progression of VWF through the early secretory pathway been appreciated as a cellular switch dictating WPB length. GBF1, a guanine-nucleotide exchange factor (GEF) for the ARF GTPase family translates environmental cues such as glucose exposure, via its phosphorylation state to modulation of anterograde ER-Golgi transport of VWF and WPB length.<sup>19</sup> Interestingly however, loss of GBF1 was accompanied by formation of giant, secretion incompetent WPBs. A recent proteomic study of the WPB interactome also identified GBF1, along with

several proteins of the anterograde trafficking pathway, including the subunits of the coat protein complex II (COPII) Sec23 and Sec24, and the v-SNARE Sec22b.<sup>20</sup>

The COPII complex is a heteropentameric protein complex that assembles at specific ER microdomains, so called ER exit sites, where it concentrates specific cargo proteins en route to the Golgi, while simultaneously initiating ER membrane budding and vesicle fission.<sup>21</sup> During this process Sec22b is also incorporated as part of the fusion machinery.<sup>22</sup> Budded off COPII vesicles are then transported towards the Golgi and fuse with the target membrane through the formation of Sec22b containing SNARE complexes.<sup>23</sup> Exocytic SNARE proteins play a key role in secretion of VWF from WPBs<sup>24–28</sup> and some have also been associated with VWF plasma levels and severity of von Willebrand disease (VWD).<sup>29,30</sup> The role of SNARE proteins in WPB biogenesis and VWF trafficking, however, is largely unknown. We have recently identified the longin-SNARE Sec22b as a novel determinant of WPB length that supports endothelial Golgi integrity and ER to Golgi transport of VWF.<sup>31</sup>

In the current study, we mapped the anterograde fusion machinery in endothelial cells using a proteomic screen of the Sec22b interactome in order to identify novel determinants of VWF trafficking. We identify a network that consists of components of the NRZ complex, the exocyst complex, SNARE-proteins and their regulatory proteins, including the t-SNARE syntaxin 5 (STX5). STX5 knockdown results in extensive fragmentation of Golgi architecture, dilation of the ER, and significantly shorter and fewer WPBs. VWF intracellular levels and regulated WPB exocytosis were significantly suppressed, highlighting STX5 as an essential component of the machinery that drives WPB formation.

## Methods

### Antibody list

For further information see Supplemental Table I.

### Cell culture, lentiviral transfection and transduction

Pooled, cryo-preserved primary human umbilical vein endothelial cells (HUVECs) were obtained from Promocell and were cultured and lentivirally transduced as described previously.<sup>25</sup> Lentiviral vectors were produced in Human embryonic kidney 293T (HEK293T) cells (ATCC) using a 3rd generation lentiviral packaging system.<sup>25</sup>

### Lentiviral DNA constructs for mEGFP-Sec22b expression and shRNA silencing of STX5

The lentiviral LVX-mEGFP-LIC vector has been described previously.<sup>32</sup> To construct human Sec22b with mEGFP tagged to its N-terminus, a synthetic Sec22b fragment was generated by gene synthesis containing all 214 codons of the Sec22b coding sequence flanked by *Bsr*GI and *Not*I sites, respectively, to facilitate cloning in frame behind mEGFP in LVX-mEGFP-LIC. Lentiviral vectors with shRNA targeting STX5 (TRCN0000059826, 5'-CCTTAGCAACA-CATTTGCCAA-3') were obtained from the MISSION® shRNA library developed by TRC at the Broad Institute of MIT and Harvard. LKO.1-puro-CMV-mEGFP-U6-shC002, which simultaneously expresses mEGFP and a non-targeting control shRNA from the CMV and U6 promoter respectively, was described previously.<sup>33</sup>

### Mass spectrometry analysis of Sec22b interactome and Sec22b- and STX5-dependent proteome

#### Sec22b interactome

HUVECs expressing lentivirally transduced mEGFP and mEGFP-Sec22b were seeded in 3 separate wells on 6 well culture plates to enable in triplicate sample preparation for pull-

downs of each condition. After 3 days of confluency, cells were rinsed 2x in PBS and subsequently lysed in mass spectrometry (MS) grade lysis buffer (10 mM Tris.HCl (pH 7.5), 150 mM NaCl, 0.5 mM EDTA, 0.5% NP40 (v/v)) supplemented with Halt protease and phosphatase inhibitor cocktail (Thermo Scientific). Lysates were centrifuged for 10 minutes at 16,000g and supernatants were transferred to fresh tubes. Cleared lysates were incubated with magnetic anti-GFP nanobody (nAb) beads or blocked control (CTRL) beads (Allele Biotech, San Diego, USA) by rotation for 2 hours at room temperature. For interactome analysis by MS, beads were collected on a magnetic stand and were washed 3 times with wash buffer (10 mM Tris.HCl (pH 7.5), 150 mM NaCl, 0.5 mM EDTA) supplemented with Halt protease and phosphatase inhibitor cocktail (Thermo Scientific) and two times with 1 ml PBS. Sample preparation, data acquisition and data analysis were performed according to.<sup>34</sup> Due to technical difficulties one of the mEGFP-Sec22b pull-down failed. The calculations were performed on all six samples, but for the statistical analysis only the successful samples were used.

#### Sec22b- and STX5-dependent whole proteome

HUVECs were lentivirally transduced with mEGFP-shSec22b as described in<sup>31</sup> and with shSTX5, along with the control shRNAs and untransduced cells, and seeded in 3 separate wells in 6-well plates. After reaching confluency cells were lysed, samples were processed for mass spectrometry and analyzed as previously described in.<sup>24</sup>

#### Fluorescence microscopy

Imaging of immunostained cells was performed as previously described<sup>24</sup> using a Leica SP8 confocal microscope (Leica). WPBs were visualized using mouse monoclonal anti-VWF CLB-RAg20.<sup>35</sup> TGN was stained used sheep polyclonal anti-TGN46 (Bio-Rad; AHP500GT) Nuclei were stained using Hoechst nuclear dye (Life Technologies; H-1399). Images were processed and analyzed using ImageJ (<https://imagej.nih.gov/ij/>). WPB length (major axis of cigar-shaped VWF positive structures) and TGN area (periphery of TGN46 staining) were measured as pixels and automatically converted in  $\mu\text{m}$  scale in ImageJ; box graphs were plotted in GraphPad Prism 8.

#### Secretion assay

ECs were grown in 6-well plates and cultured for 7 days prior to the experiment with regular medium replacement. Basal VWF release was determined as unstimulated secretion over 24 hours. For histamine-induced secretion cells were stimulated with 100  $\mu\text{M}$  histamine (Sigma-Aldrich; H7125). Lysates were obtained in NP-40 based lysis buffer supplemented with Halt protease and Phosphatase inhibitor cocktail.<sup>36</sup> VWF levels were determined by ELISA as described previously.<sup>25</sup> Secretion is expressed as relative proportion of intracellular VWF in lysates of unstimulated cells.

#### Electron microscopy

Endothelial cells were processed for electron microscopy imaging essentially according to.<sup>25</sup> Examination of the sections was done on a Fei Tecnai Twin transmission electron microscope (FEI, Eindhoven, Netherlands). Overlapping images were collected and stitched together into separate images, as previously described.<sup>37</sup>

#### Data and statistical analysis

Statistical analysis was by student's t-test and using GraphPad Prism 8 (Graphpad, La Jolla, CA, USA). Significance values are shown in the Figures and in Figure legends. Data are shown as box graphs (min. to max.), as mean  $\pm$  SEM or as contingency stacked bar graphs.

## Results

### Sec22b interactome in endothelial cells: anterograde, retrograde and intra-Golgi protein trafficking.

Sec22b has previously been described to be part of an ER-to-Golgi SNARE complex *in vitro* and in living cells.<sup>38</sup> In endothelial cells depletion of Sec22b blocks transfer of VWF from ER to Golgi and results in short WPBs,<sup>31</sup> suggesting it is an essential component of the trafficking machinery of VWF. In order to determine the composition of the ER-to-Golgi SNARE complexes and additional regulatory components that control VWF trafficking and WPB biogenesis, we employed an unbiased affinity purification-mass spectrometry (AP-MS) approach, using mEGFP-tagged Sec22b as bait. mEGFP-Sec22b and mEGFP (control) were immunoprecipitated from HUVECs and their interacting proteins were analyzed by MS.

A total of 70 proteins were statistically significantly enriched in both conditions with 46 being enriched in mEGFP-Sec22b compared to the control mEGFP samples (Figure 1A; Supplemental Table II). In order to pinpoint the biological processes that the Sec22b interactome is involved in, we conducted a STRING analysis (Figure 1B). The generated network showed that Sec22b and its interacting partners collaborate in 82 enriched biological processes that are mainly involved in anterograde and retrograde ER-Golgi trafficking, intra-Golgi trafficking as well as Golgi organization and assembly (Supplemental Table III).

Interestingly, we found interactions of Sec22b with Qa-SNARE STX5 and Qb-SNARE GosR2, which are part of the COPII anterograde SNARE complex, and of Sec22b with its cognate Qa-SNARE STX18, which facilitates COPI-dependent Golgi-to-ER trafficking (reviewed in<sup>39,40</sup>). Another cluster comprises components of the vesicle-tethering NRZ complex (NAPA, NBAS, SCFD1, SCFD2, ZW10, C19orf25), which regulates SNARE complex formation of incoming vesicles on the ER membrane.<sup>41</sup> Also, three members of the exocyst complex (EXOC2, EXOC5 and EXOC8) were identified, suggesting an until now unappreciated link of Sec22b with the post-Golgi vesicle-plasma membrane tethering complex.<sup>42</sup> A last notable component of the Sec22b interactome is the ARFGEF GBF1, which was previously implicated in ER-Golgi transport of VWF.<sup>19</sup> Taken together, our interactomic screen of Sec22b has uncovered a large protein network containing known and unknown candidates of protein trafficking in the endothelial early secretory pathway.

### STX5 silencing results in altered VWF trafficking and loss of the Golgi architecture.

It has previously been demonstrated that ER-to-Golgi trafficking plays an important role in determining the morphology of forming WPBs.<sup>18,19,31</sup> One of the prominent hits within the Sec22b interactome was the Qa-SNARE STX5, which takes part both in anterograde COPII-dependent ER-to-Golgi trafficking and in retrograde COPI-dependent intra-Golgi trafficking.<sup>40</sup> To address a potential role in VWF trafficking we silenced STX5 expression in HUVECs using shRNA interference and investigated WPB and Golgi morphology by immunostaining for VWF and TGN46, respectively (Figure 2). STX5 is expressed in a long (~40 kDa) and a short (~34 kDa) isoform, as a result of an alternative start codon,<sup>43</sup> however both isoforms are targeted by the short hairpin against STX5 used in this study as evidenced by the efficient depletion of STX5 after silencing (Figure 2B). We observed that upon STX5 silencing endothelial cells lost their characteristic elongated WPBs and their peripheral localization, the remaining VWF concentrated in spherical granules mostly found in the perinuclear area (Figure 2A). Quantitative analysis of the length of VWF positive structures in shCTRL and shSTX5 cells revealed that WPB length was severely decreased after depletion of STX5 (shCTRL: 2.39 ± 0.78 μm vs. shSTX5: 1.14 ± 0.41 μm; Figure 2C). We also observed a concomitant disintegration of Golgi morphology; TGN46, a marker of the trans-Golgi network, shows a compact, continuous ribbon structure in control cells (shCTRL), whereas in shSTX5 cells TGN46 staining was found on unlinked, dispersed endomembranes (Figure

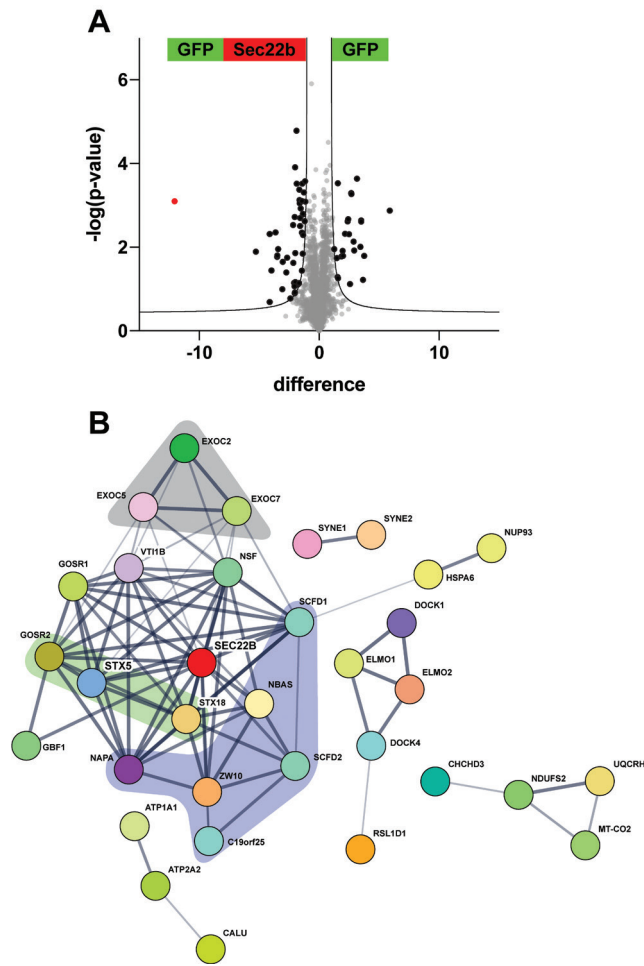


**Figure 1: Sec22b interactome in endothelial cells.** A) Volcano plot of the significantly enriched proteins in the mEGFP and mEGFP-Sec22b pull-down samples (red dot represents Sec22b that was used as bait) (FDR=0.05 and  $S_0=1$ ). B) STRING analysis of the enriched proteins in the mEGFP-Sec22b. Colored boxed regions indicate proteins from the exocyst complex (gray), proteins from the vesicle-tethering NRZ complex (purple) and SNARE proteins (green) (confidence= 0.4) (disconnected nodes are hidden).

2A). While in control cells the majority (~70%) of cells contained a Golgi in a so-called “compact” state, in shSTX5 cells the majority (~90%) of Golgi’s had disintegrated (Figure 2D). Since the VWF expression in STX5 depleted cells appeared downregulated in the confocal images along with reduced WPB numbers (Supplementary Figure I), we quantified intracellular levels of VWF by ELISA. In line with the reduction of WPBs, intracellular levels of VWF were significantly reduced upon STX5 silencing (Figure 2E). Unstimulated secretion of VWF, which is a composite of basal, WPB-derived secretion and constitutive, TGN-derived secretion,<sup>10</sup> when expressed in proportion to its intracellular level, was not altered between control and shSTX5 cells (Figure 2F). However, histamine-stimulated secretion of VWF was sharply reduced following STX5 silencing (Figure 2G), consistent with VWF not being able to reach a stimulus-sensitive compartment such as the WPB. Together these results indicate that STX5 is essential for formation of elongated WPBs, possibly through a combination of maintaining Golgi integrity and ER to Golgi trafficking of VWF.

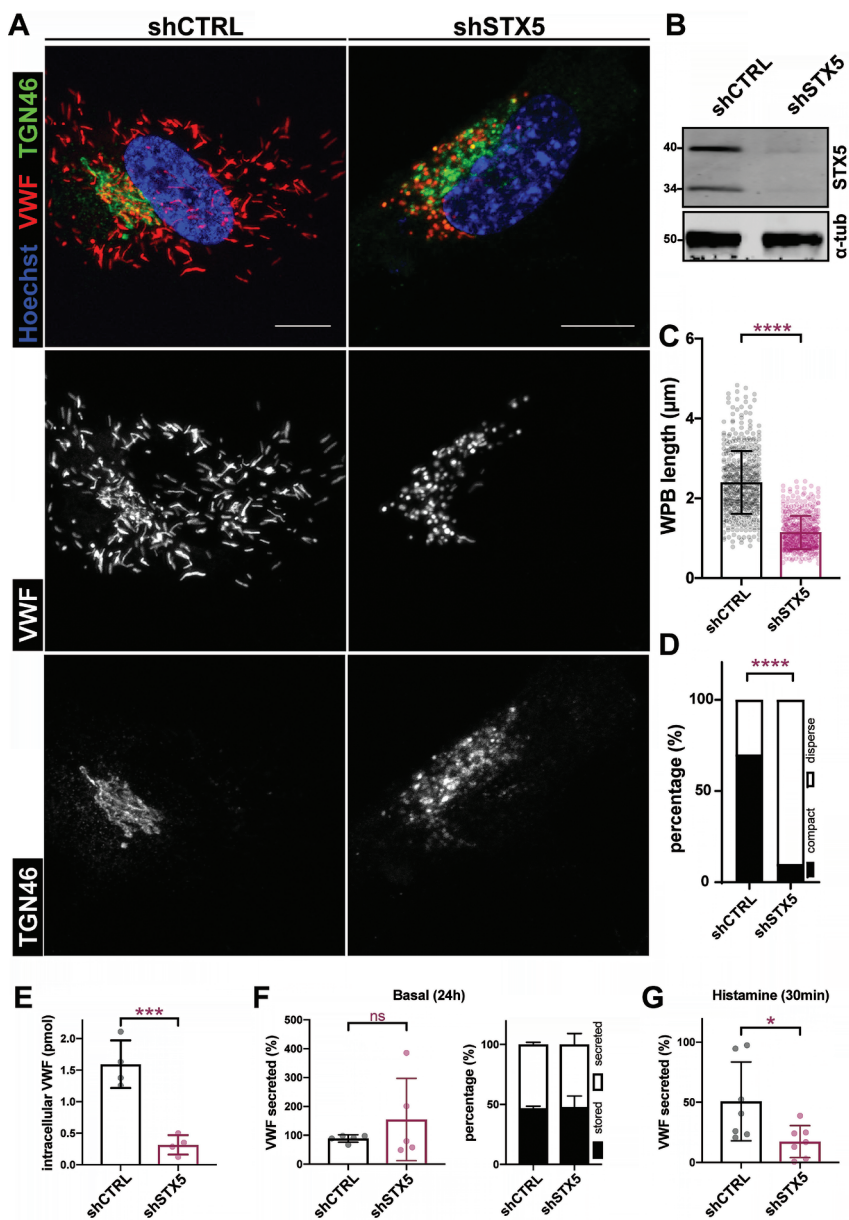


**Figure 2: STX5 downregulation results in decreased WPB length, extensive Golgi fragmentation and decreased VWF secretion.** A) (Immuno)fluorescent staining of VWF (red), TGN46 (green) and nuclei (Hoechst; blue) in control and shSTX5 endothelial cells. Individual channels are shown below in grayscale (scale bar was set at 10  $\mu$ m). B) Western blot analysis of STX5 in control and knockdown cells ( $\alpha$ -tubulin as loading control). Approximate molecular weight of protein bands is indicated on the left in kDa. C) Weibel-Palade body length in control and shSTX5 cells measured in  $\mu$ m (n=4 total of 500 WPBs, t-test with Welch correction, \*\*\*\* P<0.0001). D) Quantification of TGN fragmentation in control and shSTX5 cells. E) Intracellular VWF levels in control and shSTX5 HUVECs calculated as percentage of the intracellular VWF levels (left) and as portion of the secreted versus stored (right). G) Histamine-induced VWF release in control and shSTX5 knockdown cells (n=4, t-test with Welch correction, \* P<0.05).

### Reduction in WPB number and length and dilation of ER after STX5 silencing.

To further dissect the defect in elongated WPB formation in STX5 knockdown cells, we used transmission electron microscopy (TEM) to evaluate their (WPB) morphology (Figure 3A). Similar as earlier noted by light microscopy, we found that WPB length is decreased upon STX5 silencing (Figure 3A). Moreover, these oddly shaped WPBs were found in close proximity to the nucleus, confirming the previous observations with perinuclear localization. Similar as in Sec22b-depleted cells,<sup>31</sup> STX5 silencing also affected the morphology of the ER with a striking dilation of the rough ER (rER) (Figure 3A; rER sheets indicated with yellow arrowheads). The luminal width of rER cisternae was significantly increased in the shSTX5 ( $0.16 \mu\text{m} \pm 0.07 \mu\text{m}$ ) when compared to the control ( $0.10 \mu\text{m} \pm 0.03 \mu\text{m}$ ), indicating that upon STX5 knockdown the ER increases its volume to accommodate proteins as the trafficking pathway to the Golgi is blocked.

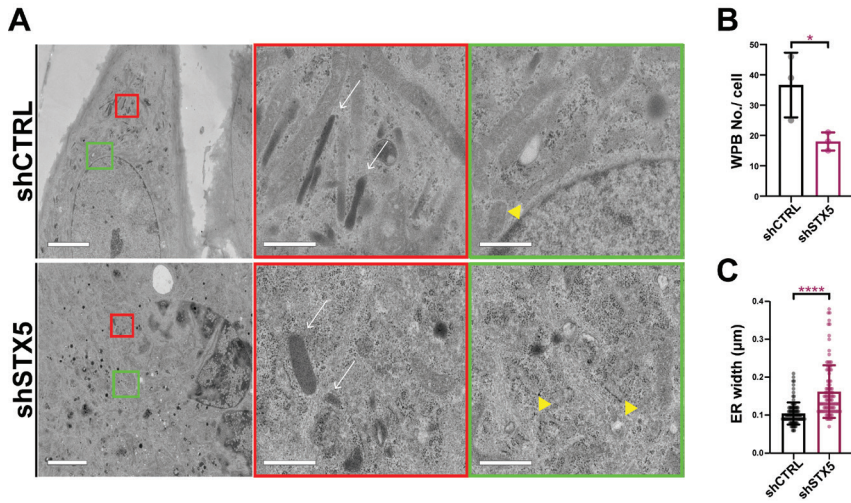


**Figure 3: STX5 downregulation results in reduced number of short WPBs and ER dilation.** A) Transmission electron microscopy (TEM) images of control and shSTX5 cells. Boxed regions are magnified on the right side with the corresponding colors, white arrows indicate WPBs and yellow arrowheads rER sheets (scale bar set at  $6 \mu\text{m}$  for overview image and at  $1 \mu\text{m}$  for the magnifications). B) rER width measured in  $\mu\text{m}$  in control and STX5 knock down cells ( $n=10$ , t-test with Welch correction, \*\*\*\*  $P < 0.0001$ ).

### Downregulation of STX5 induced significant alterations in the whole proteome of endothelial cells.

In order to further assess the dramatic changes in the WPB biogenesis and morphology, as well as the reduced intracellular VWF amount and decreased stimulated secretion, we looked into the differences on proteomic levels caused by silencing of STX5. In the same analysis we included shSec22b cells that exhibited similar phenotype to the one shSTX5, as previously described,<sup>31</sup> so as to determine the similarities and differences between the two interacting partners silencing in endothelial cells. Samples from the same condition clustered together in the principle component analysis (PCA), showing minimal variability between replicates (Figure 4A). Additionally, we observed that the shSTX5 samples were clustered further away from the rest conditions, indicating a big change in their whole proteome, followed by the shSec22b, while all the control conditions clustered together. With this type of analysis, we were able to identify changes in the whole proteome due to the lack of STX5 (and Sec22b), while normalizing the potential effects that the viral transduction delivery of the short hairpin RNAs might have on the cells (Figure 4A).



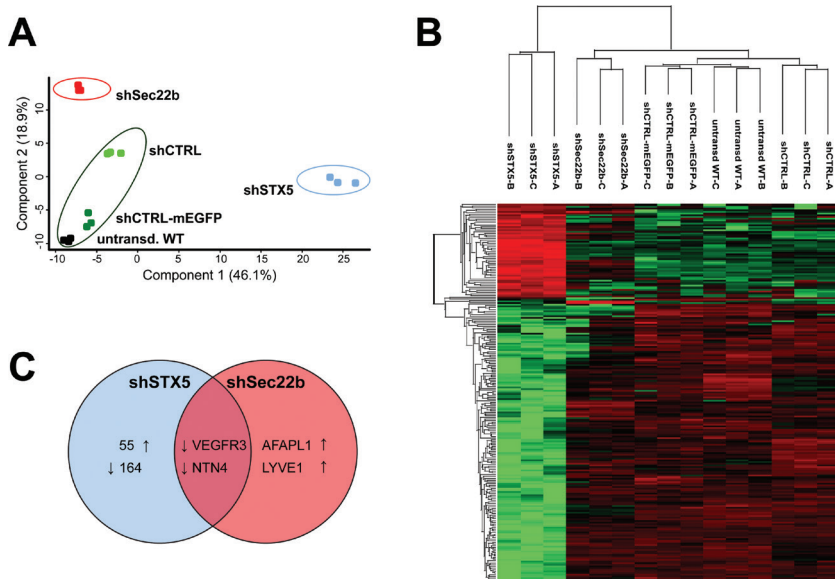


**Figure 4: Whole proteome analysis of shSTX5 and shSec22b endothelial cells.** A) Principle component analysis (PCA) of analyzed samples. B) Heatmap of Z-scored log<sub>2</sub> (LFQ) proteins with the highest variation between HUVECs transduced with shSTX5, mEGFP-shSec22b, shCTRL, mEGFP-shCTRL and untransduced HUVECs (ANOVA  $S_0=0.4$ , FDR = 0.05). C) Venn diagram of the shared and non-shared proteins changed in STX5 and Sec22b knockdown cells.

Interestingly, although STX5 was identified as an interacting partner of Sec22b and both facilitated WPB formation with their downregulation resulting in a similar WPB phenotype, i.e. shorter and stubbier WPBs, STX5 depletion affected the cell's proteome more drastically when compared to shSec22b treatment. As shown in the heat map, where red indicates upregulation and green downregulation, STX5 depleted cells had a total of 221 significantly changed proteins, whereas in shSec22b cells only 4 proteins were altered (Figure 4B). Between shSTX5 and shSec22b condition, only 2 proteins were shared, vascular endothelial growth factor receptor 3 (VEGFR3) and netrin-4, as illustrated in the Venn diagram in Figure 4C. VEGFR3 and netrin-4 have been previously implicated in the regulation of angiogenesis,<sup>44,45</sup> suggesting that STX5/ Sec22b-dependent intracellular trafficking may be additionally regulating the transport of proteins with angiogenic properties.

When we examined further the changes on protein level in the STX5-depleted cells, we confirmed the decreased intracellular VWF levels in addition to other extracellular proteins, like collagen alpha-1(XII) and alpha-1(XVIII) chain (COL12A1 and COL18A1, respectively). Moreover, several proteins involved in regulated secretion and cell adhesion, along with proteins like RaB3D that have been previously implicated in WPB formation and exocytosis<sup>46</sup> were significantly downregulated in shSTX5 cells, highlighting the importance of STX5-mediated protein transport.

## Discussion

SNARE proteins are the key machinery that promotes membrane fusion during vesicle transport.<sup>47</sup> We have previously identified several SNARE proteins involved in WPB maturation and exocytosis, while recently we have shown the critical role of Sec22b, an ER-to-Golgi SNARE, in VWF trafficking and WPB formation.<sup>24,25,31</sup> In this study, we used a mass

spectrometry-based approach, in order to determine the Sec22b interactome in endothelial cells and identify novel WPB formation regulators. From these interactors, we focused our research on STX5, cognate SNARE protein that is primarily found on the Golgi and has been shown to facilitate ER-to-Golgi and intra-Golgi protein trafficking.<sup>40</sup> We silenced the expression of STX5 by means of viral delivery of short hairpin RNAs and we discovered a severe defect in WPB biogenesis accompanied by dispersal of the TGN and decreased secretagogue-induced VWF release.

Silencing of STX5 negatively affected the Golgi morphology, which disintegrated into perinuclear puncta. It has been previously reported that STX5 is an integral member of the Golgi apparatus and has been suggested to participate in the Golgi reassembly after mitosis.<sup>48</sup> STX5 is a component of both NFS and p97 reassembly pathways,<sup>48</sup> thus, reduced levels of STX5 in endothelial cells could potentially interfere with the cell's ability entering in the post-mitotic Golgi reorganization, leading to permanent Golgi dispersal. As Golgi disassembled, this had a severe effect on the WPB biogenesis. WPBs is known to bud off from the TGN containing VWF condensed tubules and their morphology is directly linked to the Golgi continuous cisternae.<sup>18</sup> A continuous Golgi allows the integration of more VWF units, the so-called VWF quanta, resulting in larger WPBs, while Golgi mini-stacks give rises to shorter and stubbier WPBs.<sup>18</sup> Therefore, in the STX5 depleted cells with dispersed Golgi, similar to shSec22b knock down cells, WPBs length is significantly reduced. This suggest that STX5 works with Sec22b in ER-to-Golgi transport, facilitating protein trafficking and depletion of either one negatively changes the Golgi morphology, which in turn influences WPB biogenesis.

STX5 depletion affected also the ER morphology, whose intraluminal width was significantly increased when compared to control. Similar ER dilation has been previously described in Sec22b and GBF1 knock down endothelial cells, due to cargo retention in the ER and temporary storage in the ER-derived ribosome studded electron-dense round vesicles.<sup>19,31</sup> However, although the ER was enlarged, an absence of these electron-dense structures was observed in the shSTX5 knock down cells, indicating that the SNARE pair Sec22b/STX5 may affect ER-to-Golgi trafficking in a different way. Although we have shown that Sec22b-dependent membrane fusion is indispensable for the anterograde cargo delivery, including VWF dimers, it has been suggested that STX5 may not play a central role in vesicle transportation.<sup>49</sup> Notwithstanding some minor alterations in the vesicle trafficking kinetics in STX5 downregulated cells, membrane proteins like VSVG were able to be transported through the secretion pathway to the plasma membrane, indicating that STX5 depletion may be compensated by other Golgi SNAREs.<sup>49</sup> Similarly, STX5 may primarily regulate Golgi morphology and subsequently WPB formation in endothelial cells, while its role in ER-to-Golgi trafficking may be of less significance, as we do not observe any ER retention comparable to Sec22b-depleted cells.

VWF release can be separated into three modes: constitutive secretion of low molecular weight VWF (primarily) to the basolateral side, and basal and regulated (stimulus-induced) VWF secretion, both (primarily) to the apical side.<sup>50</sup> Interestingly, only stimulated VWF secretion was affected in STX5 depleted cells, while unstimulated release (which is composed of constitutive and basal secretion) was normal with a small increased trend. This could be explained by the strongly affected stimulus-sensitive compartment, i.e. reduced number of perinuclearly localized short WPBs, and reduced intracellular VWF expression levels. Therefore, we can hypothesize that STX5 role is to maintain a continuous Golgi that in turn can store VWF in WPBs.

In summary, we used Sec22b as a bait in a mass spectrometry-based approach to identify novel regulators of WPB biogenesis. We focused on STX5, a Golgi SNARE protein that participates in anterograde, retrograde and intra-Golgi protein trafficking. STX5 was found to play a major role in maintaining a continuous Golgi morphology, which in turn positively regulates WPB biogenesis and length. STX5 depletion results in severely fragmented Golgi

puncta, reduced production of short WPBs that subsequently showed a defected stimulus-induced secretory behavior. Our data point to a crucial role for STX5-containing SNARE complexes in the endothelial cell's ability to efficiently store and secrete VWF.

### **Authorship**

EK, FvA and AM performed research and analyzed data; DG, MvdB and CJ contributed vital reagents and expertise; EK, JV and RB designed the research; EK, JV and RB wrote the paper.

### **Acknowledgements**

This study was supported by grants from the Landsteiner Stichting voor Bloedtransfusie Research (LSBR-1707), the Netherlands Ministry of Health (PPOC-2015-24P) and the Dutch Thrombosis Foundation (TSN 2017-01).

## References

- Sadler JE. von Willebrand factor assembly and secretion. *J. Thromb. Haemost.* 2009;7:24–27.
- Zhou Y-F, Eng ET, Zhu J, et al. Sequence and structure relationships within von Willebrand factor. *Blood.* 2012;120(2):449–58.
- Zhou Y-F, Eng ET, Nishida N, et al. A pH-regulated dimeric bouquet in the structure of von Willebrand factor. *EMBO J.* 2011;30(19):4098–4111.
- Purvis AR, Gross J, Dang LT, et al. Two Cys residues essential for von Willebrand factor multimer assembly in the Golgi. *Proc. Natl. Acad. Sci. U. S. A.* 2007;104(40):15647–52.
- Zenner HL, Collinson LM, Michaux G, Cutler DF. High-pressure freezing provides insights into Weibel-Palade body biogenesis. *J. Cell Sci.* 2007;120(Pt 12):2117–2125.
- Mourik MJ, Faas FG, Zimmermann H, et al. Content delivery to newly forming Weibel-Palade bodies is facilitated by multiple connections with the Golgi apparatus. *Blood.* 2015;125(22):3509–16.
- Schillemans M, Kat M, Westeneng J, et al. Alternative trafficking of Weibel-Palade body proteins in CRISPR/Cas9-engineered von Willebrand factor-deficient blood outgrowth endothelial cells. *Res. Pract. Thromb. Haemost.* 2019;3(4):718–732.
- Wagner DD, Saffaripour S, Bonfanti R, et al. Induction of specific storage organelles by von Willebrand factor propolypeptide. *Cell.* 1991;64(2):403–13.
- Voorberg J, Fontijn R, Calafat J, et al. Biogenesis of von Willebrand factor-containing organelles in heterologous transfected CV-1 cells. *EMBO J.* 1993;12(2):749–758.
- Schillemans M, Karampini E, Kat M, Bierings R. Exocytosis of Weibel-Palade bodies: how to unpack a vascular emergency kit. *J. Thromb. Haemost.* 2019;17(1):6–18.
- De Ceunynck K, De Meyer SF, Vanhoorelbeke K. Unwinding the von Willebrand factor strings puzzle. *Blood.* 2013;121(2):270–277.
- Lopes da Silva M, Cutler DF. von Willebrand factor multimerization and the polarity of secretory pathways in endothelial cells. *Blood.* 2016;128(2):277–85.
- Metcalfe DJ, Nightingale TD, Zenner HL, Lui-Roberts WW, Cutler DF. Formation and function of Weibel-Palade bodies. *J. Cell Sci.* 2008;31(9):882–888.
- Valentijn KM, Valentijn JA, Jansen KA, Koster AJ. A new look at Weibel-Palade body structure in endothelial cells using electron tomography. *J. Struct. Biol.* 2008;161(3):447–458.
- Berriman JA, Li S, Hewlett LJ, et al. Structural organization of Weibel-Palade bodies revealed by cryo-EM of vitrified endothelial cells. *Proc. Natl. Acad. Sci. U. S. A.* 2009;106(41):17407–17412.
- Streetley J, Fonseca A-V, Turner J, et al. Stimulated release of intraluminal vesicles from Weibel-Palade bodies. *Blood.* 2019;133(25):2707–2717.
- Ferraro F, Mafalda Lopes da S, Grimes W, et al. Weibel-Palade body size modulates the adhesive activity of its von Willebrand Factor cargo in cultured endothelial cells. *Sci. Rep.* 2016;6(March):32473.
- Ferraro F, Kriston-Vizi J, Metcalf DJ, et al. A two-tier golgi-based control of organelle size underpins the functional plasticity of endothelial cells. *Dev. Cell.* 2014;29(3):292–304.
- Lopes-da-Silva M, McCormack JJ, Burden JJ, et al. A GBF1-Dependent Mechanism for Environmentally Responsive Regulation of ER-Golgi Transport. *Dev. Cell.* 2019;1–16.
- Holthenrich A, Drexler HCAA, Chehab T, Naß J, Gerke V. Proximity proteomics of endothelial Weibel-Palade bodies identifies novel regulator of von Willebrand factor secretion. *Blood.* 2019;134(12):979–982.
- Jensen D, Schekman R. COPII-mediated vesicle formation at a glance. *J. Cell Sci.* 2011;124(Pt 1):1–4.
- Mancias JD, Goldberg J. The Transport Signal on Sec22 for Packaging into COPII-Coated Vesicles Is a Conformational Epitope. 2007;403–414.
- Brandizzi F, Barlowe C. Organization of the ER-Golgi interface for membrane traffic control. *Nat. Rev. Mol. Cell Biol.* 2013;14(6):382–92.
- Karampini E, Schillemans M, Hofman M, et al. Defective AP-3-dependent VAMP8 trafficking impairs Weibel-Palade body exocytosis in Hermansky-Pudlak Syndrome type 2 blood outgrowth endothelial cells. *Haematologica.* 2019;haematol.2018.207787.
- Schillemans M, Karampini E, van den Eshof B, et al. The Weibel-Palade body localized SNARE syntaxin-3 modulates von Willebrand factor secretion from endothelial cells. *Arterioscler. Thromb. Vasc. Biol.* 2018;in press:1–31.
- Zhu Q, Yamakuchi M, Lowenstein CJ. SNAP23 regulates endothelial exocytosis of von Willebrand Factor. *PLoS One.* 2015;10(8):14–22.
- Pulido IR, Jahn R, Gerke V. VAMP3 is associated with endothelial Weibel-Palade bodies and participates in their Ca(2+)-dependent exocytosis. *Biochim. Biophys. Acta.* 2011;1813(5):1038–1044.
- Fu J, Naren AP, Gao X, Ahmed GU, Malik AB. Protease-activated receptor-1 activation of endothelial cells induces protein kinase Ca-dependent phosphorylation of syntaxin 4 and Munc18c: Role in signaling P-selectin expression. *J. Biol. Chem.* 2005;280(5):3178–3184.
- van Loon JE, Sanders Y V, de Wee EM, et al. Effect of genetic variation in STXBP5 and

- STX2 on von Willebrand factor and bleeding phenotype in type 1 von Willebrand disease patients. *PLoS One*. 2012;7(7):e40624.
30. Van Loon J, Dehghan A, Weihong T, et al. Genome-wide association studies identify genetic loci for low von Willebrand factor levels. *Eur. J. Hum. Genet.* 2016;24(7):1035–1040.
  31. Karampini E, Olins J, Mulder A, et al. Sec22b determines Weibel-Palade body length by controlling anterograde ER-Golgi transport. 2020;
  32. van Breevoort D, Snijders AP, Hellen N, et al. STXBP1 promotes Weibel-Palade body exocytosis through its interaction with the Rab27A effector Slp4-a. *Blood*. 2014;123(20):3185–94.
  33. Lenzi C, Stevens J, Osborn D, et al. Synaptotagmin 5 regulates Ca<sup>2+</sup>-dependent Weibel-Palade body exocytosis in human endothelial cells. *J. Cell Sci.* 2019;132(5):.
  34. Schillemans M, Karampini E, Hoogendijk AJ, et al. Interaction networks of Weibel-Palade body regulators syntaxin-3 and syntaxin binding protein 5 in endothelial cells. *J. Proteomics*. 2019;in revision.
  35. Stel H V, Sakariassen KS, de Groot PG, van Mourik JA, Sixma JJ. Von Willebrand factor in the vessel wall mediates platelet adherence. *Blood*. 1985;65(1):85–90.
  36. van Hooren KWEM, van Breevoort D, Fernandez-Borja M, et al. Phosphatidylinositol-3,4,5-triphosphate-dependent Rac exchange factor 1 regulates epinephrine-induced exocytosis of Weibel-Palade bodies. *J. Thromb. Haemost.* 2014;12(2):273–81.
  37. Faas FGA, Avramut MC, van den Berg BM, et al. Virtual nanoscopy: generation of ultra-large high resolution electron microscopy maps. *J. Cell Biol.* 2012;198(3):457–69.
  38. Xu D, Joglekar AP, Williams AL, Hay JC. Subunit structure of a mammalian ER/Golgi SNARE complex. *J. Biol. Chem.* 2000;275(50):39631–39639.
  39. Malsam J, Söllner TH. Organization of SNAREs within the Golgi stack. *Cold Spring Harb. Perspect. Biol.* 2011;3(10):a005249.
  40. Linders PT, Horst CV, Beest MT, et al. Stx5-Mediated ER-Golgi Transport in Mammals and Yeast. *Cells*. 2019;8(8):780.
  41. Tagaya M, Arasaki K, Inoue H, Kimura H. Moonlighting functions of the NRZ (mammalian Dsl1) complex. *Front. cell Dev. Biol.* 2014;2(June):25.
  42. Wu B, Guo W. The Exocyst at a Glance. *J. Cell Sci.* 2015;128(16):2957–64.
  43. Hui N, Nakamura N, Sönnichsen B, et al. An isoform of the Golgi t-SNARE, syntaxin 5, with an endoplasmic reticulum retrieval signal. *Mol. Biol. Cell*. 1997;8(9):1777–87.
  44. Tammela T, Zarkada G, Wallgard E, et al. Blocking VEGFR-3 suppresses angiogenic sprouting and vascular network formation. *Nature*. 2008;454(7204):656–660.
  45. Lejmi E, Leconte L, Pédrón-Mazoyer S, et al. Netrin-4 inhibits angiogenesis via binding to neogenin and recruitment of Unc5B. *Proc. Natl. Acad. Sci. U. S. A.* 2008;105(34):12491–12496.
  46. Knop M, Aaeskjold E, Bode G, Gerke V. Rab3D and annexin A2 play a role in regulated secretion of vWF, but not tPA, from endothelial cells. *EMBO J.* 2004;23(15):2982–92.
  47. Jahn R, Scheller RH. SNAREs—engines for membrane fusion. *Nat. Rev. Mol. Cell Biol.* 2006;7(9):631–43.
  48. Rabouille C, Kondo H, Newman R, et al. Syntaxin 5 is a common component of the NSF- and p97-mediated reassembly pathways of Golgi cisternae from mitotic golgi fragments in vitro. *Cell*. 1998;92(5):603–610.
  49. Suga K, Hattori H, Saito A, Akagawa K. RNA interference-mediated silencing of the syntaxin 5 gene induces Golgi fragmentation but capable of transporting vesicles. *FEBS Lett.* 2005;579(20):4226–4234.
  50. Bierings R, Voorberg J. Up or out: polarity of VWF release. *Blood*. 2016;128(2):154–5.

## Supplemental Tables and Figures

Supplemental Table I: Antibody reagents

target	Species (isotype)	Label	Supplier	Cat.nr /clone	Application [concentration/dilution]
VWF	mouse (IgG <sub>2b</sub> )	-	described in <sup>4</sup>	CLB-RAG20	IF [1:1000]
STX5	rabbit	-	Synaptic Systems	110053	IF [2 µg/ml], WB [1 µg/ml]
α-tubulin	mouse (IgG <sub>1</sub> )	-	Sigma-Aldrich	T9026	WB [1:1000]
VWF	rabbit	-	DAKO	A0082	ELISA [6 µg/ml]
VWF	rabbit	HRP	DAKO	A0082	WB [3µg/ml], ELISA [2 µg/ml]
TGN46	sheep	-	Bio-Rad	AHP500GT	IF [1:1000]
Hoechst	-	-	Life Technologies	H-1399	IF [1:50]
rabbit IgG	donkey	680LT	Li-Cor	925-68023	WB [0.1 µg/ml]
mouse IgG	donkey	800CW	Li-Cor	925-32212	WB [0.1 µg/ml]
mouse IgG	goat	AF568	ThermoFisher	A11004	IF [2 µg/ml]
rabbit IgG	chicken	AF647	ThermoFisher	A21443	IF [2 µg/ml]

Supplemental table II: Significantly enrich proteins with LFQ values in mEGFP-Sec22b pull-down samples and mEGFP pull-down samples

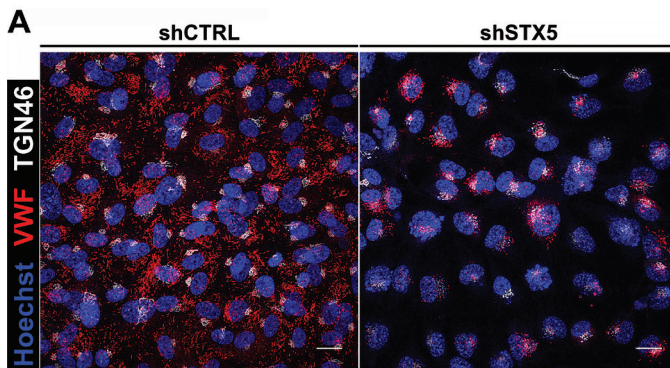
LFQ intensity mEGFP_85_A	LFQ intensity mEGFP_85_B	LFQ intensity mEGFP_85_C	LFQ intensity SEC22B_A	LFQ intensity SEC22B_B	T: Gene names
27.3382	27.304	27.4068	28.4628	28.5777	EXOC5
23.0557	21.4985	23.1988	26.0635	26.0925	SYNE1
26.0446	26.1731	26.8653	28.1191	27.5028	GOSR2
23.4481	22.5132	22.5129	26.4504	27.4439	NBAS
26.3662	26.0708	26.3033	27.7165	27.8464	GOSR1
24.9623	25.2256	25.4621	26.6878	26.6393	CHCHD3
22.8377	24.0413	22.7017	25.7075	26.0232	STX18
23.4904	23.4413	23.0538	25.2819	25.7269	SMARCB1
23.5371	23.4023	23.0682	24.8972	24.9741	CALU
23.2809	23.975	23.313	24.4725	25.9102	NUP93
23.3202	25.5194	22.8129	27.5876	28.1205	NSF
23.8773	22.7586	22.6507	25.2059	25.3181	DERL2
22.7459	22.1269	21.844	24.4577	24.0082	C19orf25
23.2586	22.7326	21.6598	26.0189	25.9317	NAPA
23.1222	22.0567	22.0492	26.1555	25.9308	ZW10
24.8117	23.1035	22.8362	25.8155	25.4523	NDUFS2
25.0794	24.9576	23.3855	37.2062	35.8567	SEC22B
23.2131	22.8698	22.3206	25.4417	27.1653	RSL1D1
27.0132	27.0638	27.2271	28.2626	28.2506	LETM1
23.2897	23.4633	23.4354	24.7252	24.6305	MT-CO2
27.2882	27.1614	27.0876	29.1966	29.1653	ATP1A1
28.5031	28.3788	28.704	29.8715	29.8935	UQCRH
27.0358	27.2763	27.3212	28.8388	28.8613	ATP2A2
23.3591	22.7543	28.9437	28.7532	29.5462	HSPA6
22.0393	24.4687	22.4517	24.9475	25.1224	SON
22.5209	21.9207	23.7411	25.8802	25.6461	CDK7
24.5205	25.8026	24.6651	27.6326	26.3408	HBB
31.6248	31.3146	31.4915	32.7599	32.6249	PRKDC
28.1281	27.9102	28.091	29.5578	29.4104	STX5
26.3552	26.2793	26.3725	28.2294	28.2284	DOCK1
26.2236	26.1049	26.606	28.3682	28.3231	ELMO2
29.3963	29.2361	29.4075	31.0877	30.9164	DOCK4
21.8027	23.9384	21.7258	24.4038	24.6263	WDR19
22.9311	20.9415	21.9829	25.0384	24.3361	SCFD2
23.2252	22.8144	21.5895	24.638	24.0135	GATAD1
23.293	23.3096	21.0679	28.1101	27.5396	SCFD1
28.9935	28.7154	28.7265	30.2034	30.1032	SYNE2
25.33	25.0607	25.3626	26.3041	26.939	GBF1
27.5699	27.7042	27.751	29.4331	29.1692	ELMO1
25.7543	22.7424	22.6161	26.2602	25.96	EXOC2
22.8003	24.7266	23.1967	25.5566	25.7801	C1orf43
23.1231	23.374	23.4099	25.0403	24.7589	TREX1
22.6996	22.1772	25.449	26.5177	26.513	CRIM1
24.9276	25.0533	24.8625	26.9009	26.7283	VTI1B
28.0342	27.9615	28.3026	29.6088	29.2792	EXOC7
24.6731	24.7714	24.759	26.2192	26.0561	DNAJC16
26.8808	26.6436	26.7384	22.772	23.7093	IKBKG
24.9117	24.9009	24.7485	23.0688	22.3258	MCC
24.504	24.9924	24.9936	22.6269	22.2731	NCOR2
24.5394	24.7124	24.5066	22.5258	21.6615	STK24
25.6333	25.5946	25.9198	22.9052	23.1685	MRPS7
25.796	26.6058	26.5843	23.4843	21.6557	NDUFA4
25.4097	25.5867	25.2171	22.708	23.2455	POP4
36.8548	36.9301	37.066	35.4006	35.383	VWF
25.7447	25.7364	26.4661	21.8878	23.2093	GTF2F2
28.8482	28.7029	28.579	23.472	22.1484	ATP6V1C1
28.4993	27.9119	28.1322	26.8908	26.9594	APEX1
25.2546	25.3911	25.3308	22.3536	21.9784	ETV6
26.7069	27.4482	26.811	25.3825	25.6377	HIST1H3A
24.5755	24.3559	24.2928	22.0694	23.0451	MRPS21
25.1724	25.2105	25.2104	23.9152	21.3174	MZT1
24.3556	24.4749	24.2176	21.8394	21.4648	ARRDC1
24.7648	24.7245	24.5795	22.2496	23.2005	AHDC1
24.4413	24.7239	24.6711	23.7086	22.4228	ZCCHC4
25.1273	24.7211	25.2406	22.573	23.5082	MED9
24.6246	24.3916	23.3982	22.3165	22.7963	TNIIK
27.6442	27.244	27.108	25.3128	22.0224	PLEKHG1
25.639	25.7149	25.7462	23.4914	22.0672	RUVBL2
25.1029	25.2067	25.0729	22.8361	21.6582	CSNK1G3
26.7042	27.5653	27.3453	23.4815	23.9024	TRIP10

**Supplemental table III: Enriched biological processes**

#term ID	term description	obs. gene count	back. gene count	FDR	matching proteins in your network (labels)
GO:0048193	Golgi vesicle transport	14	325	3,31E-11	EXOC2,EXOC5,GBF1,GOSR1,GOSR2,NAPA,NBAS,NSF,SCFD1,SEC22B,STX18,STX-5,VT11B,ZW10
GO:0061024	membrane organization	17	729	2,66E-10	ATP2A2,CHCHD3,DOCK1,ELMO1,GBF1,GOSR1,GOSR2,LETM1,NAPA,NSF,NUP93,SCF-D1,SEC22B,STX18,STX5,SYNE2,VT11B
GO:0006888	endoplasmic reticulum to Golgi vesicle-mediated transport	10	175	6,19E-09	GBF1,GOSR1,GOSR2,NAPA,NSF,SCFD1,SEC22B,STX5,VT11B,ZW10
GO:0006890	retrograde vesicle-mediated transport, Golgi to endoplasmic reticulum	8	81	1,03E-08	GBF1,NAPA,NBAS,NSF,SCFD1,SEC22B,STX18,ZW10
GO:0016192	vesicle-mediated transport	21	1699	1,28E-08	DOCK1,ELMO1,ELMO2,EXOC2,EXOC5,EXOC7,GBF1,GOSR1,GOSR2,HBB,HSPA6,NAPA,NBAS,NSF,SCFD1,SCFD2,SEC22B,STX18,STX5,VT11B,ZW10
GO:0006996	organelle organization	27	3131	1,42E-08	ATP2A2,CHCHD3,DOCK1,ELMO1,ELMO2,EXOC5,GATAD1,GBF1,GOSR1,GOSR2,LETM1,NAPA,NDUFS2,NSF,NUP93,PRKDC,SCFD1,SEC22B,SMARCB1,SON,STX18,STX-5,SYNE1,SYNE2,VT11B,WDR19,ZW10
GO:0015031	protein transport	19	1391	2,14E-08	DERL2,EXOC2,EXOC5,EXOC7,GBF1,GOSR1,GOSR2,NAPA,NBAS,NSF,NUP93,SCFD1,SCF-D2,SEC22B,STX18,STX5,VT11B,WDR19,ZW10
GO:0006901	vesicle coating	7	65	3,76E-08	GBF1,GOSR2,NAPA,NSF,SCFD1,SEC22B,STX5
GO:0061025	membrane fusion	9	170	3,76E-08	CHCHD3,GOSR1,GOSR2,NAPA,NSF,SEC22B,STX18,STX5,VT11B
GO:0071705	nitrogen compound transport	20	1690	3,8E-08	DERL2,EXOC2,EXOC5,EXOC7,GBF1,GOSR1,GOSR2,HBB,NAPA,NBAS,NSF,NUP93,SCF-D1,SCFD2,SEC22B,STX18,STX5,VT11B,WDR19,ZW10
GO:0048199	vesicle targeting, to, from or within Golgi	7	68	4,26E-08	GBF1,GOSR2,NAPA,NSF,SCFD1,SEC22B,STX5
GO:0051640	organelle localization	13	574	5,2E-08	EXOC2,EXOC5,GBF1,GOSR2,NAPA,NSF,SCFD1,SCFD2,SEC22B,STX5,SYNE2,VT11B,ZW10
GO:0008104	protein localization	21	1966	5,89E-08	DERL2,EXOC2,EXOC5,EXOC7,GBF1,GOSR1,GOSR2,NAPA,NBAS,NSF,NUP93,SCFD1,SCF-D2,SEC22B,STX18,STX5,SYNE1,SYNE2,VT11B,WDR19,ZW10
GO:0048194	Golgi vesicle budding	7	75	6,64E-08	GBF1,GOSR2,NAPA,NSF,SCFD1,SEC22B,STX5
GO:0006810	transport	29	4130	7,73E-08	ATP1A1,ATP2A2,DERL2,DOCK1,ELMO1,ELMO2,EXOC2,EXOC5,EXOC7,GBF1,GOSR1,GOSR2,HBB,HSPA6,LETM1,MT-CO2,NAPA,NBAS,NSF,NUP93,SCFD1,SCFD2,SEC22B,STX-18,STX5,SYNE2,VT11B,WDR19,ZW10
GO:0051641	cellular localization	21	2180	2,78E-07	ATP2A2,DERL2,EXOC2,EXOC5,GBF1,GOSR1,GOSR2,LETM1,NAPA,NSF,NUP93,SCF-D1,SCFD2,SEC22B,STX18,STX5,SYNE1,SYNE2,VT11B,WDR19,ZW10
GO:0048278	vesicle docking	6	58	4,89E-07	EXOC2,EXOC5,SCFD1,SCFD2,STX5,VT11B
GO:0071702	organic substance transport	20	2040	5,17E-07	DERL2,EXOC2,EXOC5,EXOC7,GBF1,GOSR1,GOSR2,HBB,NAPA,NBAS,NSF,NUP93,SCF-D1,SCFD2,SEC22B,STX18,STX5,VT11B,WDR19,ZW10
GO:0051179	localization	31	5233	5,72E-07	ATP1A1,ATP2A2,DERL2,DOCK1,DOCK4,ELMO1,ELMO2,EXOC2,EXOC5,EXOC7,GBF1,GOSR1,GOSR2,HBB,HSPA6,LETM1,MT-CO2,NAPA,NBAS,NSF,NUP93,SCFD1,SCFD2,SEC22B,STX18,STX5,SYNE1,SYNE2,VT11B,WDR19,ZW10
GO:0048208	COPII vesicle coating	6	63	6,6E-07	GOSR2,NAPA,NSF,SCFD1,SEC22B,STX5
GO:0071840	cellular component organization or biogenesis	31	5342	8,7E-07	ATP2A2,CDK7,CHCHD3,DOCK1,ELMO1,ELMO2,EXOC2,EXOC5,GATAD1,GBF1,GOSR1,GOSR2,HBB,LETM1,NAPA,NDUFS2,NSF,NUP93,PRKDC,RSL1D1,SCFD1,SEC22B,SMARCB1,SON,STX18,STX5,SYNE1,SYNE2,VT11B,WDR19,ZW10
GO:0048280	vesicle fusion with Golgi apparatus	4	10	1,18E-06	GOSR2,SEC22B,STX5,VT11B
GO:0016043	cellular component organization	30	5163	1,8E-06	ATP2A2,CDK7,CHCHD3,DOCK1,ELMO1,ELMO2,EXOC2,EXOC5,GATAD1,GBF1,GOSR1,GOSR2,HBB,LETM1,NAPA,NDUFS2,NSF,NUP93,PRKDC,SCFD1,SEC22B,SMARCB1,SON,STX-18,STX5,SYNE1,SYNE2,VT11B,WDR19,ZW10
GO:0006892	post-Golgi vesicle-mediated transport	6	83	2,39E-06	EXOC2,EXOC5,GBF1,GOSR2,SCFD1,VT11B
GO:0016050	vesicle organization	9	318	2,39E-06	GBF1,GOSR1,GOSR2,NAPA,NSF,SCFD1,SEC22B,STX5,VT11B
GO:0046907	intracellular transport	16	1390	2,39E-06	ATP2A2,DERL2,GBF1,GOSR1,GOSR2,NAPA,NSF,NUP93,SCFD1,SEC22B,STX18,STX-5,SYNE2,VT11B,WDR19,ZW10
GO:0051649	establishment of localization in cell	17	1616	2,69E-06	ATP2A2,DERL2,GBF1,GOSR1,GOSR2,LETM1,NAPA,NSF,NUP93,SCFD1,SEC22B,STX-18,STX5,SYNE2,VT11B,WDR19,ZW10
GO:0051656	establishment of organelle localization	9	387	1,1E-05	GBF1,GOSR2,NAPA,NSF,SCFD1,SEC22B,STX5,SYNE2,ZW10
GO:0048284	organelle fusion	6	120	1,74E-05	CHCHD3,GOSR1,GOSR2,SEC22B,STX5,VT11B
GO:0006891	intra-Golgi vesicle-mediated transport	4	29	3,61E-05	GOSR1,GOSR2,NAPA,VT11B
GO:0010256	endomembrane system organization	8	337	4,1E-05	ATP2A2,GBF1,NUP93,STX18,STX5,SYNE1,SYNE2,ZW10
GO:0042147	retrograde transport, endosome to Golgi	5	79	4,96E-05	GBF1,GOSR1,GOSR2,STX5,VT11B
GO:0034613	cellular protein localization	14	1367	6,19E-05	DERL2,EXOC5,GBF1,GOSR2,NAPA,NSF,NUP93,STX18,STX5,SYNE1,SYNE2,VT11B,WDR19,ZW10
GO:0006904	vesicle docking involved in exocytosis	4	38	8,27E-05	EXOC2,SCFD1,SCFD2,VT11B
GO:0006906	vesicle fusion	5	95	0,0001	GOSR1,GOSR2,SEC22B,STX5,VT11B
GO:0065003	protein-containing complex assembly	14	1514	0,00017	CDK7,EXOC2,GOSR2,HBB,LETM1,NAPA,NDUFS2,NSF,NUP93,SCFD1,SEC22B,SMARCB1,STX5,ZW10
GO:0044085	cellular component biogenesis	18	2556	0,00024	CDK7,EXOC2,EXOC5,GATAD1,GOSR2,HBB,LETM1,NAPA,NDUFS2,NSF,NUP93,RSL1D1,SCFD1,SEC22B,SMARCB1,STX5,WDR19,ZW10
GO:0022607	cellular component assembly	17	2343	0,00032	CDK7,EXOC2,EXOC5,GATAD1,GOSR2,HBB,LETM1,NAPA,NDUFS2,NSF,NUP93,SCF-D1,SEC22B,SMARCB1,STX5,WDR19,ZW10
GO:0035494	SNARE complex disassembly	2	3	0,0013	NAPA,NSF
GO:0006887	exocytosis	9	774	0,0017	EXOC2,EXOC5,EXOC7,HBB,HSPA6,NSF,SCFD1,SCFD2,VT11B
GO:1903523	negative regulation of blood circulation	3	31	0,0017	ATP1A1,ATP2A2,DOCK4
GO:0007030	Golgi organization	4	95	0,0019	GBF1,STX5,SYNE1,ZW10
GO:0006886	intracellular protein transport	9	836	0,0029	DERL2,GOSR2,NAPA,NSF,NUP93,STX18,STX5,VT11B,WDR19
GO:0090166	Golgi disassembly	2	6	0,0033	GBF1,STX5
GO:0046903	secretion	10	1070	0,0036	EXOC2,EXOC5,EXOC7,HBB,HSPA6,MT-CO2,NSF,SCFD1,SCFD2,VT11B
GO:2000535	regulation of entry of bacterium into host cell	2	7	0,0041	EXOC2,EXOC7
GO:0009987	cellular process	44	14652	0,0048	ATP1A1,ATP2A2,CALU,CDK7,CHCHD3,CRIM1,DERL2,DNAJC16,DOCK1,DOCK4,ELMO1,ELMO2,EXOC2,EXOC5,EXOC7,GATAD1,GBF1,GOSR1,GOSR2,HBB,HSPA6,LETM1,MT-CO2,NAPA,NBAS,NDUFS2,NSF,NUP93,PRKDC,RSL1D1,SCFD1,SCFD2,SEC22B,SMARCB1,SON,STX18,STX5,SYNE1,SYNE2,TREX1,UQCRRH,VT11B,WDR19,ZW10
GO:0090286	cytoskeletal anchoring at nuclear membrane	2	8	0,005	SYNE1,SYNE2
GO:0065007	biological regulation	39	11740	0,0054	ATP1A1,ATP2A2,CDK7,CHCHD3,CRIM1,DERL2,DNAJC16,DOCK1,DOCK4,ELMO1,ELMO2,EXOC2,EXOC5,EXOC7,GATAD1,GBF1,GOSR1,GOSR2,HBB,LETM1,MT-CO2,NAPA,NBAS,NSF,NUP93,PRKDC,RSL1D1,SCFD1,SEC22B,SMARCB1,SON,STX18,STX-5,SYNE1,SYNE2,TREX1,VT11B,WDR19,ZW10

GO:0060341	regulation of cellular localization	8	766	0,0077	ATP2A2,DERL2,GBF1,GOSR1,NAPA,SCFD1,STX18,VT11B
GO:0032879	regulation of localization	15	2524	0,0087	ATP1A1,ATP2A2,DERL2,DOCK1,DOCK4,GBF1,GOSR1,LETM1,NAPA,NSF,RSL1D1,SCFD1,STX18,SYNE2,VT11B
GO:0060628	regulation of ER to Golgi vesicle-mediated transport	2	12	0,0091	SCFD1,STX18
GO:1902902	negative regulation of autophagosome assembly	2	12	0,0091	SCFD1,SEC22B
GO:006896	Golgi to vacuole transport	2	13	0,0102	GOSR2,VT11B
GO:0055119	relaxation of cardiac muscle	2	13	0,0102	ATP1A1,ATP2A2
GO:0048010	vascular endothelial growth factor receptor signaling pathway	3	67	0,0106	DOCK1,ELMO1,ELMO2
GO:0050789	regulation of biological process	37	11116	0,012	ATP1A1,ATP2A2,CDK7,CHCHD3,CRIM1,DERL2,DNAJC16,DOCK1,DOCK4,ELMO1,ELMO2,EXOC2,EXOC7,GATAD1,GBF1,GOSR1,GOSR2,HBB,LETM1,MT-CO2,NAPA,NBAS,NSF,NUP93,PRKDC,RSL1D1,SCFD1,SEC22B,SMARCB1,SON,STX18,STX5,SYNE2,TREX1,VT11B,WDR19,ZW10
GO:1902115	regulation of organelle assembly	4	168	0,0122	SCFD1,SEC22B,STX18,SYNE2
GO:1903358	regulation of Golgi organization	2	15	0,0124	STX18,STX5
GO:0038096	Fc-gamma receptor signaling pathway involved in phagocytosis	3	73	0,0128	DOCK1,ELMO1,ELMO2
GO:0042775	mitochondrial ATP synthesis coupled electron transport	3	78	0,0147	MT-CO2,NDUFS2,UQCRRH
GO:0060627	regulation of vesicle-mediated transport	6	480	0,0147	ATP2A2,GOSR1,NAPA,NSF,SCFD1,STX18
GO:0032386	regulation of intracellular transport	5	335	0,0183	ATP2A2,DERL2,NAPA,SCFD1,STX18
GO:0045822	negative regulation of heart contraction	2	23	0,024	ATP1A1,ATP2A2
GO:0022411	cellular component disassembly	5	364	0,0251	GBF1,NAPA,NSF,SMARCB1,STX5
GO:2000300	regulation of synaptic vesicle exocytosis	2	24	0,0251	ATP2A2,NAPA
GO:0006623	protein targeting to vacuole	2	26	0,0285	GOSR2,VT11B
GO:0002026	regulation of the force of heart contraction	2	27	0,0303	ATP1A1,ATP2A2
GO:0031330	negative regulation of cellular catabolic process	4	234	0,0327	DERL2,NBAS,SCFD1,SEC22B
GO:0006911	phagocytosis, engulfment	2	31	0,038	DOCK1,ELMO1
GO:0016477	cell migration	7	812	0,038	DOCK1,DOCK4,ELMO1,ELMO2,GBF1,NUP93,SYNE2
GO:0042407	crisetae formation	2	31	0,038	CHCHD3,LETM1
GO:0006997	nucleus organization	3	124	0,0438	NUP93,SYNE1,SYNE2
GO:0009894	regulation of catabolic process	7	840	0,0444	DERL2,EXOC7,NBAS,NSF,SCFD1,SEC22B,STX5
GO:0006361	transcription initiation from RNA polymerase I promoter	2	35	0,0445	CDK7,SMARCB1
GO:2000772	regulation of cellular senescence	2	35	0,0445	PRKDC,RSL1D1
GO:0086004	regulation of cardiac muscle cell contraction	2	36	0,0452	ATP1A1,ATP2A2
GO:0045823	positive regulation of heart contraction	2	37	0,0471	ATP1A1,ATP2A2
GO:0050794	regulation of cellular process	34	10484	0,0471	ATP1A1,ATP2A2,CDK7,CHCHD3,CRIM1,DERL2,DNAJC16,DOCK1,DOCK4,ELMO1,ELMO2,EXOC7,GATAD1,GBF1,GOSR2,HBB,LETM1,MT-CO2,NAPA,NBAS,NSF,NUP93,PRKDC,RSL1D1,SCFD1,SEC22B,SMARCB1,SON,STX18,STX5,SYNE2,WDR19,ZW10
GO:0006928	movement of cell or subcellular component	9	1355	0,0477	ATP1A1,DOCK1,DOCK4,ELMO1,ELMO2,GBF1,NUP93,SYNE2,WDR19
GO:0033365	protein localization to organelle	6	649	0,0487	GBF1,GOSR2,SYNE1,SYNE2,VT11B,ZW10

### Supplemental Figure I



**Supplemental figure I:** (Immuno)staining of VWF (red), TGN (gray) and nuclei (Hoechst; blue) in control (shCTRL) and shSTX5 HUVECs. B) Average number of WPBs per cell in control and shSTX5 cells (n=3 independent experiments t-test, \* P<0.05).





## Chapter 5

# Exocytosis of Weibel-Palade bodies: how to unpack a vascular emergency kit

Maike Schillemans, Ellie Karampini, Marije Kat and Ruben Bierings  
*J Thromb Haemost* 2019; 17: 6–18

## Summary

The blood vessel wall minimizes blood loss and prevents or overcomes infections in the event of vascular trauma with a number of self-healing properties. Endothelial cells pre-package a cocktail of hemostatic, inflammatory and angiogenic mediators in their unique secretory organelles, the Weibel-Palade bodies (WPBs),<sup>1</sup> which can be immediately released on demand. Secretion of their content into the vascular lumen through a process called exocytosis enables the endothelium to actively participate in the arrest of bleeding and to slow down and direct leukocytes to areas of inflammation.

Owing to their remarkable elongated morphology (Figure 1) and inclusion of secretory content that spans the entire size spectrum of small chemokines all the way up to ultra-large Von Willebrand factor (VWF) multimers, WPBs are an ideal model system for studying the molecular mechanisms of secretory organelle biogenesis, exocytosis and content expulsion. Recent studies have now shown that during exocytosis WPBs can undergo several distinct modes of fusion and can utilize fundamentally different mechanisms to expel their content. In this article we will discuss recent advances in our understanding of the composition of the WPB exocytotic machinery and how, based on its configuration, it is able to support WPB release in its various forms.

## Weibel-Palade bodies: secretory organelles of the endothelium

The main cargo of WPBs is Von Willebrand factor (VWF), a large multimeric adhesive protein that mediates platelet adhesion to the endothelium and to the subendothelial matrix.<sup>2</sup> VWF also acts as a chaperone for coagulation factor VIII (FVIII) in plasma and prevents its premature clearance, which is critical for the maintenance of normal circulating FVIII levels. VWF undergoes a complex series of post-translation modifications including glycosylation, multimerization and proteolytic processing and is the driving force behind formation of WPBs. Mutations in VWF that affect its synthesis or processing and subsequent storage in WPBs are at the basis of Von Willebrand disease (VWD), the most common inherited bleeding disorder that is caused by quantitative or qualitative defects in VWF. The topics of VWF biosynthesis, WPB formation and VWD have been extensively covered in a number of excellent reviews<sup>3-5</sup> and will therefore not be in the scope of this review.

Alongside VWF a considerable number of inflammatory and angiogenic mediators are co-packaged into WPBs (Figure 1C).<sup>6,7</sup> Their simultaneous release from this vascular emergency package will also direct leukocytes to sites of inflammation and promote vessel repair. To tailor its secretory response to the prevailing vascular condition the endothelium continuously transduces cues from the local microenvironment into dynamic control over the content of WPBs by selectively including or excluding certain cargo. Conditions that mimic laminar flow lead to reduced angiotensin-2 content in WPBs.<sup>8</sup> Exposure to pro-inflammatory cytokines leads to upregulation of chemokines such as IL-8, MCP-1, eotaxin-3 and IL-6, which are packaged into newly synthesized WPBs.<sup>9</sup> Since WPBs are long-lived storage organelles with a turnover of ~24 hours,<sup>10-12</sup> endothelial cells will accumulate distinct populations of granules that differ in their levels of co-targeted WPB cargo.<sup>9,13</sup> Whether the degree of inclusion of co-targeted WPB cargo reflects the endothelial activation state of the moment the WPB was synthesized or, alternatively, if this is a result of stochastic variation following gradual redistribution of content over the WPB population through content intermixing, such as been reported for other long-lived organelles like lysosomes,<sup>14</sup> is currently unclear. Interestingly, it has been suggested that subsets of granules can be subject to differential exocytosis,<sup>15</sup> although the mechanism behind this differential release remains elusive.

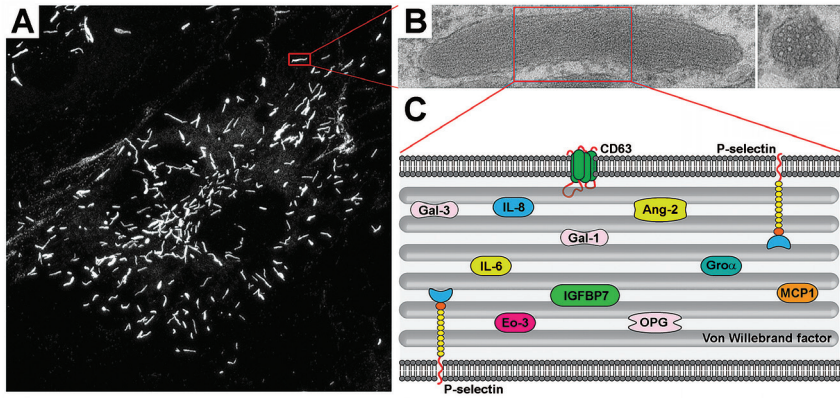


**Figure 1: Weibel-Palade bodies, secretory organelles of the endothelium.** A) Endothelial cells containing characteristic elongated WPBs visualized by VWF immunostaining. B) WPB ultrastructure with a longitudinal section (left) showing internal striations and a cross section (right) showing bundles, which represent densely packed VWF tubules. C) Cartoon representation of WPB cargo.

## The endothelial secretory pathway

VWF secretion from endothelial cells occurs via three main routes: (1) constitutive secretion and (2) basal secretion, both of which occur in the absence of stimulation, and (3) regulated secretion of WPBs in response to endothelial activation (Figure 2). Following its journey through the early secretory pathway VWF undergoes a sorting step at the level of the *trans*-Golgi network (TGN): low molecular weight (LMW) VWF multimers enter the constitutive secretory pathway in small short-lived anterograde carriers which are immediately released at the plasma membrane.<sup>16</sup> High molecular weight (HMW) VWF multimers enter the storage pathway by condensing into tubules which are packaged in nascent WPBs that bud off the TGN.<sup>17</sup> This compartment constitutes the releasable pool of HMW VWF that

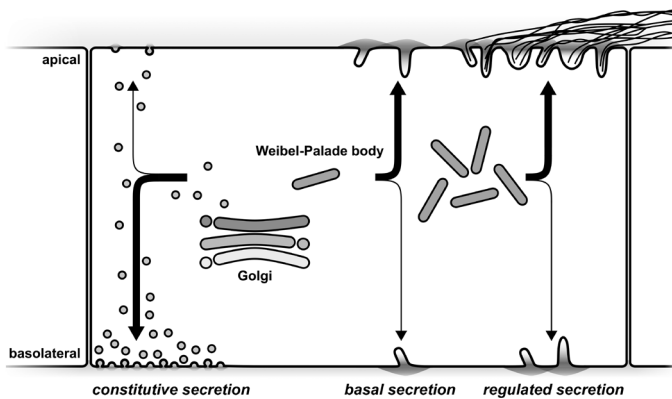


**Figure 2: The endothelial secretory pathway.** VWF secretion occurs via three pathways: (1) constitutive secretion of LMW VWF, which is primarily released at the basolateral side of the endothelium; (2) basal and (3) regulated secretion of HMW VWF from WPBs, which is primarily directed towards the apical surface. From the large number of WPBs that undergo exocytosis upon stimulated release, ultra-large VWF (UL-VWF) multimers emerge that assemble into VWF strings on the apical side of the endothelium.

is secreted upon secretagogue stimulation. The proportion of VWF that sorts into either direction has long been a matter of debate, partly because previous studies only considered constitutive and regulated secretion.<sup>16,18</sup> Careful kinetic monitoring of VWF trafficking has revealed that the storage pathway is also responsible for the majority of unstimulated VWF release through basal secretion.<sup>12</sup> This most likely reflects gradual, stochastic turnover of WPBs as VWF retention in this pathway correlates with the reported half-life of these granules.<sup>10,12</sup> It suggests that the secretory machinery of WPBs at baseline is already in a certain degree of readiness that supports low level, spontaneous release. It also reconciles earlier and recent observations that the bulk of VWF released by resting endothelial cells is of high multimeric nature.<sup>18,19</sup>

Apart from the degree of multimerization another distinction between the constitutive and basal/stimulated secretion pathway can be made based on the polarity of release. *In vivo*, the apical side of the endothelial cells faces the vascular lumen which results in VWF secretion directly into the circulation. VWF unfurls and assembles into ultra-large VWF strings that can be up to several millimeters in length. Entanglement of several of these strings leads to the formation of spiderweb-like networks that function as adhesive platforms for platelets.<sup>20</sup> In this way, VWF strings act as polymeric force sensors that upon flow expose a shear-dependent binding site for platelet GPIb.<sup>4</sup> Basolaterally released VWF is deposited in the subendothelial matrix, where it mediates platelet adhesion when the matrix is exposed following damage to the vessel wall, either directly or via self-association with plasma VWF.<sup>21,22</sup> Over 3 decades ago the idea had already arisen that secretion of such functionally distinct pools of VWF may differ in polarity, but previous studies addressing the polarity of endothelial VWF release remained inconclusive because they did not consider the contribution of spontaneous release of regulated secretory cargo via the basal route.<sup>23,24</sup> A recent study has now convincingly shown that constitutive release of LMW VWF is mainly released basolaterally whereas basal and stimulated release of HMW VWF from WPBs primarily occurs at the apical face.<sup>19</sup>

## Stimuli and signaling cascades

WPB exocytosis is triggered by a wide range of physiological (stress hormones, e.g. epinephrine; proteases, e.g. thrombin; biogenic amines, e.g. histamine and 5-hydroxytryptamine; and shear stress) and pathological (e.g. bacterial toxins) signals (reviewed in <sup>6</sup>) that use  $\text{Ca}^{2+}$  or cAMP as second messengers (Figure 3). As part of an integrated response to vascular injury  $\text{Ca}^{2+}$ -mediated secretagogues such as histamine and thrombin locally promote a prothrombotic, proinflammatory state by instantaneously causing release of large quantities of VWF and other WPB constituents while simultaneously increasing endothelial permeability and vascular tone.<sup>25,26</sup> In contrast, cAMP-mediated stimuli such as epinephrine and vasopressin act systemically, increase endothelial barrier function and when applied to cultured endothelial cells induce a slow but sustained release of WPBs.<sup>27-30</sup> This pathway can be clinically exploited to correct prolonged bleeding times in patients with mild hemophilia A or VWD through administration of the vasopressin analogue DDAVP, which mobilizes VWF from its endothelial stores following activation of the vasopressin-2 receptor (V2R).<sup>28,31</sup> Despite their distinct kinetic and physiological profile  $\text{Ca}^{2+}$ - and cAMP-dependent pathways converge at the same effector pathways which control actin remodeling and tethering and fusion of WPBs, albeit in some cases with different outcomes (Figure 3).

Elevations of intracellular free  $\text{Ca}^{2+}$  concentration ( $[\text{Ca}^{2+}]_i$ ) arise after activation of phospholipase C (PLC) by ligand bound G-protein coupled receptors (GPCRs).<sup>32</sup> Dose-dependent, subsecond release of WPBs in response to ionophores or caged  $\text{Ca}^{2+}$  implies that sustained elevation of  $[\text{Ca}^{2+}]_i$  is a sufficient transduction signal to drive WPB fusion independently from additional receptor-triggered signaling.<sup>26,33</sup> In nearly every regulated secre-

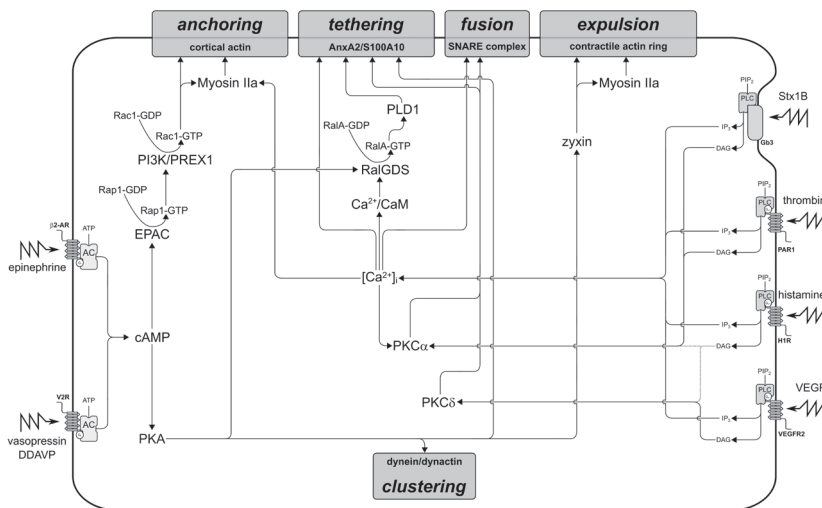


**Figure 3: Signaling cascades in WPB exocytosis.**  $\text{Ca}^{2+}$ - and cAMP-mediated secretagogues that trigger WPB exocytosis use distinct and common signalling circuits that converge at effector pathways that control anchoring, tethering, vesicle fusion and actin contractility. PIP<sub>2</sub>: phosphatidylinositol 4,5-bisphosphate; IP<sub>3</sub>: inositol 1,4,5-triphosphate; DAG: diacylglycerol; H1R: histamine H1 receptor; PAR1: protease-activated receptor 1; VEGFR2: vascular endothelial growth factor receptor 2; Gb3: ceramide trihexoside. ATP: adenosine triphosphate; cAMP: cyclic adenosine monophosphate.

tory system a vesicle-associated  $\text{Ca}^{2+}$  sensor is responsible for coupling transient elevations in  $[\text{Ca}^{2+}]_i$  to the soluble N-ethylmaleimide-sensitive factor (NSF) attachment protein receptor (SNARE) fusion machinery, but so far such a WPB-localized  $\text{Ca}^{2+}$  sensor has not been identified.<sup>34</sup> However, a number of other  $\text{Ca}^{2+}$  sensing mechanisms have been described to couple cytosolic  $\text{Ca}^{2+}$  to the endothelial exocytotic response. When  $\text{Ca}^{2+}$  is associated with the  $\text{Ca}^{2+}$ -sensor calmodulin (CaM), the  $\text{Ca}^{2+}$ /CaM complex binds to the N-terminus of the guanine nucleotide exchange factor (GEF) RalGDS, thereby unleashing its GEF activity towards the small GTPase RalA.<sup>35</sup> Activated RalA most likely coordinates a tethering step by promoting Arf6-dependent phospholipase D1 (PLD1) activity.<sup>36</sup> Local modification of phospholipids by PLD1 generates plasma membrane microdomains that recruit the  $\text{Ca}^{2+}$ - and phospholipid binding AnxA2-S100A10 complex, which in its turn links WPBs to membrane fusion sites through the WPB-localized tethering factor Munc13-4.<sup>37–39</sup>  $\text{Ca}^{2+}$ -mediated VWF secretion is also dependent on rapid changes in the actin cytoskeleton that lead to the formation of parallel arranged stress fibers, a process primarily regulated by GTPases of the Rho family.<sup>29,40,41</sup>

Triggering of the GPCR-coupled V2R and  $\beta$ 2-adrenergic receptors activates the cAMP-dependent protein kinase A (PKA) after conversion of ATP into cAMP.<sup>27,28</sup> PKA is critically involved in VWF secretion by activating a number of effector pathways,<sup>42</sup> such as tethering of WPBs through the RalGDS-RalA pathway and the AnxA2/S100A10 tethering complex<sup>30,35,38</sup> and via phosphorylation of zyxin during contractile ring assembly.<sup>43</sup> During cAMP-mediated stimulation a subset of WPBs avoids release by clustering together around the microtubule organizing center, which is the result of dynein-dynactin-dependent retrograde transport activated by PKA.<sup>42,44</sup> Whether this is a stochastic process that serves to limit the secretory response or whether these WPBs represent a specific subset of granules that are actively set aside, for instance based on their recruited membrane components, state of maturation or localization,<sup>15</sup> is still unclear. The exchange protein directly activated by cAMP (EPAC) is also activated during cAMP-mediated WPB release and catalyzes the activation of the small GTPase Rap1.<sup>45,46</sup> Via a complex of its downstream effectors PI3 kinase and the Rac exchange factor PREX1, activated Rap1 in its turn promotes activation

of the Rho GTPase Rac1.<sup>47</sup> The Rap1-Rac1 pathway is thought to promote secretion by rearranging actin into thin cortical bundles in close apposition to the plasma membrane and/or by regulating the formation or contractility of actin on the fusing WPB membrane.<sup>43</sup>

Protein kinase C (PKC) is a key signaling mediator for a number of endothelial agonists that trigger secretion of VWF. Phorbol esters, such as phorbol 12-myristate 13-acetate (PMA), are potent (nonphysiological) stimulators of VWF secretion that directly activate PKC by mimicking the action of diacylglycerol (DAG).<sup>25</sup> Histamine, VEGF and Shiga toxin Stx1B elevate  $[Ca^{2+}]_i$  in a PLC-dependent manner and simultaneously either signal through the  $Ca^{2+}$ -independent PKC $\delta$  (VEGF and histamine) or utilize the  $Ca^{2+}$ -dependent PKC $\alpha$  (Stx1B and histamine).<sup>32,48-51</sup> Among its targets are components of the SNARE machinery, the assembly of which is partly regulated through PKC-dependent phosphorylation events.<sup>52</sup> Nevertheless several ambiguities remain that suggest PKC is not always essential for VWF secretion. Both VEGF and histamine activate PKC $\delta$ , however broad range PKC inhibition or specific depletion of PKC $\delta$  significantly reduced secretory responses after VEGF but not after histamine administration.<sup>48</sup> PKC $\alpha$  is activated by Stx1B as well as histamine, but is only essential for Stx1B-induced release; inhibition of PKC $\alpha$  did not block histamine-induced VWF secretion and in some studies even enhanced it.<sup>48,51,53-55</sup> Paradoxically, 3 independent studies showed that blocking calcium signaling, which entirely blunts VWF release induced by both histamine and PKC $\alpha$ -dependent Stx1B, was not sufficient to fully inhibit VEGF-induced VWF secretion.<sup>32,48,50,53</sup> The difference in requirement of PKC and  $Ca^{2+}$  raises intriguing questions about how common signaling pathways activated by different agonists are differentially utilized and integrated to control secretion.

## Exocytotic machinery of WPBs

After emerging from the TGN immature WPBs initially are secretion incompetent because they have yet to acquire (parts of) the exocytotic machinery.<sup>56</sup> In a maturation-dependent manner WPBs recruit several GTPases of the Rab family, including Rab27A, several Rab3 isoforms and Rab15.<sup>37,56-58</sup> Rab GTPases are molecular switches that cycle between a GDP-bound “off”-state and a membrane-associated, GTP-bound “on”-state and generally contribute to defining organelle identity.<sup>59</sup> In their active GTP-bound state the Rabs are responsible for the subsequent recruitment of a set of effector proteins (MyRIP, Munc13-4 and Slp4-a) to the WPB. This process correlates with the acquisition of secretion competence<sup>56</sup> and enables WPBs to interact with the cytoskeleton and/or plasma membrane (Figure 4).<sup>56,58,60</sup> MyRIP is a Rab27A-specific effector that binds actin, directly and via the actin motor protein Myosin Va, and tethers WPBs to the actin cytoskeleton in the cell periphery.<sup>41,60,61</sup> The actin cytoskeleton plays opposing roles in the release of WPBs: On the one hand it is necessary for peripheral distribution of WPBs, which is important for releasability and depends on Myosin IIa.<sup>62</sup> On the other hand actin acts as a barrier<sup>29,40</sup> and by anchoring WPBs to the actin cytoskeleton MyRIP acts as a brake during exocytosis.<sup>41,56,60</sup> Munc13-4 binds both Rab27A and Rab15 and promotes exocytosis by tethering WPBs to release sites on the plasma membrane, which contain the Annexin A2-S100A10 complex.<sup>39,58</sup> Slp4-a interacts with Rab3 isoforms and Rab27A, with the latter in an activity-insensitive manner, and promotes WPB exocytosis<sup>56</sup> by providing the link between the WPB and members of the SNARE complex.<sup>63</sup> From this all it becomes clear that during acquisition of secretion competence WPBs recruit a cocktail of Rabs and Rab-effectors that individually perform opposing functions during secretion. Upon exocytosis, they engage in a tug of war in which the balance of effectors, their levels of activation by upstream signaling events and the efficacy of their downstream mechanisms decide the probability of release.<sup>56</sup>

In the final phase of exocytosis, the WPB fuses with the plasma membrane, which is catalyzed by a ternary complex of SNARE proteins that are positioned on the 2 opposing

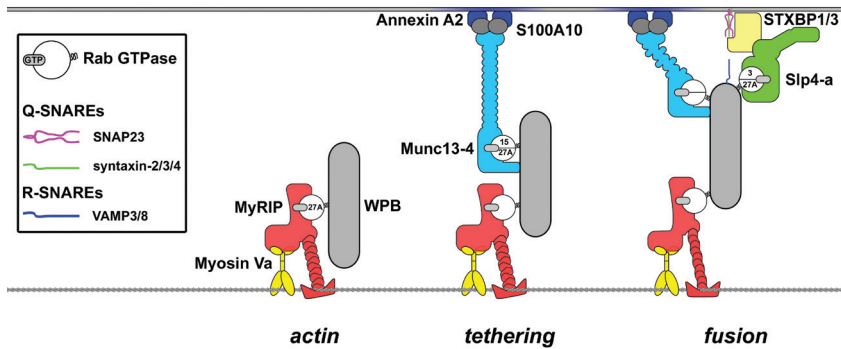


**Figure 4: The WPB exocytotic machinery.** Rab-effector complexes mediate anchoring of WPBs to the cytoskeleton, tethering to the plasma membrane and interactions with the SNARE fusion machinery. The Rab27A-MyRIP-MyoVa complex anchors WPBs to the actin cytoskeleton. Munc13-4 can be recruited by Rab GTPase-dependent (Rab15/Rab27A) or by Rab-independent mechanisms and tethers WPBs to membrane fusion sites via the Annexin A2-S100A10 complex. The Rab27A-Slp4-a complex docks WPBs and forms the link between the WPB and the SNARE complex via members of the STXBP family.

membranes. SNARE proteins can be functionally classified as t-SNAREs that are found on the target membrane and v-SNAREs that are found on the donor/vesicle membrane. The exocytotic SNARE complex consists of an v-SNARE of the VAMP family on the donor (i.e. WPB) membrane and 2 t-SNAREs (1 SNARE helix from a syntaxin, 2 SNARE helices from a SNAP25 homologue) on the acceptor (i.e. plasma) membrane (Figure 5). Together they assemble into a 4 helical bundle that when rolling up brings donor and acceptors membrane together in a zipper-like motion, thereby largely overcoming the energy barrier that normally prevents fusion of membranes. WPBs contain two v-SNAREs, VAMP3 and VAMP8, of which only VAMP3 has so far been shown to support stimulus-induced WPB release.<sup>64,65</sup> t-SNAREs that take part in WPB release include the SNAP25 homologue SNAP23 and syntaxin-3, -4 and most likely also syntaxin-2.<sup>52,63,66,67</sup> Due to their promiscuous nature, various combinations of these SNAREs exist: in endothelial cells syntaxin-4 engages with SNAP23 and VAMP3 or VAMP8.<sup>65,67</sup> Syntaxin-3 primarily interacts with VAMP8 and SNAP23<sup>67</sup>, the SNARE partners of syntaxin-2 are still unknown. This suggests that endothelial cells can employ at least three (syntaxin-4::SNAP23::VAMP3, syntaxin-4::SNAP23::VAMP8 and syntaxin-3::SNAP23::VAMP8) and possibly more distinct SNARE complexes for release of WPBs. Interestingly, while syntaxin-4 is localized on the plasma membrane, syntaxin-3 is found on WPBs<sup>67</sup>, suggesting that in certain cases WPBs can also function as the acceptor compartment during fusion.

Formation of SNARE complexes is controlled by syntaxin binding proteins (STXBPs), of which several take part in WPB release. The Slp4-a interactor STXBP1 promotes VWF secretion and interacts with syntaxin-2 or -3<sup>63</sup>, potentially controlling 2 separate downstream mechanisms towards exocytosis. Munc18c (also known as STXBP3) controls the assembly of syntaxin-4 containing SNARE complexes. Depending on a (de)phosphorylation switch controlled by PKC $\alpha$  and protein phosphatase 2B, phosphorylated Munc18c releases its grip on syntaxin-4 and allows the latter to engage with VAMP3.<sup>52,68</sup> STXBP5 was initially implicated in the WPB exocytotic machinery as a genetic modifier of circulating VWF: a polymorphism encoding the nonsynonymous N436S substitution in STXBP5 is linked to lower VWF plasma levels.<sup>69</sup> In endothelial cells STXBP5 is a negative regulator of WPB release and interacts with syntaxin-4 but not with SNAP23.<sup>70</sup> Possibly, the carboxyterminal VAMP-like domain acts as a decoy for syntaxin-4 which produces a non-fusogenic dead end, thereby lowering the number syntaxin-4 containing SNARE complexes that can support

exocytosis. Interestingly, the N436S variant of STXBP5 attenuates VWF secretion in endothelial cells<sup>70</sup>, although the mechanism through which this substitution inhibits release is still unclear. Taken together, the SNARE machinery is highly dynamic and based on its configuration may promote or attenuate secretion, but exactly how all these individual components together orchestrate WPB release remains unclear. Moreover, it raises the question why endothelial cells utilize so many different SNARE complexes for exocytosis of the same secretory organelle?

## Secretory modes of WPB exocytosis

Several different modes of stimulus-induced WPB exocytosis have been reported (Figure 5A). Initially a lipidic fusion pore is formed at the interface of vesicle and plasma membrane that establishes an aqueous channel between the WPB lumen and the extracellular space.<sup>71</sup> Recordings of fusion pore dynamics of serotonin-loaded WPBs using amperometry revealed that this transient structure exists only for a limited time (usually <200 milliseconds) before it rapidly expands within tens of milliseconds<sup>72</sup>. With its pore expanded fully the WPB undergoes full fusion resulting in delivery of soluble granule cargo into the lumen and collapse of the vesicle membrane together with its associated membrane components into the plasma membrane.<sup>26,73</sup> In a subset of cases the WPB fusion pore does not expand fully, but the pore lingers in a restricted state for some seconds before closing prematurely. The restricted diameter of the pore during this “lingering” mode of fusion, so-called lingering-kiss exocytosis, acts as a molecular size filter: small cargo, such as chemokines or the integral membrane protein CD63, are able to traverse the narrow pore that excludes passage of larger cargo proteins such as VWF, VWF propeptide (VWFpp) or P-selectin. After resealing of the unexpanded fusion pore these proteins are selectively retained in spherical WPBs, which probably owe their rounded morphology and the disruption of the orderly bundling of VWF tubules to the hydration of their paracrystalline interior.<sup>74</sup>

Apart from these heterotypic fusion modes (fusion between different compartments, i.e. WPB – plasma membrane) also homotypic fusion modes (i.e. WPB – WPB) have been described. During compound fusion several individual WPBs coalesce intracellularly prior to release and then collectively undergo exocytosis as a single entity. The first evidence for this mode of fusion in endothelial cells was provided by measurements of membrane capacitance, which is proportional to cell surface area, stepwise increases of which are due to addition of membrane during fusion of secretory organelles. A significant proportion of discrete membrane capacitance increases observed after evoking WPB exocytosis using high levels of  $[Ca^{2+}]_i$  were too large to be accounted for by the fusion of a single WPB and could only be explained by fusion of an accumulated structure made up of several WPBs.<sup>33</sup> Morphological studies of such intermediate structures have shown that they consist of enlarged, rounded structures, termed secretory pods, which contain disordered VWF tubules.<sup>75</sup> Secretory pods are prominent features following extended stimulation with PMA, but the occurrence of similar structures has also been demonstrated *in vivo* in response to factor Xa or histamine in toads and rats, respectively.<sup>76,77</sup> Despite the loss of tubular organization of VWF multimers in the spherical secretory pods, VWF strings can eventually emerge from the extruded material.<sup>78</sup> Finally, by monitoring the redistribution of EGFP-CD63 through the membranes of fusing granules a related but mechanistically distinct mode of homotypic WPB fusion, termed sequential or cumulative exocytosis, was observed.<sup>79</sup> In this mode a post-fusion WPB is used as a membrane fusion site for subsequent cumulative fusion of additional WPBs, culminating in the ginger root-like fusion structures that were observed in ultrastructural studies.<sup>76,80</sup>

A number of questions remain. First, what is the molecular basis for all these different release mechanisms? Specificity of membrane fusion during exocytosis is mediated by the





fusion machinery from the plasma membrane such as the cognate SNAREs for WPB-localized VAMPs. (Figure 5Bii) This also raises the possibility that secretory pods represent an intermediate state during cumulative fusion into WPBs that previously underwent lingering-kiss exocytosis.

Secondly, what's the use of all these distinct modes of exocytosis? Indirect or incomplete fusion modes are in certain cases energetically favorable. Homotypic fusion modes can serve to concentrate cargo release at hotspots when access to fusion sites on the membrane becomes limiting. It may also augment the secretory response by providing indirect access to the plasma membrane to a pool of WPBs situated deeper into the cytoplasm.<sup>80</sup> Lingering kiss fusion not only saves vesicle reformation and retrieval of vesicle membrane proteins, but may also help in preserving a delicate balance between endocytosis and exocytosis by limiting membrane expenditure. Exocytosis-endocytosis coupling is pertinent to the choice of secretory mode since pharmacological blocking of compensatory endocytosis resulted in a shift from full fusion towards cumulative exocytosis, possibly due to the inability to retrieve membrane components from the post-fusion WPBs.<sup>80</sup> Distinct fusion modes also allow the endothelium to fine-tune its secretory response to specific vascular conditions: lingering kiss fusion only releases a subset of molecules such as chemokines while pro-thrombotic cargo remains stuck within.<sup>74</sup> Post-fusion entanglement of VWF tubules in compound as well as cumulative fusion structures does not preclude the eventual formation of VWF strings but results in shorter strings when cumulative fusion was promoted.<sup>78,80</sup>

## Content expulsion

Secretory cargo expulsion is dependent on lateral tension in the plasma membrane; relaxation of this tension through the addition of new membrane from fusing granules opens the fusion pore and provides a force to drive secretory cargo out, which is then followed by full collapse of the vesicle into the plasma membrane.<sup>83</sup> However, the near-solid VWF paracrystal presents a significant hurdle for release as its enormous size and state will naturally resist discharge and membrane collapse. Recent studies have shown that endothelial cells, depending on their type of activation, can utilize fundamentally different modes of secretory content expulsion.

The rapid process of content expulsion during  $\text{Ca}^{2+}$ -mediated full fusion of WPBs bears the hallmarks of a jack-in-the-box mechanism that is often observed when condensed, poly-ionic molecules such as VWF need to undergo a phase transition before release.<sup>84</sup> Exchange of ions and entry of water molecules into the vesicle interior through the stalk-shaped fusion pore leads to hydration of the vesicle core and rapid neutralization of the acidic milieu of the WPB.<sup>26</sup> Dissolution of the proton gradient and other cationic species such as  $\text{Ca}^{2+}$  that are crucial for the condensed tubular packing of VWF<sup>85,86</sup> will result in loss of shielding of negative charges in VWF. The consequential charge repulsion within and between VWF multimers leads to decondensation of cargo as evidenced by the swelling of the granule and increased separation between VWF tubules.<sup>71</sup> This is followed by an explosive discharge of ultra-large VWF multimers and other cargo on a subsecond timescale, consistent with a mechanism in which VWF tubules act as electrostatic springs.<sup>26,73,87,88</sup>

An alternative mechanism of VWF expulsion has been observed in response to  $\text{Ca}^{2+}$ -independent secretagogues, such as cAMP-mediated agonists or phorbol esters. Prior to fusion, local rearrangements of cortical actin lead to formation of actin frameworks that appear to engage WPBs. Formation of such frameworks is dependent on the tension-sensitive focal adhesion protein zyxin following its phosphorylation by PKA and appositions WPBs close to the membrane.<sup>43</sup> Then, shortly after opening of the fusion pore an actomyosin ring is assembled coating the distal end of the fusing granule, a process that involves *de novo* actin polymerization.<sup>43,89</sup> Inhibition of the myosin IIa-dependent contractility of the

actomyosin ring prevented VWF release from fusing WPBs, while not affecting the secretory fate of P-selectin<sup>89</sup> (but not in<sup>62</sup>), leading to the hypothesis that contraction of such rings provides a necessary physical force to squeeze VWF out of the fusing granule. It is currently unclear what initiates actomyosin ring formation on the post-fusion WPB, but the involvement of the tension sensor zyxin<sup>43</sup> suggests that changes in local (membrane)-tension such as on a swelling granule may be an important parameter in this process. Actomyosin ring contractility is regulated by phosphorylation of myosin IIa, which has been shown to involve zyxin-dependent recruitment of casein kinase II.<sup>62</sup> Interestingly, zyxin depletion did not impair VWF release by thrombin or histamine, which is consistent with the observation that actomyosin rings do not play an important role in expulsion of VWF during Ca<sup>2+</sup>-mediated WPB exocytosis.<sup>43,87</sup>

## Weibel-Palade bodies in health and disease

Circulating levels of VWF vary widely across the human population.<sup>90</sup> The clinical manifestations at the far ends of this distribution highlight the pivotal role that VWF plays in vascular health. Low levels of plasma VWF lead to bleeding, such as in the inherited bleeding disorder Von Willebrand disease (VWD).<sup>5</sup> In some cases this is the result of mutations in *VWF* that lead to altered WPB morphology and decreased releasability such as evident in VWD blood outgrowth endothelial cells.<sup>91</sup> Increased levels of circulating VWF are associated with cardiovascular morbidity such as coronary heart disease, ischemic stroke and venous and arterial thrombosis<sup>92,93</sup>, pathologies for which the risks are reduced in VWD patients.<sup>94</sup> The variation in VWF plasma levels across the population is largely genetically determined.<sup>95</sup> Population-based linkage analyses in healthy individuals have identified a number of genetic loci that are associated with VWF levels, including the *ABO* locus and clearance receptors *CLEC4M* and *STAB2*, but also several components of the SNARE machinery (*STX2* and *STXBP5*).<sup>69,96</sup> One of the SNPs in *STXBP5* that was linked with higher VWF levels is also associated with venous thrombosis.<sup>97</sup> Variants in both *STX2* and *STXBP5* are also associated with VWF levels and disease severity in VWD patients.<sup>98</sup> Together this points out that SNARE-mediated secretion from WPBs is an important determinant of VWF plasma levels. This fits with the current consensus that the lion's share of circulating VWF, which primarily consists of high multimer VWF, originates from the storage pathway rather than from constitutive secretion.<sup>12,18,19</sup> Whether this arises from the basal or stimulated compartment may be less evident. Several of the Rab- and SNARE-(associated) regulators of stimulated WPB exocytosis also affect the basal secretion of VWF,<sup>56,63,67</sup> suggesting that the same SNARE fusion machinery is also responsible for basal release. Basal secretion accounts for the bulk of VWF that endothelial cells produce and release over time. How reflective this is of the situation *in vivo* where some areas of the vasculature may be under continuous influence of low-level stimulation by hormones such as epinephrine or vasopressin, is unclear. However, based on extrapolation of the ratio of basal versus stimulated release from cultured endothelial cells, the required area of vascular bed to be maximally activated at any given time to match what is secreted basally makes it unlikely that stimulated release contributes significantly to steady state VWF levels.<sup>19</sup>

Other pathologies that may arise from disturbed release from WPBs include angiodysplasia, which is a common complication in VWD patients that causes recurrent gastrointestinal bleedings through small vascular malformations in the gut. Recent studies have shown that VWF regulates angiogenesis, either extracellularly via controlling the cell surface expression of alphaVbeta3-integrin and/or indirect via influencing the release of one of its WPB co-residents, the angiogenic mediator Ang-2.<sup>99</sup> In the absence of its storage compartment, such as in severe VWD type 3, Ang-2 is secreted constitutively, promoting vessel destabilization. Apart from Ang-2, a number of other angiogenic mediators such as IGFBP7 and

galectin-1 and -3 are found in WPBs<sup>7,100</sup> and may be subject to similar dysregulated release in the absence of VWF, which potentially further contributes to pathological angiogenesis.

## Conclusions and future directions

Endothelial cells control secretion from their WPBs using a remarkably complex exocytotic machinery of which the outlines are now starting to become clear. However, our knowledge on the exact composition of this machinery is incomplete and importantly we are still a long way from understanding how all these components are able to direct the different modes of WPB fusion. Also, we currently do not understand how expansion of the fusion pore is regulated or what drives content expulsion in response to different endothelial activation states. To come to a deeper understanding of these processes we will need to determine changes to the characteristic ultrastructure of WPBs during fusion and content expulsion and to link these changes to individual components of the exocytotic machinery. Understanding the mechanism and purpose of the endothelium's ability to fine-tune its secretory response to vascular events would potentially allow us to exploit this mechanism for therapeutic benefit in the treatment of hematologic and cardiovascular disease.

## Disclosure of Conflicts of Interest

The authors state that they have no conflict of interest.

## Acknowledgements

We apologize to all authors whose work has been omitted owing to space restrictions, and for not always citing primary literature. Work in our lab is supported by grants from the Landsteiner Stichting voor Bloedtransfusie Research (LSBR-1244 and LSBR-1707), the Netherlands Ministry of Health (PPOC-2015-24P and PPOC-2018-21), the Dutch Thrombosis Foundation (TSN-56-2015 and TSN-2017-01) and a Research Fellowship from the European Hematology Association (EHA).

## References

1. Weibel ER, Palade GE. New cytoplasmic components in arterial endothelia. *J. Cell Biol.* 1964;23(1):101–12.
2. Ruggeri ZM. Von Willebrand factor, platelets and endothelial cell interactions. *J. Thromb. Haemost.* 2003;1(7):1335–1342.
3. Valentijn KM, Sadler JE, Valentijn JA, Voorberg J, Eikenboom J. Functional architecture of Weibel-Palade bodies. *Blood.* 2011;117(19):5033–5043.
4. Springer TA. von Willebrand factor, Jedi knight of the bloodstream. *Blood.* 2014;124(9):1412–1426.
5. Leebeek FWG, Eikenboom J. Von Willebrand's Disease. *N. Engl. J. Med.* 2016;375(21):2067–2080.
6. Rondaj MG, Bierings R, Kragt A, Van Mourik JA, Voorberg J. Dynamics and plasticity of Weibel-Palade bodies in endothelial cells. *Arterioscler. Thromb. Vasc. Biol.* 2006;26(5):1002–1007.
7. van Breevoort D, van Agtmaal EL, Dragt BS, et al. Proteomic screen identifies IGFBP7 as a novel component of endothelial cell-specific Weibel-Palade bodies. *J. Proteome Res.* 2012;11(5):2925–36.
8. van Agtmaal EL, Bierings R, Dragt BS, et al. The shear stress-induced transcription factor KLF2 affects dynamics and angiopoietin-2 content of Weibel-Palade bodies. *PLoS One.* 2012;7(6):e38399.
9. Knipe L, Meli A, Hewlett L, et al. A revised model for the secretion of tPA and cytokines from cultured endothelial cells. *Blood.* 2010;116(12):2183–2191.
10. Kobayashi T, Vischer UM, Rosnoble C, et al. The tetraspanin CD63/lamp3 cycles between endocytic and secretory compartments in human endothelial cells. *Mol. Biol. Cell.* 2000;11(5):1829–1843.
11. Fiedler U, Scharpfenecker M, Koidl S, et al. The Tie-2 ligand Angiopoietin-2 is stored in and rapidly released upon stimulation from endothelial cell Weibel-Palade bodies. *Blood.* 2004;103(11):4150–4156.
12. Giblin JP, Hewlett LJ, Hannah MJ. Basal secretion of von Willebrand factor from human endothelial cells. *Blood.* 2008;112(4):957–64.
13. Bierings R, van den Biggelaar M, Kragt A, et al. Efficiency of von Willebrand factor-mediated targeting of interleukin-8 into Weibel-Palade bodies. *J. Thromb. Haemost.* 2007;5(12):2512–2519.
14. Deng YP, Storrie B. Animal cell lysosomes rapidly exchange membrane proteins. *Proc. Natl. Acad. Sci. U. S. A.* 1988;85(11):3860–4.
15. Cleator JH, Zhu WQ, Vaughan DE, Hamm HE, Dc W. Differential regulation of endothelial exocytosis of P-selectin and von Willebrand factor by protease-activated receptors and cAMP. *Blood.* 2012;107(7):2736–2744.
16. Sporn LA, Marder VJ, Wagner DD. Inducible secretion of large, biologically potent von Willebrand factor multimers. *Cell.* 1986;46(2):185–90.
17. Zenner HL, Collinson LM, Michaux G, Cutler DF. High-pressure freezing provides insights into Weibel-Palade body biogenesis. *J. Cell Sci.* 2007;120(Pt 12):2117–2125.
18. Tsai HM, Nagel RL, Hatcher VB, Seaton AC, Sussman II. The high molecular weight form of endothelial cell von Willebrand factor is released by the regulated pathway. *Br. J. Haematol.* 1991;79(2):239–45.
19. Da Silva ML, Cutler DF. Von Willebrand factor multimerization and the polarity of secretory pathways in endothelial cells. *Blood.* 2016;128(2):277–285.
20. De Ceunynck K, De Meyer SF, Vanhoorelbeke K. Unwinding the von Willebrand factor strings puzzle. *Blood.* 2013;121(2):270–7.
21. Stel H V, Sakariassen KS, de Groot PG, van Mourik JA, Sixma JJ. Von Willebrand factor in the vessel wall mediates platelet adherence. *Blood.* 1985;65(1):85–90.
22. Savage B, Sixma JJ, Ruggeri ZM. Functional self-association of von Willebrand factor during platelet adhesion under flow. *Proc. Natl. Acad. Sci.* 2002;99(1):425–430.
23. van Buul-Wortelboer MF, Brinkman HJ, Dingemans KP, et al. Reconstitution of the vascular wall in vitro. A novel model to study interactions between endothelial and smooth muscle cells. *Exp. Cell Res.* 1986;162(1):151–158.
24. Sporn LA, Marder VJ, Wagner DD. Differing polarity of the constitutive and regulated secretory pathways for von Willebrand factor in endothelial cells. *J. Cell Biol.* 1989;108(4):1283–1289.
25. Loesberg C, Gonsalves MD, Zandbergen J, et al. The effect of calcium on the secretion of factor VIII-related antigen by cultured human endothelial cells. *Biochim. Biophys. Acta.* 1983;763(2):160–8.
26. Erent M, Meli A, Moiso N, et al. Rate, extent and concentration-dependence of histamine-evoked Weibel-Palade body exocytosis determined from individual fusion events in human endothelial cells. *J. Physiol.* 2007;583(Pt 1):195–212.
27. Vischer UM, Wollheim CB. Epinephrine induces von Willebrand factor release from cultured endothelial cells: involvement of cyclic AMP-dependent signalling in exocytosis. *Thromb. Haemost.* 1997;77(6):1182–8.
28. Kaufmann JE, Oksche A, Wollheim CB, et al. Vasopressin-induced von Willebrand factor secretion from endothelial cells involves V2 receptors and cAMP. *J. Clin. Invest.* 2000;106(1):107–16.
29. Vischer UM, Barth H, Wollheim CB. Regulated von Willebrand factor secretion is associated with agonist-specific patterns of cytoskeletal remodeling in cultured endothelial cells. *Arterioscler. Thromb. Vasc. Biol.* 2000;20(3):883–891.

30. Rondaij MG, Sellink E, Gijzen K a, et al. Small GTP-binding protein Ral is involved in cAMP-mediated release of von Willebrand factor from endothelial cells. *Arterioscler. Thromb. Vasc. Biol.* 2004;24(7):1315–20.
31. Mannucci PM, Ruggeri ZM, Pareti FI, Capitanio A. 1-Deamino-8-d-arginine vasopressin: a new pharmacological approach to the management of haemophilia and von Willebrands' diseases. *Lancet (London, England)*. 1977;1(8017):869–72.
32. Xiong Y, Huo Y, Chen C, et al. Vascular endothelial growth factor (VEGF) receptor-2 tyrosine 1175 signaling controls VEGF-induced von Willebrand factor release from endothelial cells via phospholipase C-gamma 1- and protein kinase A-dependent pathways. *J. Biol. Chem.* 2009;284(35):23217–24.
33. Zupancic G, Ogden D, Magnus CJ, Wheeler-Jones C, Carter TD. Differential exocytosis from human endothelial cells evoked by high intracellular Ca(2+) concentration. *J. Physiol.* 2002;544(Pt 3):741–55.
34. Pang ZP, Südhof TC. Cell Biology of Ca<sup>2+</sup>-Triggered Exocytosis. *Curr. Opin. Cell Biol.* 2010;22(4):496–505.
35. Rondaij MG, Bierings R, van Agtmaal EL, et al. Guanine exchange factor RalGDS mediates exocytosis of Weibel-Palade bodies from endothelial cells. *Blood.* 2008;112(1):56–63.
36. Disse J, Vitale N, Bader M-FF, Gerke V. Phospholipase D1 is specifically required for regulated secretion of von Willebrand factor from endothelial cells. *Blood.* 2009;113(4):973–80.
37. Knop M, Aareskjold E, Bode G, Gerke V. Rab3D and annexin A2 play a role in regulated secretion of vWF, but not tPA, from endothelial cells. *EMBO J.* 2004;23(15):2982–92.
38. Brandherm I, Disse J, Zeuschner D, Gerke V. cAMP-induced secretion of endothelial von Willebrand factor is regulated by a phosphorylation/dephosphorylation switch in annexin A2. *Blood.* 2013;122(6):1042–1051.
39. Chehab T, Santos NC, Holthenrich A, et al. A novel Munc13-4/S100A10/annexin A2 complex promotes Weibel–Palade body exocytosis in endothelial cells. *Mol. Biol. Cell.* 2017;28(12):1688–1700.
40. Klarenbach SW, Chipiuk A, Nelson RC, Hollenberg MD, Murray AG. Differential actions of PAR2 and PAR1, in stimulating human endothelial cell exocytosis and permeability: The role of Rho-GTPases. *Circ. Res.* 2003;92(3):272–278.
41. Conte IL, Hellen N, Bierings R, et al. Interaction between MyRIP and the actin cytoskeleton regulates Weibel-Palade body trafficking and exocytosis. *J. Cell Sci.* 2016;129(3):592–603.
42. Vischer UM, Wollheim CB. Purine nucleotides induce regulated secretion of von Willebrand factor: involvement of cytosolic Ca<sup>2+</sup> and cyclic adenosine monophosphate-dependent signaling in endothelial exocytosis. *Blood.* 1998;91(1):118–27.
43. Han X, Li P, Yang Z, et al. Zyxin regulates endothelial von Willebrand factor secretion by reorganizing actin filaments around exocytic granules. *Nat. Commun.* 2017;8:1–11.
44. Rondaij MG, Bierings R, Kragt A, et al. Dynein-dynactin complex mediates protein kinase A-dependent clustering of Weibel-Palade bodies in endothelial cells. *Arterioscler. Thromb. Vasc. Biol.* 2006;26(1):49–55.
45. Øynebråten I, Barojs N, Hagelsteen K, et al. Characterization of a novel chemokine-containing storage granule in endothelial cells: evidence for preferential exocytosis mediated by protein kinase A and diacylglycerol. *J. Immunol.* 2005;175(8):5358–69.
46. van Hooren KWEM, van Agtmaal EL, Fernandez-Borja M, et al. The Epac-Rap1 signaling pathway controls cAMP-mediated exocytosis of Weibel-Palade bodies in endothelial cells. *J. Biol. Chem.* 2012;287(29):24713–20.
47. van Hooren KWEM, van Breevoort D, Fernandez-Borja M, et al. Phosphatidylinositol-3,4,5-triphosphate-dependent Rac exchange factor 1 regulates epinephrine-induced exocytosis of Weibel-Palade bodies. *J. Thromb. Haemost.* 2014;12(2):273–81.
48. Lorenzi O, Frieden M, Villemin P, et al. Protein kinase C-delta mediates von Willebrand factor secretion from endothelial cells in response to vascular endothelial growth factor (VEGF) but not histamine. *J. Thromb. Haemost.* 2008;6(11):1962–9.
49. Wheeler-Jones C, Abu-Ghazaleh R, Cospedal R, et al. Vascular endothelial growth factor stimulates prostacyclin production and activation of cytosolic phospholipase A2 in endothelial cells via p42/p44 mitogen-activated protein kinase. *FEBS Lett.* 1997;420(1):28–32.
50. Matsushita K, Yamakuchi M, Morrell CN, et al. Vascular endothelial growth factor regulation of Weibel-Palade-body exocytosis. *Blood.* 2005;105(1):207–14.
51. Huang J, Haberichter SL, Sadler JE. The B subunits of Shiga-like toxins induce regulated VWF secretion in a phospholipase D1-dependent manner. *Blood.* 2012;120(5):1143–9.
52. Fu J, Naren AP, Gao X, Ahmmed GU, Malik AB. Protease-activated receptor-1 activation of endothelial cells induces protein kinase Ca-dependent phosphorylation of syntaxin 4 and Munc18c: Role in signaling P-selectin expression. *J. Biol. Chem.* 2005;280(5):3178–3184.
53. Liu F, Huang J, Sadler JE. Shiga toxin (Stx)1B and Stx2B induce von Willebrand factor secretion from human umbilical vein endothelial cells through different signaling pathways. *Blood.* 2011;118(12):3392–8.
54. Carew MA, Paleolog EM, Pearson JD. The roles of protein kinase C and intracellular Ca<sup>2+</sup> in the secretion of von Willebrand factor from human vascular endothelial cells.

- Biochem. J.* 1992;286 ( Pt 2):631–5.
55. Huwiler A, Döll F, Ren S, et al. Histamine increases sphingosine kinase-1 expression and activity in the human arterial endothelial cell line EA.hy 926 by a PKC- $\alpha$ -dependent mechanism. *Biochim. Biophys. Acta - Mol. Cell Biol. Lipids.* 2006;1761(3):367–376.
  56. Bierings R, Hellen N, Kiskin N, et al. The interplay between the Rab27A effectors Slp4-a and MyRIP controls hormone-evoked Weibel-Palade body exocytosis. *Blood.* 2012;120(13):2757–2767.
  57. Hannah MJ, Hume AN, Arribas M, et al. Weibel-Palade bodies recruit Rab27 by a content-driven, maturation-dependent mechanism that is independent of cell type. *J. Cell Sci.* 2003;116(Pt 19):3939–3948.
  58. Zografou S, Basagiannis D, Papafotika A, et al. A complete Rab screening reveals novel insights in Weibel-Palade body exocytosis. *J. Cell Sci.* 2012;125(Pt 20):4780–90.
  59. Barr FA. Rab GTPases and membrane identity: causal or inconsequential? *J. Cell Biol.* 2013;202(2):191–9.
  60. Nightingale TD, Pattni K, Hume AN, Seabra MC, Cutler DF. Rab27a and MyRIP regulate the amount and multimeric state of VWF released from endothelial cells. *Blood.* 2009;113(20):5010–5018.
  61. Rojo Pulido I, Nightingale TD, Darchen F, et al. Myosin Va acts in concert with Rab27a and MyRIP to regulate acute von-Willebrand factor release from endothelial cells. *Traffic.* 2011;12(10):1371–1382.
  62. Li P, Wei G, Cao Y, et al. Myosin IIa is critical for cAMP-mediated endothelial secretion of von Willebrand factor. 2018.
  63. Van Breevoort D, Snijders AP, Hellen N, et al. STXBP1 promotes Weibel-Palade body exocytosis through its interaction with the Rab27A effector Slp4-a. *Blood.* 2014;123(20):3185–3194.
  64. Matsushita K, Morrell CN, Cambien B, et al. Nitric oxide regulates exocytosis by S-nitrosylation of N-ethylmaleimide-sensitive factor. *Cell.* 2003;115(2):139–150.
  65. Pulido IR, Jahn R, Gerke V. VAMP3 is associated with endothelial Weibel-Palade bodies and participates in their Ca<sup>2+</sup>-dependent exocytosis. *Biochim. Biophys. Acta.* 2011;1813(5):1038–1044.
  66. Zhu Q, Yamakuchi M, Lowenstein CJ. SNAP23 regulates endothelial exocytosis of von Willebrand Factor. *PLoS One.* 2015;10(8):14–22.
  67. Schillemans M, Karampini E, van den Eshof BL, et al. Weibel-Palade Body Localized Syntaxin-3 Modulates Von Willebrand Factor Secretion From Endothelial Cells. *Arterioscler. Thromb. Vasc. Biol.* 2018;38(7):1549–1561.
  68. Nolasco LH, Gushiken FC, Turner NA, et al. Protein phosphatase 2B inhibition promotes the secretion of von Willebrand factor from endothelial cells. *J. Thromb. Haemost.* 2009;7(6):1009–18.
  69. Smith NL, Chen MH, Dehghan A, et al. Novel associations of multiple genetic loci with plasma levels of factor VII, factor VIII, and von willebrand factor: The charge (cohorts for heart and aging research in genome epidemiology) consortium. *Circulation.* 2010;121(12):1382–1392.
  70. Zhu Q, Yamakuchi M, Ture S, et al. Syntaxin-binding protein STXBP5 inhibits endothelial exocytosis and promotes platelet secretion. *J. Clin. Invest.* 2014;124(10):4503–4516.
  71. Berriman J a, Li S, Hewlett LJ, et al. Structural organization of Weibel-Palade bodies revealed by cryo-EM of vitrified endothelial cells. *Proc. Natl. Acad. Sci. U. S. A.* 2009;106(41):17407–17412.
  72. Cookson EA, Conte IL, Dempster J, Hannah MJ, Carter T. Characterisation of Weibel-Palade body fusion by amperometry in endothelial cells reveals fusion pore dynamics and the effect of cholesterol on exocytosis. *J. Cell Sci.* 2013;126(Pt 23):5490–9.
  73. Hannah MJ, Skehel P, Erent M, et al. Differential kinetics of cell surface loss of von Willebrand factor and its propolypeptide after secretion from Weibel-Palade bodies in living human endothelial cells. *J. Biol. Chem.* 2005;280(24):22827–22830.
  74. Babich V, Meli A, Knipe L, et al. Selective release of molecules from Weibel-Palade bodies during a lingering kiss. *Blood.* 2008;111(11):5282–5290.
  75. Valentijn KM, van Driel LF, Mourik MJ, et al. Multigranular exocytosis of Weibel Palade bodies in vascular endothelial cells. *Blood.* 2010;116(10):1807–1816.
  76. Fujimoto S. Degranulation of endothelial specific granules of the toad aorta after treatment with compound 48/80. *Anat. Rec.* 1982;203(2):197–204.
  77. Richardson M, Tinlin S, De Reske M, et al. Morphological alterations in endothelial cells associated with the release of von Willebrand factor after thrombin generation in vivo. *Arterioscler. Thromb.* 1994;14(6):990–999.
  78. Mourik MJ, Valentijn J a, Voorberg J, et al. von Willebrand factor remodeling during exocytosis from vascular endothelial cells. *J. Thromb. Haemost.* 2013;11(11):2009–19.
  79. Kiskin NI, Babich V, Knipe L, Hannah MJ, Carter T. Differential cargo mobilisation within weibel-palade bodies after transient fusion with the plasma membrane. *PLoS One.* 2014;9(9):1–12.
  80. Stevenson NL, White IJ, McCormack JJ, et al. Clathrin-mediated post-fusion membrane retrieval influences the exocytic mode of endothelial Weibel-Palade bodies. *J. Cell Sci.* 2017;130(15):2591–2605.
  81. Behrendorff N, Dolai S, Hong W, Gaisano HY, Thorn P. Vesicle-associated membrane protein 8 (VAMP8) is a SNARE (soluble N-ethylmaleimide-sensitive factor attachment protein receptor) selectively required

- for sequential granule-to-granule fusion. *J. Biol. Chem.* 2011;286(34):29627–29634.
82. Zhu D, Koo E, Kwan E, et al. Syntaxin-3 regulates newcomer insulin granule exocytosis and compound fusion in pancreatic beta cells. *Diabetologia.* 2013;56(2):359–369.
  83. Kozlov MM, Chernomordik L V. Membrane tension and membrane fusion. *Curr. Opin. Struct. Biol.* 2015;33:61–67.
  84. Verdugo P. Goblet cells secretion and mucogenesis. *Annu. Rev. Physiol.* 1990;52:157–76.
  85. Wagner DD, Mayadas T, Marder VJ. Initial glycosylation and acidic pH in the Golgi apparatus are required for multimerization of von Willebrand factor. *J. Cell Biol.* 1986;102(4):1320–4.
  86. Huang R-H, Wang Y, Roth R, et al. Assembly of Weibel-Palade body-like tubules from N-terminal domains of von Willebrand factor. *Proc. Natl. Acad. Sci. U. S. A.* 2008;105(2):482–487.
  87. Conte IL, Cookson E, Hellen N, et al. Is there more than one way to unpack a Weibel-Palade body? *Blood.* 2015;126(18):2165–7.
  88. Michaux G, Abbitt KB, Collinson LM, et al. The physiological function of von Willebrand's factor depends on its tubular storage in endothelial Weibel-Palade bodies. *Dev. Cell.* 2006;10(2):223–232.
  89. Nightingale TD, White IJ, Doyle EL, et al. Actomyosin II contractility expels von Willebrand factor from Weibel-Palade bodies during exocytosis. *J. Cell Biol.* 2011;194(4):613–629.
  90. SADLER JE. von Willebrand factor: two sides of a coin. *J. Thromb. Haemost.* 2005;3(8):1702–1709.
  91. Wang JW, Bouwens EAMM, Pintao MC, et al. Analysis of the storage and secretion of von willebrand factor in blood outgrowth endothelial cells derived from patients with von Willebrand disease. *Blood.* 2013;121(14):2762–2772.
  92. Koster T, Blann AD, Briët E, Vandenbroucke JP, Rosendaal FR. Role of clotting factor VIII in effect of von Willebrand factor on occurrence of deep-vein thrombosis. *Lancet (London, England).* 1995;345(8943):152–5.
  93. Sonneveld MAH, De Maat MPM, Leebeek FWG. Von Willebrand factor and ADAMTS13 in arterial thrombosis: A systematic review and meta-analysis. *Blood Rev.* 2014;28(4):167–178.
  94. Sanders Y V, Eikenboom J, de Wee EM, et al. Reduced prevalence of arterial thrombosis in von Willebrand disease. *J. Thromb. Haemost.* 2013;11(5):845–854.
  95. Desch KC, Ozel AB, Siemieniak D, et al. Linkage analysis identifies a locus for plasma von Willebrand factor undetected by genome-wide association. *Proc. Natl. Acad. Sci. U. S. A.* 2013;110(2):588–93.
  96. van Loon JE, Leebeek FWG, Deckers JW, et al. Effect of genetic variations in syntaxin-binding protein-5 and syntaxin-2 on von Willebrand factor concentration and cardiovascular risk. *Circ. Cardiovasc. Genet.* 2010;3(6):507–12.
  97. Smith NL, Rice KM, Bovill EG, et al. Genetic variation associated with plasma von Willebrand factor levels and the risk of incident venous thrombosis. *Blood.* 2011;117(22):6007–11.
  98. Sanders Y V, van der Bom JG, Isaacs A, et al. CLEC4M and STXBP5 gene variations contribute to von Willebrand factor level variation in von Willebrand disease. *J. Thromb. Haemost.* 2015;13(6):956–66.
  99. Starke RD, Ferraro F, Paschalaki KE, et al. Endothelial von Willebrand factor regulates angiogenesis. *Blood.* 2016;117(3):1071–1081.
  100. Saint-lu N, Oortwijn BD, Pegon JN, et al. Identification of Galectin-1 and Galectin-3 as Novel Partners for Von Willebrand Factor. *Arterioscler. Thromb. Vasc. Biol.* 2012;32:894–901.





## Chapter 6

# Defective AP-3-dependent VAMP8 trafficking impairs Weibel-Palade body exocytosis in Hermansky-Pudlak Syndrome type 2 blood outgrowth endothelial cells

Ellie Karampini\*, Maaïke Schillemans\*, Menno Hofman, Floris van Alphen, Martin de Boer, Taco W. Kuijpers, Maartje van den Biggelaar, Jan Voorberg and Ruben Bierings

*\* These authors contributed equally*

*Haematologica* 2019 Oct;104(10):2091-2099

## Abstract

Weibel-Palade bodies are endothelial secretory organelles that contain von Willebrand factor, P-selectin and CD63. Release of von Willebrand factor from Weibel-Palade bodies is crucial for platelet adhesion during primary hemostasis. Endosomal trafficking of proteins like CD63 to Weibel-Palade bodies during maturation is dependent on the adaptor protein complex 3 complex. Mutations in the *AP3B1* gene, which encodes the adaptor protein complex 3  $\beta 1$  subunit, result in Hermansky-Pudlak syndrome 2, a rare genetic disorder that leads to neutropenia and a mild bleeding diathesis. This is caused by abnormal granule formation in neutrophils and platelets due to defects in trafficking of cargo to secretory organelles. The impact of these defects on the secretory pathway of the endothelium is largely unknown.

In this study we have investigated the role of adaptor protein complex 3-dependent mechanisms in trafficking of proteins during Weibel-Palade body maturation in endothelial cells. An *ex vivo* patient-derived endothelial model of Hermansky-Pudlak syndrome 2 was established using blood outgrowth endothelial cells that were isolated from a patient with compound heterozygous mutations in *AP3B1*. Hermansky-Pudlak syndrome 2 endothelial cells and CRISPR-Cas9-engineered *AP3B1*<sup>-/-</sup> endothelial cells contain Weibel-Palade bodies that are entirely devoid of CD63, indicative of disrupted endosomal trafficking. Hermansky-Pudlak syndrome 2 endothelial cells have impaired Ca<sup>2+</sup>- and cAMP-mediated exocytosis. Whole proteome analysis revealed that apart from adaptor protein complex 3  $\beta 1$  also the  $\mu 1$  subunit and the v-SNARE VAMP8 were depleted. Stimulus-induced von Willebrand factor secretion was impaired in CRISPR-Cas9-engineered *VAMP8*<sup>-/-</sup> endothelial cells.

Our data show that defects in adaptor protein complex 3 dependent maturation of Weibel-Palade bodies impairs exocytosis by affecting the recruitment of VAMP8.

## Introduction

Weibel-Palade bodies (WPBs) are the storage and secretory compartment of endothelial cells and play an important role in hemostasis, inflammation and angiogenesis.<sup>1</sup> Secretion of their main cargo, the hemostatic protein von Willebrand factor (VWF), promotes platelet adhesion at the site of injury.<sup>2</sup> Apart from VWF, WPBs also store angiopoietin-2, IGFBP7 and various chemokines, along with the transmembrane protein P-selectin and the integral membrane protein CD63.<sup>1,3</sup> Simultaneous release of this cocktail of inflammatory and angiogenic mediators from WPBs also promotes extravasation of leukocytes and vessel repair mechanisms.

WPBs belong to the lysosome-related organelles (LROs), a heterogeneous group of sub-cellular organelles that share features with lysosomes through acquisition of recycled cargo and/or membrane components from the endo-lysosomal system.<sup>4</sup> Biogenesis and subsequent degranulation of LROs is fundamental to the function of a wide variety of (circulating) cells, including granulocytes, T cells, platelets and endothelial cells. Although their function and cargo differ between cell types, the mechanisms and core components that control LRO biogenesis, maturation and degranulation are shared and operate in all cells with LROs. In endothelial cells, biogenesis of WPBs starts at the *trans*-Golgi Network (TGN) and is driven by the biosynthesis of VWF. At this point other soluble cargo as well as P-selectin are also included in newly forming WPBs. In a subsequent post-Golgi step during WPB maturation additional key components such as CD63 are transferred from adaptor protein complex 3 (AP-3)-positive endosomes to maturing WPBs.<sup>5-7</sup> AP-3 is a heterotetrameric complex, consisting of four subunits:  $\beta 1$ ,  $\delta 1$ ,  $\mu 1$  and  $\sigma 1$ , previously also referred to as  $\beta 3A$ -,  $\delta 3$ -,  $\mu 3A$ - and  $\sigma 3A$ -adaptins, respectively.<sup>8</sup> The AP-3  $\mu 1$  subunit is known to interact with membrane proteins through linear sequences of amino acid residues in their cytoplasmic tail, such as the di-leucine ([DE]XXX[LI]) and the tyrosine (YXX $\Phi$ ) motifs,<sup>9,10</sup> the latter of which

is also present in CD63 (GYEVM).<sup>11</sup> When its tyrosine motif is altered or the expression of AP-3 $\beta$ 1 is downregulated, CD63 shows impaired trafficking to WPBs, suggestive of a direct interaction between the AP-3 complex and CD63.<sup>7</sup>

Defective formation and degranulation of LROs is at the basis of a number of poorly understood congenital storage pool disorders (SPDs) that affect secretory responses of cells. Since the mechanisms of LRO formation and degranulation are shared between different cell types SPDs are often poly-systemic, affecting many cell types at the same time which leads to complex disease symptoms. Hermansky-Pudlak syndrome (HPS) is a group of autosomal recessive disorders characterized by hypopigmentation and platelet storage pool deficiency, due to defective maturation of melanosomes and platelet dense granules, respectively.<sup>12</sup> HPS-2, a subtype of HPS, affects the expression and functionality of the AP-3 complex by mutations in the *AP3B1* gene, which encodes the AP-3 complex  $\beta$ 1 subunit.<sup>13</sup> Apart from the shared HPS features of platelet dysfunction and albinism, HPS-2 is also uniquely characterized by CD8<sup>+</sup> cytotoxic T cell dysfunction and neutropenia.<sup>14-16</sup>

Given the polysystemic nature of SPDs, we sought to determine how genetic deficiencies in the AP-3 sorting machinery impact the secretory function of endothelial cells. Here we show, using blood outgrowth endothelial cells (BOECs) from an HPS-2 patient, that defects in AP-3 dependent maturation of WPBs impairs the exocytotic potential of WPBs by affecting the recruitment of the WPB-localized member of the SNARE fusion machinery VAMP8.

## Methods

### Cell culture and isolation of BOECs

BOECs were isolated as previously described and cultured in EGM-2 (Lonza, Basel, Switzerland, CC-3162) supplemented with 18% fetal calf serum (FCS) (Bodinco, Alkmaar, The Netherlands) (EGM-18).<sup>17</sup> HPS-2 BOECs were isolated from venous blood from a patient diagnosed with HPS-2 (described in<sup>16</sup>), caused by compound heterozygote *AP3B1* mutations (c.177delA, p.K59Nfs\*4 and c.1839-1842delTAGA, p.D613Efs\*38). The study was performed according to national regulations regarding the use of human materials. The patient's parents signed an informed consent form for participation. Control BOECs were isolated from healthy, anonymized donors participating in the voluntary internal blood donor system of Sanquin Blood Supply following written consent. The study was approved by the Medical Ethical Committee of the Academic Medical Center in Amsterdam and was conducted in accordance with the Declaration of Helsinki.

### DNA constructs

The mEGFP-LIC and LVX-mEGFP-LIC vectors have been described before.<sup>18,19</sup> The EGFP-AP-3 $\beta$ 1 plasmid encoding AP-3 $\beta$ 1 with EGFP fused to its aminotermisus was a gift from Dr. Adolfo Saiardi.<sup>20</sup> To construct LVX-mEGFP-AP3- $\beta$ 1, a 3317 bp fragment containing the AP-3 $\beta$ 1 coding sequence was cut from EGFP-AP-3 $\beta$ 1 using BsrGI and SacII and pasted in frame behind mEGFP using the same sites in mEGFP-LIC. In a second step, the AP-3 $\beta$ 1 coding sequence was excised from mEGFP-AP-3 $\beta$ 1 using BsrGI and NotI and pasted in frame behind mEGFP in the LVX-mEGFP-LIC vector.

### CRISPR genome engineering

gRNAs were designed to target exon 1 of the *AP3B1* gene and exon 1 and 2 of the *VAMP8* gene using the CRISPR Design tool (<http://crispr.mit.edu>). gRNAs [(*AP3B1* exon 1: gRNA-4: TACAATGAGCAGTCCGAGG and gRNA-5: ACAATGAGCAGTCCG GAGGA); (*VAMP8* exon 1: gRNA-4: GAATGTGGAGCGGATCCTGG and gRNA-5: AGA ATGTGGAGCG-GATCCTG; exon 2: gRNA-3: CTGGAGCGACTCGAGATGCG)] were selected based on the specificity score with the minimum amount of off-target effects and were subsequently

cloned as hybridized oligos [(*AP3B1*: gRNA-4: RBNL306 5'-CA CCGTACAATGAGCAGTC-CGGAGG-3' and RBNL307 5'-AAACCTCCGGACTGCTCA TTGTAC-3'; gRNA-5: RBNL308 5'-CACCGACAATGAGCAGTCCGGAGGA-3' and RBNL309 5'-AAACTCCTCCGGACTGCT-CATTGT C-3'), (*VAMP8*: gRNA-3: RBNL318 5'-CACCGGTGGAGAAATGATCGTGTG-3' and RBNL319 5'-AAACCACACGATCATT TCCTCCACC-3'; gRNA-4: RBNL320 5'-CACCGAT-TCACTTACTGACCGCCT-3' and RBNL321 5'-AAACAGCCGGTCAGTAAGTGAATC-3'; gRNA-5: RBNL322 5'-CACCGA TCACTTACTGACCGCCT-3' and RBNL323 5'-AAACG-GCCGGTCTCAGTAAAGTAA TTC-3')] into BsmBI-digested LentiCRISPR\_v2 vector (a gift from Dr. Feng Zhang; Addgene #52961). A detailed protocol on transduction and clonal selection of knockout BOECs has been previously described.<sup>21</sup>

### CD63 and CD62P membrane exposure

Endothelial cells were cultured in gelatin-coated 6-well plates until confluency for 3–4 days prior to the experiment. In order to measure CD63 surface exposure in WT and HPS-2 BOECs under steady conditions, cells were washed twice with PBS, detached with Accutase (Sigma, A6964), and stained with FITC-conjugated anti-CD63 antibody at 4°C for 30 minutes in the dark. After incubation, cells were washed with PBS, spun down at 250×g, 4°C for 2 minutes and suspended in PBS containing 0.01% (v/v) NaN<sub>3</sub>. Samples were measured by flow cytometry (BD FACSCANTO II, BD Biosciences). In order to measure CD62P levels on the plasma membrane upon stimulation, cells were pre-incubated in RM for at least 30 minutes. Stimulation was performed in RM supplemented with 100 μM histamine for 5 minutes. After stimulation, cells were treated with ice-cold PBS and detached by Accutase. Staining for CD62P exposure was performed at 4°C in the dark with a PE-conjugated anti-CD62P antibody for 20 minutes. Cells were centrifuged at 4°C at 250×g for 2 minutes and subsequently resuspended in PBS containing 0.01% (v/v) NaN<sub>3</sub>.

Further details on materials and methods are found in the *Online Supplemental Materials and Methods*.

## Results

### AP3B1 deficient endothelial cells exhibit impaired intracellular protein trafficking from endosomes to WPBs

To study the role of the AP-3 complex in primary endothelial cells we isolated BOECs from peripheral blood mononuclear cells of an HPS-2 patient with mutations in the *AP3B1* gene that encodes for the β1 subunit of the heterotetrameric AP-3 complex. The patient, who has previously been described in <sup>16</sup>, is a compound heterozygote with both mutations (exon 2: c.177delA, p.K59Nfs4; exon 17: c.1839-1842delTAGA, p.D613Efs\*38) leading to a frame shift and a premature stop codon (Figure 1A). As expected, Western blot analysis of lysates of BOECs confirmed that the expressed levels of AP-3 β1 were not detectable (Figure 1Bi-ii). The truncated AP-3β1 protein products, generated in the HPS-2 BOECs, are most likely rapidly degraded as previously reported in HPS-2 fibroblasts.<sup>13</sup> In order to test whether there is any remaining functionality of the AP-3 complex in HPS-2 BOECs, we determined the localization of proteins that are subject to AP-3 dependent trafficking. Both the tetraspanin CD63 and the leukocyte receptor CD62P continuously cycle between plasma membrane and WPBs.<sup>5,6</sup> However, after endocytic retrieval, CD63 is incorporated in maturing WPBs through transfer from AP-3 positive endosomes, while P-selectin diverges to the trans-Golgi network where it is incorporated in nascent WPBs.<sup>7</sup> Therefore, we stained HPS-2 and healthy control BOECs for VWF and CD63 or P-selectin. We observed that CD63 is not detectable in WPBs in HPS-2 BOECs and can only be observed in round endosome-like structures (Figure 1Ei). Quantitative evaluation of our imaging data showed that in WT BOECs, nearly a third of cellular CD63 is associated with WPBs (Figure 1Eii) and that on

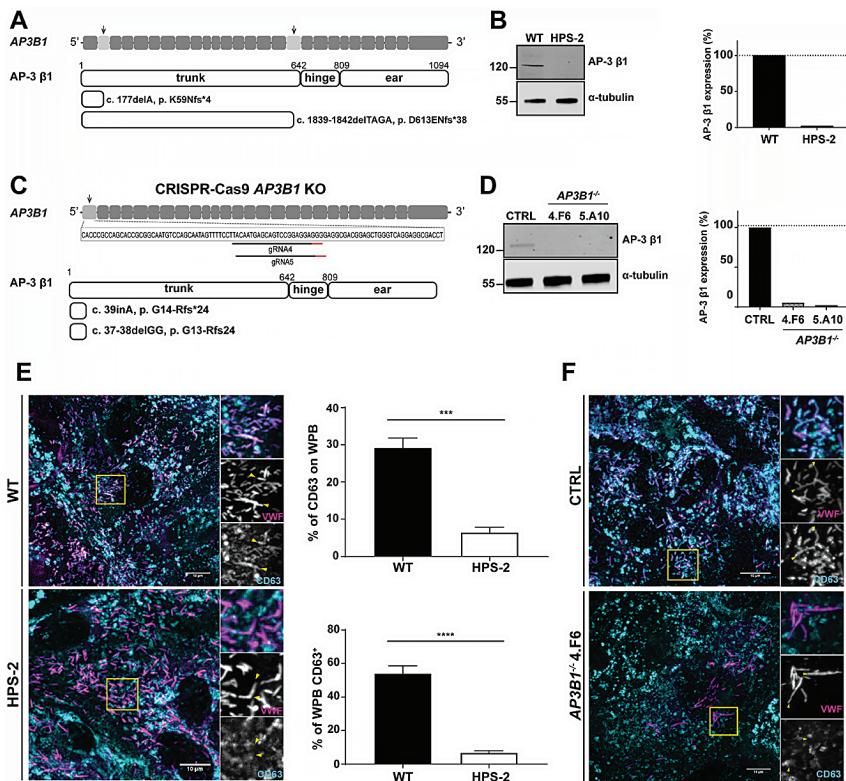


**Figure 1: Disrupted trafficking of CD63 to WPBs in ex vivo patient-derived HPS-2 BOECs and CRISPR-Cas9-engineered *AP3B1*<sup>-/-</sup> BOECs.** A) Cartoon depicting the mutations of the HPS-2 patient in the *AP3B1* gene and the corresponding predicted truncated protein products relative to the full length AP-3β1 domain structure. B) Expression of AP-3β1 in WT and HPS-2 BOECs. Bi) Healthy control (WT) and HPS-2 BOEC lysates were separated with SDS-PAGE and were immunoblotted for AP-3β1; α-tubulin was used as a loading control. Molecular weight standards are indicated on the left (kDa). Bii) Quantification of relative AP-3β1 expression in HPS-2 BOECs normalized to AP-3β1 in healthy control BOECs (WT). C) Cartoon representation of the CRISPR-Cas9-engineering strategy to generate *AP3B1*<sup>-/-</sup> BOEC lines. Guide RNAs (gRNA4 and gRNA5) are shown underneath a fragment of *AP3B1* exon 1 sequence with their protospacer adjacent motif (PAM) indicated in red. The mutations and the corresponding predicted truncated protein products of 2 *AP3B1*<sup>-/-</sup> clones (4.F6 and 5.A10, respectively) are shown relative to the full length AP-3β1 domain structure. D) Loss of AP-3β1 expression in *AP3B1*<sup>-/-</sup> BOECs. Di) Lysates of clonal control BOECs (CTRL) and 2 clonal *AP3B1*<sup>-/-</sup> BOEC lines (4.F6 and 5.A10) were separated with SDS-PAGE and were immunoblotted for AP-3β1; α-tubulin was used as a loading control. Dii) Quantification of relative AP-3β1 expression in clonal *AP3B1*<sup>-/-</sup> BOEC lines normalized to AP-3β1 in clonal control BOECs (CTRL). E-F) Immunostaining of BOECs for VWF (magenta) and CD63 (cyan) in WT vs. HPS-2 BOECs (Ei) and CTRL vs. *AP3B1*<sup>-/-</sup> 4.F6 BOECs (F), respectively. Boxed areas are magnified in the right part. Yellow arrowheads indicate the position of WPBs in both channels. Scale bars represent 10 μm. Eii) Proportion of CD63 immunoreactivity that is found on WPBs. Eiii) Proportion of WPBs that contain CD63 immunoreactivity. Student t-test, \*\*\*: p-value<0.001, \*\*\*\*: p-value<0.0001.

average about 60% of the WPBs are CD63 positive (Figure 1Eiii), numbers that are both in close accordance with previous studies.<sup>7,22</sup> We observed a sharp reduction in these parameters in HPS-2 BOECs (Figure 1Eii-iii), pointing to a defect in CD63 trafficking. P-selectin trafficking to WPBs is unaffected by the lack of AP-3 β1 (Supplemental Figure IA). We also measured CD63 surface expression in HPS-2 and healthy control BOECs under steady state conditions using flow cytometry. We observed that CD63 surface levels were significantly increased in HPS-2 BOECs (Supplemental Figure IB). Together these data point to defective AP-3 dependent trafficking mechanisms in HPS-2 BOECs.

To further corroborate the role of AP-3 in trafficking of CD63 we also generated *AP3B1* knock out primary endothelial cells using CRISPR-Cas9 gene editing. Using lentiviral transduction of cord blood BOECs (cbBOECs) with guide RNAs targeting the first exon of the *AP3B1* gene we generated 3 clonal cbBOEC lines containing indels that led to frame shifts and subsequent premature stop codons in the *AP3B1* gene (Figure 1C). This resulted in complete abolishment of AP-3 $\beta$ 1 expression in all three clonal lines (Figure 1Di-ii). Similar to what we observed in HPS-2 BOECs and to what has been reported in endothelial cells after siRNA-mediated AP-3  $\beta$ 1 silencing,<sup>7</sup> WPBs of *AP3B1*<sup>-/-</sup> cbBOECs did not contain CD63 (Figure 1F and Supplemental Figure II).

### **AP3B1 deficient HPS-2 BOECs have an unstable AP-3 complex and lack the WPB v-SNARE VAMP8**

To better understand the phenotypic effect of loss of AP-3  $\beta$ 1 expression we performed a comparative analysis of the whole proteome between HPS-2 and healthy control BOECs by means of label-free LC-MS/MS. We identified 5812 proteins, from which 4323 were quantifiable following the selection criteria. To include the natural variation in our analysis, we compared HPS-2 BOECs to 4 independent healthy control donors. Z-scored LFQ values of the proteins with the highest variation between samples ( $S_0=0.4$ , FDR = 0.05) are shown in the heatmap in Figure 2A. Following this approach, we were able to confirm the AP-3  $\beta$ 1 depletion in HPS-2 BOECs (Figure 2B). Moreover, we observed that the expression of AP-3  $\mu$ 1, an AP-3 subunit encoded by *AP3M1*, was also significantly reduced. However, expression levels of AP-3  $\delta$ 1 and AP-3  $\sigma$ 1, the other 2 subunits of the AP-3 complex, were not significantly different and only modestly reduced (Figure 2B). A similar observation has previously been made in HPS-2 fibroblasts<sup>23</sup> and in murine *pe* fibroblasts (pearl, *pe*, mouse model of HPS-2), where  $\delta$ 1 and  $\sigma$ 1 subunits remained as a heterodimer and showed cytosolic rather than membrane-associated localization.<sup>24</sup> The tight correlation of  $\beta$ 1 and  $\mu$ 1 expression levels suggests that loss of AP-3  $\beta$ 1 and consequential disintegration of the AP-3 complex destabilizes the AP-3 $\mu$ 1 subunit. This was supported by the observation that lentivirally expressed mEGFP-AP-3  $\beta$ 1 was able to rescue the expression of AP-3  $\mu$ 1 in HPS-2 BOECs (Figure 2C).

Interestingly, among the downregulated proteins, we discovered that the expression of the WPB-localized SNARE protein VAMP8 is severely diminished (Figure 2A and Supplemental Figure III). This was specific for VAMP8 as the expression levels of other SNARE proteins that have been implicated in WPB exocytosis were not significantly altered (Supplemental Figure II). Western blot analysis also revealed a complete depletion of VAMP8 expression in HPS-2 BOECs compared to healthy controls (Figure 2D). Moreover, immunofluorescent staining in healthy control and HPS-2 BOECs for VAMP8 and VWF, showed that WPBs in HPS-2 BOECs lack VAMP8 immunoreactivity (Figure 2E). In addition, in the *AP3B1* knockout BOEC lines VAMP8 was strongly reduced when compared to the control cbBOEC (Supplemental Figure IV).

### **Ex vivo HPS-2 endothelial cells have impaired stimulus-induced WPB exocytosis.**

To investigate the contribution of AP-3 dependent maturation on the degranulation efficiency of WPBs in endothelial cells, we measured the stimulus-induced VWF release in HPS-2 BOECs. We observed that under unstimulated conditions the release of VWF is unaffected in the HPS-2 BOECs compared to WTs (Figure 3A). However, upon stimulation HPS-2 BOECs showed a clear defect in VWF release with both Ca<sup>2+</sup>- (histamine) and cAMP-mediated (forskolin) secretagogues (Figure 3B). As an alternative measurement of WPB exocytosis we also investigated how other WPB proteins respond to histamine treatment. We stimulated WT and HPS-2 BOECs and measured CD62P exposure on the plasma membrane (Figure 3C). We found that significantly less CD62P was expressed on HPS-2 BOEC plasma membrane when compared to healthy control BOEC upon histamine stimulation.

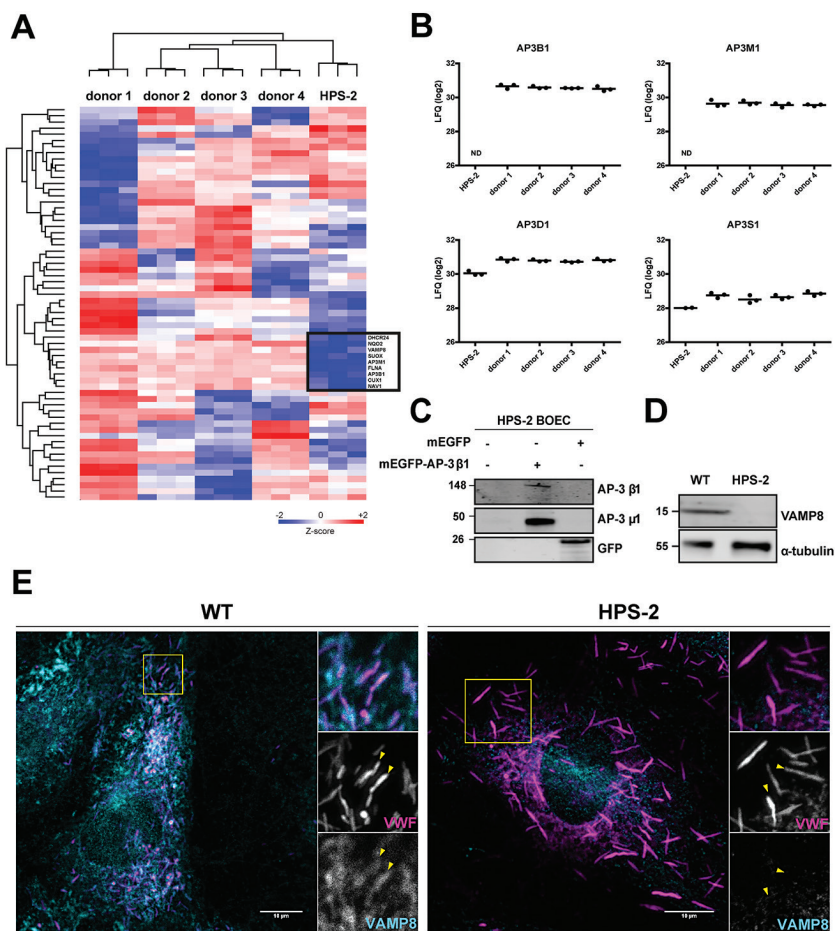


**Figure 2: HPS-2 BOECs lack components of the AP-3 complex and the WPB v-SNARE VAMP8.** A-B) Whole proteome analysis of HPS-2 BOECs. (A) Heatmap of Z-scored LFQ (log<sub>2</sub>) values of the proteins with the highest variation between BOECs derived from 4 individual healthy donors and HPS2derived BOECs (ANOVA S0=0.4, FDR = 0.05) B) Graph representing LFQ (log<sub>2</sub>) values for AP3B1, AP3D1, AP3M1 and AP3S1. C) HPS-2 BOECs lentivirally transduced with mEGFP-AP-3β1 and mEGFP (control). Lysates were separated with SDS-PAGE and were immunoblotted for AP-3β1, AP-3μ1 and GFP; molecular weight standards are indicated on the left (kDa). D) Immunoblot analysis of VAMP8 in lysates of HPS-2 and WT BOECs; α-tubulin was used as a loading control. E) Immunofluorescent stainings for VWF (magenta) and VAMP8 (cyan) in healthy controls and HPS-2 BOECs. Boxed areas are magnified in the right part. Yellow arrowheads indicate the position of WPBs in both channels. Scale bars represent 10 μm.

The reduction in the stimulus-induced surface expression of CD62P and release of VWF in HPS-2 BOECs suggests that defects in the AP-3 dependent maturation of WPBs alter the exocytotic potential of these organelles in endothelial cells.

### The WPB v-SNARE protein VAMP8 promotes WPB exocytosis.

Expression of the SNARE protein VAMP8 is reduced in the absence of AP-3 β1, in HPS-2 patient BOECs as well as in CRISPR-Cas9 engineered *AP3B1* knockout endothelial cells. SNARE proteins are key regulators of intracellular membrane fusion events, such as during exocytosis or during fusion between organelles. To further investigate the role of VAMP8 in endothelial cells, we first studied the intracellular localization of VAMP8 with confocal

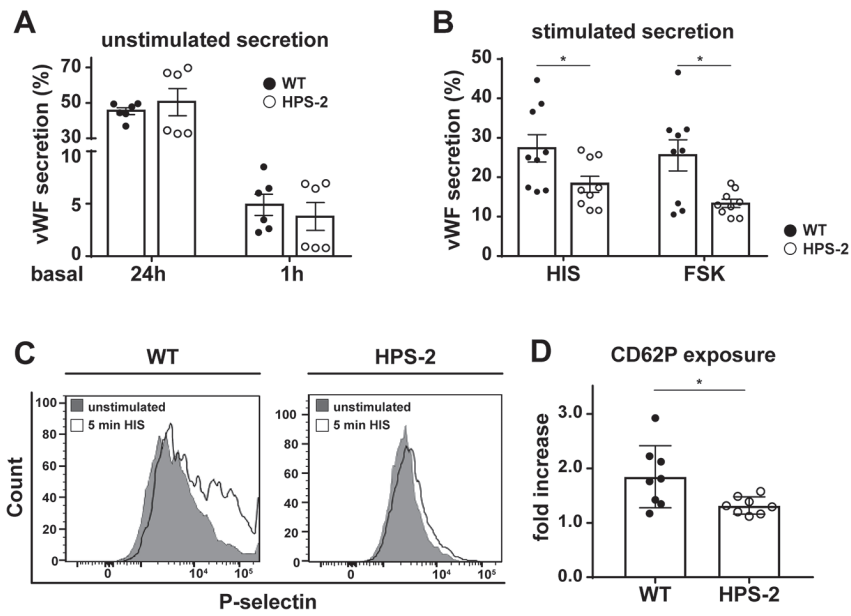


**Figure 3: Impaired stimulus-induced VWF secretion and P-selectin cell surface exposure in HPS-2 BOECs.** A) Basal (unstimulated) secretion of VWF in conditioned media after 24 hours and 1 hour from WT HPS-2 (black) and HPS-2 (white) BOECs ( $n=6$ , from 2 independent experiments). B) Stimulated VWF secretion after 30 minutes treatment with 100  $\mu\text{M}$  histamine (HIS) or 10  $\mu\text{M}$  forskolin + 100  $\mu\text{M}$  IBMX (FSK) from WT (black) and HPS-2 (white) BOECs. Secretion is expressed as relative proportion of intracellular VWF in lysates of unstimulated cells ( $n=9$ , from 3 independent experiments). Ci) Representative histograms of P-selectin (CD62P) cell surface expression before (close gray) and after 5 minutes stimulation with 100  $\mu\text{M}$  histamine (open black line) Cii) CD62P exposure after histamine stimulation expressed as fold increase over unstimulated cells ( $n=8$ , from 4 independent experiments). Two tailed student t-test, \*:  $p$ -value $<0.05$ .

microscopy in HUVEC / healthy control BOECs. In line with what was previously reported, VAMP8 was localized on a subset of WPBs and on spherical organelles of the endosomal system (Supplemental Figure V).<sup>21,25</sup> Interestingly, VAMP8-positive WPBs and VAMP8-positive endosomes both contained CD63, suggesting their shared itinerary may be indicative of a common AP-3 dependent trafficking pathway.

To explore the role of VAMP8 in endothelial cells we generated clonal CRISPR-Cas9 knockout BOECs by introducing a mutation in the first and second exon (Figure 4Ai) and evaluated the knockout efficiency by Western blot (Figure 4Aii) and immunofluorescence (Supplemental Figure VI A). We investigated both AP-3-dependent intracellular protein trafficking as well as the efficiency of WPB to exocytose upon stimulation in two clonal *VAMP8*<sup>-/-</sup> BOEC lines. To assess the involvement of VAMP8 in a fusion step between WPBs and the endosomal compartment during CD63 recruitment, we checked the localization of CD63 in control and VAMP8 deficient cell lines. Immunofluorescent staining of CD63 and VWF in the *VAMP8*<sup>-/-</sup> lines exhibit a similar pattern when compared to the control cell lines, with CD63 being found on endosome-like structures as well as WPBs (Supplemental Figure VIB). This suggests that membrane transfer between endosomes and WPBs during CD63 trafficking does not depend on VAMP8. We next examined the involvement of VAMP8 in WPB exocytosis by testing stimulus-induced VWF release in CRISPR-edited *VAMP8*<sup>-/-</sup> BOECs. Our data show that the intracellular levels of VWF are similar for VAMP8-deficient and control cell lines (Figure 4B), showing that the process of CRISPR-Cas9 genetic modification and clonal selection does not affect VWF biosynthesis and/or WPB biogenesis. However, upon Ca<sup>2+</sup>-mediated stimulation of WPB release with histamine, VAMP8 knockout endo-



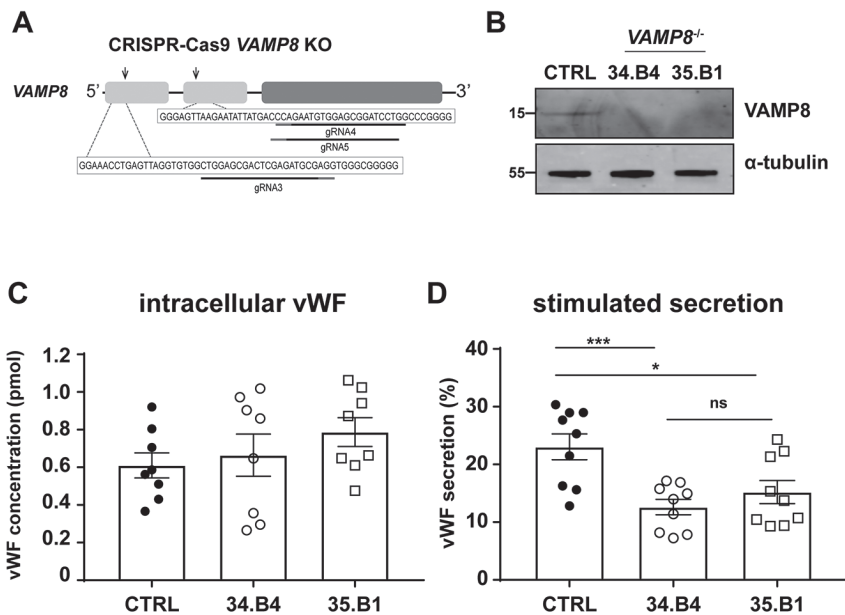


**Figure 4: CRISPR-Cas9-engineered *VAMP8*<sup>-/-</sup> BOECs have decreased histamine-induced VWF secretion.** A) Generation of clonal *VAMP8* deficient BOEC lines using CRISPR-Cas9 genome-editing. Ai) Cartoon representation of the CRISPR-Cas9-engineering strategy to generate *VAMP8*<sup>-/-</sup> BOEC lines. Guide RNAs targeting exon 1 and exon 2 (gRNA3 and gRNA4&5, respectively) are shown underneath fragments of *VAMP8* exon 1 and 2 sequences with their protospacer adjacent motif (PAM) indicated in red. Aii) Loss of *VAMP8* expression in clonal *VAMP8*<sup>-/-</sup> BOECs. Lysates of clonal control BOECs (CTRL) and 2 clonal *VAMP8*<sup>-/-</sup> BOEC lines (34.B4 and 35.B1) were separated with SDS-PAGE and were immunoblotted for *VAMP8*;  $\alpha$ -tubulin was used as a loading control. Molecular weight standards are indicated on the left (kDa). B) Intracellular levels of VWF in lysates from control and 2 clonal *VAMP8*<sup>-/-</sup> BOEC lines (34.B4 and 35.B1) as determined by ELISA (n=9). C) Stimulated VWF secretion after 30 minutes treatment with 100  $\mu$ M histamine (HIS) from CTRL (close black) and 2 clonal *VAMP8*<sup>-/-</sup> BOEC lines (34.B4 and 35.B1) (open circle and square respectively). Secretion is expressed as relative proportion of intracellular VWF in lysates of unstimulated cells (n=9 from 3 independent experiments). Two tailed student t-test, ns: p-value>0.05, \*: p-value<0.05, \*\*\*: p-value<0.001.

thelial cells secreted significantly less VWF when compared to the control lines (Figure 4C). These findings demonstrate that *VAMP8* promotes stimulus-induced VWF secretion and establish *VAMP8* as a novel component of the WPB exocytotic machinery.

## Discussion

The AP-3 complex regulates the formation and maturation of lysosome-related organelles in many different cell types.<sup>8</sup> In this study we show that mutations in the *AP3B1* gene that lead to HPS-2 result in loss of AP-3  $\beta$ 1 and rapid degradation of the AP-3  $\mu$ 1 subunit of the AP-3 complex. While the  $\delta$ 1 and  $\sigma$ 1 subunits are still expressed, the consequential destabilization of the AP-3 complex leads to a failure to traffic proteins to the WPBs. Two of these, CD63 and *VAMP8*, normally co-reside on endosomes and WPBs. However, in the absence of AP-3-dependent sorting, their fates differ radically. Blockade of the route from the endosomal compartment to the WPB causes an increase of CD63 on the cell surface, possibly caused by a global redistribution of CD63 in the absence of its storage compartment. This has previously been reported for other cell types derived from HPS-2 patients such as cyto-

toxic T-lymphocytes and fibroblasts.<sup>13-15,23</sup> VAMP8 expression is severely reduced in both HPS-2 BOECs and in CRISPR-engineered *AP3B1* KO BOECs, for which we currently do not have an explanation. Contrary to CD63, VAMP8 does not contain any of the known sorting motifs that would allow it to directly interact with the AP-3 complex.<sup>9,10</sup> VAMP7, a v-SNARE that is found on a number of LROs, has been shown to interact with the AP-3 complex on early endosomes, via a direct interaction between the AP-3  $\delta 1$  subunit and the N-terminal longin domain of VAMP7.<sup>26,27</sup> Destabilization of the AP-3 complex, such as in *mocha* mice which lack the  $\delta 1$  subunit of AP-3, leads to mistargeting of VAMP7.<sup>27</sup> It has also been suggested that AP-3 indirectly traffics STX13 to maturing melanosomes via VAMP7.<sup>28</sup> Although VAMP8 does not contain a longin domain, it may be possible that during WPB maturation a similar mechanism exist in which VAMP8 catches a ride on the back of another AP-3 interacting partner.

In this study we further explored the effect of WPB maturation on regulated secretion and identify VAMP8 as a novel component of the exocytotic fusion machinery. Previous studies have found that WPBs contain the v-SNAREs VAMP3 and VAMP8, but so far only VAMP3 has been implicated in  $\text{Ca}^{2+}$ -dependent WPB exocytosis.<sup>25</sup> We have previously established that VAMP8 is a direct interactor of both syntaxin-3 (STX3) and syntaxin-4 (STX4).<sup>21</sup> STX4, which is found at the plasma membrane, has been implicated in thrombin-induced release of WPBs through the formation of a complex with WPB-localized VAMP3.<sup>25,29</sup> We have recently shown that STX3 is localized on WPBs and that absence of STX3 from endothelial cells results in impaired basal and hormone-evoked VWF secretion.<sup>21</sup> The decrease in histamine-evoked VWF secretion in VAMP8 knock out endothelial cells indicates an active involvement of VAMP8 in stimulus-induced WPB exocytosis. Based on its ability to interact with STX4 and STX3, VAMP8 can potentially support exocytosis via direct (WPB-plasma membrane) or homotypic (WPB-WPB) fusion modes. Further research on this topic should address the involvement of VAMP8 in the different modes of fusion.

*In vivo*, *VAMP8*<sup>-/-</sup> mice show delayed and decreased thrombus formation.<sup>30</sup> Although that study found that defective thrombus formation correlated with impaired dense granule release from *VAMP8*<sup>-/-</sup> platelets, it was not tested whether lack of VAMP8 in endothelial cells also contributed to defects in thrombus formation. A more pronounced defect in thrombus formation was also observed in *ruby eye* mice, a murine model for HPS-6, which lack platelet dense granules.<sup>31</sup> Contributing to this phenotype was (1) the inability to secrete protein disulfide isomerase (PDI) from so called T-granules, a tubular secretory compartment in platelets that contains VAMP8<sup>32</sup> and (2) defective thrombin-induced secretion of PDI and VWF from endothelial cells after silencing of HPS6.<sup>31</sup> A recent study also found that endothelial secretion of VWF in response to administration of the vasopressin analogue 1-deamino-8-D-arginine vasopressin (DDAVP) was delayed and/or decreased in *pallid*, *ruby eye* and *pale ear* mice, murine models of HPS-9, HPS-6 and HPS-1, respectively.<sup>33</sup> This provides an explanation for earlier observations that long bleeding times in *ruby eye* and *pale ear* mice were not corrected by DDAVP,<sup>34</sup> but possibly also for the variable response of HPS patients to DDAVP.<sup>35-37</sup> Taken together this suggests that defects in maturation of WPBs decrease their ability to undergo exocytosis.

In this study we show that BOECs from an HPS-2 patient have a moderate (but not complete) defect in stimulated VWF secretion, a phenotype that we found to be closely correlated with the absence of VAMP8 on mature WPBs. We propose that during maturation LROs also acquire components of their fusion machinery, thereby increasing their ability to undergo exocytosis. In some LROs, such as dense granules, defects in LRO maturation result in the absence of the secretory granule at issue, which obscures a secretory defect by the lack of the fusion machinery recruitment. This becomes apparent in LROs such as WPBs, which have already been formed before their failure to interact with the endo/lysosomal system, preventing them from acquiring additional content (CD63) or fusion machinery components (VAMP8) (Figure 5).

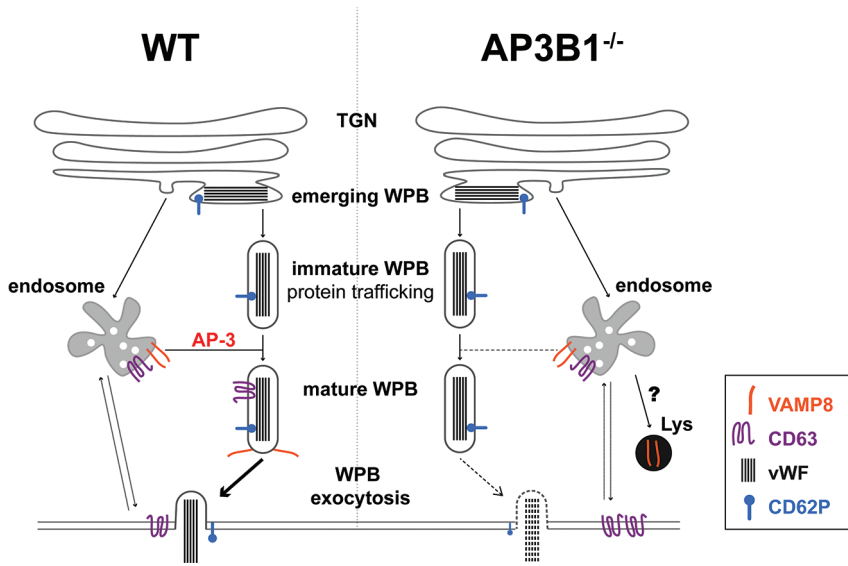


**Figure 5: Proposed model of (defective) AP-3 dependent acquisition of VAMP8 during WPB maturation.** WPBs in normal endothelial cells (WT, left) emerge from the *trans*-Golgi network (TGN) and mature by acquisition of recycled membrane proteins, such as CD63 and VAMP8, through endosomal trafficking to the WPB membrane via an AP-3 dependent pathway. Recruitment of VAMP8 promotes the secretion competence of WPBs by supporting the formation of trans-SNARE complexes with STX3 and STX4<sup>21</sup>, which will allow WPBs to undergo exocytosis upon cellular activation. After membrane fusion, CD63 and VAMP8 are retrieved and, via the early endosome (EE) make their way to another WPB. In the absence of a function AP-3 complex (right), such as in HPS-2 or *AP3B1*<sup>-/-</sup> BOECs, WPBs fail to recruit CD63 from the early endosomes. This leads to a global redistribution of cellular CD63, increasing its presence on the cell surface during steady state conditions. WPBs also fail to acquire (part of) their fusion machinery such as VAMP8, resulting in attenuated WPB exocytosis in response to cellular activation. Following its failure to transfer to the WPB membrane, VAMP8 is possibly rerouted to the lysosome where it is degraded.

### Authorship

EK, MS, MH, FvA, MdB, MvdB and RB performed research and analyzed data; TK contributed vital reagents and expertise; JV and RB designed the research; EK and RB wrote the paper. The authors report no disclosures.

### Acknowledgements

This study was supported by grants from the Landsteiner Stichting voor Bloedtransfusie Research (LSBR-1244, LSBR-1517 and LSBR-1707), Sanquin (PPOC-2015-24P and PPOC-2018-21) and the Dutch Thrombosis Foundation (TSN 56-2015 and 2017-01). RB is supported by a European Hematology Association Research Fellowship.

## References

- Schillemans M, Karampini E, Kat M, Bierings R. Exocytosis of Weibel-Palade bodies: how to unpack a vascular emergency kit. *J Thromb Haemost* [Epub ahead of print].
- Metcalfe DJ, Nightingale TD, Zenner HL, Lui-Roberts WW, Cutler DF. Formation and function of Weibel-Palade bodies. *J Cell Sci* 2008;31(9):882–888.
- Rondaj MG, Bierings R, Kragt A, van Mourik J a, Voorberg J. Dynamics and plasticity of Weibel-Palade bodies in endothelial cells. *Arterioscler Thromb Vasc Biol* 2006;26(5):1002–1007.
- Marks MS, Heijnen HFG, Raposo G. Lysosome-related organelles: Unusual compartments become mainstream. *Current Opinion in Cell Biology* 2013;25(4):495–505.
- Kobayashi T, Vischer UM, Rosnoblet C, et al. The tetraspanin CD63/lamp3 cycles between endocytic and secretory compartments in human endothelial cells. *Mol Biol Cell* 2000;11(5):1829–1843.
- Arribas M, Cutler DF. Weibel-Palade body membrane proteins exhibit differential trafficking after exocytosis in endothelial cells. *Traffic* 2000;1(10):783–793.
- Harrison-Lavoie KJ, Michaux G, Hewlett L, et al. P-selectin and CD63 use different mechanisms for delivery to Weibel-Palade bodies. *Traffic* 2006;7(6):647–662.
- Robinson MS, Bonifacino JS. Adaptor-related proteins. *Curr Opin Cell Biol* 2001;13(4):444–453.
- Bonifacino JS, Traub LM. Signals for sorting of transmembrane proteins to endosomes and lysosomes. *Annu Rev Biochem* 2003;72395–72447.
- Newell-Litwa K, Seong E, Burmeister M, Faundez V. Neuronal and non-neuronal functions of the AP-3 sorting machinery. *J Cell Sci* 2007;120(Pt 4):531–541.
- Rous BA, Reaves BJ, Ihrke G, et al. Role of adaptor complex AP-3 in targeting wild-type and mutated CD63 to lysosomes. *Mol Biol Cell* 2002;13(3):1071–1082.
- Wei ML. Hermansky-Pudlak syndrome: a disease of protein trafficking and organelle function. *Pigment cell Res* 2006;19(1):19–42.
- Dell'Angelica EC, Shotelersuk V, Aguilar RC, Gahl WA, Bonifacino JS. Altered trafficking of lysosomal proteins in Hermansky-Pudlak syndrome due to mutations in the beta 3A subunit of the AP-3 adaptor. *Mol Cell* 1999;3(1):11–21.
- Clark RH, Stinchcombe JC, Day A, et al. Adaptor protein 3-dependent microtubule-mediated movement of lytic granules to the immunological synapse. *Nat Immunol* 2003;4(11):1111–1120.
- Wenham M, Grieve S, Cummins M, et al. Two patients with Hermansky Pudlak syndrome type 2 and novel mutations in AP3B1. *Haematologica* 2010;95(2):333–337.
- de Boer M, van Leeuwen K, Geissler J, et al. Hermansky-Pudlak syndrome type 2: Aberrant pre-mRNA splicing and mislocalization of granule proteins in neutrophils. *Hum Mutat* 2017;38(10):1402–1411.
- Martin-Ramirez J, Kok MGM, Hofman M, et al. Individual with subclinical atherosclerosis have impaired proliferation of blood outgrowth endothelial cells, which can be restored by statin therapy. *PLoS One* 2014;9(6):e99890.
- Bierings R, Hellen N, Kiskin N, et al. The interplay between the Rab27A effectors Slp4-a and MyRIP controls hormone-evoked Weibel-Palade body exocytosis. *Blood* 2012;120(13):2757–2767.
- van Breevoort D, Snijders AP, Hellen N, et al. STXBP1 promotes Weibel-Palade body exocytosis through its interaction with the Rab27A effector Slp4-a. *Blood* 2014;123(20):3185–3194.
- Azevedo C, Burton A, Ruiz-Mateos E, Marsh M, Saiardi A. Inositol pyrophosphate mediated pyrophosphorylation of AP3B1 regulates HIV-1 Gag release. *Proc Natl Acad Sci U S A* 2009;106(50):21161–21166.
- Schillemans M, Karampini E, van den Eshof BL, et al. Weibel-Palade Body Localized Syntaxin-3 Modulates Von Willebrand Factor Secretion From Endothelial Cells. *Arterioscler Thromb Vasc Biol* 2018;38(7):1549–1561.
- Poeter M, Brandherm I, Rossaint J, et al. Annexin A8 controls leukocyte recruitment to activated endothelial cells via cell surface delivery of CD63. *Nat Commun* 2014;5(3738):3738.
- Liu L, Sutton J, Woodruff E, Villalta F, Spearman P, Dong X. Defective HIV-1 particle assembly in AP-3-deficient cells derived from patients with Hermansky-Pudlak syndrome type 2. *J Virol* 2012;86(20):11242–11253.
- Peden AA, Rudge RE, Lui WWY, Robinson MS. Assembly and function of AP-3 complexes in cells expressing mutant subunits. *J Cell Biol* 2002;156(2):327–336.
- Pulido IR, Jahn R, Gerke V. VAMP3 is associated with endothelial Weibel-Palade bodies and participates in their Ca(2+)-dependent exocytosis. *Biochim Biophys Acta* 2011;1813(5):1038–1044.
- Martinez-Arca S, Rudge R, Vacca M, et al. A dual mechanism controlling the localization and function of exocytic v-SNAREs. *Proc Natl Acad Sci U S A* 2003;100(15):9011–9006.
- Kent HM, Evans PR, Schäfer IB, et al. Structural basis of the intracellular sorting of the SNARE VAMP7 by the AP3 adaptor complex. *Dev Cell* 2012;22(5):979–988.
- Jani RA, Purushothaman LK, Rani S, Bergam P, Setty SRG. STX13 regulates cargo delivery from recycling endosomes during melanosome biogenesis. *J Cell Sci* 2015;128(17):3263–3276.
- Fu J, Naren AP, Gao X, Ahmmed GU, Malik

- AB. Protease-activated receptor-1 activation of endothelial cells induces protein kinase Calpha-dependent phosphorylation of syntaxin 4 and Munc18c: role in signaling p-selectin expression. *J Biol Chem* 2005;280(5):3178–3184.
30. Graham GJ, Ren Q, Dilks JR, Blair P, Whiteheart SW, Flaumenhaft R. Endobrevin/VAMP-8-dependent dense granule release mediates thrombus formation in vivo. *Blood* 2009;114(5):1083–1090.
  31. Sharda A, Kim SH, Jasuja R, et al. Defective PDI release from platelets and endothelial cells impairs thrombus formation in Hermansky-Pudlak syndrome. *Blood* 2015;125(10):1633–1642.
  32. Thon JN, Peters CG, Machlus KR, et al. T granules in human platelets function in TLR9 organization and signaling. *J Cell Biol* 2012;198(4):561–574.
  33. Ma J, Zhang Z, Yang L, Kriston-Vizi J, Cutler DF, Li W. BLOC-2 subunit HPS6 deficiency affects the tubulation and secretion of von Willebrand factor from mouse endothelial cells. *J Genet Genomics* 2016;43(12):686–693.
  34. Sweeney JD, Novak EK, Reddington M, Takeuchi KH, Swank RT. The RIIIS/J inbred mouse strain as a model for von Willebrand disease. *Blood* 1990;76(11):2258–2265.
  35. Van Dorp DB, Wijermans PW, Meire F, Vrensen G. The Hermansky-Pudlak syndrome. Variable reaction to 1-desamino-8D-arginine vasopressin for correction of the bleeding time. *Ophthalmic Paediatr Genet* 1990;11(3):237–244.
  36. Zatik J, Póka R, Borsos A, Pfliegler G. Variable response of Hermansky-Pudlak syndrome to prophylactic administration of 1-desamino 8D-arginine in subsequent pregnancies. *Eur J Obstet Gynecol Reprod Biol* 2002;104(2):165–166.
  37. Cordova A, Barrios NJ, Ortiz I, Rivera E, Cadilla C, Santiago-Borrero PJ. Poor response to desmopressin acetate (DDAVP) in children with Hermansky-Pudlak syndrome. *Pediatr Blood Cancer* 2005;44(1):51–54.

## Supplemental Materials and Methods

### Antibodies

Antibodies used in this study are listed in Supplemental Table I.

### Lentiviral transfection and transduction

HEK293T cells, cultured in DMEM-F12 (Lonza, Basel, Switzerland) supplemented with 10% FCS, were seeded on collagen coated plates or flasks. HEK293T cells were transfected with lentiviral transfer (see in section DNA constructs, Materials and Methods), 3rd generation packaging (MDL and REV) and envelop (VGV-G) plasmids using *transit-LT1* (Mirus Bio LLC, Madison, WI, USA) and following the supplier's protocol. Virus particles were collected 24 and 48 hours following transfection. Virus particles were filtered through 0.45  $\mu\text{m}$  pore filters in EGM-18. Two batches of virus were used to transduce BOECs or cord blood BOECs (cbBOECs) for the period of 48 hours. Transduced endothelial cells were selected by puromycin (0.5  $\mu\text{g}/\text{ml}$ ) that was added to the medium for 72 hours after the second virus installment.

### Immunoblotting

Endothelial cells were grown to confluency and lysed in NP-40 based lysis buffer (0.5% NP-40, 0.5 mM EDTA, 10 mM Tris HCl, 150 mM NaCl), supplemented with Complete protease inhibitor cocktail (Roche, 05056489001). Proteins were separated on a Novex® NuPAGE® 4-12% Bis-Tris gel (ThermoFisher, NP0321/NP0323) and transferred onto a nitrocellulose membrane (iBlot Transfer Stack, ThermoFisher, IB3010). Membranes were blocked with Odyssey blocking buffer (LI-COR Biosciences, Lincoln, USA, LI 927) and probed with primary antibodies and subsequently with IRDye conjugated secondary antibodies (see Supplemental Table I). Visualization of IRDye conjugated antibodies was performed by means of LI-COR Odyssey Infrared Imaging System (LI-COR Biosciences). Blot analysis for band intensities was done in Image Studio Lite (V4.0, LI-COR Biosciences) and when needed intensities were normalized to the intensity of  $\alpha$ -tubulin which was used as a loading control.

### Whole-proteome analysis

Whole proteome analysis was performed as described previously.<sup>2</sup> In short, BOECs were cultured in 10 cm culture dishes in triplicate. Upon confluency, cells were lysed and processed into tryptic peptides using the Filter Aided Sample Preparation method.<sup>3</sup> Tryptic peptides were desalted using Empore-C18 StageTips<sup>4</sup> and separated by nanoscale C18 reverse phase chromatography coupled online to an Orbitrap Fusion Tribrid Mass Spectrometer via a nanospray Flex Ion Source (Thermo Scientific, Waltham, MA, USA) using the same settings as described previously.<sup>5</sup> All MS data were acquired with Xcalibur software (Thermo Scientific). The RAW mass spectrometry files were processed with the MaxQuant computational platform, version 1.5.2.8.<sup>6</sup> Proteins and peptides were identified using the Andromeda search engine by querying the human Uniprot database, (downloaded February 2015). Standard settings with the additional options match between runs, label-free quantification, and unique peptides for quantification were selected. The generated proteingroups.txt table was filtered for reverse hits, only identified by site and potential contaminants using Perseus 1.5.1.6. The label-free quantification values were transformed in log<sub>2</sub> scale. Samples were grouped per BOEC donor (HPS-2 patient (ID 8621), 4 healthy controls (IDs 7908, 7950, 7958 and 7977); 5 groups, 3 samples per group), and proteins were filtered for at least 3 valid values in at least 1 of the 5 groups. Missing values were imputed by normal distribution (width = 0.3, shift = 1.8), assuming these proteins were close to the detection limit. Global changes in protein levels were assessed using ANOVA (false discovery rate, 0.05, S0: 0.4). Z-scored LFQ (log<sub>2</sub>) values were represented using a heatmap combined with hierarchical clustering. The .raw MS files and search/identification

files obtained with MaxQuant have been deposited in the ProteomeXchange Consortium (<http://proteomecentral.proteomexchange.org/cgi/GetDataset>) via the PRIDE partner repository<sup>7</sup> with the data set identifier PXD011294.

### Fluorescence microscopy

Immunostaining and fluorescence imaging of fixed cells was performed as previously described.<sup>2</sup> Immunostained cells were mounted in MOWIOL mounting medium and images were acquired using a Leica SP8 confocal microscope (Leica, Wetzlar, Germany). Images were processed and analyzed using ImageJ or IMARIS Digital Imaging software (Bitplane AG, Zürich, Switzerland).

### Secretion assay

Endothelial cells were grown in 6-well wells and cultured for the period of 7 days prior to the experiment. Unstimulated VWF release was determined for 1 and 24 hours in release medium [serum-free M199 (Thermofisher, 22340) supplemented with 0.2% (w/v) bovine serum albumin (BSA) (Merck, 112018)] and EGM-18 medium, respectively. Cells were pre-incubated in RM medium for 15-30 minutes prior to stimulated VWF secretion. Cells were stimulated in RM medium supplemented with 0.1-100  $\mu$ M histamine (Sigma-Aldrich, H7125), 10  $\mu$ M forskolin (Sigma-Aldrich, F6886) with 100  $\mu$ M IBMX (Sigma-Aldrich, I7018), or vehicle (unstimulated) for 30 minutes, unless stated otherwise. Lysates were obtained in RM medium supplemented with 1% Triton X-100. VWF levels were determined by ELISA as described previously.<sup>2</sup> Secretion is expressed as relative proportion of intracellular VWF in lysates of unstimulated cells.

### Data and statistical analysis

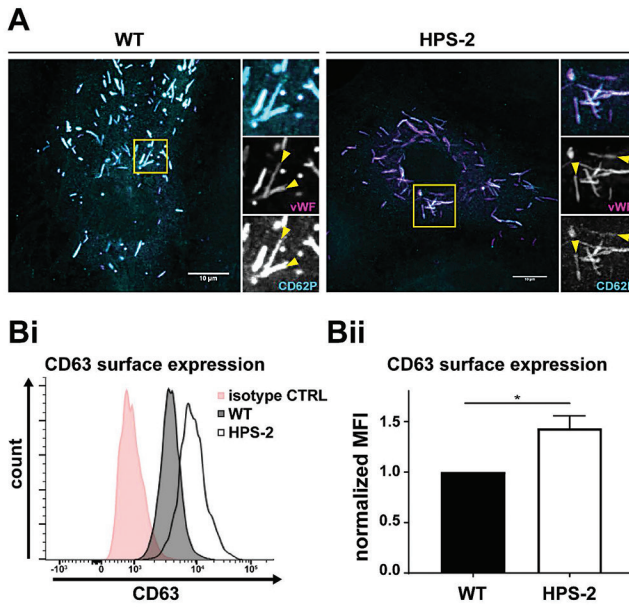
Flow cytometry data was analyzed using FlowJo version 10 (Ashland, OR, USA). Statistical analysis was by student's t-test and using GraphPad Prism 7.04 (Graphpad, La Jolla, CA, USA). Significance values are shown in the Figures or in Figure legends. Data are shown as mean  $\pm$  SEM.

## Supplemental Figures and Tables

**Supplemental Table I: Antibody reagents**

Target	Species (isotype)	Label	Supplier	Cat.nr / clone	Use [concentration/dilution]
VWF	mouse (IgG <sub>2b</sub> )	-	described in <sup>1</sup>	CLB-RAG20	IF [1:1000]
$\alpha$ -tubulin	mouse (IgG <sub>1</sub> )	-	Sigma-Aldrich	T9026	WB [1:1000]
VWF	rabbit	-	DAKO	A0082	ELISA [6 $\mu$ g/ml]
VWF	rabbit	HRP	DAKO	A0082	ELISA [2 $\mu$ g/ml]
AP-3 $\beta$ 3A	rabbit		proteintech	13384-1-AP	WB (1:500)
AP-3 $\mu$ 3	rabbit		Abcam	ab201227	WB (1:1000)
GFP	sheep		BIORAD	4745-1051	WB [0.5 $\mu$ g/ml]
CD63	mouse (IgG <sub>1</sub> )	AF488	Sanquin	CLB-gran/12	IF [0.4 $\mu$ g/ml]
CD62P	mouse (IgG <sub>1</sub> )	AF488	AbD Serotec	MCA796	IF [2 $\mu$ g/ml]
CD62P	mouse (IgG <sub>1</sub> )	PE	BioLegend	304906	FCM (1:100)
VAMP8	rabbit		Synaptic Systems	104303	WB, IF [1 $\mu$ g/ml]
rabbit IgG	donkey	680LT	Li-Cor	925-68023	WB [0.1 $\mu$ g/ml]
mouse IgG	donkey	800CW	Li-Cor	925-32212	WB [0.1 $\mu$ g/ml]
rabbit IgG	goat	AF633	ThermoFisher	A11011	IF [2 $\mu$ g/ml]
mouse IgG	goat	AF568	ThermoFisher	A11004	IF [2 $\mu$ g/ml]
mouse IgG	goat	AF488	ThermoFisher	A11004	IF [2 $\mu$ g/ml]
rabbit IgG	chicken	AF647	ThermoFisher	A21443	IF [2 $\mu$ g/ml]

## Supplemental Figure I

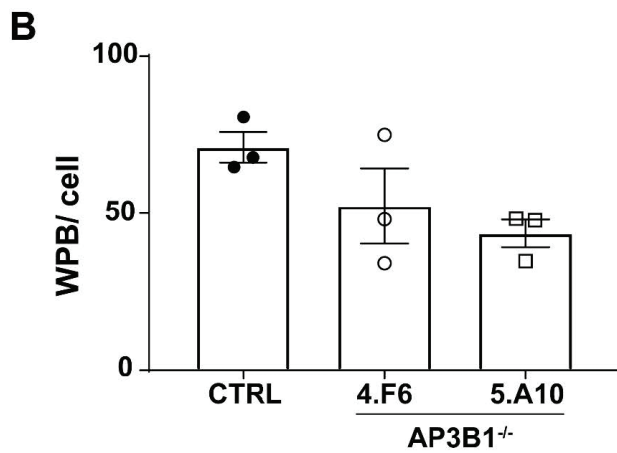
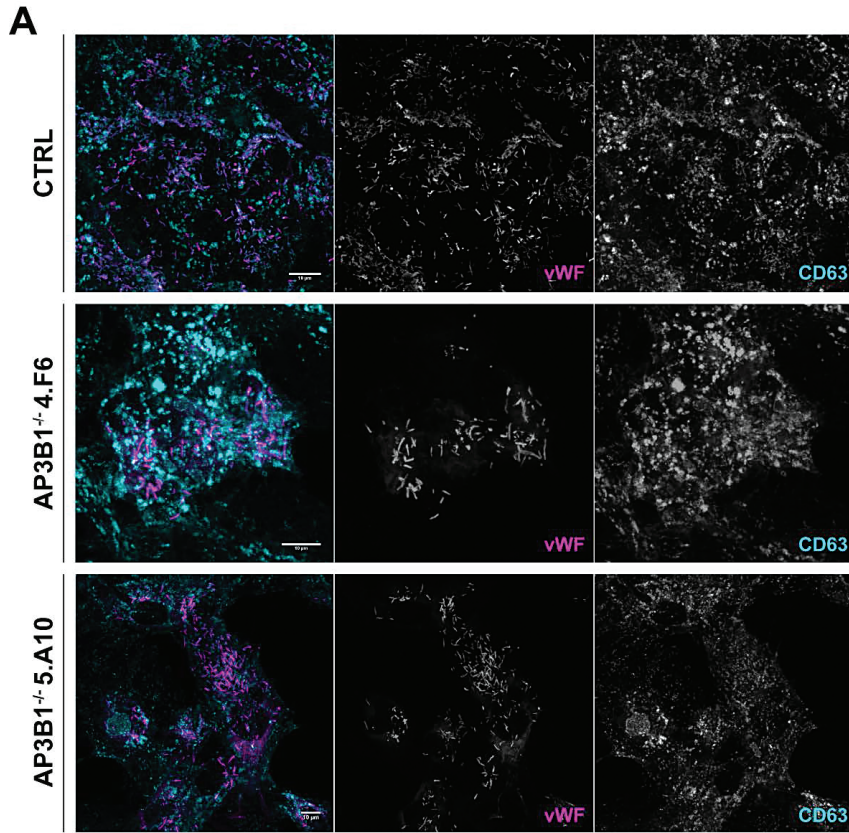


**Supplemental Figure I: P-selectin (CD62P) and CD63 trafficking in HPS-2 BOECs.** A) WT and HPS-2 BOECs were immunostained for vWF (magenta) and CD62P (cyan). Boxed regions are magnified on the right. The yellow arrowheads show WPB in both channels. In both WT and HPS-2 BOEC WPBs are positive for CD62P. B) Flow cytometric analysis of CD63 membrane expression under steady state conditions in WT and HPS-2 BOECs. Bi) Representative histogram plot of WT and HPS-2 BOEC stained with mouse anti-CD63 Bii) Quantification of 6 independent experiments. CD63 is significantly increased on the plasma membrane of HPS-2 BOEC. (Paired two-tailed Student's t-test, \*  $p < 0.05$ ).

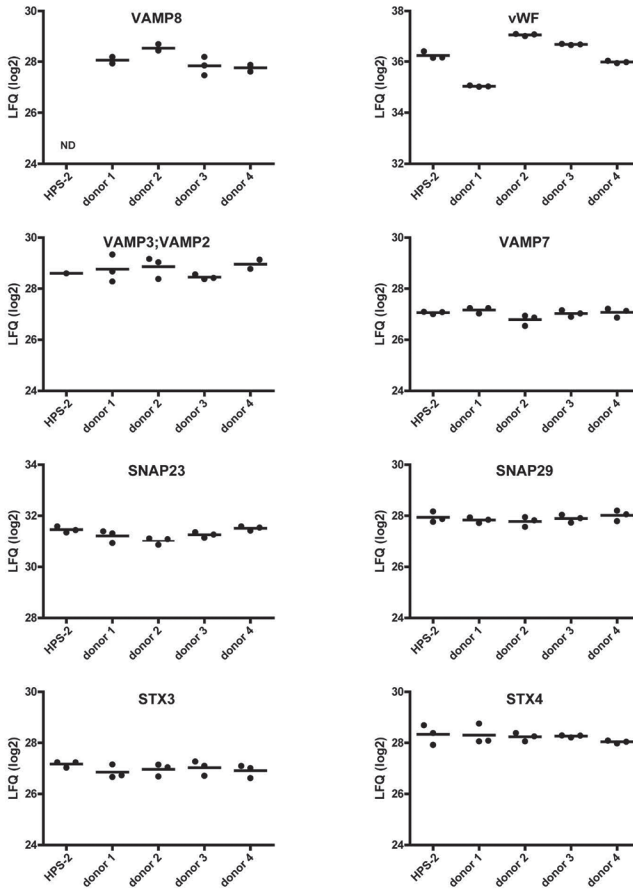


## Supplemental Figure II

Supplemental Figure II: WPB formation and maturation (CD63 delivery) in *AP3B1*<sup>-/-</sup> BOEC lines. A) Control and *AP3B1*<sup>-/-</sup> BOEC were immunostained for VWF (magenta) and CD63 (cyan). B) average amount of WPB per cell in control and *AP3B1*<sup>-/-</sup> BOEC.

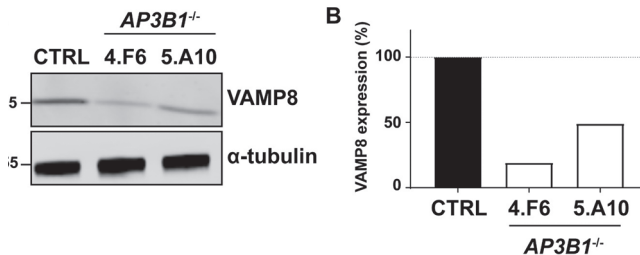


## Supplemental Figure III



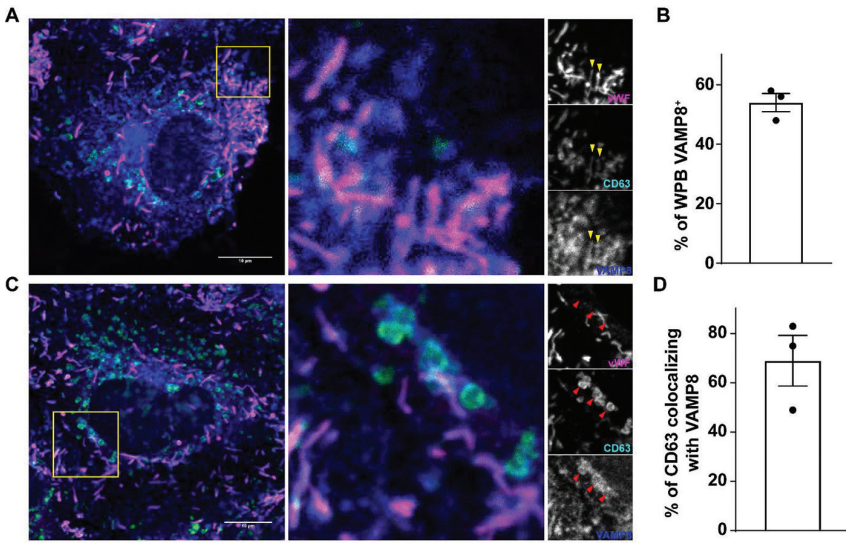
Supplemental Figure III: Expression of exocytotic SNARE proteins in healthy control and HPS-2 BOECs. Graph representing LFQ (log<sub>2</sub>) values for VAMP8, VAMP3, VAMP7, SNAP23, SNAP29, STX3, STX4 and vWF.

## Supplemental Figure IV



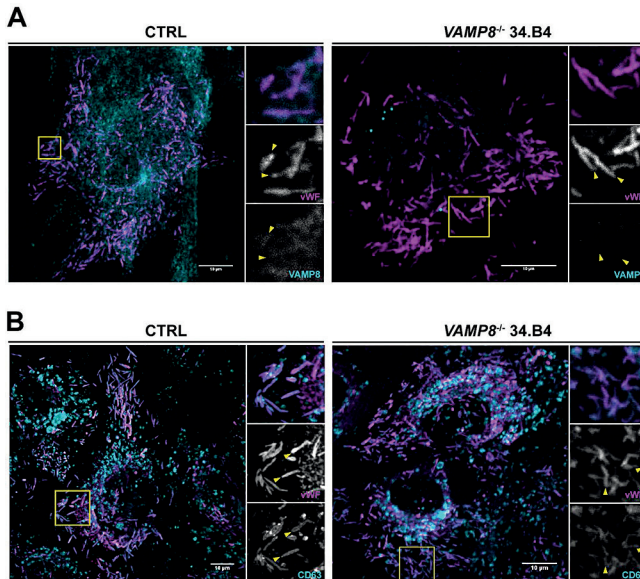
Supplemental Figure IV: Reduced expression of VAMP8 in *AP3B1*<sup>-/-</sup> BOEC lines. A) Western blot analysis of VAMP8 expression in lysates from two clonal *AP3B1*<sup>-/-</sup> BOEC lines (4.F6 and 5.A10) compared to clonal control BOEC.  $\alpha$ -tubulin is used as loading control. Molecular weight standards are indicated on the left (kDa). B) Quantification of relative VAMP8 expression in clonal *AP3B1*<sup>-/-</sup> BOEC lines normalized to VAMP8 in clonal control BOEC (CTRL). VAMP8 expression is severely affected in both clones with one, 4.F6, expressing less than 20%, while the other, 5.A10 having expression below 50%.

## Supplemental Figure V



**Supplemental Figure V: VAMP8 and CD63 expression in healthy control endothelial cells.** A) Control BOECs were immunostained for vWF (magenta), CD63 (green) and VAMP8 (blue). Boxed regions are magnified on the right. WPBs are indicated by yellow arrowheads that are positive for both VAMP8 and CD63. B) Proportion of WPB that contain CD63 immunoreactivity. C) Control BOEC were immunostained for VWF (magenta), CD63 (green) and VAMP8 (blue). Boxed regions are magnified on the right. CD63 positive endosome-like structures are indicated by red arrowheads. These structures are only positive for CD63 and VAMP8, but lack VWF. D) Proportion of CD63 that co-localizes with VAMP8. Scale bars represent 10  $\mu$ m.

## Supplemental Figure VI



**Supplemental Figure VI: CD63 trafficking in VAMP8 knockout cell lines.** A) Control and *VAMP8*<sup>-/-</sup> BOECs were immunostained for vWF (magenta) and VAMP8 (cyan), demonstrating the lack of VAMP8 immunoreactivity on WPBs in *VAMP8*<sup>-/-</sup> BOECs. B) Control and *VAMP8*<sup>-/-</sup> BOEC were immunostained for vWF (magenta) and CD63 (cyan). In both control and *VAMP8*<sup>-/-</sup> BOEC WPBs are positive for CD63. Boxed regions are magnified on the right. The yellow arrowheads show WPB in both channels. Scale bars represent 10  $\mu$ m.

## Supplemental References

1. van Agtmaal EL, Bierings R, Dragt BS, et al. The shear stress-induced transcription factor KLF2 affects dynamics and angiopoietin-2 content of Weibel-Palade bodies. *PLoS One* 2012;7(6):e38399.
2. Schillemans M, Karampini E, van den Eshof BL, et al. Weibel-Palade Body Localized Syntaxin-3 Modulates Von Willebrand Factor Secretion From Endothelial Cells. *Arterioscler Thromb Vasc Biol* 2018;38(7):1549–1561.
3. Wiśniewski JR, Zougman A, Nagaraj N, Mann M. Universal sample preparation method for proteome analysis. *Nat Methods* 2009;6(5):359–62.
4. Rappsilber J, Ishihama Y, Mann M. Stop And Go Extraction tips for matrix-assisted laser desorption/ionization, nanoelectrospray, and LC/MS sample pretreatment in proteomics. *Anal Chem* 2003;75(3):663–670.
5. Gazendam RP, van de Geer A, van Hamme JL, et al. Impaired killing of *Candida albicans* by granulocytes mobilized for transfusion purposes: A role for granule components. *Haematologica* 2016;101(5):587–596.
6. Cox J, Mann M. MaxQuant enables high peptide identification rates, individualized p.p.b.-range mass accuracies and proteome-wide protein quantification. *Nat Biotechnol* 2008;26(12):1367–72.
7. Vizcaíno J, Deutsch EEW, Wang R, et al. ProteomeXchange provides globally coordinated proteomics data submission and dissemination. *Nat Biotech* 2014;32(3):223–226.



## Chapter 7

# Weibel-Palade body localized syntaxin-3 modulates von Willebrand factor secretion from endothelial cells

Maike Schillemans, Ellie Karampini, Bart L van den Eshof, Anastasia Gangaev, Menno Hofman, Dorothee van Breevoort, Henriët Meems, Hans Janssen, Aat A Mulder, Carolina R Jost, Johanna C Escher, Rüdiger Adam, Tom Carter, Abraham J Koster, Maartje van den Biggelaar, Jan Voorberg and Ruben Bierings  
*Arteriosclerosis, Thrombosis, and Vascular Biology* 2018; 38: 1549–1561

## Abstract

### Objective

Endothelial cells store von Willebrand factor (VWF) in rod-shaped secretory organelles, called Weibel-Palade bodies (WPBs). WPB exocytosis is coordinated by a complex network of Rab GTPases, Rab-effectors and SNARE proteins. We have previously identified STXBP1 as the link between the Rab27A-Slp4-a complex on WPBs and the SNARE proteins syntaxin-2 and -3. In this study we investigate the function of syntaxin-3 in VWF secretion.

### Approach and Results

In human umbilical vein endothelial cells (HUVECs) and in blood outgrowth endothelial cells (BOECs) from healthy controls endogenous syntaxin-3 immunolocalized to WPBs. A detailed analysis of BOECs isolated from a patient with variant microvillus inclusion disease (MVID), carrying a homozygous mutation in *STX3* (*STX3*<sup>-/-</sup>), showed a loss of syntaxin-3 protein and absence of WPB-associated syntaxin-3 immunoreactivity. Ultrastructural analysis revealed no detectable differences in morphology or prevalence of immature or mature WPBs in control versus *STX3*<sup>-/-</sup> BOECs. VWF multimer analysis showed normal patterns in plasma of the MVID patient, and media from *STX3*<sup>-/-</sup> BOECs, together indicating WPB formation and maturation are unaffected by absence of syntaxin-3. However, a defect in basal as well as Ca<sup>2+</sup>- and cAMP-mediated VWF secretion was found in the *STX3*<sup>-/-</sup> BOECs. We also show that syntaxin-3 interacts with the WPB-associated SNARE protein VAMP8.

### Conclusions

Our data reveal syntaxin-3 as a novel WPB-associated SNARE protein that controls WPB exocytosis.

### Nonstandard Abbreviations and Acronyms

VWF	Von Willebrand factor
WPB	Weibel/Palade body
SNARE	Soluble NSF Attachment Protein Receptor
MVID	Microvillus inclusion disease
BOEC	blood outgrowth endothelial cell
HUVEC	Human umbilical vein endothelial cell

## Introduction

Von Willebrand factor (VWF) is a multimeric adhesive glycoprotein that is critically involved in hemostasis by mediating adhesion of platelets to sites of vascular damage and by acting as a chaperone for coagulation factor VIII in plasma. The importance of VWF for vascular homeostasis is illustrated by the pathophysiological phenotypes that are associated with abnormal levels of circulating VWF. Low levels of VWF are associated with bleeding, such as in the inherited bleeding disorder Von Willebrand disease, while elevated levels of VWF are associated with increased risk of thrombosis and cardiovascular disease.<sup>1</sup> The majority of VWF is synthesized by endothelial cells, where it is stored in secretory organelles called Weibel-Palade bodies (WPBs). VWF, together with a number of inflammatory and angiogenic mediators, is rapidly released from WPBs upon shear stress or damage to the vessel wall.<sup>2</sup>

The mechanisms that regulate biogenesis and exocytosis of WPBs are complex and poorly understood. During biogenesis and maturation, WPBs recruit a set of Rab GTPases (Rab27A, Rab3B/D, Rab15) and Rab-effectors (MyRIP, Slp4-a, Munc13-4), that mediate interactions with the cytoskeleton and plasma membrane. Recruitment of these molecules coin-

cides with the acquisition of WPB secretion competence and provides the link with Soluble NSF Attachment Protein Receptor (SNARE) complex proteins.<sup>3-9</sup> SNARE complexes are molecular machines that catalyze the fusion of lipid bilayers, which plays a central role in the exocytosis of secretory vesicles. They typically consist of four SNARE helices: 1 provided by a v-SNARE/R-SNARE on the donor compartment (VAMPs) and 3 Q-SNAREs provided by a t-SNARE complex (1 by syntaxins and 2 by SNAP25 homologues) on the acceptor compartment. Assembly of v- and t-SNAREs into a parallel 4 helix bundle produces a mechanical force that brings the vesicle and target membranes in close proximity, lowering the energetic barrier for fusion. A number of SNARE and SNARE associated proteins have been implicated in WPB exocytosis.<sup>10-14</sup> Despite this, we currently do not know the exact composition of the WPB exocytotic machinery and how all these individual components together orchestrate WPB release. Recently, syntaxin-3 was found as part of a complex with STXBPI and the Rab27A-effector Slp4-a, which both have been identified as positive regulators of WPB exocytosis.<sup>7,12</sup>

In this study we show that syntaxin-3 localizes to WPBs. VWF secretion is significantly impaired in *ex vivo* *STX3*<sup>Δ</sup> endothelial cells derived from a patient with variant microvillus inclusion disease (MVID), whereas WPB abundance and morphology are unaffected. We identified VAMP8, another WPB localized SNARE, as an interaction partner of syntaxin-3. Together, the data identify syntaxin-3 as a new component of the SNARE machinery regulating WPB exocytosis and VWF secretion.

## Materials and Methods

The whole-proteome analysis .raw MS files and search/identification files obtained with MaxQuant are available through the ProteomeXchange Consortium (<http://proteomecentral.proteomexchange.org/cgi/GetDataset>) via the PRIDE partner repository<sup>15</sup> with the dataset identifier PXD006176.

### Antibodies

Antibodies used in this study are listed in Supplemental Table I.

### Cell culture and blood outgrowth endothelial cell (BOEC) isolation

Pooled, cryo-preserved primary human umbilical vein endothelial cells (HUVECs) were obtained from Promocell (Heidelberg, Germany) and were cultured as described.<sup>12</sup> BOECs were isolated as previously described and cultured in EGM-2 medium (Lonza, Basel, Switzerland, CC-3162) supplemented with 18% FCS (Bodinco, Alkmaar, Netherlands).<sup>12</sup> Experiments were always performed at passage 5-6. Venous blood was drawn from an individual with variant MVID, caused by a homozygous 2-bp insertion (c.372\_373dup, p.Arg125Leufs\*7) in *STX3* (patient 2 in<sup>16</sup>), and from both parents. Blood from an additional variant MVID patient with a homozygous nonsense mutation (c.739C>T, p.Arg247\*) in *STX3* (patient 1 in<sup>16</sup>) and the mother of the patient was drawn, but isolation of BOECs was only successful for the heterozygous mother. Control BOECs from healthy donors were isolated from the internal blood donor system at Sanquin Blood Supply. The patient's parents signed an informed consent form for participation. The study was conducted in accordance with the Declaration of Helsinki.

### Immunocytochemistry

Endothelial cells were grown on gelatin-coated glass coverslips (Marienfeld, Lauda-Königshofen, Germany). Cells were fixed at room temperature with EM-grade 4% formaldehyde (Electron Microscopy Sciences, Hatfield, USA) in PBS for 15 min followed by simultaneous permeabilization and quenching using 0.2% saponin, 50 mM NH<sub>4</sub>Cl in PBS.

Immunostaining was performed in PGAS (PBS, 0.2% gelatin, 0.02% NaN<sub>3</sub>, 0.02% saponin). Immunostained cells were mounted in Mowiol 40-88® (Sigma-Aldrich, Steinheim, Germany, 324590) and images were acquired by confocal microscopy using a Leica SP8 (Leica Microsystems, Wetzlar, Germany).

### Subcellular fractionation

HUVECs were grown to confluency and after 4 days they were homogenized using a ball-bearing homogenizer (Isobiotec, Heidelberg, Germany) essentially as described previously.<sup>17</sup> Subcellular fractions were obtained by density gradient ultracentrifugation using a Beckmann Optima™ LX-100 XP ultracentrifuge equipped with a Ti50.2 fixed angle rotor. Briefly, homogenates were fractionated by two subsequent Percoll (GE Healthcare, Eindhoven, Netherlands) density gradients followed by one Nycodenz (Progen Biotechnik, Heidelberg, Germany) density gradient.<sup>17</sup> Percoll fractions and Nycodenz fractions containing the WPBs were identified by VWF ELISA.<sup>18</sup> Selected fractions were analyzed by immunoblotting for syntaxin-3.

### Immunoblotting

Endothelial cells were grown to confluency and lysed in NP-40 based lysis buffer (1% NP-40, 10% glycerol, 1 mM EDTA, 1 mM EGTA, 50 mM Tris HCL, 100 mM NaCL), supplemented with Complete protease inhibitor cocktail (Roche, 05056489001). Proteins were separated on a Novex® NuPAGE® 4-12% Bis-Tris gel (ThermoFisher, NP0321/NP0323) and transferred onto a nitrocellulose membrane (iBlot Transfer Stack, ThermoFisher, IB3010). Membranes were blocked with Odyssey blocking buffer (LI-COR Biosciences, Lincoln, USA, LI 927) and probed with primary antibodies followed by IRDye conjugated secondary antibodies. IRDye conjugated antibodies were visualized by LI-COR Odyssey Infrared Imaging System (LI-COR Biosciences). Image Studio Lite (V4.0, LI-COR Biosciences) was used to analyze band intensities, when needed intensities were normalized to the intensity of  $\alpha$ -tubulin which was used as a loading control.

### Whole-proteome analysis of BOECs.

BOECs were cultured in 10 cm culture dishes in triplicate. Upon confluency, cells were rinsed 3x in PBS and subsequently scraped in 100 ml SDS lysis buffer consisting of 4% SDS, 100 mM DTT, 100 mM Tris.HCl pH 7.5, supplemented with MS grade Halt protease and phosphatase inhibitor cocktail (Thermo Scientific, 78440). Next, cell lysates were incubated for 5 minutes at 95°C, sonicated using a Branson Sonifier 250 (Branson Ultrasonics S.A., Geneva, Switzerland) and centrifuged for 10 minutes at 16,000g. The cleared lysates were obtained and the protein concentration was determined by Bradford. 50  $\mu$ g of protein was processed into tryptic peptides using the Filter Aided Sample Preparation method.<sup>19</sup> 10  $\mu$ g peptides were desalted and concentrated using Empore-C18 StageTips and eluted with 0.5% (v/v) acetic acid, 80% (v/v) acetonitrile as described before.<sup>20,21</sup> Sample volume was reduced by SpeedVac and supplemented with 2% (v/v) acetonitrile, 0.1% (v/v) TFA to a final volume of 5  $\mu$ l. Three  $\mu$ l was injected in the Mass Spectrometer (Orbitrap Fusion, Thermo Scientific, Waltham, MA, USA).

Tryptic peptides were separated by nanoscale C18 reverse chromatography coupled online to an Orbitrap Fusion Tribrid mass spectrometer (Thermo Scientific) via a nanoelectrospray ion source (Nanospray Flex Ion Source, Thermo Scientific), using the same settings as described in.<sup>21</sup> All MS data were acquired with Xcalibur software (Thermo Scientific).

The RAW mass spectrometry files were processed with the MaxQuant computational platform, 1.5.2.8.<sup>22</sup> Proteins and peptides were identified using the Andromeda search engine by querying the human Uniprot database (downloaded February 2015).<sup>23</sup> Standard settings with the additional options match between runs, label free quantification, and unique peptides for quantification were selected. The generated 'proteingroups.txt' table



was filtered for reverse hits, 'only identified by site' and potential contaminants using Perseus 1.5.1.6. The label free quantification values were transformed in log<sub>2</sub> scale. Samples were grouped per BOEC donor (*STX3*<sup>-/-</sup> patient, 4 healthy controls) (5 groups, 3 samples per group) and proteins were filtered for at least 3 valid values in at least one of the 5 groups. Missing values were imputed by normal distribution (width = 0.3, shift = 1.8), assuming these proteins were close to the detection limit. Global changes in protein levels were assessed employing four separate volcano plots where the syntaxin-3 patient BOECs were pair wise compared with the healthy control BOECs (FDR 0.05, S0: 0.4). Proteins with a significantly changed level were defined as proteins with a significantly changed expression in all four pair wise comparisons.

The .raw MS files and search/identification files obtained with MaxQuant have been deposited in the ProteomeXchange Consortium (<http://proteomecentral.proteomexchange.org/cgi/GetDataset>) via the PRIDE partner repository<sup>15</sup> with the dataset identifier PXD006176.

### Electron microscopy

BOECs were grown in a petri dish to 5 days post-confluence and were fixed with Karnovsky's fixative followed by 1% osmiumtetroxide post fixation, en-bloc staining with Ultrastain1 (Leica Microsystems) and dehydration by ethanol series. Beem capsules were filled with EPON and the open side of the capsules were positioned on the fixed cells. After polymerization of the EPON, beem capsules were snapped off the surface of the wells of the culture dish. Ultrathin sections (70 nm) parallel to the surface of the beem specimen containing the cultured cells were made on a Reichert Ultracut S (Leica Microsystems). Sections were post stained with uranylacetate and lead citrate. Electron microscopy images were obtained in a Fei Tecnai Twin transmission electron microscope (FEI, Eindhoven, Netherlands) operating on 120 kV using a Gatan OneView (Gatan, Pleasanton, USA) camera. About 2100 pics per stitch were taken on binning 2. Overlapping images were collected and stitched together into a big image as described.<sup>24</sup> Single WPB images were taken from 7 different cells from stitches of both healthy control BOECs and *STX3*<sup>-/-</sup> BOECs (control: n=135, *STX3*<sup>-/-</sup>: n=128). All images were randomized after which 6 researchers independently scored the maturation status of all 263 WPB images. Images that were not unanimously recognized as WPBs were excluded (31 from control, 18 from stitch *STX3*<sup>-/-</sup>), which led to a final maturity scoring of 104 WPBs from healthy control BOECs and 110 from *STX3*<sup>-/-</sup> MVID BOECs.

### Secretion assay

Endothelial cells were grown in 6-well wells or on 24 mm polyester Transwell membranes with 0.4 μm pores (3450, Costar) and cultured at full confluence for 4-5 days. Unstimulated VWF release was determined in conditioned EGM-18 medium after 24 hour incubation. Stimulated VWF release was assayed following a 15 minute pre-incubation in serum-free medium M199 (ThermoFisher, 22340) supplemented with 0.2% (w/v) BSA (Merck, 112018). Cells were stimulated in serum-free medium supplemented with 0.1-100 μM histamine (Sigma-Aldrich, H7125), 10 μM forskolin (Sigma-Aldrich, F6886) with 100 μM IBMX (Sigma-Aldrich, I7018), or vehicle (unstimulated) for 30 minutes, unless stated otherwise. Lysates were made in serum-free media supplemented with 1% Triton X-100 and protease inhibitors. Polarized VWF secretion was assayed essentially as described<sup>25</sup> and conditioned media were collected separately from the top (apical) and bottom compartment (basolateral). VWF and VWFpp levels were determined by ELISA.

### VWF and VWFpp ELISA

For determination of VWF secretion and intracellular content a sandwich ELISA was performed using (0.5 mg/well) rabbit polyclonal anti-hVWF as coating antibody and HRP-conjugated rabbit polyclonal anti-hVWF (0.5 mg/ml) for detection. Secreted and intracellular

VWFpp was detected by sandwich ELISA using mouse monoclonal anti-hVWFpp (1.0 mg/well) as coating antibody and HRP-conjugated mouse monoclonal anti-hVWFpp (0.125 mg/ml) for detection. Blocking, washing and detection steps were performed in TWEB buffer (0.1% Tween-20, 0.2% gelatin, and 1 mM EDTA in PBS). HRP activity was measured by colorimetric detection of ortho-phenylenediamine conversion using a Spectramax Plus 384 microplate reader (Molecular Devices, Sunnyvale, USA). Normal plasma from a pool of 30 donors served as a standard for determination of VWF antigen levels in plasma samples.<sup>26</sup> For lysates and media samples concentrated conditioned media from HEK293Ts stably expressing human wildtype VWF,<sup>27</sup> which was calibrated against the plasma standard, was used as a standard.

### DNA construct and transfection

For construction of mEGFP tagged to the N-terminus of human STX3 the STX3 coding sequence was amplified with RBNL175 (5'-GGGCGCGCCTGGTGGGGCCATGAAGGACCGTCTGGAGCAGCTG-3') and RBNL176 (5'-GCGGCCGCTGCTCGTCCATTAATT CAGCCCAACGGAAAGTCC-3') using a human STX3 cDNA clone (clone ID 3010338, Thermo Scientific) as template. The 908 bp PCR product containing the entire STX3 coding sequence was cloned in frame behind mEGFP in the mEGFP-LIC vector by ligation independent cloning, resulting in mEGFP-STX3. STX3 and VAMP8 were cloned into a lentiviral vector by digestion of the inserts from mEGFP-STX3 using BsrGI and NotI or from pEGFP-VAMP8<sup>28</sup> (a kind gift from Thierry Galli; Addgene #42311) using BsrGI and MluI. Fragments were inserted into the previously described LVX-mEGFP-LIC backbone, using the same restriction enzymes, respectively.<sup>12</sup> To construct lentiviral myc-STX3 the 10 residue myc-epitope from myc-LIC<sup>7</sup> was used to replace mEGFP in LVX-mEGFP-LIC through cut and paste cloning with SbfI and BsrGI, resulting in LVX-myc-LIC. STX3 was excised from LVX-mEGFP-STX3 using BsrGI and NotI and cloned in frame behind myc, resulting in LVX-myc-STX3. All constructs were verified by sequence analysis. Transfection of HUVECs was performed by nucleofection as described.<sup>29</sup> Lentivirus was produced in HEK293T cells cultured in EGM18 as described.<sup>12</sup> Puromycin was used to select for transduced endothelial cells.

### Immunoprecipitation

ECs expressing lentivirally transduced mEGFP-fusion proteins were lysed in lysis buffer (0.5% NP40, 10mM Tris.HCl (pH7.5), 150 mM NaCl and 0.5 mM EDTA) supplemented with Complete Protease Inhibitor Cocktail. Lysates were incubated with magnetic GFP-nanobody beads (Allele Biotech, San Diego, USA, ABP-NAB-GFPM100) or blocked control beads (ABP-NAB-MCCTRL5) by rotation for 2 hours at room temperature. Alternatively, lysates of native HUVECs were lysed and incubated with magnetic protein G dynabeads (Thermo Scientific, 10004D) coupled with antibody as described in the figure. After incubation, beads were washed 4 times with lysis buffer. Co-immunoprecipitates and lysates were analyzed by immunoblotting.

### CRISPR/Cas9 engineering of BOECs

gRNAs were designed to exon 1 and exon 2 of the *STX3* gene using the CRISPOR Design tool (<http://crispor.tefor.net/crispor.py>). gRNAs (gRNA-A exon 1: CTTCAGGATGAAGGACCGTC; gRNA-B exon 2: GACGAGTCTTTTCTGAGGT) were selected based on the specificity score with the minimum amount of off-target effects and were subsequently cloned as hybridized oligos (gRNA-A: RBNL358 5'-CACCGCTTCAGGATGAAGGACCGTC-3' and RBNL359 5'-AAACGACGGTCTTCATCCTGAAGC-3'; gRNA-B: RBNL364 5'-CACCGGACGAGTTCTTTTCTGAGGT-3' and RBNL365 5'-AAACACCTCAGAAAAGAACTCGTCC-3') into BsmBI-digested LentiCRISPR v2 vector<sup>30</sup> (a kind gift from Feng Zhang; Addgene #52961). BOECs were transduced with LentiCRISPR constructs containing gRNA-A or gRNA-B or without gRNA insertion (control) as described above. Puromycin selected cells

were single cell sorted using an antibody against VE-cadherin and plated in 96-well format. Clonal colonies were tested for the expression of syntaxin-3 by immunoblot and STX3 null clones were expanded. To identify the mutations in *STX3*, genomic DNA was isolated using the DNeasy Blood and Tissue kit (QIAGEN, Venlo, NL) from the *STX3*<sup>-/-</sup> clones. PCR products amplified using primers for exon 1 (RBNL366: 5'-CGGACGCTCCTCCTAGCTAG-3' and RBNL367: 5'-GTGGTGAAGGGACCCCTG AC-3') and exon 2 (RBNL368: 5'-CCCAGCAATTG-GTAGAGCTAGG-3' and RBNL402: 5'-CATG GTTGTGATCCTATGGTTGATTCTG-3') were subjected to Sanger sequencing and Next Generation Sequencing.

### Statistical analysis

Statistical analysis was by two-tailed *t*-test using GraphPad Prism 7.04 (Graphpad, La Jolla, CA), either paired or unpaired as mentioned in the Figure legends. Prior to performing a paired *t*-test normality was confirmed using the Shapiro-Wilk test on small (N=3-6) sample sizes. Prior to performing an unpaired *t*-test normality was approached by a log-transformation and an F-test was used to confirm equal variance in larger data sets (N<100). Significance values are shown in the Figures or in Figure legends. Data are shown as mean  $\pm$  SEM.

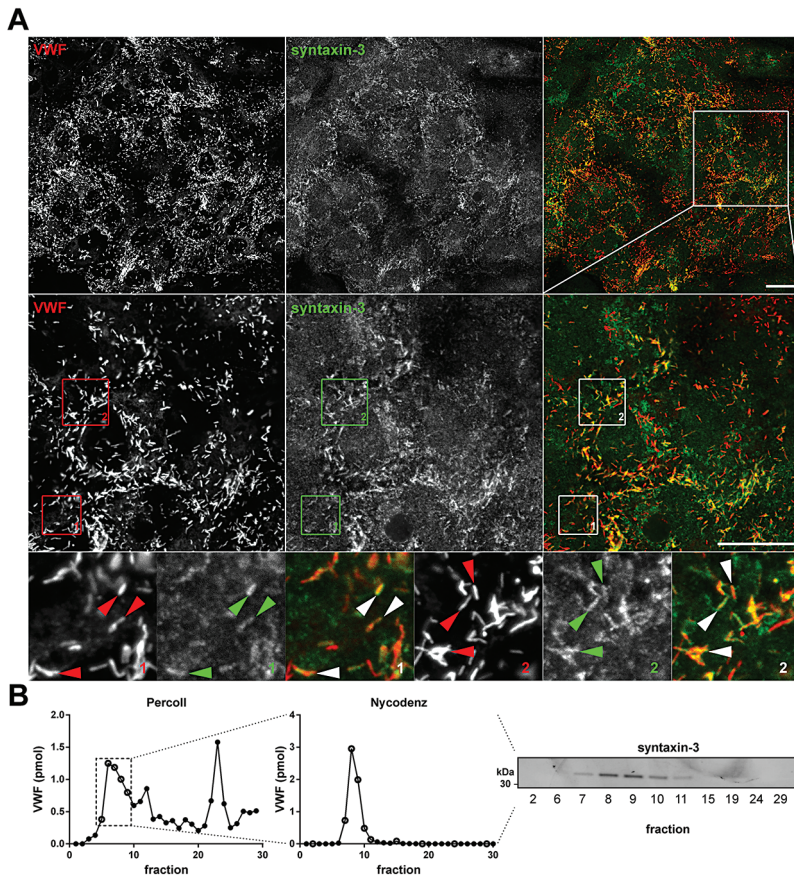
## Results

### The SNARE-protein syntaxin-3 is found on WPBs

In an unbiased proteomic pull down screen for endothelial Slp4-a interaction partners, we have previously identified STXBP1, together with syntaxin-2 and syntaxin-3.<sup>12</sup> Here we determined the intracellular localization of syntaxin-3 in endothelial cells by immunocytochemistry. Endogenous syntaxin-3 immunoreactivity was primarily associated with WPBs in HUVECs (Figure 1A). In an earlier report Fu and colleagues looked at the cellular distribution of syntaxin-3 in lung microvascular endothelial cells and found that this protein was found primarily at cell-cell contacts and some intracellular punctate structures, but it remained inconclusive whether these represented WPBs.<sup>11</sup> To further test the WPB localization of syntaxin-3 we undertook subcellular fractionation of HUVECs using density gradient ultracentrifugation.<sup>17,18</sup> Consistent with localization on the WPB, syntaxin-3 immunoreactivity co-sedimented with VWF in WPB containing subcellular fractions (Figure 1B). This was further confirmed by expression of mEGFP-tagged or myc-tagged syntaxin-3 (Supplemental Figure I & II), which labels WPBs, although interestingly at ectopic expression a significant proportion was also found on the plasma membrane. Possibly, at normal expression levels, syntaxin-3 is targeted to the WPBs, but at expression levels higher than normal, such as achieved by overexpression of epitope-tagged STX3, this SNARE can also be targeted to alternative locations.

### Ex vivo MVID blood outgrowth endothelial cells are an endothelial deficiency model for syntaxin-3

To assess the function of syntaxin-3 we established an *ex vivo* patient-derived model of syntaxin-3 deficiency using blood outgrowth endothelial cells (BOECs) from an MVID patient with a loss-of-function mutation in *STX3*. MVID is a rare but severe congenital gastrointestinal disorder that manifests itself by chronic diarrhea, malabsorption, metabolic acidosis and severe dehydration. The abnormal morphology of the enterocytes, which involves microvillus atrophy, intracellular microvillus inclusion bodies and loss of intestinal epithelial cell polarity, is caused by defective membrane trafficking events as a result of genetic defects in (primarily) *MYO5B* and *STXBP2*.<sup>31,32</sup> Recently, two atypical MVID patients have been described with homozygous loss-of-function mutations in *STX3* (Figure 2A).<sup>16</sup> Both patients and several heterozygous, non-affected family members participated in our study. Table 1



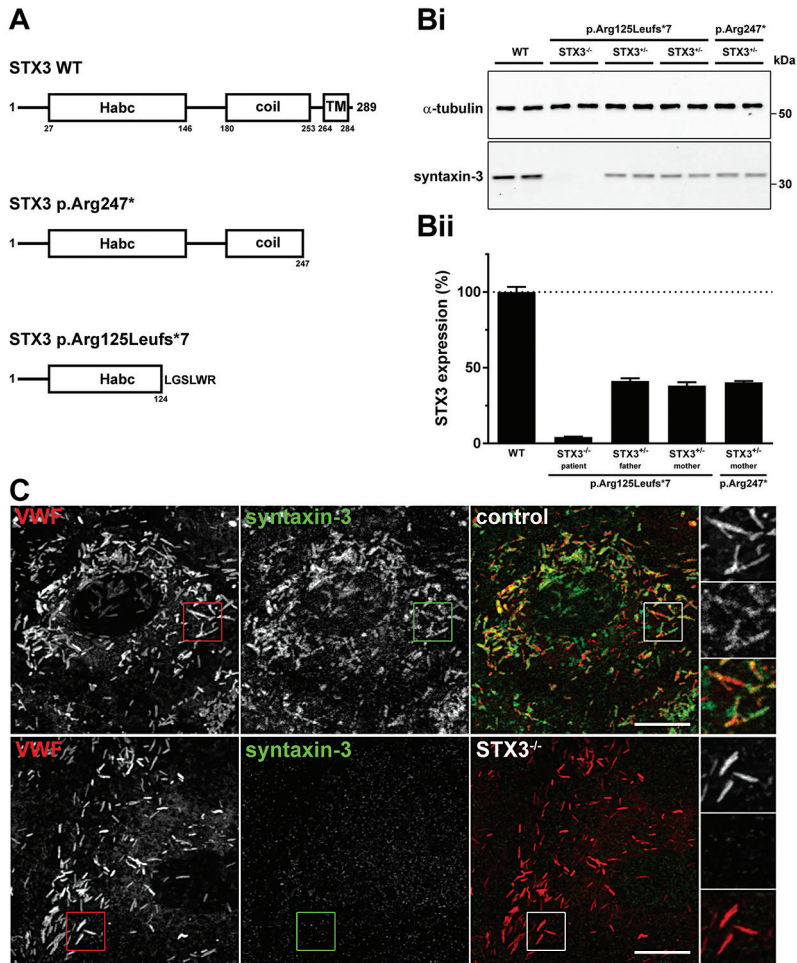
**Figure 1. Syntaxin-3 is a WPB-associated SNARE.** A) HUVECs were immunostained for endogenous VWF (red) and syntaxin-3 (green). Arrowheads indicate syntaxin-3 positive WPBs. Scale bar represents 20  $\mu\text{m}$ . B) Sub-cellular fractionation of HUVECs using density ultracentrifugation. Fractions were assayed for VWF by ELISA to identify WPB containing fractions. Syntaxin-3 presence was assayed using immunoblotting with anti-syntaxin-3 antibodies.

Table 1. Levels of circulating VWF measured in MVID patients and relatives

Subject	VWF:Ag (IU/ml)
Patient 1 ( <i>STX3</i> <sup>-/-</sup> : c.372_373dup, p.Arg125Leufs*7)	0.6
Mother of patient 1 ( <i>STX3</i> <sup>+/-</sup> )	2.2
Father of patient 1 ( <i>STX3</i> <sup>+/-</sup> )	1.1
Patient 2 ( <i>STX3</i> <sup>-/-</sup> : c.739C>T, p.Arg247*)	0.6
Mother of patient 2 ( <i>STX3</i> <sup>+/-</sup> )	1.1

shows the VWF:Ag levels in plasma, which are moderately lower in both patients.

Blood outgrowth endothelial cells were isolated from peripheral blood mononuclear cells, which was successful for all participants except patient 2. In BOECs from patient 1, who carries a homozygous frame-shifting 2-bp insertion leading to a premature stop (c.372\_373dup, p.Arg125Leufs\*7) in exon 6 of *STX3*, we were unable to detect syntaxin-3 in its full length or predicted truncated form. BOECs from both heterozygous parents and also the mother of patient 2, who has a heterozygous nonsense mutation leading to a premature stop (c.739C>T, p.Arg247\*) in exon 9 of *STX3*, contained approximately 50%



**Figure 2: BOECs from a 2-year old MVID patient with a homozygous *STX3* mutation are devoid of syntaxin-3.** A) Schematic representation of *STX3* domain structure and the predicted patient truncations. p.Arg247\* lacks the carboxyterminal transmembrane domain (TM), while p.Arg125Leufs\*7 lacks both the TM and the coil domain but includes a 6 residue de novo peptide (LGSLWR) at the carboxyterminus. Bi) Healthy control (WT), *STX3*<sup>-/-</sup> MVID and *STX3*<sup>-/-</sup> BOEC lysates were separated with SDS-PAGE and were immunoblotted for syntaxin-3; α-tubulin was used as a loading control. Bii) Quantification of syntaxin-3 expression in *STX3*<sup>-/-</sup> MVID and *STX3*<sup>-/-</sup> BOECs normalized to syntaxin-3 in healthy control BOECs (WT). C) Healthy control and *STX3*<sup>-/-</sup> MVID BOECs were immunostained for VWF (red) and syntaxin-3 (green). Arrowheads point to WPBs. Scale bar represents 10 μm.

reduced levels of syntaxin-3 (Figure 2B). This was further confirmed by mass spectrometry analysis of the whole proteome of MVID patient BOECs, which was compared to that of 4 healthy control BOECs (Supplemental Figure III). Interestingly, 5 out of 6 peptides that were found for syntaxin-3 in the healthy control BOECs mapped in the area before the truncation, however we were unable to accurately detect these in the MVID patient BOECs (not shown). Most probably, both mutations lead to depletion of syntaxin-3 due to either reduced protein stability<sup>16</sup> or nonsense mediated decay of the mutant transcripts. Consistent with the absence of syntaxin-3 expression, WPBs in BOECs from the MVID patients showed a loss of syntaxin-3 immunoreactivity, while the abundance, distribution and size of WPBs appeared unaltered (Figure 2C and Supplemental Figure IV & V). CRISPR/Cas9-engineered *STX3*<sup>-/-</sup> BOECs (Supplemental Figure VI) also showed loss of syntaxin-3

immunoreactivity but like in the patient BOECs this did not lead to altered morphology of the WPBs (Supplemental Figure VII).

### Syntaxin-3 deficiency does not perturb WPB formation or recruitment of key membrane components

SNAREs are key regulators of protein trafficking by facilitating membrane fusion between organelles or during exocytosis. As syntaxin-3, in contrast to syntaxin-4,<sup>11,33</sup> localizes to WPBs rather than the plasma membrane, we investigated whether syntaxin-3 functions in WPB formation and maturation. Throughout its life cycle the WPB can engage in several membrane fusion steps that contribute to biogenesis, (membrane) content acquisition or exocytosis.<sup>34</sup> Biogenesis of secretory organelles is generally thought to involve a number

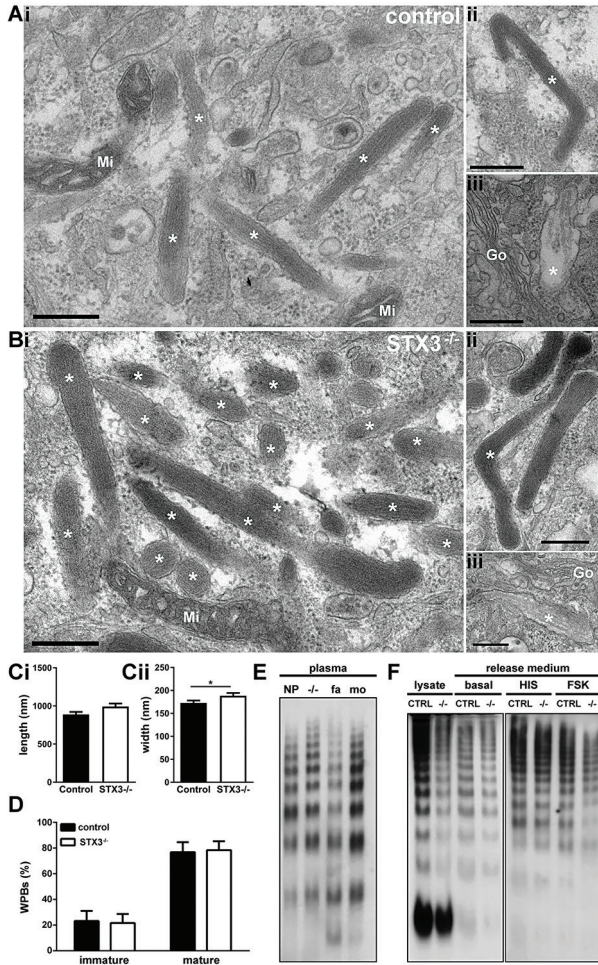


**Figure 3: Syntaxin-3 deficiency does not affect WPB maturation.** A–D) Healthy control BOECs (A) and *STX3*<sup>-/-</sup> BOECs (B) were cultured at full confluency for 4–5 days before fixation for EM stitches. A–B) Representative images taken from EM stitches showing grouped WPBs (i), hinged WPBs (ii) and immature WPBs (iii), indicated with asterisks. Mi = mitochondrium; Go = Golgi. Scale bars represent 400 nm. C–D) Images of single WPBs were taken from healthy control (n=104) and *STX3*<sup>-/-</sup> (n=110) EM stitch images. Length and width were measured (C) and WPB maturity was scored by 6 individuals. D) Statistical analysis was performed using a 2-tailed t-test on log-transformed values to approach normal distribution. Error bars represent SEM. \*P<0.05. E) Multimer analysis of VWF in plasma samples taken from a *STX3*<sup>-/-</sup> MVID patient (-/-) and his *STX3*<sup>-/-</sup> father (fa) and mother (mo) compared to pooled normal plasma (NP). F) Multimer analysis of VWF in lysates and release medium of healthy control (C) and *STX3*<sup>-/-</sup> BOECs (-/-). Release medium was taken after 24 hours without stimulation (basal) or after 30 minutes of stimulation with 100 mM histamine (HIS) or 10 mM forskolin + 100 mM IBMX (FSK).

of discrete steps: cargo condensation in the trans-Golgi network (1), budding of nascent / immature secretory granules from the trans-Golgi network (2), homotypic fusion of immature secretory granules (3) and removal of excess membrane (4).<sup>35</sup> To which extent this also applies to WPB biogenesis is still under debate, but there is evidence for the existence of immature WPBs as well as fusion of WPBs.<sup>36-38</sup> We carried out ultrastructural analysis of the morphology of large numbers of mature and immature WPBs using TEM stitches of control and *STX3*<sup>-/-</sup> BOECs. The numbers and morphometric characteristics of mature WPBs, characterized by intensely condensed cargo, were very similar in both WT and *STX3*<sup>-/-</sup> samples. When measured, no significant difference in WPB length (WT: 889 nm +/- 335 nm vs. *STX3*<sup>-/-</sup>: 991 nm +/- 414 nm) but a small, statistically significant difference in width (WT: 173 nm +/- 52 nm vs. *STX3*<sup>-/-</sup>: 188 nm +/- 61 nm) was observed (Figure 3A-D). Immature WPBs, characterized by one or a few discrete VWF tubules loosely surrounded by membrane (Figure 3Aiii, Biii), were also found in similar proportions in WT and *STX3*<sup>-/-</sup> samples (Figure 3D). WPBs containing hinges (e.g. Figure 3Aii, Bii) are thought to result from head-on fusion between WPBs.<sup>37</sup> Hinged WPBs were routinely observed in both WT and *STX3*<sup>-/-</sup> samples. We also observed normal VWF multimers in plasma from the MVID patient and his parents (Figure 3E & Supplemental Figure VIII), as well as stored in and secreted from cultured *STX3*<sup>-/-</sup> BOECs (Figure 3F).

To determine if syntaxin-3 plays a role in delivery of key membrane components to the WPB we first studied the localization of the tetraspanin CD63. The endosome-lysosome marker CD63 is thought to be delivered to WPBs through an AP-3- and annexin-8-dependent interaction/fusion with endosomal compartments.<sup>39-41</sup> Comparison of control and *STX3*<sup>-/-</sup> BOECs showed no obvious differences in CD63 localization (Figure 4). In both cases CD63 was found in abundance in WPBs and also in VWF-negative spherical organelles, most probably representing late endosomes, which in some cases were also syntaxin-3 positive (Figure 4). Localization of the WPB v-SNAREs, VAMP3 and VAMP8,<sup>33</sup> (Supplemental Figure IX) and the WPB membrane associated proteins P-selectin, Rab27A and Slp4-a (Supplemental Figure X-XI) were also unaffected in *STX3*<sup>-/-</sup> BOECs.<sup>3,7,42,43</sup> Taken together our data suggest that syntaxin-3 does not play a key role in the formation and maturation of WPBs and their content, nor in the recruitment of membrane components to the WPB.

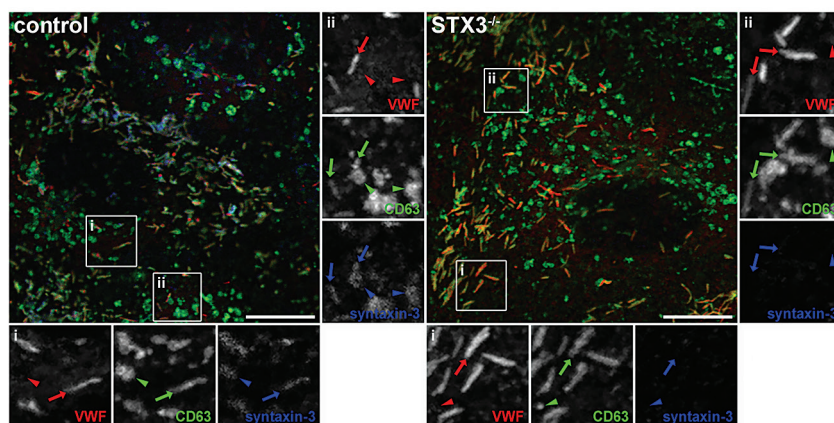


**Figure 4: WPB targeting of CD63 is not dependent on syntaxin-3.** Healthy control (control) and *STX3*<sup>-/-</sup> MVID (*STX3*<sup>-/-</sup>) BOECs were grown at full confluence for 5-7 days before fixation. Cells were immunostained with mouse IgG2b-CD63 (green), mouse IgG1 anti-VWF (red) and rabbit anti-syntaxin-3 (blue). Arrows indicate WPBs that are positive for CD63 and in the control cells also for syntaxin-3. Arrowheads indicate potential endosomes positive for CD63 and in the control cells also syntaxin-3. Scale bars are 10 μm.

## Ex vivo MVID endothelial cells deficient for syntaxin-3 have impaired basal and hormone-evoked WPB exocytosis

To investigate the role of syntaxin-3 in WPB exocytosis, we measured hormone-evoked VWF propeptide (VWFpp) release from *STX3*<sup>-/-</sup> BOECs. We chose to assay VWFpp because after release from the WPB, VWFpp has a lower retention to the cellular surface than VWF and is therefore a more direct measure of WPB degranulation.<sup>44,45</sup> Intracellular levels of VWFpp were comparable between *STX3*<sup>-/-</sup> BOECs and those from a healthy control donor (Figure 5A). However, *STX3*<sup>-/-</sup> BOECs showed a significantly reduced release of VWFpp in unstimulated conditions (Figure 5B). Also, *STX3*<sup>-/-</sup> BOECs showed a clear stimulus-induced secretion defect: upon stimulation with both Ca<sup>2+</sup>- (histamine) as well as cAMP-mediated (forskolin) secretagogues a significant decrease in VWFpp release was observed (Figure 5C) and this was augmented when lower concentrations of histamine were used (Figure 5D). Essentially similar results were obtained when assaying for secretion of mature VWF (Supplemental Figure XII)

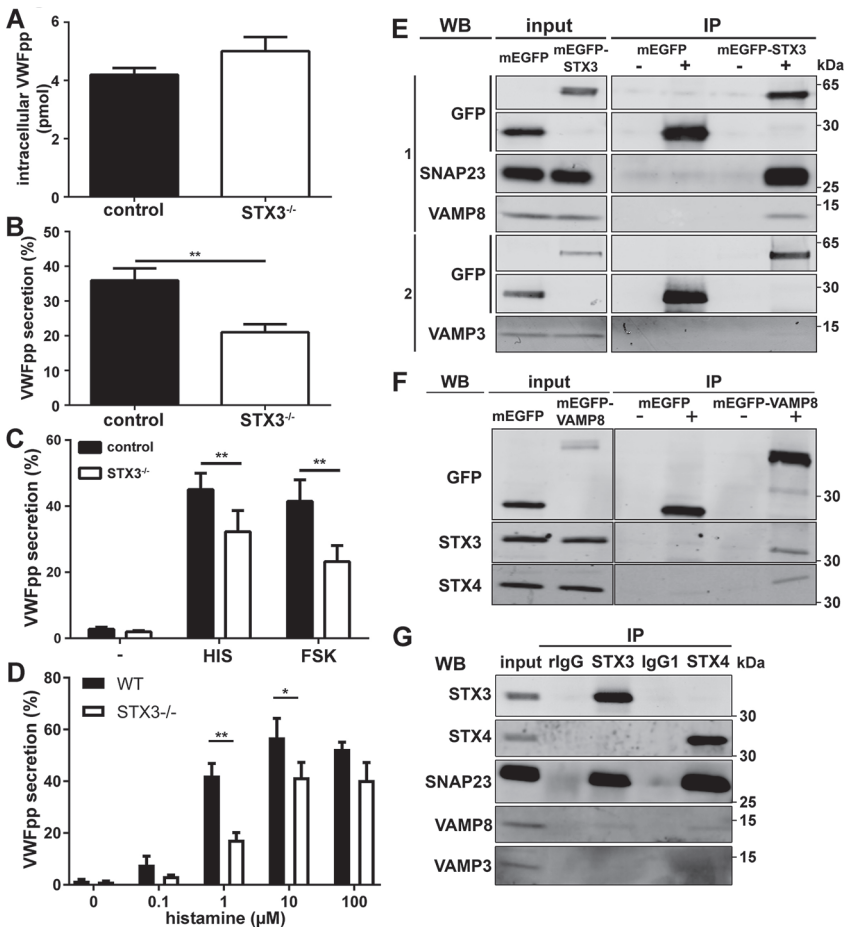


**Figure 5: VWFpp release is impaired in *STX3*<sup>-/-</sup> MVID BOECs.** A) Intracellular VWFpp levels in healthy control and *STX3*<sup>-/-</sup> MVID BOECs. (n=6) B) VWFpp levels in 24 hours conditioned medium from control and *STX3*<sup>-/-</sup> BOECs. (n=6) C) VWFpp release from control and *STX3*<sup>-/-</sup> BOECs after 30 minute stimulation with 100 mM histamine (HIS) or 10 mM forskolin + 100 mM IBMX (FSK). Release of VWFpp is expressed as percentage of intracellular VWFpp (n=6). D) Dose dependency of histamine-stimulated VWFpp release from control and *STX3*<sup>-/-</sup> BOECs (n=3). Statistical analyses were performed using paired 2-tailed t-tests (A–D). Error bars represent SEM. \*P<0.05 \*\*P<0.01. E–F) Lysates of endothelial cells expressing mEGFP, mEGFP-STX3 (E) or mEGFP-VAMP8 (F) were incubated with magnetic beads covalently coupled with anti-GFP nanobody (+) or control beads (-). G) HUVEC lysates were incubated with magnetic beads covalently coupled with rabbit anti-syntaxin-3 IgG or an equivalent amount of naive



In a recent report it was shown that unstimulated/basal as well as stimulus-induced VWF secretion are primarily directed towards the endothelial lumen while constitutive secretion of VWF is mostly directed to the basolateral side of the endothelium.<sup>25</sup> To test whether syntaxin-3 contributes to the polarity of VWF secretion we performed Transwell secretion assays. (Supplemental Figure XIII). Interestingly, while the decrease in stimulated secretion in MVID BOECs is on both sides, the decrease observed in unstimulated VWF secretion was almost entirely caused by a deficit on the apical side (Supplemental Figure XIII Bi-ii and Ci-ii). Proportionally, while both stimulus-induced and unstimulated VWF release are both released primarily in the apical direction, the polarity of unstimulated release is lost in MVID BOECs (Supplemental Figure XIII Biii-iv and Ciii-iv). This suggests that syntaxin-3 supports apically directed basal release of WPBs, which during strong activation such as upon 100  $\mu$ M histamine stimulation, can be partially compensated for, possibly by other SNARE complexes.

To study the mechanism by which syntaxin-3 can promote WPB exocytosis we looked for interactors that have been previously implicated in WPB exocytosis, such as the WPB associated v-SNAREs VAMP3 and -8 and the t-SNARE SNAP23.<sup>14,42</sup> Co-immunoprecipitation experiments using mEGFP-syntaxin-3 as bait showed that syntaxin-3 predominantly interacts with SNAP23 and VAMP8 and to a lesser extent with VAMP3 (Figure 5E). Similarly, reciprocal pull down using mEGFP-VAMP8 showed co-precipitation of syntaxin-3, but also syntaxin-4 (Figure 5F). This was further confirmed using precipitation of endogenous syntaxin-3 and syntaxin-4 from endothelial cells. VAMP8 and SNAP23 co-precipitated with both endogenous syntaxin-3 and syntaxin-4 (Figure 5G). However, we were unable to confirm endogenous VAMP3 interaction with either syntaxin-3 or syntaxin-4.

## Discussion

Circulating levels of VWF are determined by environmental as well as genetic factors, with the heritability of variation being estimated up to 75%.<sup>46-48</sup> In approximately 30% of cases low VWF is caused by mutations outside the *VWF* gene, implying that other genetic loci are involved in regulation of VWF levels.<sup>49</sup> Genome-wide association studies for genetic determinants of VWF levels have identified a number of new regulators that are suggested to affect secretory processes (*STXBP5* and *STX2*),<sup>13,50</sup> arguing that SNARE-mediated exocytosis of WPBs is a significant determinant of VWF levels. In this study we have characterized a new component of the WPB regulatory machinery, syntaxin-3, previously identified as a downstream target of the Rab27A – Slp4-a – STXBP1 complex.<sup>12</sup>

The main finding of our study is the identification of SNARE protein syntaxin-3 as a secretory granule localized regulator of WPB exocytosis. The SNARE fusion machinery underlies exocytosis in all secretory cells. Endothelial cells express several members of the SNARE complex, which includes a mixture of t-SNAREs; SNAP23, syntaxin-2, -3 and -4, and WPB-localized v-SNAREs; VAMP3 and VAMP8.<sup>11,12,14,33</sup> The SNARE complexes formed are in turn regulated by SNARE-associated proteins including STXBP1, STXBP3 and STXBP5.<sup>11-13</sup> However, the precise number and composition of SNARE complex(es) and their specific roles in controlling VWF secretion remains unclear. In the context of such a complex cocktail of SNAREs it can prove challenging to single out the contribution of an individual component, especially since residual levels of SNAREs that remain upon depletion using RNA interference have been reported to suffice for their function.<sup>51</sup> Therefore we took the opportunity to study the role of syntaxin-3 in a patient-derived endothelial model of complete syntaxin-3 deficiency using blood outgrowth endothelial cells from a MVID patient with mutations in *STX3*. Our results show that complete loss of syntaxin-3 leads to a significant attenuation of VWFpp and VWF secretion.

In syntaxin-3 deficient MVID patients circulating levels of VWF are at the low end of the normal range for the general population, although not associated with bleeding complications. Plasma levels of VWF are thought to be maintained by unstimulated VWF secre-

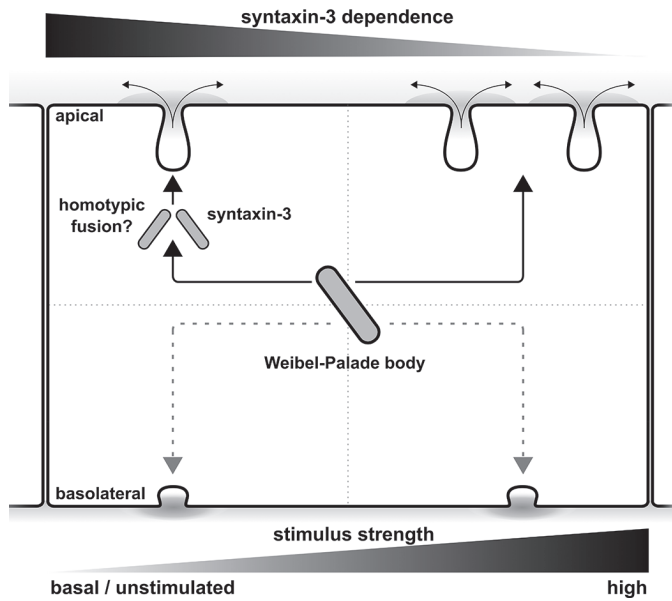


**Figure 6: Proposed model of syntaxin-3 function in WPB exocytosis.** Cartoon representation of a WPB undergoing polarized release as a function of stimulus intensity. Depending on the strength of stimulus, WPBs can undergo syntaxin-3 dependent and -independent release, both of which occur primarily at the apical face of endothelial cells (Supplemental Figure XIII). During conditions of low concentration secretagogue stimulus or during basal release WPBs utilize a syntaxin-3 dependent pathway, possibly by an exocytotic mode that involves homotypic fusion of WPBs through SNARE pairing of syntaxin-3 with v-SNARE VAMP8 at opposing WPBs (Figure 5E-G), which is primarily directed to the apical side of the endothelium. At elevated levels of endothelial activation the inhibition of (polarized) VWF secretion in the absence of syntaxin-3 is (partly) overcome (Figure 5 and Supplemental Figure XIII) due to the increasing contribution of syntaxin-3 independent pathways that are able to compensate for the loss of syntaxin-3.

tion by the endothelium, which arises primarily from basal release of WPBs.<sup>25,52</sup> In line with this, analysis of *STX3*<sup>-/-</sup> BOECs showed a small but statistically significant reduction in unstimulated VWF and VWFpp secretion (Figure 5B). There was also clear defect of stimulus-induced secretion in *STX3*<sup>-/-</sup> BOECs: we observed a significant reduction of VWFpp and VWF secretion upon challenging with Ca<sup>2+</sup>- or cAMP-mediated secretagogues. However, WPB release was not completely abolished which most likely reflects functional redundancy through syntaxin-3-independent SNARE complexes that are able to partially compensate for the loss of syntaxin-3. Because VWF secretion from the endothelium is such a critically important process, as illustrated by patients with type III Von Willebrand disease, a high degree of redundancy in the molecular regulation of VWF secretion may reflect an evolutionary drive to maintain this vital process. Indeed, of the SNARE-(associated) mediators of WPB release identified so far, the consequence of depletion of any one factor leads, in the majority of cases, to only a partial reduction of stimulated WPB release.<sup>7,11,12,14,33</sup> This may also explain why genetic disorders affecting a single component of the WPB exocytosis machinery are often not accompanied by significant hemostatic complications or why genetic variations such as identified in genome-wide association studies are associated with modest effects on VWF levels.<sup>53-55</sup> Employing several distinct SNARE complexes potentially also enables the endothelium to have greater control over its secretory response (e.g. release of different subsets of WPBs), support different modes of exocytosis or control release at specific sites. Attempts to experimentally rescue the secretory defect in *STX3* deficient BOECs using ectopically expressed *STX3* were unsuccessful and even attenuated

stimulated VWF release in both *STX3*<sup>-/-</sup> and control BOECs (data not shown), possibly due to mistargeting of a pool of epitope-tagged STX3 (Supplemental Figures I-II). Whether this was the result of the epitope-tag or the inability to experimentally control the ectopic expression levels remains unclear, but this may be further indication that the proper function of syntaxin-3 in WPB exocytosis depends on its localization on the secretory vesicle.

Microvillus inclusion disease is characterized by a failure of enterocytes, polarized intestinal epithelial cells, to target microvilli to their apical surface. This manifests as a loss of brush-border microvilli, basolateral targeting of microvilli and the formation of microvillus inclusion bodies. Syntaxin-3, which contains an N-terminal apical targeting motif, is normally found at the apical side where it supports delivery of apical membrane proteins involved in the formation of microvilli. Loss of syntaxin-3, such as in the MVID patient from whom we established *STX3*<sup>-/-</sup> BOECs, leads to a loss of polarity and mistargeting of apical cargo to the basolateral side where syntaxin-4 is found.<sup>16,56–58</sup> Endothelial cells also exhibit apical/basolateral polarity with the apical side facing the vessel lumen, while the basolateral side is connected to the subendothelial matrix. Recently, evidence has been presented that endothelial cells secrete high molecular weight VWF from a stored WPB pool predominantly at the apical side, where it is ideally positioned to support platelet adherence. In contrast, low molecular weight VWF is secreted constitutively at the basolateral side.<sup>25</sup> The mechanisms that dictate this preference for the apical side are still unknown, but our data suggest that syntaxin-3 supports apical release of WPBs.

Membrane fusion events in the regulated secretory pathway can be heterotypic (fusion between different compartments, i.e. WPB–plasma membrane) or homotypic (fusion of similar intracellular compartments, for example WPB–WPB). One previously described homotypic fusion mode is compound fusion, in which several WPBs fuse intracellularly prior to exocytosis. Upon compound fusion, enlarged, rounded structures are formed, termed “secretory pods”, that contain disordered VWF tubules.<sup>59,60</sup> A related but distinct mode of WPB fusion, termed sequential or cumulative exocytosis, has recently been reported.<sup>61,62</sup> In this mode a post-fusion WPB provides a membrane site for subsequent cumulative fusion of additional WPBs. The mechanisms underlying homotypic WPB fusion are not known, however, in mast and pancreatic acinar cells, cumulative fusion is the predominant form of exocytosis and has been studied more extensively. In both cell types syntaxin-3 is found on the secretory organelles.<sup>63,64</sup> In acinar cells, syntaxin-3 was found to pair with SNAP23 and VAMP8, the latter of which is also found on WPBs, while syntaxin-2 complexed with VAMP2 and SNAP23. During sequential exocytosis syntaxin-2 and syntaxin-3 containing SNARE machineries were found to support distinct steps: primary granules were released via syntaxin-2, while the subsequent secondary steps were dependent on syntaxin-3.<sup>65</sup> A similar mechanism was described in insulin granule exocytosis from pancreatic beta cells, where syntaxin-3 regulates exocytosis of a secondary, “newcomer” granule.<sup>66</sup> One difference between compound and cumulative fusion is the strength of stimulus required to set these pathways in motion: in eosinophils compound fusion becomes more prevalent in conditions of high stimulus while the incidence of cumulative fusion is increased at low levels of stimulus.<sup>67</sup> In that respect it is noteworthy that at lower concentration of histamine the loss of syntaxin-3 leads to a more prominent decrease in VWFpp secretion. (Figure 5D and Supplemental Figure XIID).

Taken together, our data identify syntaxin-3 as a novel WPB-localized regulator of VWF secretion which, depending on the degree of endothelial activation, takes a prominent role in WPB release at the apical side of endothelial cells. Based on its interactions with (WPB-localized) SNAREs that have been previously implicated in VWF secretion, we speculate that a homotypic fusion mode of WPBs is the underlying mechanisms by which syntaxin-3 facilitates exocytosis (Figure 6). Future studies should address whether assembly of *trans*-complexes of t-SNAREs and v-SNAREs on opposing WPBs contribute to homotypic fusion modes, such as compound or sequential/cumulative fusion.

### **Acknowledgements**

We would like to thank Martin de Boer and Karin van Leeuwen for assistance with NGS analysis of CRISPR clones.

### **Sources of Funding**

This study was supported by grants from the Center for Translational Molecular Medicine (INCOAG-01C-201-04), the Landsteiner Stichting voor Bloedtransfusie Research (LSBR-1244), Sanquin (PPOC-2015-24P) and the Dutch Thrombosis Foundation (TSN 56-2015 and 2017-01). TC is supported by an UK MRC grant MC\_PC\_13053. RB is supported by a European Hematology Association Research Fellowship.

### **Disclosures**

The authors report no conflicts of interest.

## References

1. Sadler JE. von Willebrand factor: two sides of a coin. *J Thromb Haemost.* 2005;3(8):1702-1709.
2. Rondaj MG, Bierings R, Kragt A, Van Mourik JA, Voorberg J. Dynamics and plasticity of Weibel-Palade bodies in endothelial cells. *Arterioscler Thromb Vasc Biol.* 2006;26(5):1002-1007.
3. Hannah MJ, Hume AN, Arribas M, et al. Weibel-Palade bodies recruit Rab27 by a content-driven, maturation-dependent mechanism that is independent of cell type. *J Cell Sci.* 2003;116(Pt 19):3939-3948.
4. Knop M, Aareskjold E, Bode G, Gerke V. Rab3D and annexin A2 play a role in regulated secretion of vWF, but not tPA, from endothelial cells. *EMBO J.* 2004;23(15):2982-2992.
5. Nightingale TD, Pattni K, Hume AN, Seabra MC, Cutler DF. Rab27a and MyRIP regulate the amount and multimeric state of VWF released from endothelial cells. *Blood.* 2009;113(20):5010-5018.
6. Rojo Pulido I, Nightingale TD, Darchen F, Seabra MC, Cutler DF, Gerke V. Myosin Va acts in concert with Rab27a and MyRIP to regulate acute von-Willebrand factor release from endothelial cells. *Traffic.* 2011;12(10):1371-1382.
7. Bierings R, Hellen N, Kiskin N, et al. The interplay between the Rab27A effectors Slp4-a and MyRIP controls hormone-evoked Weibel-Palade body exocytosis. *Blood.* 2012;120(13):2757-2767.
8. Zografou S, Basagiannis D, Papafotika A, et al. A complete Rab screening reveals novel insights in Weibel-Palade body exocytosis. *J Cell Sci.* 2012;125(Pt 20):4780-4790.
9. Conte IL, Hellen N, Bierings R, et al. Interaction between MyRIP and the actin cytoskeleton regulates Weibel-Palade body trafficking and exocytosis. *J Cell Sci.* 2016;129(3):592-603.
10. Matsushita K, Morrell CN, Cambien B, et al. Nitric oxide regulates exocytosis by S-nitrosylation of N-ethylmaleimide-sensitive factor. *Cell.* 2003;115(2):139-150.
11. Fu J, Naren AP, Gao X, Ahmed GU, Malik AB. Protease-activated receptor-1 activation of endothelial cells induces protein kinase Calpha-dependent phosphorylation of syntaxin 4 and Munc18c: role in signaling p-selectin expression. *J Biol Chem.* 2005;280(5):3178-3184.
12. van Breevoort D, Snijders AP, Hellen N, et al. STXBP1 promotes Weibel-Palade body exocytosis through its interaction with the Rab27A effector Slp4-a. *Blood.* 2014;123(20):3185-3194.
13. Zhu Q, Yamakuchi M, Ture S, et al. Syntaxin-binding protein STXBP5 inhibits endothelial exocytosis and promotes platelet secretion. *J Clin Invest.* 2014;124(10):4503-4516.
14. Zhu QM, Zhu Q, Yamakuchi M, Lowenstein CJ. SNAP23 Regulates Endothelial Exocytosis of von Willebrand Factor. *PLoS One.* 2015;10(8):e0118737.
15. Vizcaíno J, Deutsch EEW, Wang R, et al. ProteomeXchange provides globally coordinated proteomics data submission and dissemination. *Nat Biotech.* 2014;32(3):223-226.
16. Wiegierinck CL, Janecke AR, Schneeberger K, et al. Loss of syntaxin 3 causes variant microvillus inclusion disease. *Gastroenterology.* 2014;147(1):65-68.e10.
17. van Breevoort D, van Agtmaal EL, Dragt BS, et al. Proteomic screen identifies IGFBP7 as a novel component of endothelial cell-specific Weibel-Palade bodies. *J Proteome Res.* 2012;11(5):2925-2936.
18. Bierings R, van den Biggelaar M, Kragt A, Mertens K, Voorberg J, van Mourik JA. Efficiency of von Willebrand factor-mediated targeting of interleukin-8 into Weibel-Palade bodies. *J Thromb Haemost.* 2007;5(12):2512-2519.
19. Wisniewski JR, Zougman A, Nagaraj N, Mann M. Universal sample preparation method for proteome analysis. *Nat Meth.* 2009;6(5):359-362.
20. Rappsilber J, Ishihama Y, Mann M. Stop And Go Extraction tips for matrix-assisted laser desorption/ionization, nanoelectrospray, and LC/MS sample pretreatment in proteomics. *Anal Chem.* 2003;75(3):663-670.
21. Gazendam RP, van de Geer A, van Hamme JL, et al. Impaired killing of *Candida albicans* by granulocytes mobilized for transfusion purposes: A role for granule components. *Haematologica.* 2016;101(5):587-596.
22. Cox J, Mann M. MaxQuant enables high peptide identification rates, individualized p.p.b.-range mass accuracies and proteome-wide protein quantification. *Nat Biotechnol.* 2008;26(12):1367-1372.
23. Bateman A, Martin MJ, O'Donovan C, et al. UniProt: A hub for protein information. *Nucleic Acids Res.* 2015;43(D1):D204-D212.
24. Faas FGA, Avramut MC, van den Berg BM, Mommaas AM, Koster AJ, Ravelli RBG. Virtual nanoscopy: generation of ultra-large high resolution electron microscopy maps. *J Cell Biol.* 2012;198(3):457-469.
25. Lopes da Silva M, Cutler DF. von Willebrand factor multimerization and the polarity of secretory pathways in endothelial cells. *Blood.* 2016;128(2):277-285.
26. van Mourik JA, Boertjes R, Huisveld IA, et al. von Willebrand factor propeptide in vascular disorders: A tool to distinguish between acute and chronic endothelial cell perturbation. *Blood.* 1999;94(1):179-185.
27. van den Biggelaar M, Bierings R, Storm G, Voorberg J, Mertens K. Requirements for cellular co-trafficking of factor VIII and von Willebrand factor to Weibel-Palade bodies. *J Thromb Haemost.* 2007;5(11):2235-2242.

28. Paumet F, Le Mao J, Martin S, et al. Soluble NSF Attachment Protein Receptors (SNAREs) in RBL-2H3 Mast Cells: Functional Role of Syntaxin 4 in Exocytosis and Identification of a Vesicle-Associated Membrane Protein 8-Containing Secretory Compartment. *J Immunol.* 2000;164(11):5850-5857.
29. Knipe L, Meli A, Hewlett L, et al. A revised model for the secretion of tPA and cytokines from cultured endothelial cells. *Blood.* 2010;116(12):2183-2191.
30. Sanjana NE, Shalem O, Zhang F. Improved vectors and genome-wide libraries for CRISPR screening. *Nat Methods.* 2014;11(8):783-784.
31. Müller T, Hess MW, Schiefermeier N, et al. MYO5B mutations cause microvillus inclusion disease and disrupt epithelial cell polarity. *Nat Genet.* 2008;40(10):1163-1165.
32. Stepensky P, Bartram J, Barth TF, et al. Persistent defective membrane trafficking in epithelial cells of patients with familial hemophagocytic lymphohistiocytosis type 5 due to STXBP2/MUNC18-2 mutations. *Pediatr Blood Cancer.* 2013;60(7):1215-1222.
33. Pulido IR, Jahn R, Gerke V. VAMP3 is associated with endothelial Weibel-Palade bodies and participates in their Ca<sup>2+</sup>-dependent exocytosis. *Biochim Biophys Acta.* 2011;1813(5):1038-1044.
34. Valentijn KM, Sadler JE, Valentijn J a, Voorberg J, Eikenboom J. Functional architecture of Weibel-Palade bodies. *Blood.* 2011;117(19):5033-5043.
35. Tooze SA, Martens GJ, Huttner WB. Secretory granule biogenesis: rafting to the SNARE. *Trends Cell Biol.* 2001;11(3):116-122.
36. Zenner HL, Collinson LM, Michaux G, Cutler DF. High-pressure freezing provides insights into Weibel-Palade body biogenesis. *J Cell Sci.* 2007;120(Pt 12):2117-2125.
37. Valentijn KM, Valentijn JA, Jansen KA, Koster AJ. A new look at Weibel-Palade body structure in endothelial cells using electron tomography. *J Struct Biol.* 2008;161(3):447-458.
38. Ferraro F, Kriston-Vizi J, Metcalf DJ, et al. A two-tier Golgi-based control of organelle size underpins the functional plasticity of endothelial cells. *Dev Cell.* 2014;29(3):292-304.
39. Kobayashi T, Vischer UM, Rosnoblet C, et al. The tetraspanin CD63/lamp3 cycles between endocytic and secretory compartments in human endothelial cells. *Mol Biol Cell.* 2000;11(5):1829-1843.
40. Harrison-Lavoie KJ, Michaux G, Hewlett L, et al. P-selectin and CD63 use different mechanisms for delivery to Weibel-Palade bodies. *Traffic.* 2006;7(6):647-662.
41. Poeter M, Brandherm I, Rossaint J, et al. Annexin A8 controls leukocyte recruitment to activated endothelial cells via cell surface delivery of CD63. *Nat Commun.* 2014;5(3738):3738.
42. Pulido IR, Jahn R, Gerke V. VAMP3 is associated with endothelial Weibel-Palade bodies and participates in their Ca<sup>2+</sup>-dependent exocytosis. *Biochim Biophys Acta - Mol Cell Res.* 2011;1813(5):1038-1044.
43. McEver RP, Beckstead JH, Moore KL, Marshall-Carlson L, Bainton DF. GMP-140, a platelet alpha-granule membrane protein, is also synthesized by vascular endothelial cells and is localized in Weibel-Palade bodies. *J Clin Invest.* 1989;84(1):92-99.
44. Hannah MJ, Skehel P, Erent M, Knipe L, Ogden D, Carter T. Differential kinetics of cell surface loss of von Willebrand factor and its propolypeptide after secretion from Weibel-Palade bodies in living human endothelial cells. *J Biol Chem.* 2005;280(24):22827-22830.
45. Hewlett L, Zupančič G, Mashanov G, et al. Temperature-dependence of Weibel-Palade body exocytosis and cell surface dispersal of von Willebrand factor and its propolypeptide. *PLoS One.* 2011;6(11):e27314.
46. de Lange M, Snieder H, Ariëns RA, Spector TD, Grant PJ. The genetics of haemostasis: a twin study. *Lancet (London, England).* 2001;357(9250):101-105.
47. Bladbjerg EM, de Maat MPM, Christensen K, Bathum L, Jespersen J, Hjelmberg J. Genetic influence on thrombotic risk markers in the elderly—a Danish twin study. *J Thromb Haemost.* 2006;4(3):599-607.
48. Desch KC, Ozel AB, Siemieniak D, et al. Linkage analysis identifies a locus for plasma von Willebrand factor undetected by genome-wide association. *Proc Natl Acad Sci U S A.* 2013;110(2):588-593.
49. Leebeek FWG, Eikenboom JCJ. Von Willebrand's Disease. *N Engl J Med.* 2016;375(21):2067-2080.
50. Smith NL, Chen MH, Dehghan A, et al. Novel associations of multiple genetic loci with plasma levels of factor VII, factor VIII, and von willebrand factor: The charge (cohorts for heart and aging research in genome epidemiology) consortium. *Circulation.* 2010;121(12):1382-1392.
51. Bethani I, Werner A, Kadian C, Geumann U, Jahn R, Rizzoli SO. Endosomal fusion upon SNARE knockdown is maintained by residual SNARE activity and enhanced docking. *Traffic.* 2009;10(10):1543-1559.
52. Giblin JP, Hewlett LJ, Hannah MJ. Basal secretion of von Willebrand factor from human endothelial cells. *Blood.* 2008;112(4):957-964.
53. Van Gele M, Dynodot P, Lambert J. Griscelli syndrome: A model system to study vesicular trafficking. *Pigment Cell Melanoma Res.* 2009;22(3):268-282.
54. Stamberger H, Nikanorova M, Willemsen MH, et al. STXBP1 encephalopathy: A neurodevelopmental disorder including epilepsy. *Neurology.* 2016;86(10):954-962.
55. Smith NL, Rice KM, Bovill EG, et al. Genetic variation associated with plasma

- von Willebrand factor levels and the risk of incident venous thrombosis. *Blood*. 2011;117(22):6007-6011.
56. Sharma N, Low SH, Misra S, Pallavi B, Weimbs T. Apical targeting of syntaxin 3 is essential for epithelial cell polarity. *J Cell Biol*. 2006;173(6):937-948.
  57. Knowles BC, Weis VG, Yu S, et al. Rab11a regulates syntaxin 3 localization and microvillus assembly in enterocytes. *J Cell Sci*. 2015;128(8):1617-1626.
  58. Vogel GF, Klee KMC, Janecke AR, Müller T, Hess MW, Huber LA. Cargo-selective apical exocytosis in epithelial cells is conducted by Myo5B, Slp4a, Vamp7, and Syntaxin 3. *J Cell Biol*. 2015;211(3):587-604.
  59. Zupancic G, Ogden D, Magnus CJ, Wheeler-Jones C, Carter TD. Differential exocytosis from human endothelial cells evoked by high intracellular Ca(2+) concentration. *J Physiol*. 2002;544(Pt 3):741-755.
  60. Valentijn KM, van Driel LF, Mourik MJ, et al. Multigranular exocytosis of Weibel Palade bodies in vascular endothelial cells. *Blood*. 2010;116(10):1807-1816.
  61. Kiskin NI, Babich V, Knipe L, Hannah MJ, Carter T. Differential cargo mobilisation within Weibel-Palade bodies after transient fusion with the plasma membrane. *PLoS One*. 2014;9(9):e108093.
  62. Stevenson NL, White JJ, McCormack JJ, Robinson C, Cutler DF, Nightingale TD. Clathrin-mediated post-fusion membrane retrieval influences the exocytic mode of endothelial Weibel-Palade bodies. *J Cell Sci*. 2017;130(15):2591-2605.
  63. Gaisano HY, Ghai M, Malkus PN, et al. Distinct cellular locations of the syntaxin family of proteins in rat pancreatic acinar cells. *Mol Biol Cell*. 1996;7(12):2019-2027.
  64. Brochetta C, Suzuki R, Vita F, et al. Munc18-2 and syntaxin 3 control distinct essential steps in mast cell degranulation. *J Immunol*. 2014;192(1):41-51.
  65. Behrendorff N, Dolai S, Hong W, Gaisano HY, Thorn P. Vesicle-associated membrane protein 8 (VAMP8) is a SNARE (soluble N-ethylmaleimide-sensitive factor attachment protein receptor) selectively required for sequential granule-to-granule fusion. *J Biol Chem*. 2011;286(34):29627-29634.
  66. Zhu D, Koo E, Kwan E, et al. Syntaxin-3 regulates newcomer insulin granule exocytosis and compound fusion in pancreatic beta cells. *Diabetologia*. 2013;56(2):359-369.
  67. Hafez I, Stolpe A, Lindau M. Compound Exocytosis and Cumulative Fusion in Eosinophils. *J Biol Chem*. 2003;278(45):44921-44928.

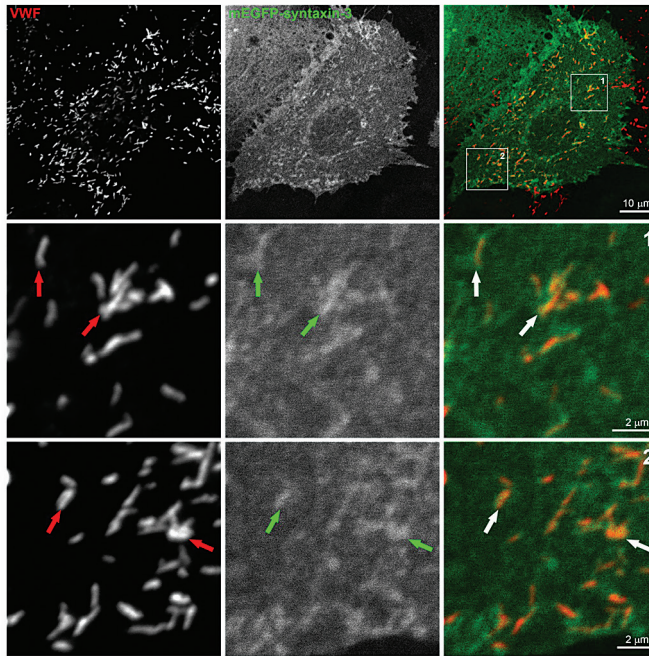
## Supplemental Figures and Tables

Supplemental Table I: Antibody reagents

Target	Species (isotype)	Label	Supplier	Cat.nr / clone	Use [concentration/dilution]
VWF	mouse (IgG <sub>2b</sub> )	-	described in <sup>1</sup>	CLB-RAg20	IF [1:1000]
syntaxin-3	rabbit	-	Synaptic Systems	110033	IF, WB [2 µg/ml]
α-tubulin	mouse (IgG <sub>1</sub> )	-	Sigma-Aldrich	T9026	WB [1:1000]
VWF	rabbit	-	DAKO	A0082	ELISA [6 µg/ml]
VWF	rabbit	HRP	DAKO	A0082	ELISA [2 µg/ml]
VWFpp	mouse	-	described in <sup>2</sup>	CLB-pro35	ELISA [1:2500]
VWFpp	mouse	HRP	described in <sup>2</sup>	CLB-pro14-3	ELISA [1:2500]
GFP	rabbit		GeneTex	GTX113617	WB [0.5 µg/ml]
Slp4-a	mouse (IgG <sub>1</sub> )		Santa Cruz	sc-374544	IF [1 µg/ml]
CD63	mouse (IgG <sub>1</sub> )	AF488	Sanquin	CLB-gran/12	IF [0.4 µg/ml]
CD62P	mouse (IgG <sub>1</sub> )	AF488	AbD Serotec	MCA796	IF [2 µg/ml]
Rab27A	rabbit		described in <sup>3</sup>		IF [1:100]
VAMP3	rabbit		Synaptic Systems	104203	WB [1 µg/ml], IF [2 µg/ml]
VAMP8	rabbit		Synaptic Systems	104303	WB, IF [1 µg/ml]
syntaxin-4	Mouse (IgG <sub>1</sub> )		BD Biosciences	610439	WB [0.25 µg/ml]
SNAP23	rabbit		Synaptic Systems	111203	WB [1 µg/ml]
VE-cadherin	Goat		Santa Cruz	sc-6458	IF [0.4 µg/ml]
F-actin	(Phalloidin)	AF670	Tebu-Bio	PHDN1-A	IF [28 nM]
c-myc	Mouse (IgG <sub>1</sub> )		Invitrogen	13-2500	IF [2.5 µg/ml]
rabbit IgG	donkey	680LT	Li-Cor	925-68023	WB [0.1 µg/ml]
mouse IgG	donkey	680LT	Li-Cor	925-68022	WB [0.1 µg/ml]
rabbit IgG	donkey	800CW	Li-Cor	925-32213	WB [0.1 µg/ml]
mouse IgG	donkey	800CW	Li-Cor	925-32212	WB [0.1 µg/ml]
rabbit IgG	goat	AF405	ThermoFisher	A31556	IF [2 µg/ml]
rabbit IgG	chicken	AF488	ThermoFisher	A21441	IF [2 µg/ml]
rabbit IgG	goat	AF568	ThermoFisher	A11011	IF [2 µg/ml]
rabbit IgG	chicken	AF647	ThermoFisher	A21443	IF [2 µg/ml]
mouse IgG	chicken	AF488	ThermoFisher	A21200	IF [2 µg/ml]
mouse IgG	goat	AF568	ThermoFisher	A11004	IF [2 µg/ml]
mouse IgG	chicken	AF647	ThermoFisher	A21463	IF [2 µg/ml]
goat IgG	donkey	AF488	ThermoFisher	A11055	IF [2 µg/ml]
goat IgG	donkey	AF568	ThermoFisher	A11057	IF [2 µg/ml]
goat IgG	chicken	AF647	ThermoFisher	A21469	IF [2 µg/ml]

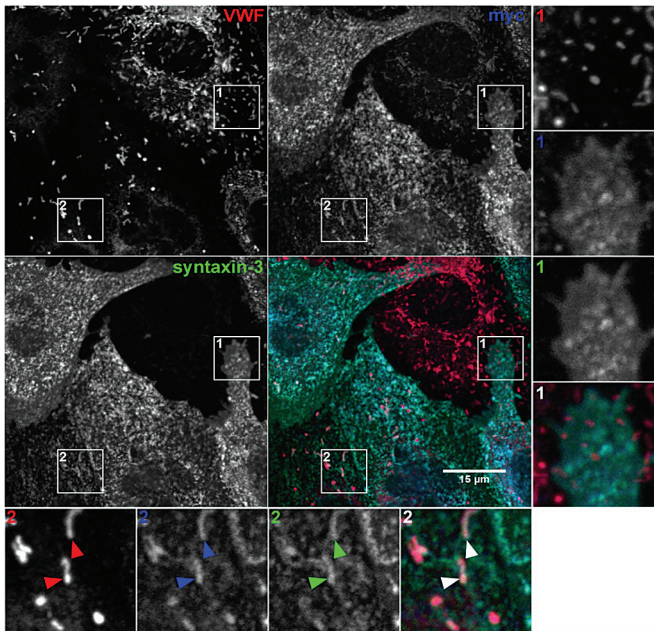


## Supplemental Figure I



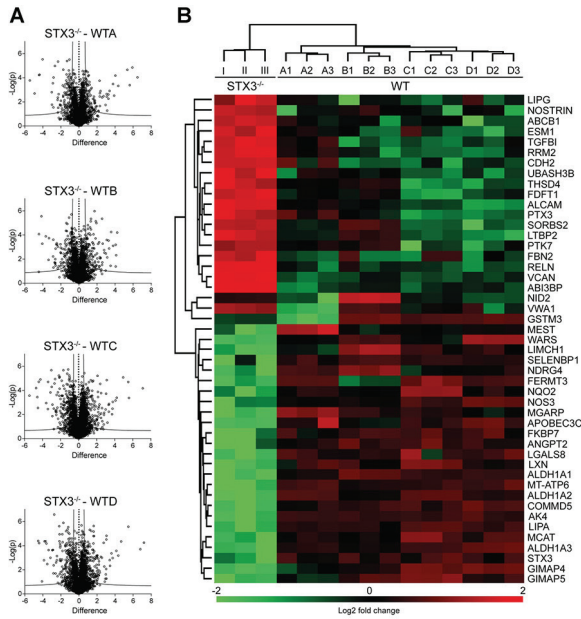
**Supplemental Figure I: mEGFP-syntxin-3 labels WPBs and plasma membrane.** 48 hours after Nucleofection with mEGFP-syntxin-3 (green) HUVECs were fixed and immunostained for VWF (red). Boxed areas in the top panels are magnified below. Arrows indicate syntxin-3 positive WPBs.

## Supplemental Figure II



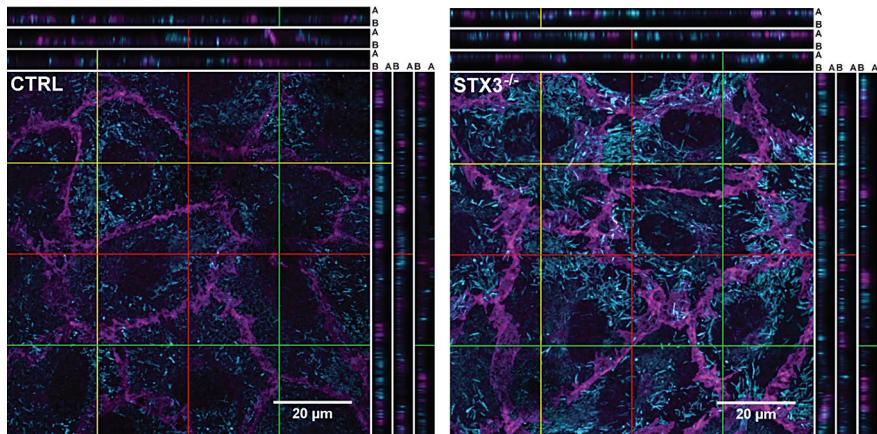
**Supplemental Figure II: myc-STX3 labels WPBs and plasma membrane.** 5 days after transduction with myc-syntxin-3 BOECs were fixed and immunostained for VWF (red), syntxin-3 (green) and myc (blue). Boxed areas in the panels are shown as magnifications, displaying membranous (1) and WPB (2) localization of myc-STX3. Arrowheads indicate syntxin-3 positive WPBs.

### Supplemental Figure III



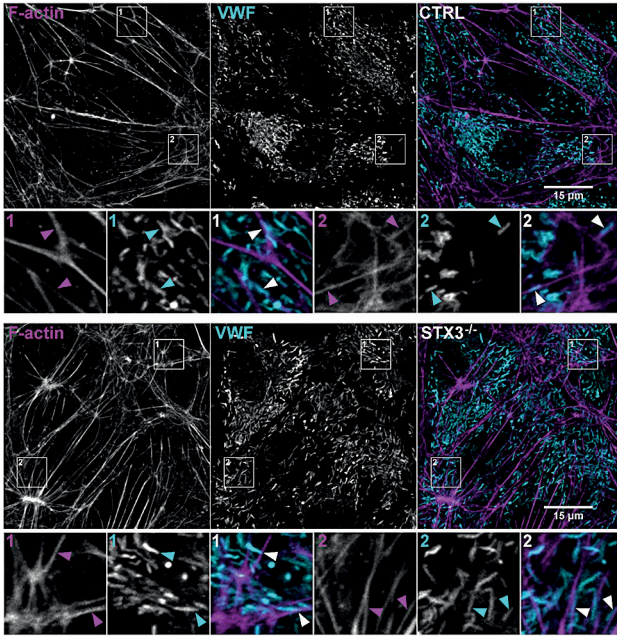
**Supplemental Figure III: BOECs from a 2-year old MVID patient with a homozygous STX3 mutation are devoid of syntaxin-3.** A) Differentially expressed proteins between the STX3<sup>-/-</sup> BOECs and 4 healthy control BOECs are shown in four separate volcano plots. N=3 per patient/healthy control, FDR = 0.05 and S0 = 0.4. (B) Heat map and hierarchical clustering (based on average Euclidean distance and pre-processed with k-means) of proteins with significantly changed levels (defined as significantly changed expression in all four volcano plots of the STX3<sup>-/-</sup> BOECs and healthy control BOECs). Proteins are indicated by gene names. Heat map colors (see legend) are based on the z-scored label free quantification data (log2).

### Supplemental Figure IV



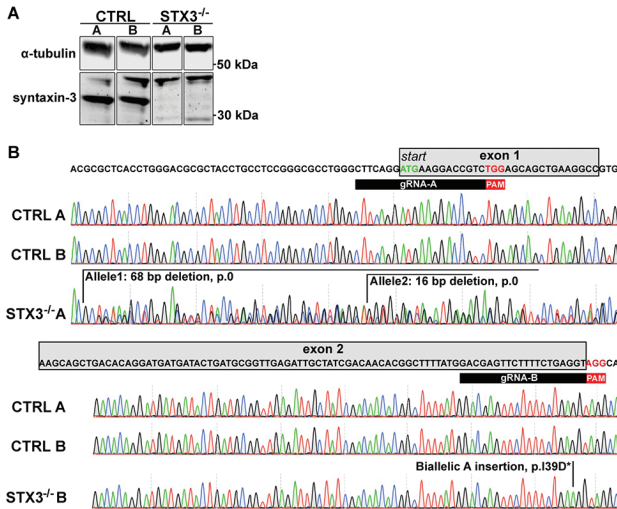
**Supplemental Figure IV: Weibel-Palade body distribution is similar in control and syntaxin-3 deficient cells.** Control and syntaxin-3 deficient MVID BOEC were culture at confluency for 4-5 days, fixed and immunostained for VWF (cyan) and VE-cadherin (magenta). Shown are single XY plane and orthogonal XZ and YZ projections with apical (A) and basolateral (B) directions indicated

Supplemental Figure V



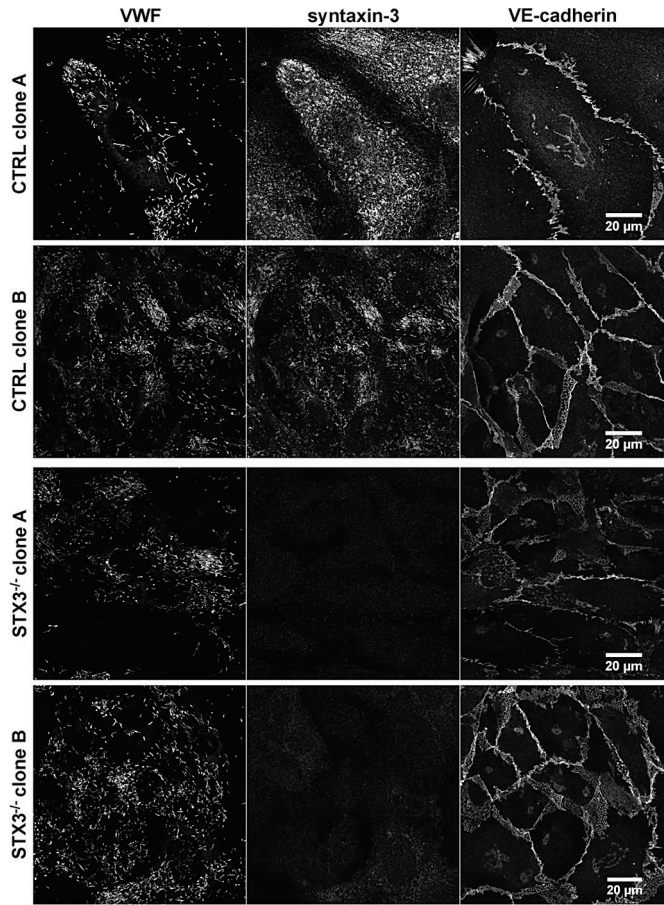
**Supplemental Figure V: WPB distribution relative to actin cytoskeleton is unaffected by syntaxin-3 deficiency.** Control and syntaxin-3 deficient MVID BOECs were cultured at confluency for 4-5 days, fixed and stained for filamentous actin (magenta) and VWF (cyan). Arrow heads indicate WPBs in contact with F-actin.

Supplemental Figure VI



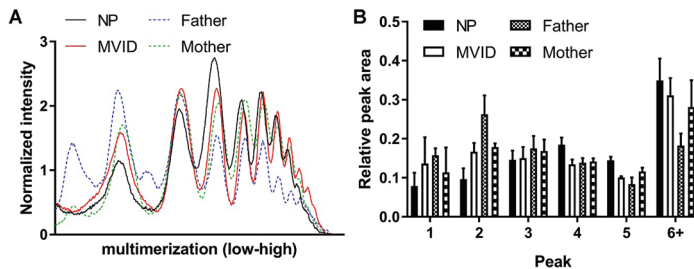
**Supplemental Figure VI: CRISPR/Cas9-engineered STX3<sup>-/-</sup> BOECs.** A) Syntaxin-3 immunoblot showing syntaxin-3 expression in 2 selected control clones and lack of syntaxin-3 expression in 2 selected STX3<sup>-/-</sup> CRISPR clones obtained by targeting exon 1 (STX3<sup>-/-</sup> A) or exon 2 (STX3<sup>-/-</sup> B). α-tubulin is shown as a loading control. B) DNA sequence analysis of the same clones, showing CRISPR events in exon 1 and 2 at the expected sites for double strand break close to the protospacer adjacent motif (PAM) site of the respective gRNA target sites. Predicted null mutations based on Sanger and Next Generation Sequencing of the clones are indicated in the chromatograms.

## Supplemental Figure VII



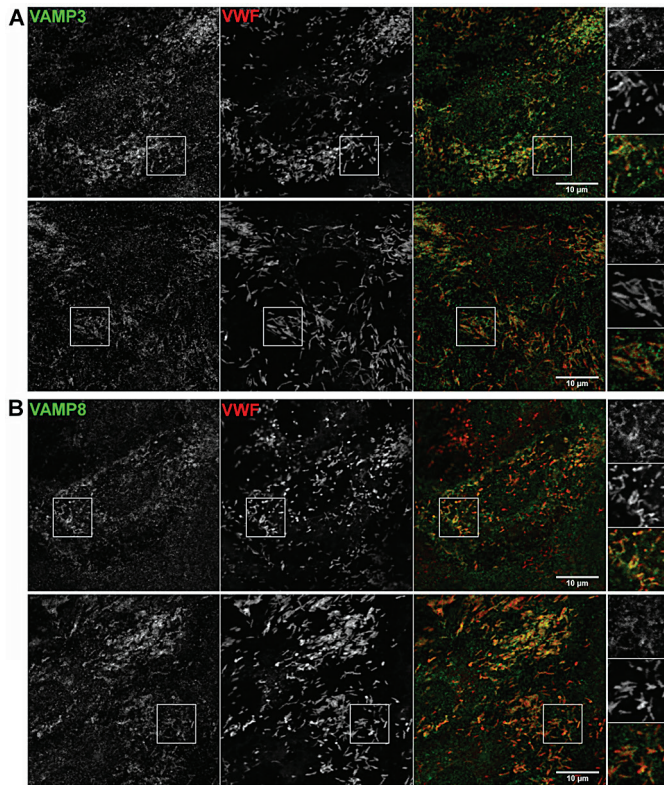
**Supplemental Figure VII: Morphological analysis of CRISPR-engineered *STX3*<sup>-/-</sup> BOECs.** Control and CRISPR *STX3*<sup>-/-</sup> BOEC clones were cultured at confluency for 4–5 days, fixed and immunostained for VWF, syntaxin-3 and VE-cadherin.

## Supplemental Figure VIII



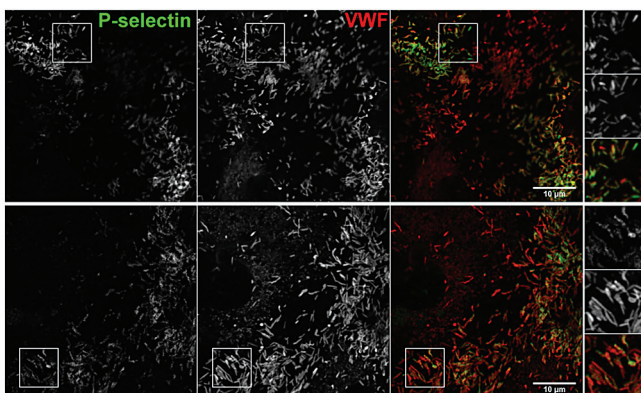
**Supplemental Figure VIII: Densitometry analysis of patient and parent plasma does not show a defect in VWF multimerization.** A) Representative graph of the densitometry of a VWF multimer blot (see Figure 3E in main text) of plasma from patient and both heterozygous parents compared to normal plasma (NP). Signal intensity was normalized to the mean intensity of each sample. B) Analysis of the areas under the curve for peak 1 to 5, representing the lower multimers, and peaks 6+, representing the higher multimers. Values are normalized to the total area under the curve. Error bars represent SEM, N=3.

## Supplemental Figure IX



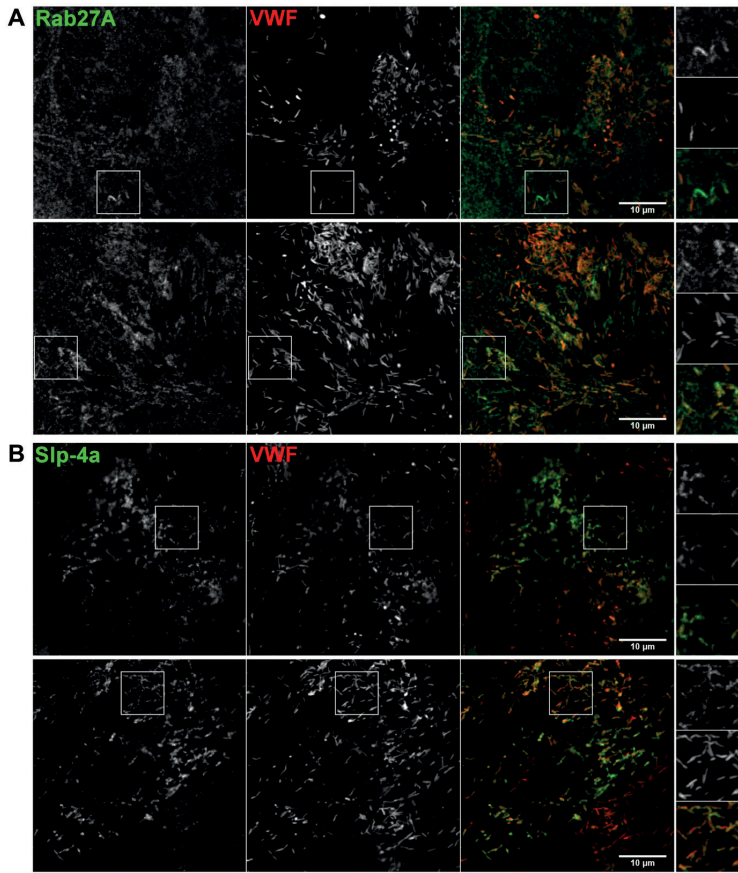
**Supplemental Figure IX: WPB targeting of VAMP3 and VAMP8 is not affected by syntaxin-3 deficiency.** Healthy control (top panels) and *STX3*<sup>-/-</sup> MVID BOECs (bottom panels) were fixed after 5–7 days of confluence and immunostained for VWF (red) and WPB associated SNARE proteins VAMP3 (A) or VAMP8 (B) (green).

## Supplemental Figure X



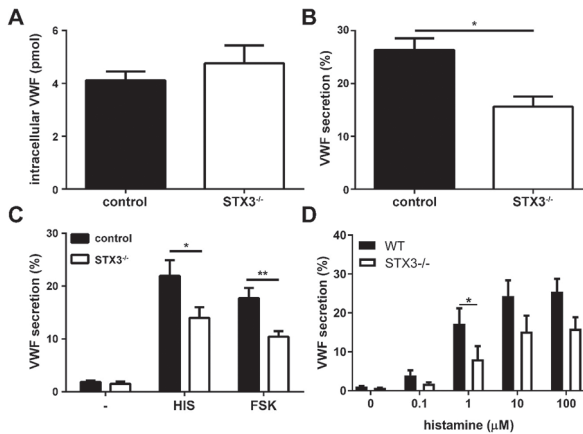
**Supplemental Figure X: WPB targeting of P-selectin is not affected by syntaxin-3 deficiency.** Healthy control (top panels) and *STX3*<sup>-/-</sup> MVID BOECs (bottom panels) were fixed after 5–7 days of confluence and immunostained for VWF (red) and P-selectin (green).

## Supplemental Figure XI



**Supplemental Figure XI: WPB targeting of Rab27A and Slp4-a is not affected by syntaxin-3 deficiency.** Healthy control (top panels) and *STX3*<sup>-/-</sup> MVID BOECs (bottom panels) were fixed after 5–7 days of confluence and immunostained for VWF (red) and Rab27A (A) or Slp4-a (B) (green).

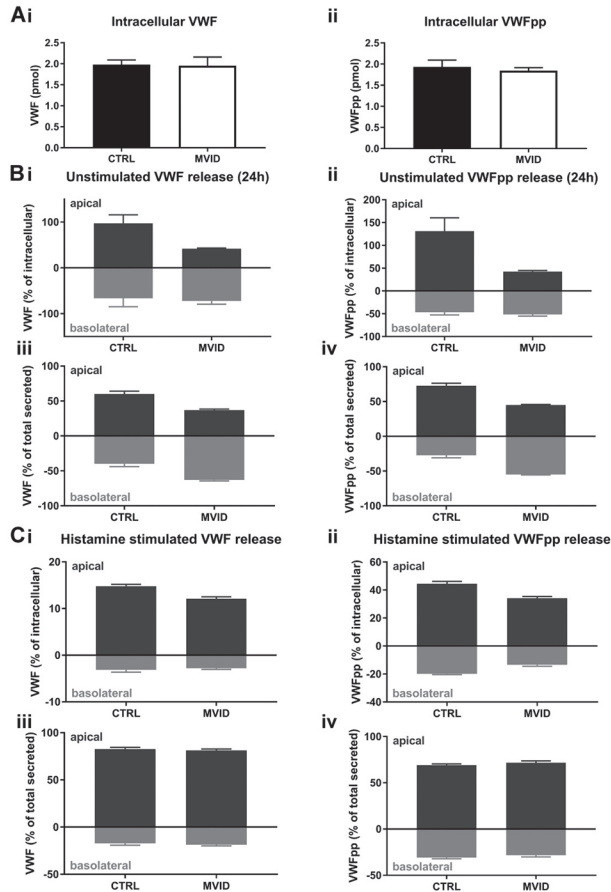
## Supplemental Figure XII



**Supplemental Figure XII: VWF release is impaired in *STX3*<sup>-/-</sup> MVID BOECs.** A) Intracellular VWF levels in healthy control and *STX3*<sup>-/-</sup> MVID BOECs. (n=6) B) VWF levels in 24 hours conditioned medium from control and *STX3*<sup>-/-</sup> BOECs. (n=6) C) VWF release from control and *STX3*<sup>-/-</sup> BOECs after 30 minute stimulation with 100 mM histamine (HIS) or 10 mM forskolin + 100 mM IBMX (FSK). Release of VWF is expressed as percentage of

intracellular VWF (n=6). D) Dose dependency of histamine-stimulated VWF release from control and *STX3*<sup>-/-</sup> BOECs (n=3). Statistical analyses were performed using paired 2-tailed t-tests (A-D). \*P<0.05 \*\*P<0.01. Error bars represent SEM.

### Supplemental Figure XIII



**Supplemental Figure XIII: Syntaxin-3 deficiency affects polarity of release.** Control and syntaxin-3 deficient MVID BOECs were cultured at confluency for 4–5 days on 0.4  $\mu$ m pore size Transwell inserts. A) Lysates were made to measure intracellular VWF. B–C) Release medium was collected from the top (apical) and bottom (basolateral) Transwell compartments from unstimulated (B) and histamine (100  $\mu$ M) stimulated (C) cells. Release of VWF/VWFpp is expressed as percentage of intracellular VWF/VWFpp (Bi-ii and Ci-ii) or as a percentage of total (apical+basolateral) secretion (Biii-iv and Ciii-iv). Secretion assays were performed in triplicate. Error bars represent SEM.

## Supplemental References

1. van Agtmaal EL, Bierings R, Dragt BS, Leyen T a, Fernandez-Borja M, Horrevoets AJG, Voorberg J. The shear stress-induced transcription factor KLF2 affects dynamics and angiotensin-2 content of Weibel-Palade bodies. *PLoS One*. 2012;7:e38399.
2. Borchiellini A, Fijnvandraat K, ten Cate JW, Pajkrt D, van Deventer SJ, Pasterkamp G, Meijer-Huizinga F, Zwart-Huinink L, Voorberg J, van Mourik JA. Quantitative analysis of von Willebrand factor propeptide release in vivo: effect of experimental endotoxemia and administration of 1-deamino-8-D-arginine vasopressin in humans. *Blood*. 1996;88:2951-2958.
3. Bierings R, Hellen N, Kiskin N, Knipe L, Fonseca A-V, Patel B, Meli A, Rose M, Hannah MJ, Carter T. The interplay between the Rab27A effectors Slp4-a and MyRIP controls hormone-evoked Weibel-Palade body exocytosis. *Blood*. 2012;120:2757-2767.





# Chapter 8

## General discussion

Ellie Karampini

## Endothelial cells as a model for lysosome-related organelle biogenesis

Lysosome-related organelles (LROs) consist of a heterogeneous group of intracellular organelles that share features with lysosomes.<sup>1</sup> LROs can be found in many different cell types, where they function as a (temporary) storage compartment for cell specific cargo. In most, if not all cases their content is then released into the extracellular lumen or delivered to the plasma membrane.<sup>1</sup> LRO's biogenesis falls into shared pathways between cell types, that include an endosomal or trans-Golgi network (TGN) origin and a complex maturation process, where the forming LRO acquires more endosomal protein content.<sup>1</sup> So far the melanosomes, which are pigment granules found in melanocytes and retina pigment epithelial cells and which store and traffic melanin,<sup>2,3</sup> are probably the best studied examples of the LRO family. Since melanocyte isolation and experimental manipulation is relatively straightforward and melanosome biogenesis can be monitored *in vitro* by light and electron microscopy,<sup>3-5</sup> melanosomes have been extensively used as a model system for LRO formation and their findings have often been extrapolated to other cell types. However, similar advantages also apply to endothelial cells and Weibel Palade bodies (WPBs), making these a powerful new model system to study the biogenesis of hemostatic LROs. In view of the similarities in contents and regulation of release studies on WPBs may be particularly relevant for the functionally closely related platelet LROs such as  $\alpha$ - and  $\delta$ -granules.

WPBs are the LRO of ECs that primarily store von Willebrand factor (VWF). WPB biogenesis starts at the TGN, where VWF tubules are tightly packaged in the forming from the TGN membrane organelle, followed by an adaptor-protein complex 3 (AP-3) dependent cargo delivery from the endosomes and acquisition of exocytotic machinery.<sup>1,6</sup> WPB formation relies upon several check points, including ER-to-Golgi VWF trafficking (**chapter 3**), preserved Golgi morphology (**chapter 4**) and proper function of the AP-3 complex, correctly delivering proteins (**chapter 6**), so as the mature WPB can respond optimally to stimuli from its microenvironment (**chapter 6 and 7**). Since there is quite an overlap in the mechanisms between biogenesis of LROs, highlighted by multisystemic storage pool disorders, ECs can be a useful alternative model system in future hemostatic LRO research. In particular, blood outgrowth endothelial cells (BOECs), can be easily isolated from patients (**chapter 6 and 7**), as well as expand and maintain a stable culture *in vitro*.<sup>7</sup> These patient derived BOECs can provide an advantageous *ex vivo* disease model, that allows for studying the effects of patient mutations on the biogenesis and release of LROs. Additionally, ECs can be genetically modified by means of either short hairpin RNAs (shRNAs) in order to create knockdowns (**chapter 3 and 4**) or CRISPR/Cas9 gene editing and clonal selection in order to create knockout cell lines in primary cells (**chapter 3, 6 and 7**). This allows for the simultaneous screening of multiple genes and proteins, while it provides an additional outlet for data corroboration when patient material is scarce, as we showed in this thesis. Moreover, ECs can easily be reprogrammed into induced pluripotent stem cells (iPSCs), creating immortal cells that can subsequently differentiate in any desired cell type (Figure 1). This can provide for a platform where the role of mutated genes can be easily evaluated in different cells types in parallel, identifying similarities and differences in the cellular mechanisms of LRO formation. We have recently generated iPSCs from both wild type and HPS-2 BOECs that were described in Chapter 6 of this thesis. The generated iPSCs were successfully differentiated into megakaryocytes (see Figure 1). This approach allows for exploring the contribution of the AP3-complex (which is absent in HPS-2) in cargo delivery to LROs in megakaryocytes. Similarly, iPSC-derived megakaryocytes generated from other patient-derived or genetically CRISPR/Cas9 engineered BOECs could be used to study the biogenesis of LROs in megakaryocytes. For the aforementioned reasons, we propose that ECs provide a highly accessible and easily manipulated platform to further advance our knowledge on the mechanisms driving the biogenesis and release of LROs.

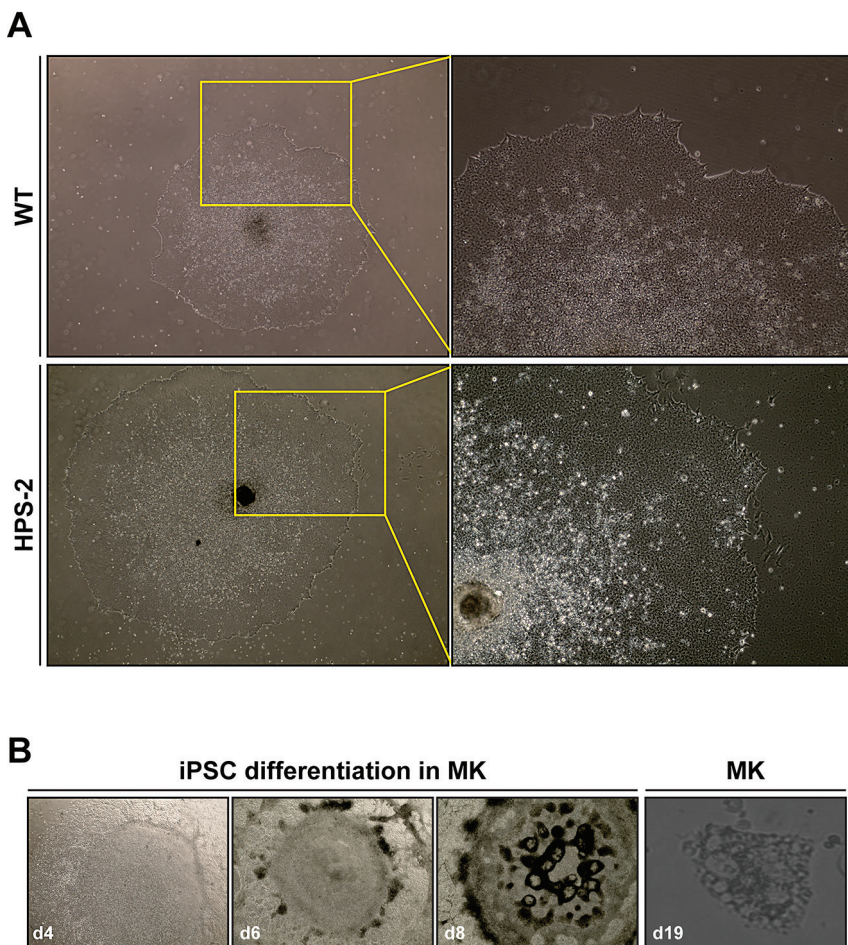


**Figure 1: Generation and differentiation of iPSCs from WT and HPS-2 BOECs.** A) iPSC generated from WT and HPS-2 BOECs from the patient described in chapter 6, boxed regions are magnified on the right side. B) iPSC differentiation in megakaryocytes (MK) after 4, 6 and 8 days of treatment and mature MK after 19 days.

## ER-to-Golgi protein influx is the first step in WPB and LRO formation

ER-to-Golgi trafficking is the initial point in the early secretory pathway.<sup>8</sup> Proteins that are properly produced and destined for the Golgi or beyond are packaged in the ER-into exiting ribosome-depleted COPII vesicles.<sup>8</sup> It has been shown that depletion of factors that comprise the COPII complex, negatively affects ER-to-Golgi transport and the biogenesis of secretory vesicles such as the zymogen granules.<sup>9,10</sup> However, only recently, the role of ER-to-Golgi trafficking has been appreciated as the first step in the biogenesis of LROs. Two independent studies have highlighted the importance of anterograde trafficking by looking into ER-to-Golgi vesicle trafficking regulators in megakaryotic cell lines and ECs.<sup>11,12</sup> In the first case, downregulation of RAB1B, due to RUNX1 haplodeficiency, negatively affects ER-to-Golgi protein transport, including VWF, that subsequently results in abnormal platelet granule formation and stimulated release.<sup>11,13,14</sup> In ECs, Lopes da Silva *et al.* showed that GBF1, a GEF for the anterograde vesicle formation regulator family (ADP-ribosylation factors (ARFs)), supports secretory protein transport, including VWF, which in turn controls WPB formation.<sup>12</sup> To further elucidated the molecular mechanisms involved in the

ER-to-Golgi, we looked into the SNARE proteins, which are known regulators of membrane fusion events between vesicles and target membranes (heterotypic fusion).<sup>8</sup> In **chapter 3** we targeted Sec22b, a SNARE protein that is incorporated on COP-II vesicles through a conformational epitope.<sup>15</sup> Silencing of Sec22b or expression of a non-fusogenic Sec22b construct in ECs altered the ER-to-Golgi VWF transport, along with other proteins, that gave rise to abnormally short WPBs. Interestingly, the ER dilated in order to accommodate the retained protein cargo in ribosome-studded ER vesicles that in most cases maintained their connections to the ER. This suggests that VWF follows a Sec22b/COPII dependent pathway when entering the early secretory pathway. Yet, how ECs regulate the rate of protein influx to the Golgi is still unknown.

An interesting role of intracellular signaling in response to environmental cues during ER-to-Golgi trafficking and how this affects the WPB formation, potentially also other LROs, has been demonstrated for GBF1.<sup>12</sup> GBF1 has multiple phosphorylation sites that, upon AMPK-dependent phosphorylation, regulate its activity in response to glucose levels and subsequently modulate WPB formation.<sup>12</sup> Of relevance, SNARE proteins also contain phosphorylation sites that regulate their activity through controlling SNARE complex formation.<sup>16,17</sup> Interestingly, it has been demonstrated that SNARE proteins of the secretory machinery, along with SNARE proteins and SNARE interacting proteins of anterograde, retrograde and intra-Golgi trafficking are phosphorylated during thrombin activation of ECs.<sup>18</sup> In this group of SNAREs, Sec22b was found to have two phosphorylation sites, with early increased phosphorylation levels, similar to its interacting partner (**chapter 4**) Vt1ba with a later response.<sup>18</sup> This suggests that environmental cues like ECs activation stimuli and perhaps also metabolic changes may affect the efficiency of ER-to-Golgi transport through phosphorylation-dependent modulation as consequence of SNARE complex formation and fusogenic activity.

## Maintenance of the Golgi architecture: effects on WPB biogenesis

After VWF has entered in the early secretory pathway as a dimer and transported at the Golgi, possibly by a Sec22b/STX5-dependent manner, it is further modified into mature VWF multimers.<sup>19</sup> Subsequently the multimers are condensed into VWF tubules that are tightly packaged into WPBs that emerge from the trans-Golgi network (TGN).<sup>20,21</sup> It has been established that Golgi morphology directly affects WPB biogenesis and the hemostatic properties of its main cargo, VWF.<sup>22,23</sup> Co-packaging of discrete amounts of VWF, known as VWF quanta, into nascent WPBs is a stochastic process; a continuous Golgi ribbon therefore results in longer WPBs.<sup>22</sup> In contrast, when the Golgi is fragmented this leads to short and stubby WPBs, which can affect the adhesive activity of VWF upon stimulation.<sup>22,23</sup> Golgi dispersal occurs when there is a disequilibrium in anterograde and retrograde protein influx and is an attributed feature to neurodegenerative disorders, including Parkinson disease.<sup>24-26</sup> Therefore, when ER-to-Golgi protein trafficking is impeded due to the depletion of Sec22b and STX5, this has an immediate impact on the Golgi morphology that rapidly fragments, as shown in **chapter 3 and 4**. Consequently, the production of WPBs is altered, giving rise to a reduced number of short WPBs, which negatively influence the stimulus-induced VWF release.

We and others have demonstrated that STX5 is a binding partner of Sec22b (**chapter 4**), and plays an active role in ER-to-Golgi transport,<sup>27,28</sup> nonetheless, the extent of its requirement in vesicle transport is in question.<sup>29</sup> It has been suggested that although STX5 is an inextricable part of the Golgi architecture, it may have a secondary role in anterograde transport of membrane and secretory proteins, since STX5 depletion only has minor effects on the kinetics of protein transport.<sup>29</sup> However, this does not exclude its involvement in

trafficking of proteins important for the structural and functional organization of the Golgi, like Golgins and Golgi reassembly stacking proteins (GASPs).<sup>30,31</sup> The hypothesis that STX5 may not play a major role in trafficking of membrane and secretory proteins can explain the morphological differences we observed in the ER between Sec22b and STX5 depleted cells. Although STX5 knockdown ECs display an increased intraluminal width of ER cisternae, they lack the ribosome-studded round vesicles that contain VWF aggregates, presented in Sec22b knock down ECs. A similar phenotype as in Sec22b-depleted cells has also been described in COPII-depleted cells as discussed above, suggestive of defected anterograde protein transport.<sup>9,10</sup> This implies, that despite the comparable effect on Golgi morphology, Sec22b and STX5 may not affect ER-to-Golgi transport in a similar manner and STX5 might have an additional role in Golgi architecture, for instance through its role in retrograde and intra-Golgi transport.

The Golgi is a dynamic compartment that undergoes changes during the cell cycle. It is known that Golgi cisternae continuously fragment during mitosis, with the Golgi fragments being distributed over the daughter cells.<sup>32</sup> Post-mitosis, these Golgi parts then reassemble into continuous Golgi stacks.<sup>32</sup> It has been demonstrated that STX5 is actively involved in disassembly and reassembly of the Golgi through ubiquitin-dependent mechanisms during the cell cycle,<sup>33</sup> which further explains the induction of Golgi dispersal upon STX5 silencing. Interestingly, we observed in the Sec22b interactome that apart from STX5, ZW10 coimmunoprecipitated and was identified as a Sec22b binding partner (**chapter 4**). ZW10 is a diverse protein with an identified role as a mitotic checkpoint, as well as an implication in membrane trafficking between ER and Golgi.<sup>34,35</sup> Moreover, ZW10 depletion affects the Golgi architecture, as it displays a dispersed phenotype and a reducing in Golgi enzymes trafficking to the ER.<sup>36,37</sup> By extension, ZW10 may play a role in WPB biogenesis via controlling the Golgi morphology during cell cycle, however, more experiments on the topic should be held. Finally, we have identified several binding partners of Sec22b (**chapter 4**) that are implicated in Golgi disassembly during mitosis and post-mitosis reassembly in addition to their role in anterograde and retrograde transport. Therefore, we suggest that the WPB biogenesis may depend on ER-to-Golgi protein influx, which is regulated according to the cell cycle phase.

## Intracellular trafficking of SNARE proteins: AP-3 dependent WPB maturation

After WPBs have formed at the TGN, including within their initial cargo proteins like VWF and P-selectin (CD62P), they undergo an AP-3 dependent maturation process during which they acquire more proteins from the endosomal compartment.<sup>21,38,39</sup> The heterotetrameric AP-3 complex recognizes sorting signals in the cytoplasmic tail of transmembrane proteins, like the tyrosine motif on the tetraspanin CD63, and transports them to their correct destination.<sup>40</sup> Mutations on the  $\beta 1$  subunit of the AP-3 complex result in a Hermansky-Pudlak syndrome type 2 (HPS-2), a rare, recessive multisystemic disorder that is characterized by malformed LROs in many different cell types and which often leads to a bleeding diathesis.<sup>41</sup> In **chapter 6**, we were able to isolate BOECs from an HPS-2 patient with mutations in *AP3B1* that led to loss of AP-3  $\beta 1$  expression which, together with CRISPR-engineered *AP3B1* knockout BOECs, were used as models for AP-3-dependent WPB maturation. While confirming the mistrafficking of known AP-3 cargo, like CD63, which is mislocalized on the plasma membrane, we identified a potentially new target of the AP-3-dependent route, the SNARE protein VAMP8. Although the AP-3 complex has been associated with the SNARE protein VAMP7, more specifically by virtue of the latter's N-terminal longin domain,<sup>42</sup> it had not been described before to affect the SNARE maturation process of WPBs. We observed mislocalization and decreased expression of VAMP8, a WPB SNARE protein that

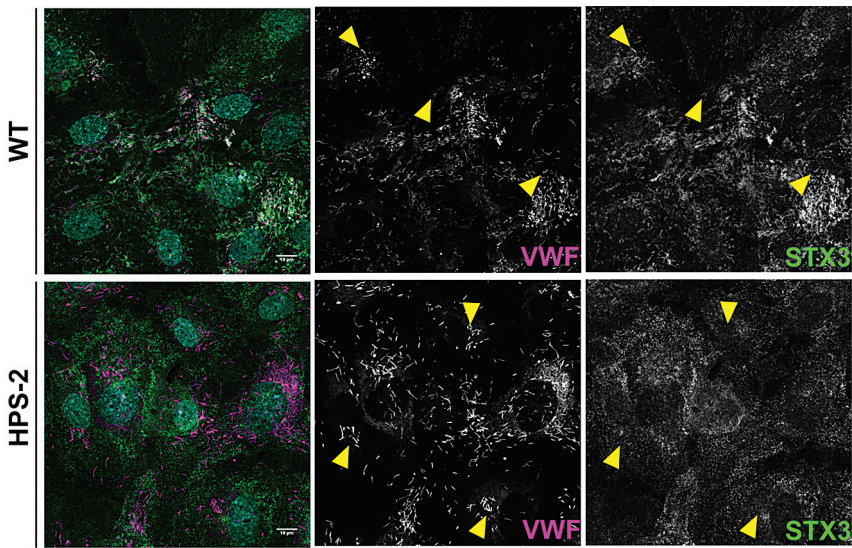


**Figure 2: Absence of STX3 on WPBs in HPS-2 BOECs.** Immunofluorescent staining of VWF (magenta) and STX3 (green) in WT and HPS-2 BOECs. Below the merged picture the magenta and green channel are shown. Yellow arrowheads indicate WPBs in the VWF and the corresponding areas in the STX3 channel (WPBs are positive for STX3 in WT cells and negative in HPS-2). Scale is shown on the bottom right and is set at 10  $\mu\text{m}$ .

takes part in stimulus-induced WPB release (**chapter 6**). Interestingly, VAMP8 intracellular localization correlates with CD63, which may indicate either a form of “piggyback trafficking” with VAMP8 ending up on WPBs as “bycatch” of the AP-3 dependent CD63 route or may involve a yet unidentified recognition motive on cytosolic exposed parts of VAMP8 for AP-3 to bind to. Finally, initial experiments revealed that syntaxin-3, another WPB SNARE that is normally found on WPBs and on endosomal vesicles, was no longer recruited to WPBs of HPS-2 BOECs (Figure 2). This may indicate that the AP-3-dependent transport pathway is a universal trafficking route for SNAREs from the endosomal compartment to maturing LROs such as WPBs.

## Exocytotic machinery of endothelial cells

SNARE proteins catalyze the fusion of opposing membranes through the formation of the SNARE complex. A functional SNARE complex consists of a v-SNARE on the donor membrane, usually a VAMP on a vesicle, i.e. WPB, and t-SNAREs on the target membrane, usually a STX and a SNAP on i.e. the plasma membrane.<sup>43</sup> Several SNAREs have been described so far to participate in the stimulus-induced WPB exocytosis (**chapter 5**). In **chapter 6 and 7**, we showed that both VAMP8 and STX3 are key components in the histamine-evoked WPB release, with their downregulation resulting in reduced VWF secretion. However, depletion of either SNARE protein does not block the WPB exocytosis completely, but rather reduces it by approximately half, indicating that WPB exocytosis may rely on more than one SNARE at a time in a complicated exocytotic scheme. Additionally, based on their intracellular localization on WPBs, VAMP8 and STX3 could also participate in content delivery during WPB maturation, however, the normal CD63 staining in both VAMP8 and STX3 knock out ECs indicates a rather more prominent role of both SNAREs in WPB exocytosis (**chapter 6 and 7**). In order to further understand the role of these SNAREs in WPB release and how they pair with each other, we used STX3 and VAMP8 as baits and looked into their interacting partners. Interestingly, while VAMP8 interacts with both STX3 and STX4,

a t-SNARE localized on the plasma membrane involved in WPB exocytosis,<sup>44</sup> STX3 interacts mainly with VAMP8 and only slightly with VAMP3, a v-SNARE described to also play a role in WPB/ VWF release.<sup>45</sup> This suggests that the SNARE pairs can be interchangeable although there might be preferential combinations of one over the other. Moreover, as several modes of exocytosis have been described, like sequential and compound (**chapter 5**), different SNARE pairs may assist different modes. In the case of sequential fusion, the order of SNARE pairing may include an initial VAMP8-3/ STX4 interaction in order to create the “hotspot” for WPB release, followed by an interaction between STX3 on the first WPB with VAMP8 on the next. In the case of compound fusion, the order would be reversed with a STX3/ VAMP8 pairing in order to create the secretory pod, that subsequently would fuse with the plasma membrane through a STX4/ VAMP8/3 complex formation. Nonetheless, in order to further understand the series of the SNARE complex formation in the different modes of exocytosis, more experiments should be held, including experiments with fluorescence resonance energy transfer (FRET) of living cells that could potentially decipher the SNARE complexes in a time dependent manner. Finally, the interchangeability and redundancy of SNARE proteins may be a cellular mechanism to prevent sole dependency on a specific SNARE pair that mutations could have devastating effects on its functionality. However, more experiments should be conducted with double knock out endothelial cells, in order to further understand the SNARE complex formation with respect to WPB exocytosis.

## Mutations outside the *VWF* gene that lead to reduced VWF release and Von Willebrand Disease

VWD is the most common congenital bleeding disorder that affects from 0.1% to 1% of the general population with 1:10.000 patients seeking medical care.<sup>46–48</sup> VWD is categorized in 3 main types: type 1 (VWD1) with partial quantitative deficiency, type 3 (VWD3) with almost complete lack of VWF and type 2 (VWD2) with qualitative defects that is further subcategorized in four types (2A, 2B, 2M and 2N) depending on the VWF function perturbed.<sup>49</sup> VWD1 is most prevalent form of VWD, accounting for up to 70% of the all cases in some studies, however is still the least understood form.<sup>48,50</sup> Mutations in the *VWF* gene can be found from the promoter region to exon 52, with blood group O being present in 65% of the patients.<sup>49</sup> The main reason for reduced VWF plasma levels is either intracellular retention, for instance because of dominant negative mutations that affect its intracellular processing or because of rapid clearance of VWF.<sup>49</sup> However, for ~30% of the cases of VWD1 or low VWF, this is not caused by mutations in the *VWF* gene,<sup>51</sup> which means that there are other modifiers of VWF levels at play.

Recent population-based studies with over 23,000 participants of European ancestry from 5 cohorts have shown that, in addition to *VWF* and *ABO*, variations in genes that encode for SNAREs, such as *STXBP5* and *STX2*, are associated with circulating levels of VWF.<sup>52</sup> Although these novel genetic loci only explain part of the genetic regulation of VWF levels,<sup>53</sup> their intracellular partners and the pathways they take part in open a whole array of potential regulators of VWF plasma levels that can contribute to the bleeding phenotypes of patients with known or (currently) unknown cause of bleeding. In **chapter 6** and **7**, we showed that downregulation of either VAMP8 or STX3 results in significantly reduced VWF secretion upon histamine stimulation. Like *STXBP5* and *STX2*, these are SNAREs that function in the process of exocytosis. In **chapter 3** and **4**, we demonstrated how early secretory pathway SNARE also contribute to the correct trafficking of VWF prior to its storage in WPBs. Both Sec22b and *STX5* positively regulate WPB formation and elongation, with Sec22b regulating the VWF turn over in the Golgi apparatus. Sec22b depletion results in VWF retention in ribosome-studded round vesicles in the ER, similar to the dilated ER observed in HEK293T cells expression VWF mutants identified in VWD patients.<sup>54,55</sup> It can

therefore be expected that genes that encode proteins in this pathway, for instance such as those that were discovered in the Sec22b interactome (**chapter 3**), may contain mutations or single-nucleotide polymorphisms (SNPs) that are linked with abnormal circulating VWF levels due to defects in intracellular protein trafficking or WPB exocytosis. Recent proteomic surveys of the WPB regulatory machinery such as in **chapter 3** (but also <sup>56-59</sup>) can therefore be very helpful for the interpretation of future Whole Genome Sequencing and Whole Exosome Sequencing efforts directed at identifying causes of bleeding or low VWF in patients that currently lack a molecular diagnosis of their disease.

## Future perspective

In this thesis we discussed the pathways involved in the biogenesis and maturation of WPBs in endothelial cells. We particularly were interested in the SNARE-mediated fusion steps that play an important role in intracellular VWF trafficking and WPB biogenesis in addition to basal and stimulus-induced exocytosis after WPB maturation (Figure 3). Understanding the cellular and molecular mechanisms involved in WPB formation can shed light to the yet unknown pathways involved in the formation of other LROs like platelet granules. Additionally, increasing our knowledge on the mechanisms that drive the formation and release of LROs may lead to a better understanding of multisystemic disorders like HPS and bleeding disorders like VWD. Eventually, this may result in improved diagnosis and treatment of patients with LRO-related disorders. Moreover, BOECs and iPSCs may be a powerful platform for *in vitro* disease correction testing, that would be the basis for cellular therapy with gene corrected hematopoietic stem cells (HSCs) of patients with storage pool disorders. Finally, since WPBs and platelet granules play an important role in hemostasis, figuring out how protein targeting takes place and how cells regulate the size of their storage organelles may be beneficial in creating “super” LROs containing additional hemostatic factors that would be superior in controlling bleeding and or regulation of thrombosis in individuals with hemostatic disorders.



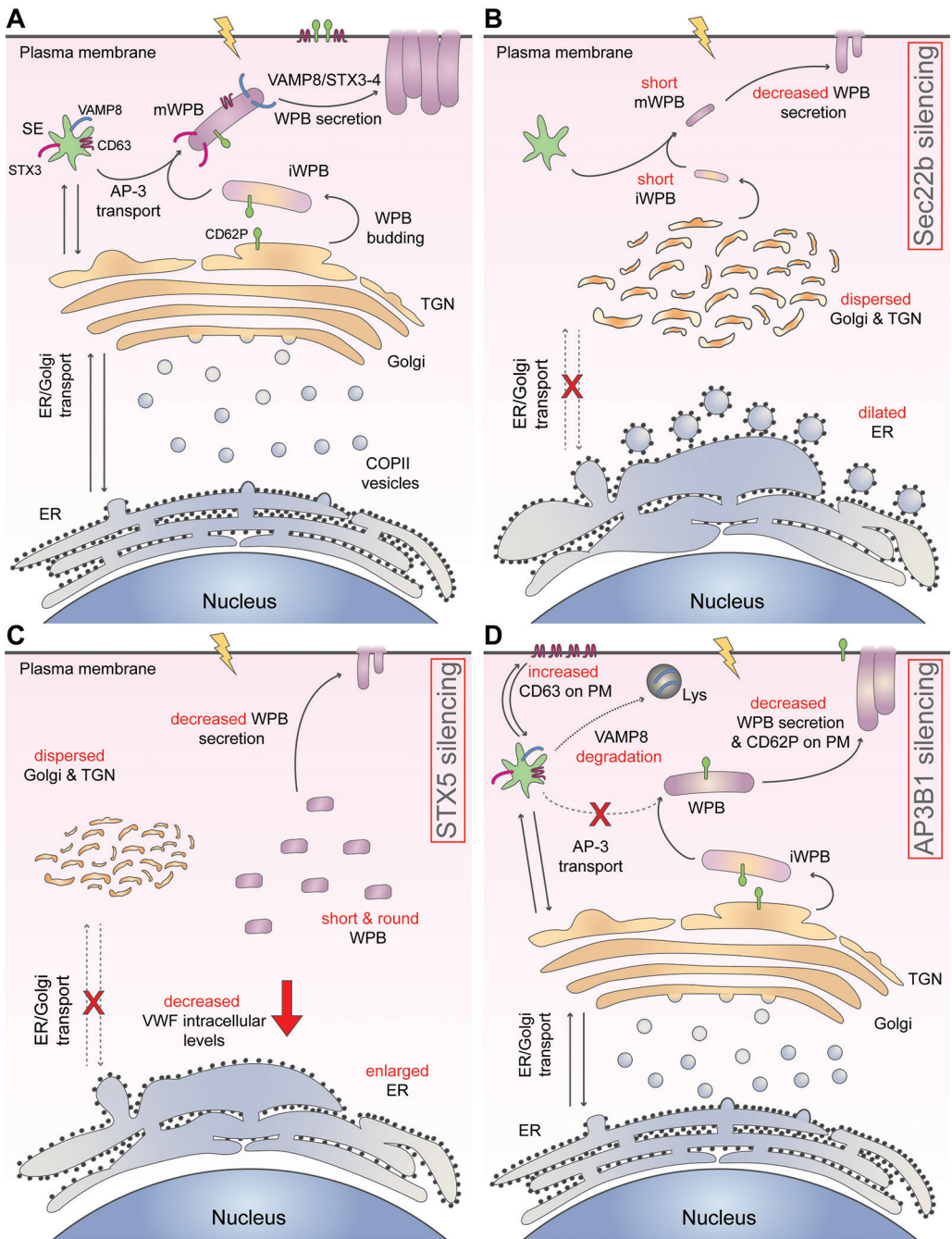


**Figure 3: Proposed models of VWF trafficking and WPB biogenesis and maturation.** A) WT and control cells with normal anterograde transport store VWF in elongated WPBs that mature in an AP-3 dependent manner and become positive for VAMP8 and possibly STX3 prior to a VAMP8/ STX3-4 dependent exocytosis. B) Upon Sec22b silencing, anterograde transport is blocked and VWF and other proteins are retained in ribosome-studded round vesicle closely related to the rER, which results in Golgi fragmentation and short WPBs, leading to decreased stimulus-induced VWF release. C) When STX5 is silenced, WPB biogenesis is negatively affected, with WPBs being short, round and in perinuclear localization, due to defective ER-to-Golgi transport and Golgi dispersal, which subsequently affects the exocytotic behavior of WPBs. D) obstructed WPB maturation due to mutation in AP-3 related genes in HPS-2, induce abnormal WPB content (mislocalization of CD63 and potentially STX3 and depletion of VAMP8), which alters the secretagogue-evoked VWF release, with HPS-2 and VAMP8 KO cells secrete significantly less.

## References

- Marks, M. S., Heijnen, H. F.G., Raposo G. Lyso-some-related organelles: Unusual compartments become mainstream. *Curr Opin Cell Biol.* 2014;25(4):495–505.
- Ambrosio AL, Di Pietro SM. Storage pool diseases illuminate platelet dense granule biogenesis. *Platelets.* 2017;28(2):138–146.
- Wasmeier C, Hume AN, Bolasco G, Seabra MC. Melanosomes at a glance. *J. Cell Sci.* 2008;121(24):3995–3999.
- Raposo G, Marks MS. Melanosomes - Dark organelles enlighten endosomal membrane transport. *Nat. Rev. Mol. Cell Biol.* 2007;8(10):786–797.
- Tsuji T, Karasek M. A procedure for the isolation of primary cultures of melanocytes from newborn and adult human skin. *J. Invest. Dermatol.* 1983;81(2):179–180.
- Valentijn KM, Sadler JE, Valentijn J a, Voorberg J, Eikenboom J. Functional architecture of Weibel-Palade bodies. *Blood.* 2011;117(19):5033–5043.
- Martin-Ramirez J, Hofman M, van den Biggelaar M, Hebbel RP, Voorberg J. Establishment of outgrowth endothelial cells from peripheral blood. *Nat Protoc.* 2012;7(9):1709–1715.
- Alberts B, Johnson A, Lewis J, et al. Transport from the ER through the Golgi Apparatus. *Mol. Biol. Cell, 4th Ed.* 2002;
- Tao J, Zhu M, Wang H, et al. SEC23B is required for the maintenance of murine professional secretory tissues. *Proc. Natl. Acad. Sci. U. S. A.* 2012;109(29):.
- Ohisa S, Inohaya K, Takano Y, Kudo A. Sec24d encoding a component of COPII is essential for vertebra formation, revealed by the analysis of the medaka mutant, vbi. *Dev. Biol.* 2010;342(1):85–95.
- Jalagadugula G, Goldfinger LE, Mao G, Lambert MP, Rao AK. Defective RAB1B-related megakaryocytic ER-to-Golgi transport in RUNX1 haplo deficiency: impact on von Willebrand factor. *Blood Adv.* 2018;2(7):.
- Lopes-da-Silva M, McCormack JJ, Burden JJ, et al. A GBF1-Dependent Mechanism for Environmentally Responsive Regulation of ER-Golgi Transport. *Dev. Cell.* 2019;1–16.
- Sun L, Mao G, Rao AK. Association of CBFA2 mutation with decreased platelet PKC- $\theta$  and impaired receptor-mediated activation of GPIIb-IIIa and pleckstrin phosphorylation: Proteins regulated by CBFA2 play a role in GPIIb-IIIa activation. *Blood.* 2004;103(3):948–954.
- Mao GF, Goldfinger LE, Fan DC, et al. Dysregulation of PLDN (pallidin) is a mechanism for platelet dense granule deficiency in RUNX1 haplo deficiency. *J. Thromb. Haemost.* 2017;15(4):792–801.
- Mancias JD, Goldberg J. The Transport Signal on Sec22 for Packaging into COPII-Coated Vesicles Is a Conformational Epitope. 2007;403–414.
- Malmersjö S, Di Palma S, Diao J, et al. Phosphorylation of residues inside the SNARE complex suppresses secretory vesicle fusion. *EMBO J.* 2016;35(16):1810–1821.
- Snyder DA, Kelly ML, Woodbury DJ. SNARE complex regulation by phosphorylation. *Cell Biochem. Biophys.* 2006;45(1):111–123.
- Van Den Biggelaar M, Hernández-Fernaund JR, Van Den Eshof BL, et al. Quantitative phosphoproteomics unveils temporal dynamics of thrombin signaling in human endothelial cells. *Blood.* 2014;123(12):22–37.
- Sadler JE. von Willebrand factor assembly and secretion. *J. Thromb. Haemost.* 2009;7:24–27.
- Zenner HL, Collinson LM, Michaux G, Cutler DF. High-pressure freezing provides insights into Weibel-Palade body biogenesis. *J. Cell Sci.* 2007;120(Pt 12):2117–2125.
- Mourik MJ, Faas FG, Zimmermann H, et al. Content delivery to newly forming Weibel-Palade bodies is facilitated by multiple connections with the Golgi apparatus. *Blood.* 2015;125(22):3509–16.
- Ferraro F, Kriston-Vizi J, Metcalf DJ, et al. A two-tier golgi-based control of organelle size underpins the functional plasticity of endothelial cells. *Dev. Cell.* 2014;29(3):292–304.
- Ferraro F, Mafalda Lopes da S, Grimes W, et al. Weibel-Palade body size modulates the adhesive activity of its von Willebrand Factor cargo in cultured endothelial cells. *Sci. Rep.* 2016;6(March):32473.
- Campadelli G, Brandimarti R, Di Lazzaro C, et al. Fragmentation and dispersal of Golgi proteins and redistribution of glycoproteins and glycolipids processed through the Golgi apparatus after infection with herpes simplex virus 1. *Proc. Natl. Acad. Sci. U. S. A.* 1993;90(7):2798–2802.
- Cole NB, Sciakly N, Marotta A, Song J, Lippincott-Schwartz J. Golgi dispersal during microtubule disruption: Regeneration of Golgi stacks at peripheral endoplasmic reticulum exit sites. *Mol. Biol. Cell.* 1996;7(4):631–650.
- Rendón WO, Martínez-Alonso E, Tomás M, Martínez-Martínez N, Martínez-Menárguez JA. Golgi fragmentation is Rab and SNARE dependent in cellular models of Parkinson's disease. *Histochem. Cell Biol.* 2013;139(5):671–684.
- Xu D, Joglekar AP, Williams AL, Hay JC. Subunit structure of a mammalian ER/Golgi SNARE complex. *J. Biol. Chem.* 2000;275(50):39631–39639.
- Dascher C, Matteson J, Balch WE. Syntaxin 5 regulates endoplasmic reticulum to Golgi transport. *J. Biol. Chem.* 1994;269(47):29363–29366.
- Suga K, Hattori H, Saito A, Akagawa K. RNA interference-mediated silencing of the syntaxin 5 gene induces Golgi fragmentation but capable of transporting vesicles. *FEBS Lett.* 2005;579(20):4226–4234.

30. Xiang Y, Wang Y. GRASP55 and GRASP65 play complementary and essential roles in Golgi cisternal stacking. *J. Cell Biol.* 2010;188(2):237–51.
31. Wang T, Grabski R, Sztul E, Hay JC. p115-SNARE interactions: a dynamic cycle of p115 binding monomeric SNARE motifs and releasing assembled bundles. *Traffic.* 2015;16(2):148–71.
32. Tang D, Mar K, Warren G, Wang Y. Molecular mechanism of mitotic golgi disassembly and reassembly revealed by a defined reconstitution assay. *J. Biol. Chem.* 2008;283(10):6085–6094.
33. Huang S, Tang D, Wang Y. Monoubiquitination of Syntaxin 5 Regulates Golgi Membrane Dynamics during the Cell Cycle. *Dev. Cell.* 2016;38(1):73–85.
34. Vallee RB, Varma D, Dujardin DL. ZW10 function in mitotic checkpoint control, dynein targeting and membrane trafficking: Is dynein the unifying theme? *Cell Cycle.* 2006;5(21):2447–2451.
35. Hirose H, Arasaki K, Dohmae N, et al. Implication of ZW10 in membrane trafficking between the endoplasmic reticulum and Golgi. *EMBO J.* 2004;23(6):1267–1278.
36. Varma D, Dujardin DL, Stehman SA, Vallee RB. Role of the kinetochore/cell cycle checkpoint protein ZW10 in interphase cytoplasmic dynein function. *J. Cell Biol.* 2006;172(5):655–662.
37. Sun Y, Shestakova A, Hunt L, et al. Rab6 Regulates Both ZW10/RINT-1 and COG Complex Dependent Golgi Trafficking and Homeostasis. *Mol Biol Cell.* 2007;
38. Arribas M, Cutler DF. Weibel-Palade body membrane proteins exhibit differential trafficking after exocytosis in endothelial cells. *Traffic.* 2000;1(10):783–93.
39. Harrison-Lavoie KJ, Michaux G, Hewlett L, et al. P-selectin and CD63 use different mechanisms for delivery to Weibel-Palade bodies. *Traffic.* 2006;7(6):647–662.
40. Bonifacino JS, Traub LM. Signals for sorting of transmembrane proteins to endosomes and lysosomes. *Annu. Rev. Biochem.* 2003;72:395–447.
41. Wei ML. Hermansky-Pudlak syndrome: a disease of protein trafficking and organelle function. *Pigment cell Res.* 2006;19(1):19–42.
42. Kent HM, Evans PR, Schäfer IB, et al. Structural Basis of the Intracellular Sorting of the SNARE VAMP7 by the AP3 Adaptor Complex. *Dev. Cell.* 2012;22(5):979–988.
43. Gerst JE. SNAREs and SNARE regulators in membrane fusion and exocytosis. *Cell. Mol. Life Sci.* 1999;55(5):707–734.
44. Zhu Q, Yamakuchi M, Lowenstein CJ. SNAP23 regulates endothelial exocytosis of von Willebrand Factor. *PLoS One.* 2015;10(8):14–22.
45. Pulido IR, Jahn R, Gerke V. VAMP3 is associated with endothelial Weibel-Palade bodies and participates in their Ca(2+)-dependent exocytosis. *Biochim. Biophys. Acta.* 2011;1813(5):1038–1044.
46. Werner EJ, Broxson EH, Tucker EL, et al. Prevalence of von Willebrand disease in children: A multiethnic study. *J. Pediatr.* 1993;123(6):893–898.
47. Rodeghiero F, Castaman G, Dini E. Epidemiological investigations of the prevalence of von Willebrand's disease. *Blood.* 1987;69(2):454–459.
48. Goodeve A, Paula James. Von Willebrand disease. *GeneReviews*®. 2017;
49. Goodeve A. Diagnosing von Willebrand disease: Genetic analysis. *Hematology.* 2016;2016(1):678–682.
50. Goodeve A. Genetics of type 1 von Willebrand disease. *Curr. Opin. Hematol.* 2007;14(5):444–449.
51. Goodeve A, Eikenboom J, Castaman G, et al. Phenotype and genotype of a cohort of families historically diagnosed with type 1 von Willebrand disease in the European study, Molecular and Clinical Markers for the Diagnosis and Management of Type 1 von Willebrand Disease (MCMDM-1VWD). *Blood.* 2007;109(1):112–121.
52. Smith NL, Chen MH, Dehghan A, et al. Novel associations of multiple genetic loci with plasma levels of factor VII, factor VIII, and von willebrand factor: The charge (cohorts for heart and aging research in genome epidemiology) consortium. *Circulation.* 2010;121(12):1382–1392.
53. Swystun LL, Lillcrap D. Genetic regulation of plasma von Willebrand factor levels in health and disease. *J. Thromb. Haemost.* 2018;16(12):2375–2390.
54. Wang JW, Valentijn KM, De Boer HC, et al. Intracellular storage and regulated secretion of Von Willebrand factor in quantitative Von Willebrand disease. *J. Biol. Chem.* 2011;286(27):24180–24188.
55. Wang JW, Groeneveld DJ, Cosemans G, et al. Biogenesis of Weibel-Palade bodies in von Willebrand's disease variants with impaired von Willebrand factor intrachain or interchain disulfide bond formation. *Haematologica.* 2012;97(6):859–866.
56. Van Breevoort D, Van Agtmaal EL, Dragt BS, et al. Proteomic screen identifies IGFBP7 as a novel component of endothelial cell-specific weibel-palade bodies. *J. Proteome Res.* 2012;11(5):2925–2936.
57. van Breevoort D, Snijders AP, Hellen N, et al. STXBP1 promotes Weibel-Palade body exocytosis through its interaction with the Rab27A effector Slp4-a. *Blood.* 2014;123(20):3185–94.
58. Schillemans M, Karampini E, Hoogendijk AJ, et al. Interaction networks of Weibel-Palade body regulators syntaxin-3 and syntaxin binding protein 5 in endothelial cells. *J. Proteomics.* 2019;in revision.
59. Holthenrich A, Drexler HCAA, Chehab T, Naß J, Gerke V. Proximity proteomics of endothelial Weibel-Palade bodies identifies novel regulator of von Willebrand factor secretion. *Blood.* 2019;134(12):979–982.





# Chapter 9

## Appendix

## Summary

Endothelial cells (ECs) form the inner lining of the vasculature, separating the blood from the underlining tissue. ECs, together with megakaryocyte (MK)-derived platelets are the main cellular regulators of primary hemostasis. Briefly, upon vascular damage, ECs rapidly respond by secreting their von Willebrand factor (VWF) content that unfurls into VWF strings and provides an adhesive platform for platelets. Subsequently, arrested platelets are activated by binding to collagen which is exposed in the subendothelium. These highly coordinated processes ultimately result in the formation of a primary hemostatic plug. ECs respond to stress signals by secreting their lysosome-related organelles (LROs), known as Weibel-Palade bodies. WPBs are a storage compartment of bioactive compounds, such as VWF. WPBs also contain a number of other components with angiogenic and proinflammatory properties that are simultaneously released with VWF following agonist induced WPB release. WPB formation can be divided into two distinct steps: their biogenesis is strictly dependent on the presence of multimeric VWF which is the driving force for their generation; a subsequent AP-3 dependent maturation step serves to recruit additional endosome-derived cargo to newly formed WPBs. VWF, a large multimeric protein enters the early secretory pathway as a monomer and dimerizes in the ER. VWF dimers are transported to the Golgi for further processing which includes proteolytic cleavage of its propeptide and multimerization. VWF multimers condense into VWF helical tubules and are tightly packaged in newly generated vesicles that bud off from the trans-Golgi network (TGN) membrane. In this thesis, we aim to elucidate the molecular mechanisms involved in the biogenesis of WPBs, as well as the pathways that govern its maturation process.

In **chapter 2** we provide an overview of our recent knowledge on the biogenesis of hemostatic LROs. We discuss in depth the molecular regulators of the formation of platelet  $\alpha$ - and  $\delta$ -granules, and endothelial WPBs. We first focus on the transcription factors that have been implicated in regulating the expression of proteins that are involved in the biogenesis of platelet LROs. The biological role of protein complexes involved in assembly of LROs is subsequently discussed. Next, we summarize recent information on WPB formation focusing on the newly discovered role of ER-to-Golgi protein transport in the regulation of WPB biogenesis and their release. Finally, we summarize the current knowledge on disorders that affect the formation of platelet granules and WPBs.

In **chapter 3** and **4** we provide novel information about the ER-to-Golgi protein trafficking and how it affects WPB formation. In **chapter 3** we explore the role of Sec22b in endothelial anterograde protein transport. We show that Sec22b, a SNARE protein that facilitates fusion of ER-derived vesicles with the Golgi target membrane, is involved in VWF trafficking. Depletion of Sec22b results in VWF retention in the ER, Golgi fragmentation and generation of short and “stubby” WPBs. We proceed by identifying the endothelial Sec22b interactome and exploring the role of its binding partner, STX5, a Golgi localized SNARE in WPB biogenesis (**chapter 4**). Downregulation of STX5 in ECs, results in extensive Golgi dispersal, which in turn alters WPB biogenesis. Finally, we demonstrate that depleting either Sec22b or STX5, negatively affects stimulus induced release of WPB.

In **chapter 5** we review the current literature on WPB exocytosis. We start by exploring the WPB content, that ranges from small chemokines to large VWF multimers. We also provide an overview of the signaling cascades, as well as tethering and fusion complexes that have been implicated in stimulus-induced WPB secretion. Finally, we discuss the role of WPBs in health and disease.

After WPBs have budded from the TGN, they undergo an extensive maturation process, that involves an AP-3 dependent cargo delivery from endosomes to immature WPB. In **chapter 6** we provide new information on AP-3-dependent WPB maturation by using patient-derived and in house CRISPR engineered blood outgrowth endothelial cells (BOECs) with mutations in the *AP3B1* gene. *AP3B1* encodes for a subunit of the heterote-

trameric AP-3 complex absence of which results in a multisystemic disorder, the Hermansky-Pudlak syndrome type 2 (HPS-2). Although HPS-2 has only been associated with defective  $\delta$ -granules in platelets, which leads to bleeding tendency, we show that HPS-2 BOECs are secretagogically incompetent due to defective WPB maturation. We confirm that AP3 $\beta$ 1 depletion in both patient and CRISPR knock out (KO) BOECs affects CD63 trafficking to the WPBs. Interestingly, we provide strong evidence that VAMP8, a WPB SNARE, follows the same AP-3 dependent pathway and is the primary reason for the observed decrease in WPB release in HPS-2 BOEC. In **chapter 7** we explore the role of STX3, a binding partner of VAMP8, employing ECs isolated from a STX3 deficient patient with microvillus inclusion disease. We show that STX3 is localized on WPBs and provide evidence for its role in stimulus induced WPB release.

Finally, in **chapter 8** we provide a broader perspective on the novel findings discussed in this thesis with reference to studies performed by other investigators. We present novel unpublished primary data and relate them to findings presented in this thesis. Based on our data we provide a novel model summarizing the mechanisms that govern the biogenesis and maturation of WPBs. We end by presenting suggestions and directions for future research.

## Samenvatting

De binnenbekleding van de vaatwand wordt gevormd door een aaneengesloten, enkele laag van endotheelcellen (EC). Tesaamen vormen zij een dynamische barrière tussen het circulerende bloed en de onderliggende weefsels. Samen met de van megakaryocyten afkomstige bloedplaatjes spelen endotheelcellen een cruciale rol bij de bloedstelping. Na beschadiging van een vaatwand worden door de endotheelcellen von Willebrand Factor (VWF) polymeren uitgescheiden die lange strengen vormen waaraan bloedplaatjes kunnen binden. Door de interactie van aan VWF gebonden bloedplaatjes met collageen van weefsel onder het endotheel dat door de beschadiging bloot komt te liggen, worden de bloedplaatjes geactiveerd. Dit resulteert uiteindelijk in de vorming van een bloedplaatjes-prop die ervoor zorgt dat de de beschadigde vaatwand snel afgedicht wordt om verder bloedverlies te voorkomen.

Endotheelcellen reageren op stress-signalen door aan lysosomen gerelateerde organellen (LROs) uit te scheiden. De LROs die in endotheelcellen aanwezig zijn worden “Weibel-Palade bodies” (WPBs) genoemd. WPBs zijn het belangrijkste opslag compartiment in endotheelcellen waarin naast VWF nog een aantal andere eiwitten aanwezig zijn die een rol spelen bij ontstekingsreacties en bij de vorming van nieuwe bloedvaten. De vorming van WPBs bestaat uit twee stappen; de vorming van WPBs wordt gedreven en is afhankelijk van VWF, daarna worden aanvullende componenten vanuit endosomes naar WPB gebracht door middel van een door “adaptor protein-3” (AP-3) gecontroleerde transport-route. VWF is een zeer groot eiwit dat als monomeer gesynthetiseerd wordt; in het ER worden VWF dimeren gevormd die daarna naar het Golgi worden getransporteerd. In het Golgi worden de dimeren omgezet in multimeren die vervolgens condenseren in lange tubules die het best vergeleken kunnen worden met een telefoonsnoer. De spiraalvormige VWF tubules worden in het trans-Golgi network (TGN) door een membraan omgeven en hieruit ontstaan nieuwe WPBs. In dit proefschrift worden de moleculaire mechanismen bestudeerd die betrokken zijn bij de vorming van WPBs. Daarnaast wordt gekeken naar de mechanismen die er voor zorgen dat na de vorming van WPBs nog nieuwe componenten aan de organellen toegevoegd kunnen worden.

In **hoofdstuk 2** beschrijven we onze huidige kennis over de vorming van LROs in bloedplaatjes en endotheelcellen. De moleculaire mechanismen die betrokken zijn bij de vorming van  $\alpha$  en  $\delta$  granules in bloedplaatjes en WPBs in endotheelcellen worden besproken. Allereerst focussen we op de rol van transcriptie-factoren die betrokken zijn bij de vorming van LROs in bloedplaatjes. We bespreken de rol die bepaalde eiwit-complexen spelen bij de vorming van LRO in bloedplaatjes. Daarnaast bespreken we welke mechanismen betrokken zijn bij de vorming van WPBs in endotheelcellen. Als laatste vatten we samen wat er op dit moment bekend is met betrekking tot ziekten die geassocieerd zijn met defecten in de vorming van plaatjes granules en WPBs.

In **hoofdstuk 3 en 4** wordt aangetoond dat transport van ER naar Golgi impact heeft op de vorming van WPBs. In **hoofdstuk 3** laten we zien dat Sec22b, een SNARE-eiwit dat betrokken is bij de fusie van uit het ER afkomstige transport-vesikels met het Golgi, een belangrijke rol speelt bij de vorming van WPBs. Sec22b depletie resulteert in de retentie van VWF in het ER, fragmentering van het Golgi en de vorming van kleine, zeer compacte (“stubby”) WPBs. Met behulp van massa spectrometrie is gekeken welke binding partners van Sec22b in endotheelcellen aanwezig zijn. Syntaxin 5 (STX5), een in het Golgi aanwezig SNARE-eiwit werd geïdentificeerd als een bindingspartner van Sec22b (**hoofdstuk 4**). Depletie van STX5 resulteerde in dispersie van het Golgi waardoor de vorming van WPBs verstoord werd. Uiteindelijk resulteerde dit in een sterk verminderde secretie van WPBs na stimulatie van endotheelcellen met histamine.

In **hoofdstuk 5** vatten we onze huidige kennis met betrekking tot de biosynthese en uitscheiding van WPBs samen. In dit hoofdstuk wordt de inhoud van WPBs uitgebreid



besproken. Tevens wordt een overzicht gegeven over de mechanismen die een rol spelen bij de secretie van WPBs. De biologische functie van WPBs wordt besproken aan de hand van ziektebeelden die impact hebben op de vorming en fysiologische rol van WPBs.

Na de initiële vorming van WPB vanuit het TGN kunnen er nog nieuwe componenten aan WPBs toegevoegd worden die afkomstig zijn uit endosomen. Transport van endosomen naar WPBs wordt gereguleerd door het AP-3 complex. In **hoofdstuk 6** gebruiken we uit bloed geïsoleerde endotheelcellen (zogenaamde “blood outgrowth endothelial cells” (BOEC)) van een Hermansky-Pudlak syndrome type 2 patiënt (HPS-2) om de rol van het AP-3 complex bij de vorming van WPBs in kaart te brengen. Patiënten met HPS-2 hebben een mutatie in de beta-subunit van het hetero-tetramere AP-3 complex die ervoor zorgt dat het AP-3 complex niet functioneel is. De resultaten in **hoofdstuk 6** laten zien dat HPS-2 BOEC in vergelijking met BOEC van gezonde personen minder goed WPBs kunnen secreteren. We bevestigen in dit hoofdstuk dat het AP-3 complex betrokken is bij het transporteren van het membraan-eiwit CD63 vanuit endosomen naar WPBs. Daarnaast laten we zien dat het AP-3 complex een rol speelt bij het transport van het SNARE-eiwit VAMP8 naar WPBs. VAMP8 is betrokken bij de secretie van WPBs en we postuleren dat de afwezigheid van VAMP8 ten grondslag ligt aan de verminderde secretie van WPBs. In **hoofdstuk 7** bestuderen we de rol van syntaxin-3 (STX3), een bindingspartner van VAMP8 bij de secretie van WPBs. Hiervoor maken we gebruik van BOEC geïsoleerd afkomstig van een patiënt met “microvillus inclusion disease”. We laten zien dat STX3 op WPBs aanwezig is en dat dit eiwit betrokken is bij de secretie van WPBs.

In **hoofdstuk 8** bespreken we de resultaten zoals weergegeven in dit proefschrift. Daarnaast presenteren we een aantal niet in dit proefschrift opgenomen waarnemingen en geven we een aantal suggesties voor vervolgonderzoek.

## PhD Portfolio

**PhD period:** September 2015 – September 2019

**Promotor:** prof. dr. Jan Voorberg

**Co-promotor:** dr. Ruben Bierings

Congresses/symposia	Year	ECTS	Presentation
ETCH Congress, The Hague, Netherlands	2016	0.25	Poster
Sanquin Science Day, Amsterdam, Netherlands	2016	0.25	Poster
ISTH Congress, Berlin, Germany	2017	1.5	Oral
Sanquin Science Day, Amsterdam, Netherlands	2017	0.25	Poster
DEBS symposium, Biezenmortel, Netherlands	2017	0.25	Poster
NVTH Symposium, Koudekerke, Netherlands	2018	0.5	Oral
GRS: Endothelial Cell Phenotypes in Health and Disease, Lucca, Italy	2018	0.5	Poster
GRC: Endothelial Cell Phenotypes in Health and Disease, Lucca, Italy	2018	1.0	Poster
Sanquin Science Day, Amsterdam, Netherlands	2018	0.25	Poster
NVTH Symposium, Koudekerke, Netherlands	2019	0.5	Oral
Sanquin Spring Seminar, Amsterdam, Netherlands	2019	0.5	Oral
EHA Congress, Amsterdam, Netherlands	2019	0.25	Poster
ISTH Congress, Melbourne, Australia	2019	1.5	Oral
Courses	Year	ECTS	
NVTH AIO course - Arterial Thrombosis	2016	0.5	
Advanced Immunology	2016	2.5	
Sanquin Science Course	2016	0.5	
Bioinformatics	2016	1.0	
NVTH AIO course – Bleeding Disorder	2017	0.5	
NVTH AIO course - Venous Thrombosis	2018	0.5	
Seminars, workshops and masterclasses	Year	ECTS	
Department meetings	2015–2019	2	
Journal clubs	2015–2018	1	
Sanquin Research seminars	2015–2019	2	
Landsteiner lectures and guest speakers	2015–2019	1	
Masterclass Prof. dr. Karin Hoffmeister	2016	0.2	
Masterclass Prof. dr. Jose Cancelas	2018	0.2	
Masterclass Prof. dr. Matthias Mann	2018	0.2	
Masterclass Prof. dr. David Lillicrap,	2019	0.25	
Masterclass Prof. dr. Paul Frenette and dr. Matthew Porteus	2019	0.2	
Invited Speaker Erasmus MC, Rotterdam, Netherlands	2019	0.1	
Invited Speaker Royal College of Surgeons (RCSI), Dublin Ireland	2019	0.5	
Teaching/mentoring	Year	ECTS	
Bachelor students: Marieke van Maanen and Selin Alpagot	2017	1	
Master student: Jennifer Olins	2018–2019	3	
Parameters of Esteem	Year		
ISTH Congress Young Investigator Award	2017		
NVTH Award of Excellence	2018		
GRC NIH Travel Grant	2018		
ISTH Congress Young Investigator Award	2019		

## Publication list

### Published

Schillemans M, **Karampini E**, van den Eshof BL, Gangaev A, Hofman M, van Breevoort D, Meems H, Janssen H, Mulder AA, Jost CR, Escher JC, Adam R, Carter T, Koster AJ, Van den Biggelaar M, Voorberg J, Bierings R (2018), *Weibel-Palade body localized Syntaxin-3 modulates von Willebrand factor secretion from endothelial cells*. *Arterioscler Thromb Vasc Biol.*; 38(7):1549-1561.

Schillemans M, **Karampini E**, Kat M and Bierings, R (2019), *Exocytosis of Weibel-Palade bodies: how to unpack a vascular emergency kit*. *J Thromb Haemost*; 17(1):6-18.

**Karampini E\***, Schillemans M\*, Hofman M, van Alphen F, de Boer M, Kuijpers TW, van den Biggelaar M, Voorberg J and Bierings R (2019), *Defective AP-3-dependent VAMP8 trafficking impairs Weibel-Palade body exocytosis in Hermansky-Pudlak Syndrome type 2 blood outgrowth endothelial cells*. *Haematologica*; 104(10):2091-2099

Schillemans M\*, **Karampini E\***, Hoogendijk AJ, Wahedi M, van Alphen, FPJ, van den Biggelaar M, Voorberg J and Bierings R (2019), *Interaction networks of Weibel-Palade body regulators syntaxin-3 and syntaxin binding protein 5 in endothelial cells*. *J Proteomics*; 205:103417

### In press

**Karampini E**, Olins J, Mulder A, Jost C, Geerts D, Voorberg J and Bierings R (2020), *Sec22b determines Weibel-Palade body length by controlling anterograde ER-Golgi transport*. *Haematologica*.

### In preparation

**Karampini E**, Mulder A, van Alphen F, Geerts D, Jost C, van den Biggelaar M, Voorberg J and Bierings R (2020), *WPB biogenesis is dependent on the Golgi Qa-SNARE STX5*.

**Karampini E**, Bierings R and Voorberg J (2020), *Orchestration of primary hemostasis by platelet and endothelial lysosome-related organelles*.

\* These authors contributed equally

## Authors and affiliations

### **Rüdiger Adam**

Pediatric Gastroenterology, University Medical Centre, Mannheim, Germany

### **Floris P.J. van Alphen**

Molecular and Cellular Hemostasis, Sanquin Research and Landsteiner Laboratory, Amsterdam UMC, University of Amsterdam, The Netherlands

### **Ruben Bierings**

Hematology, Erasmus University Medical Center, Rotterdam, The Netherlands.  
Molecular and Cellular Hemostasis, Sanquin Research and Landsteiner Laboratory, Amsterdam UMC, University of Amsterdam, The Netherlands

### **Maartje van den Biggelaar**

Molecular and Cellular Hemostasis, Sanquin Research and Landsteiner Laboratory, Amsterdam UMC, University of Amsterdam, The Netherlands

### **Martin de Boer**

Blood Cell Research, Sanquin Research and Landsteiner Laboratory, Amsterdam UMC, University of Amsterdam, The Netherlands

### **Dorothee van Breevoort**

Molecular and Cellular Hemostasis, Sanquin Research and Landsteiner Laboratory, Amsterdam UMC, University of Amsterdam, The Netherlands

### **Tom Carter**

Molecular and Clinical Sciences Research Institute, St George's University of London, United Kingdom

### **Johanna C. Escher**

Pediatric Gastroenterology, Sophia Children's Hospital, Erasmus MC, Rotterdam, The Netherlands

### **Bart L. van den Eshof**

Molecular and Cellular Hemostasis, Sanquin Research and Landsteiner Laboratory, Amsterdam UMC, University of Amsterdam, The Netherlands

### **Anastasia Gangaev**

Molecular and Cellular Hemostasis, Sanquin Research and Landsteiner Laboratory, Amsterdam UMC, University of Amsterdam, The Netherlands

### **Dirk Geerts**

Medical Biology Academic Medical Center, University of Amsterdam, The Netherlands

### **Menno Hofman**

Molecular and Cellular Hemostasis, Sanquin Research and Landsteiner Laboratory, Amsterdam UMC, University of Amsterdam, The Netherlands

### **Hans Janssen**

Cell Biology, The Netherlands Cancer Institute, Amsterdam, The Netherlands

**Carolina R. Jost**

Molecular Cell Biology, Section Electron Microscopy, Leiden University Medical Center, Leiden, The Netherlands

**Ellie Karampini**

Molecular and Cellular Hemostasis, Sanquin Research and Landsteiner Laboratory, Amsterdam UMC, University of Amsterdam, The Netherlands

**Marije Kat**

Molecular and Cellular Hemostasis, Sanquin Research and Landsteiner Laboratory, Amsterdam UMC, University of Amsterdam, The Netherlands

**Abraham J. Koster**

Molecular Cell Biology, Section Electron Microscopy, Leiden University Medical Center, Leiden, The Netherlands

**Taco W. Kuijpers**

Blood Cell Research, Sanquin Research and Landsteiner Laboratory, Amsterdam UMC, University of Amsterdam, The Netherlands

Emma Children's Hospital, University of Amsterdam, The Netherlands

**Henriët Meems**

Molecular and Cellular Hemostasis, Sanquin Research and Landsteiner Laboratory, Amsterdam UMC, University of Amsterdam, The Netherlands

**Aat A. Mulder**

Molecular Cell Biology, Section Electron Microscopy, Leiden University Medical Center, Leiden, The Netherlands

**Jennifer Olins**

Molecular and Cellular Hemostasis, Sanquin Research and Landsteiner Laboratory, Amsterdam UMC, University of Amsterdam, The Netherlands

**Maaïke Schillemans**

Molecular and Cellular Hemostasis, Sanquin Research and Landsteiner Laboratory, Amsterdam UMC, University of Amsterdam, The Netherlands

**Jan Voorberg**

Molecular and Cellular Hemostasis, Sanquin Research and Landsteiner Laboratory, Amsterdam UMC, University of Amsterdam, The Netherlands

Department of Vascular Medicine, Academic Medical Center, University of Amsterdam, The Netherlands

## Thank you note

After four happy, intense, beautiful, stressed, lively years, filled with new people, experiences and places, the time to “promote” has come. It was a period of my life that I learned so much about science, myself and how the world works, and now I can genuinely say that I enjoyed all of it, with its ups and downs. Of course, I couldn’t have done this alone and therefore I would like to thank you all for being there for me in any way that you could. To my supervisors Jan and Ruben, thanks for guiding me, pushing me to become better, trusting me and helping me grow as a scientist. To my paranymphs, Nadia and Elena, girls, maybe we met a couple years or a couple decades ago, but each of you has a special place in my heart. To old and new friends, thank you for the support you provided knowingly or unknowingly and for always being there to “let’s get a drink” and have fun. To my colleagues from PE, MCB, MHC and my co-authors, all of you created a safe and stimulating environment that allowed me to achieve all of my goals and much more! Μαμά και μπαμπά, όλα αυτά τα χρόνια σταθήκατε δίπλα μου σαν ακλόνητοι φρουροί, που παρόλο που μας χωρίζουν κάποιες χιλιάδες χιλιόμετρα ποτέ δεν μου έλειψε η ζεστασιά και η αγάπη σας. Ελπίζω να σας κάνω τόσο περήφανους, όσο εσείς καθημερινά. Σας ευχαριστώ για όλα και σας αγαπώ για πάντα! Finally, Achilles, not so much needed to be said, θα σε δω στο πίτι και love you!

## Curriculum vitae

Ellie was born in Cholargos, Athens, Greece to loving parents, Mary and Alexandros. She studied Chemistry at the National and Kapodistrian University of Athens, where she performed her final internship at the Department of Environmental Chemistry, assessing the ecological status of urban streams.

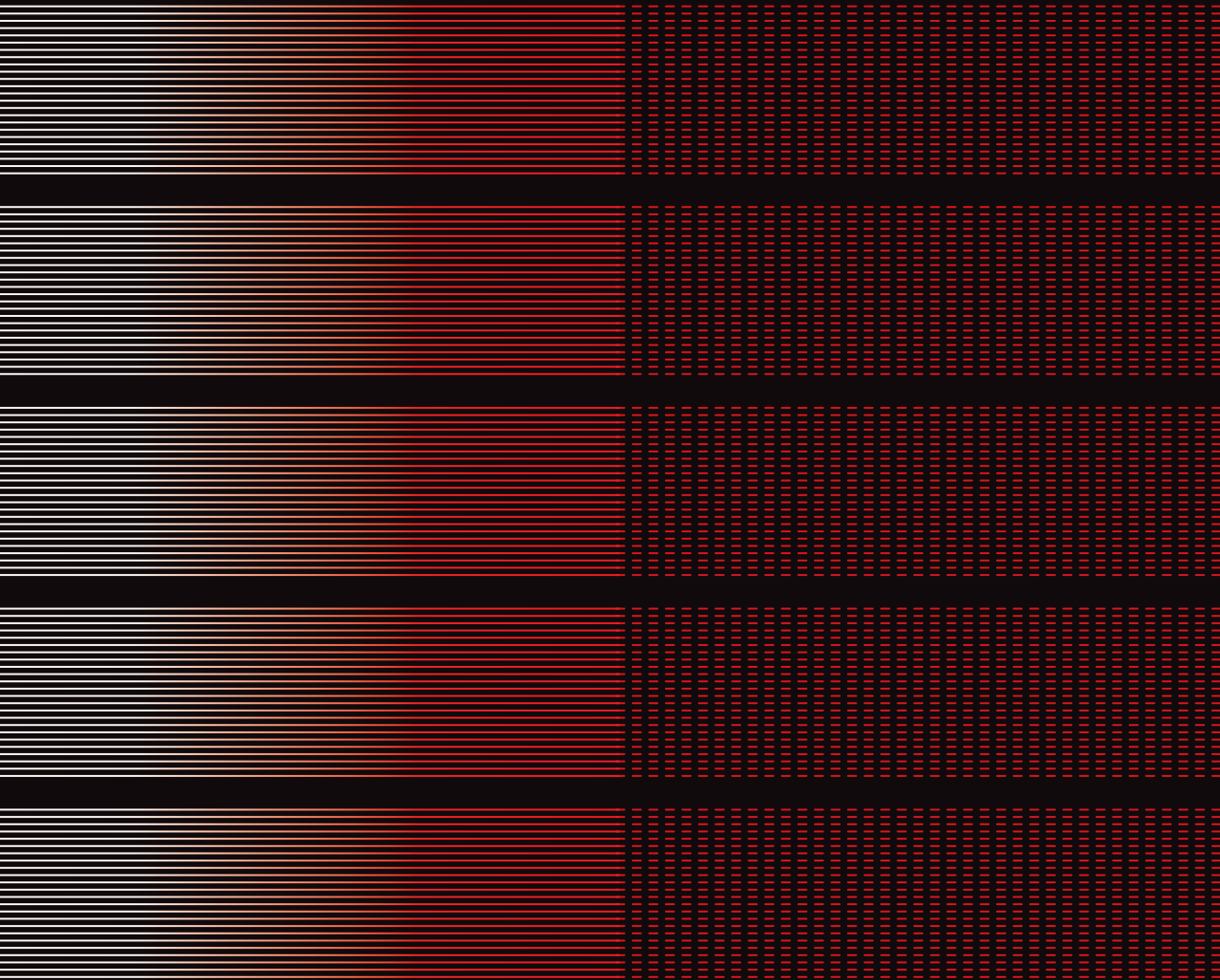
Upon obtaining her bachelor's degree (BSc), she moved to Amsterdam, where she obtained her master's degree in Analytical Chemistry (MSc) at the University of Amsterdam. During her studies, she worked in excellent groups and completed her two internships, one in statistics, and one in the group of Prof. Dr. Manfred Wuhrer, where she developed a mass spectrometry-based method for profiling urinary glycan in Fabry disease.

She went on to enter the PhD program of the University of Amsterdam, joining the Department of Molecular and Cellular Hemostasis at Sanquin Research, where worked under the supervision of Prof. Dr. Jan Voorberg and Dr. Ruben Bierings. During that time, she was able to investigate the role of SNARE proteins in intracellular protein trafficking and contribute to understanding the molecular mechanisms involved in Weibel-Palade body formation and release. Additionally, her work was nationally and internationally recognized, as she was given the prestigious award of excellence from the Dutch Society of Thrombosis and Haemostasis and two Young Investigator Awards from International Society of Thrombosis and Haemostasis.

Currently, she is based in Dublin, Ireland, where she has joined the team of James O'Donnell in the Royal College of Surgeons, working as Post-Doc in the multi-institutional Zimmerman Program for the molecular and clinical biology of von Willebrand disease.







ISBN: 978-94-028-2003-4